On the Importance of Soil Moisture for Streamflow Forecasting

Mahshid Shahrban

A thesis submitted for the degree of Doctor of Philosophy

August 2016

Department of Civil Engineering

MONASH University

Copyright notice

Abstract

Streamflow forecasting is essential for improving efficiencies in water use through reduced water losses on irrigation orders, and enhancing water management operations based on better information on inflows and off-takes in time and space. In addition, it provides valuable information on flood events for the dissemination of flood warnings with sufficient accuracy and lead time. Hydrologic forecasting models are used extensively in simulation of river flows in both flood and non-flood events. Quantitative Precipitation Forecasts (QPFs) from Numerical Weather Prediction (NWP) models are the primary source of rainfall data for input into hydrologic forecasting models, other than a forecaster's intuition.

Soil moisture is a key factor controlling the hydrological behaviour of a catchment, particularly for flood modelling, as it controls transformation of rainfall into infiltration or runoff. Advances in remote sensing technologies have provided a variety of opportunities for improved hydrologic prediction, including the observation of land surface states such as soil moisture through time and across large areas. However, there has been limited effort to utilise such remote sensing information in hydrological modelling, especially in the context of operational applications.

The principal objectives of this thesis are i) evaluation of QPFs from the Australian forecast system product, ii) understanding the impact of soil moisture on streamflow prediction skill when used in the hydrologic model calibration stages, iii) assessment of satellite-based soil moisture observation constraint of the hydrologic model and its subsequent streamflow generation, and iv) the overall impact on the streamflow forecast skill when putting all three components together.

The NWP QPFs from the Australian Community Climate Earth-System Simulator (ACCESS) are evaluated against rainfall observations from a weather radar, to understand the uncertainties transferred to the streamflow forecasting

model. The radar observations are first calibrated to remove the expected bias in the data according to in-situ rainfall observations. The QPFs evaluation indicates that significant rainfall uncertainty is expected to be propagated into the streamflow forecasting in this research.

Next, the ground-based measurement of soil moisture from research monitoring stations are used to calibrate and evaluate the soil moisture predictive capability in two rainfall-runoff models, Génie Rural 4 paramètres Horaire (GR4H) and Probability Distributed Model (PDM), and its subsequent effect on the streamflow predictions. Two calibration methods are tested; calibration to streamflow alone and joint-calibration using both streamflow and soil moisture observations. The results suggest that the GR4H model be used in Australia, in preference to PDM, and that soil moisture observations be used in the calibration process.

To investigate the impact of ongoing soil moisture constraint on streamflow forecasting, the root-zone soil wetness is first estimated from Soil Moisture and Ocean Salinity Mission (SMOS) satellites near-surface soil moisture retrievals. According to the comparisons with in-situ soil wetness data in the study area of this thesis, the exponential filtering technique is selected as the best approach. The hydrologic models are then constrained with the satellite-based root-zone estimates using a nudging approach, and the results are benchmarked against ground-based soil moisture data. It is shown that the effectiveness of soil moisture constraint depends on both catchment characteristics and the selected model for coupling soil moisture and runoff generation.

Finally, soil moisture constrained streamflow forecasts are assessed in the context of a real-time forecasting scenario, utilising both satellite-based estimates of root-zone soil moisture and NWP forecast rainfall. It is demonstrated that even with the degraded rainfall information, soil moisture constraint typically improve the streamflow forecasts, especially for moderate sized events, while for major events the forecasts are only improved for longer lead times.

Declaration

This is to certify that this thesis contains no material which has been accepted for the award of any other degree or diploma in any university or other institution, and affirms that to the best of my knowledge the thesis contains no material previously published or written by another person, except where due reference is made in the text of the thesis.

Mahshid Shahrban

23 August 2016

Acknowledgement

I am greatly indebted to many people who in some way contributed to the progress and publication of this research. First and foremost, I would like to gratefully and sincerely thank my supervisors, Prof. Jeffrey Walker at Monash University and Dr. Q.J. Wang at CSIRO Land and Water, who have supported me during the entire period of my study. Their valuable recommendations and endless inspiration have enabled me to assemble and finish my study effectively.

I deeply appreciate the constant support and advice provided by people at CSIRO. In particular, I am very grateful to Dr. David Robertson for his insightful feedback and wise comments. I have learned a great deal from his unique perspective on almost any issue in research. I would like to acknowledge Dr. Alan Seed at the Bureau of Meteorology. It has been a great opportunity to complete some stages of my research under his guidance and learn from his research expertise. Additionally, I wish to thank Dr. Peter Steinle at the Bureau of Meteorology. Despite his busy schedules, he has been very supportive to me during my study. I also would like to thank Dr. Prasantha Happuachchi, formerly at CSIRO and now at the Bureau of Meteorology, and Dr. David Enever at the Bureau of Meteorology for their assistance in setting up the SWIFT modelling and providing the data sets. At Monash University, I would like to thank Dr. Chris Rudiger and Dr. Ye Nan for sharing their generous and valuable comments during my research.

Finally and most importantly, I would like to appreciate my parents, Homa and Reza, for their encouragement and unconditional support over all these years of studies. They always gave me the inspiration to pursue my dreams. Special thanks to my husband, Vahid, who has supported me in every venture. I had little time for him during the recent years and without his understanding, patience and love I would not have made it to this point.

Table of Contents

List of Symbols

Symbols	Unit	Definitions
b	[-]	Exponent of Pareto distribution for spatial variability (PDM)
b_e	[-]	Exponent in actual evaporation function (PDM)
b_g	[-]	Exponent of recharge function (PDM)
c	mm	Storage capacity (PDM)
c_{max}	mm	Maximum soil moisture storage capacity (PDM)
c_{min}	mm	Minimum soil moisture storage capacity (PDM)
c_{minrat}	[-]	The ratio of c_{min} to c_{max} (PDM)
D_c	km	Distance between centroids of observed and forecast rain objects
D	d	Number of days in the time windows in moving average
d_i	mm	Rate of drainage (PDM)
E_i	mm	Potential evaporation (PDM)
E'_i	mm	Actual evaporation (PDM)
E_n	mm	Evapotranspiration (GR4H)
E_s	mm	Actual evaporation rate (GR4H)
F	mm	Ground water exchange function (GR4H)
f(c)	[-]	Probability Density Function (PDM)
F_{pdm}	[-]	Cumulative distribution function (PDM)
F_{SF}	m^6/s^2	Objective function for streamflow calibration
F_{joint}	[-]	Objective function for joint-calibration
G	[-]	Weighting parameter in nudging approach
I	m^3/s	Inflow (Muskingum routing)
k	s	Storage time constant parameter (Muskingum routing)
k_b	h mm^2	Baseflow time constant (PDM)
k_g	h mm^{bg-1}	Groundwater recharge time constant (PDM)
k_1	h	Time constant of cascade of linear reservoirs (PDM)
k_2	h	Time constant of cascade of linear reservoirs (PDM)
M_k	[-]	Model operator matrix
n	[-]	Number of time steps for calibration

O	m^3/s	Outflow (Muskingum routing)
Perc	mm	Percolation leakage from the production store (GR4H)
P_n	mm	Net rainfall (GR4H)
P_r	mm	Total runoff (GR4H)
P_s	mm	Infiltration to the production store (GR4H)
$Q_{obs,i}$	m^3/s	Observed streamflow at the i_{th} time step
$Q_{sim,i}$	m^3/s	Simulated streamflow at the i_{th} time step
q_b	m^3/s	Subsurface flow (PDM)
q_s	m^3/s	Surface runoff (PDM)
R	mm/h	radar rainfall rate
R'	mm/h	Gauge rainfall rate
R_{eff}	km	Effective radius of observed rain object
S	mm	Model Soil water level (GR4H, PDM)
S_m	m^3	Storage within the routing reach (Muskingum routing)
St_{ratio}	[-]	The ratio of soil tension storage capacity to C_{max} (PDM)
$SM_{sim,i}$	%	Simulated soil moisture at the i^{th} time step
SSM	m^3/m^3	Satellite near-surface soil moisture retrieval
SWI	%	Soil wetness index
$SW_{ass,i}$	%	Updated soil wetness at the i^{th} time step
$SW_{obs,i}$	%	Observed soil wetness at the i^{th} time step
$\overline{SW}_{obs}$	%	Average of soil wetness observations
$SW_{sim,i}$	%	Simulated soil wetness at the i^{th} time step
S_1	[-]	Soil moisture storage (PDM)
S_{21}	[-]	Linear reservoir (PDM)
S_{22}	[-]	Linear reservoir (PDM)
S_3	[-]	Nonlinear storage (PDM)
T	d	Characteristic time length parameter in exponential filtering
w_i	[-]	Multiplicative weight
x	[-]	Weighting factor parameter (Muskingum routing)
$\hat{X}_k^a$	mm	Analysis
X_k^b	mm	Model initial state
x_1	mm	Maximum production store capacity (GR4H)

x_2	mm	Groundwater exchange coefficient (GR4H)
x_3	mm	Maximum routing store capacity (GR4H)
x_4	h	Time base of unit hydrograph UH1 (GR4H)
α	[-]	Multiplicative parameter in radar conversion equation
β	[-]	Exponent in radar conversion equation
θ_i	m^3/m^3	Average volumetric soil moisture at the i^{th} time step
θ_{max}	m^3/m^3	Maximum volumetric soil moisture
θ_{min}	m^3/m^3	Minimum volumetric soil moisture
σ^2_{obs}	[-]	Soil wetness observation variance
σ^2_{sim}	[-]	Soil wetness prediction variance

List of Abbreviations

ACCESS	Australian Community Climate Earth-System Simulator
ACCESS-A	Australian Community Climate Earth-System Simulator with Australian domain
ACCESS-G	Australian Community Climate Earth-System Simulator with Global domain
ACCESS-R	Regional Australian Community Climate Earth-System Simulator
ACCESS-VT	Australian Community Climate Earth-System Simulator for Victoria-Tasmania region
ALOS	Advanced Land Observing Satellite
AMI	Active Microwave Instrument
AMSR-E	Advanced Microwave Scanning Radiometer-EOS
AMSR2	Advanced Microwave Scanning Radiometer 2
ARMA	AutoRegressive Moving Average
ASCAT	Advanced SCATterometer
AVHRR	Advanced Very High Resolution Radiometer
AWAP	Australian Water Availability Project
AWBM	Australian Water Balance Model
BoM	Bureau of Meteorology
CATDS	Center Aval de Traitemnet des Donnees SMOS
CDF	Cumulative Density Function
CLSM	Catchment-based Land Surface Model
DGG	Discrete Global Grid
DHSVM	Distributed Hydrology Soil Vegetation Model
DI	Direct Insertion
DM	Deutschland-Modell
DMSP	Defense Meteorological Satellite Program
EASE	Equal Area Scalable Earth

DWD	Deutscher Wetterdienst
EC	European Commission
EDA	Evolutionary Data Assimilation
EFAS	European Flood Awareness System
EKF	Extended Kalman Filter
EM	Europa-Modell
EnKF	Ensemble Kalman Filter
EnKS	Ensemble Kalman Smoother
EnSRF	Ensemble Square Root Filter
ERS	European Remote Sensing Satellites
ESA	European Space Agency
ESA CCI	ESA’s Water Cycle Multi-mission Observation Strategy and Climate Change Initiative
EUMETSAT	Exploitation of Meteorological Satellites
FAR	False Alarm Ratio
FBI	Frequency Bias Index
FDP	Forecast Demonstration Project
FSS	Fractions Skill Score
GASP	Global Assimilation and Prediction System
GM	Global Model
GOES	Geostationary Operational Environmental Satellites
GR3J	Génie Rural 3 paramètres Journalier
GR4H	Génie Rural 4 paramètres journalier Hourly version
GR4J	Génie Rural 4 paramètres Journalier
HBV	Hydrologiska Byråns Vattenavdelning
IHACRES	Identification of unit Hydrographs and Component flows from Rainfall, Evaporation and Streamflow data
IMS	Ice Mapping System
ISURF	Integrated Sensitivity and UnceRtainty analysis Framework

KNN	K-Nearest Neighbour
LAI	Leaf Area Index
LAPS	Limited Area and Prediction System
LM	Lokal-Modell
LM COSMO	Lokall Model of the COSMO consortium
L-MEB	L-band Microwave Emission of the Biosphere
LPRM	Land Parameter Retrieval Model
MAE	Mean Absolute Error
MDB	Murray Darling Basin
ME	Mean Error
MetOp	Meteorological Operational satellite programme
MIKE-SHE	MIKE System Hydrologique European
MIRAS	Microwave Imaging Radiometer with Aperture Synthesis
MODIS	MODerate-resolution Imaging Spectrometer
MSE	Mean Squared Error
NCEP	National Centres for Environmental Prediction
NOAA	National Oceanic and Atmospheric Administration
NSE	Nash-Sutcliffe Efficiency
NWP	Numerical Weather Prediction
PALSAR	Phased Array type L-band SAR
PDM	Probability Distributed Model
POD	Probability of detection
QPE	Quantitative Precipitation Estimation
QPF	Quantitative Precipitation Forecasting
RE	Relative Error
RMSD	Root Mean Square Difference
RMSE	Root Mean Square Error
SAC	Sacramento

SAC-SMA	Sacramento Soil Moisture Accounting
SAR	Synthetic Aperture Radar
SCA	Snow Covered Area
SCE-UA	Shuffled Complex Evolution developed at the University of Arizona
SCS-CN	Soil Conservation Service-Curve Number
SFB	Surface inFiltration Baseflow
SIM	Safran-Isba-Modcou
SimHYD	Simplified HYDROLOG model
SCRRM	Simplified Continuous Rainfall–Runoff model
SMA	Soil Moisture Accounting
SMAP	Soil Moisture Active Passive
SMAR	Soil Moisture Accounting Runoff
SMAR	Soil Moisture Accounting and Routing
SMARG	SMAR with a Groundwater component added
SMMR	Scanning Multichannel Microwave Radiometer
SMOS	Soil Moisture and Ocean Salinity Mission
SSM/I	Special Sensor Microwave/Imager
STEPS	Short-Term Ensemble Prediction System
SWAT	Soil and Water Assessment Tool
SWB	Soil Water Balance
SWE	Snow Water Equivalent
SWI	Soil Wetness Index
SWIFT	Short-Term Water Information Forecasting Tool
TATE	Time-area Topographic Extension
TMI	TRMM Microwave Imager
TOPKAPI	TOPographic Kinematic APproximation and Integration
TOPLATS	TOPmodel-based Land-Atmosphere Transfer Scheme
TOPMODEL	Topography-based Hydrologic Model

TRMM	Tropical Rainfall Measuring Mission
TUWIEN	Vienna University of Technology
TSS	True Skill Statistics
UH2	Second Unit Hydrograph
UM	Unified Model
URBS	Unified River Basin Simulator
Vol E	Volumetric Error
VUA	Vrije Universiteit Amsterdam
WGNE	Working Group of Numerical Experimentation

List of Figures

List of Tables

Chapter 1
Introduction

This thesis contributes to the development of an advanced continuous streamflow modelling system, utilising satellite soil moisture observations coupled with numerical weather prediction forecasts of precipitation, with the aim of improving streamflow forecasting skill. The Murrumbidgee catchment in south-eastern Australia is used as a demonstration test-bed because of the extensive in-situ soil moisture and rain gauge data available there. Moreover, these developments are made within the new Bureau of Meteorology operational flood warning system that is currently in progress for catchments across Australia. The streamflow modelling system developments have been assessed through i) an evaluation of quantitative precipitation forecasts capability from the Australian numerical weather forecast system for application in streamflow forecasting, ii) evaluation of satellite-based soil moisture estimates using the in-situ measurements, and iii) application of in-situ and/or satellite-based soil moisture data to constrain the initial soil moisture states.

1.1 Problem Statement

Floods have been extensive world-wide in recent times. Thousands of people have lost their lives while many others have been left homeless as a consequence of floods (Kundzewicz, 2012). Many researchers are trying to improve hydrological modelling capabilities (Parker and Fordham, 1996; Cloke and Pappenberger, 2009; Hapuarachchi et al., 2011; Biondi and De Luca, 2013), such that there will be a reduced loss of life and property from these events, by providing accurate flood warnings with sufficient lead time for people to react (Glantz, 2004; Basha et al., 2008). In addition, better continuous streamflow prediction may improve efficiencies in water use through reduced water losses on irrigation orders, adjusting environmental releases, and enhancing water management operations based on better information on inflows and off-takes in time and space (Hamlet et al., 2002; Dong et al., 2006; Bravo et al., 2009). While hydrological models are used extensively in simulation of river flows in both flood and non-flood events, these predictions are uncertain for a range of reasons, including model development error (Beven, 1989), parameter value uncertainty and error in calibration (Moradkhani et al., 2005), forcing data errors and uncertainty in initial conditions (Grayson and Blöschl, 2000). Though hydrological model skill has improved substantially over the last 10 years (Liu and Gupta, 2007), there is still a need to increase the predictive power of the models.

The most important input to streamflow prediction models is precipitation (Larson and Peck, 1974). Hydrological models are strongly dependent on precipitation input, and accurate forecast precipitation is crucial for reliable hydrological forecasting in both flood and non-flood conditions of a catchment (Silvestro and Rebora, 2014). Numerical weather prediction (NWP) models can provide information on forecast precipitation with national coverage for different spatial and temporal resolutions and with lead times out to several days, but the accuracy of this information is uncertain. Therefore, to enhance hydrological modelling forecasts, there is a need to evaluate and correct forecast precipitation before their application in hydrological forecasting. In addition, antecedent land surface conditions such as soil moisture and snow are also important for accurate forecasting of time to flood peak and the peak level (Senarath et al., 2000; Gao et al., 2010), as soil moisture controls the partitioning of precipitation into infiltration and surface runoff, thus influencing the amount of storage and flow path to the river (Bindlish et al., 2009; Lacava et al., 2010), while snowpack amount affects the spring-time release of water due to snow melt (Thirel et al., 2011).

It is difficult to estimate the soil moisture from ground-based measurements across the catchment because of high spatial variability (Brocca et al., 2010a). Remote sensing provides an alternative approach to estimating the soil moisture content, which can then be used to constrain land surface and hydrological model predictions (Owe and de Jeu, 2001). However, it only gives an estimate of the top few centimetres at most with a temporal repeat every two to three days (Brocca et al., 2010b; Dharssi et al., 2011). Similarly, satellite remote sensing of the snow water equivalent or snow coverage has proved promising for determining areal snow pack water storage (Tsutsui et al., 2006). Given the essential role of initial soil moisture and snow conditions of a catchment for flood prediction, the improvement in flow predictions that might be possible through the use of such data has to be investigated. It is also essential to evaluate remote sensing estimations prior to the application in the hydrological modelling.

1.2 Research Objective

The aim of this research is to determine the possible skill improvement in the current operational flood modelling system in Australia, by constraining the antecedent soil moisture state of the continuous hydrologic model with satellite observations. Additionally, the research investigates the uncertainties in numerical weather prediction forecasts of precipitation, and thus their utility for application in hydrological prediction models. This work uses rainfall and soil moisture observational data from the OzNet monitoring stations in the Murrumbidgee catchment of south-eastern Australia (Smith et al., 2012), snow cover data from the MOD-MADI product (Bormann et al., 2012), soil moisture data from the Soil Moisture and Ocean Salinity (SMOS; Kerr et al., 2001 ; Kerr et al., 2010) satellite mission, real-time observational rainfall data from the Australian Bureau of Meteorology (BoM), rainfall observations from the Yarrawonga weather radar, rainfall forecasts from the Australian Community Climate Earth-System Simulator (ACCESS; BoM, 2010), real-time streamflow observations from the New South Wales office of Water (http://www.water.nsw.gov.au/realtime-data/default.aspx), and potential evapotranspiration data from Australian Water Availability Project data set (AWAP; Raupach *et al*., 2009). These data are used to evaluate the proposed algorithm for streamflow modelling in the Murrumbidgee study area.

The specific objectives to be addressed by this study are:

- Investigating the importance of snow in steamflow modelling of the chosen study area.
- Evaluation of forecast rainfall from Australian forecast system product against gauge-based and weather radar rainfall data.
- Understanding the impact of soil moisture on streamflow prediction skill when used in the hydrological model calibration stage.
- Evaluation of estimated satellite-based root-zone soil moisture as compared to in-situ observations.
- Assessment of in-situ/satellite soil moisture observation impact on the streamflow prediction skill.
- Assessment of satellite-based soil moisture estimates impact on the streamflow forecast skill.

1.3 Outline of Approach

The objectives of this research are addressed through several stages. The schematic of the overall thesis approach is presented in Figure 1.1. As an initial step, the impact of snow on the runoff generation in the Murrumbidgee catchment is investigated to understand the contribution of snow melt in the streamflow generation of the study catchment. The next steps are delineation of the study area, considering all modelling limitation such as dams and regulated areas, and available monitoring stations for application in the research.

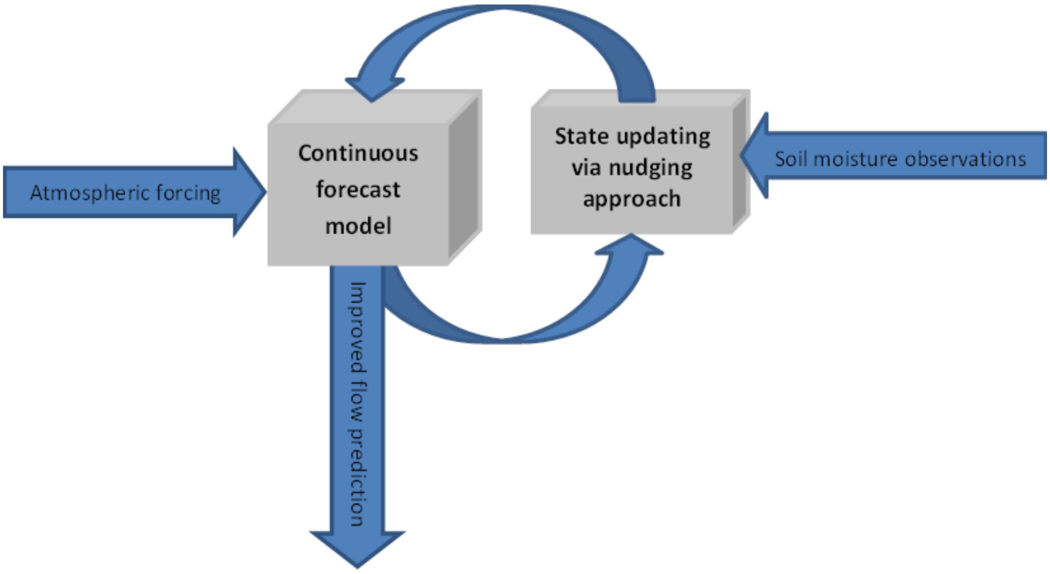

Figure 1.1: The schematic of the overall thesis approach.

Forecast precipitation from ACCESS-A NWP model and Yarrawonga radar observations are evaluated through a comparison against OzNet gauge observations for specific points and at various lead times. This is then followed by an assessment of the forecast precipitation against radar observations over the radar coverage area. For this task, radar rainfall data are calibrated to the OzNet rain gauge observations.

Next, two rainfall-runoff models have been selected based on i) the available models in the modelling toolkit developed for operational flood forecasting in the BoM, ii) the aims for using soil moisture observations, and iii) availability of the input data required for the models. These models are calibrated with rainfall data from the BoM real-time rain gauge network for the whole area, and rainfall observations from OzNet monitoring stations in two subcatchments (Upper Kyeamba and Adelong Creek) where such rain gauges were available. This enables the uncertainties in the sparse real-time rain gauge network data set to be accounted for. Two separate calibration procedures have been conducted: a) calibration to streamflow alone, and b) calibration to both streamflow and soil moisture observations. This allowed the additional streamflow forecast skill from constraint to soil moisture observations to be evaluated for the test catchment.

The next step is to investigate the effect of including remote sensing soil moisture observation data in the streamflow prediction models for the whole study area. As the models that have been used in this research have a single soil moisture storage, the entire root-zone moisture needs to be updated in the model. Therefore, empirical approximation of root-zone soil moisture from the near-surface satellite data is used prior to application in streamflow prediction model. In addition, soil moisture predictions in the models have been separately updated using root-zone soil moisture estimate from in-situ soil moisture monitoring station data for the two subcatchments where it was available. This gave important insight into the streamflow skill improvement that could be gained from constraint to satellite soil moisture data. In this research, a nudging approach is used for the state updating as the hydrologic models chosen from the operational flood forecasting toolkit have only a single layer, and therefore the benefit of more complex approaches that allow propagation of corrections to unobserved soil layers is not warranted, given the crude assumptions typically made in defining the weighting factors used for taking into account observation and model errors.

Finally, there is an application of SMOS soil moisture and forecast rainfall data area to real-time streamflow forecasting in the whole study area, with the aim of demonstrating the proposed approach at the city of Wagga Wagga, which suffered from several significant flood events during the study period.

1.4 Thesis Organization

This thesis is divided into seven chapters. **Chapter 2** presents an extensive review of the literature supporting this thesis and the existing data assimilation methods. **Chapter 3** makes the assessment of rainfall forecast from the ACCESS-A numerical weather prediction model against OzNet rain gauge sites and Yarrawonga weather radar data. **Chapter 4** describes the calibration results using streamflow observations alone, and the combined constraint to root zone soil moisture and streamflow. The soil moisture assimilation experiments are then presented using the in-situ data and the SMOS data in **Chapter 5**. This is followed by an application of SMOS soil moisture and ACCESS-A rainfall forecasts in a real-time condition in **Chapter 6**. Conclusions of the research and recommendations for the future work are given in **Chapter 7**.

Some parts of the thesis are based on the following publications:

- Shahrban, M., Walker, J.P., Wang, Q.J. Seed, A., Steinle, P. 2016. An evaluation of numerical weather prediction based rainfall forecasts, Hydrological Sciences Journal, 61, 2704-2717.
- Shahrban, M., Walker, J.P., Wang, Q.J. Robertson, D.E. 2015. On the importance of soil moisture in calibration of rainfall-runoff modelling: Two case studies, submitted to Hydrological Processes Journal, Under review.
- Shahrban, M., Walker, J.P., Wang, Q.J. 2015. Application of satellite-based soil moisture estimation to streamflow prediction in the Murrumbidgee catchment, In preparation.
- Shahrban, M., Walker, J.P., Wang, Q.J. 2015. Application of satellite-based soil moisture estimations to real-time streamflow forecasting in the Murrumbidgee catchment, In preparation.
- Shahrban, M., Walker, J.P., Wang, Q.J. Seed, A., Steinle, P. 2011. Comparison of weather radar, numerical weather prediction and gauge-based rainfall estimates. MODSIM, 19th International Congress on Modelling and Simulation, Modelling and Simulation Society of Australia and New Zealand, Perth, Australia, 3384-3390.

Chapter 2

Literature Review

This chapter presents an overview of rainfall-runoff models used for hydrological predictions and the importance of precipitation. It also presents the importance of hydrological model initialisation, and data assimilation methods used by flood forecasting models. Consequently, different types of rainfall-runoff models and their application especially in Australian catchments are described. In addition, the methods used for evaluation of precipitation are investigated, with an emphasis given to forecast precipitation data. The methods used for soil moisture estimation and the current status of assimilation of discharge, soil moisture or snow observations into hydrological models are also reviewed. Based on the key findings in literature, an algorithm for streamflow forecasting is proposed to address the objectives of this thesis.

2.1 Background

Hydrological models developed as far back as the 1960's have been trying to simulate the process of transforming of rainfall into streamflow using three main steps: i) hillslope runoff by rainfall-runoff models, ii) translation from the hillslope to the streams by catchment routing models , and iii) translation along the stream by channel routing models (Kokkonen et al., 2001). Rainfall-runoff models are the mathematical algorithm used to describe the partitioning of precipitation into runoff, evaporation, changes in soil moisture and its lateral movement out of the catchment via catchment routing models. Such models simulate the transport of water from the hillslope to the stream via surface and sub-surface flow paths, while channel routing models convey the flows through the channel network to the catchment outlet (Linsley, 1982). Although rainfall-runoff models are extensively used in streamflow prediction, the performance depends on factors such as the accuracy of the rainfall input and initial land surface conditions prior to an event.

Soil moisture plays a major role in the hydrological behaviour of a catchment, particularly for operational flood modelling, as it is a key variable that controls transformation of rainfall into infiltration or runoff (Wagner et al., 2007). Snow is also an important component as the snow packs can store a huge quantity of water in the winter time that may be quickly released in the spring time, and hence significantly affecting the amount of streamflow in a catchment. One examples of such an event is the Mississippi River floods in April and May 2011, which were among the largest and most damaging recorded in the U.S (Jung et al., 2012). This occurred when two major rainfall events were combined with the springtime snowmelt. A better estimation of initial state variables such as soil moisture and snow in the catchment is therefore expected to lead to more accurate simulation of the rainfall-runoff process. Consequently, to have a good prediction of flow, there is a need to have an accurate estimation of the initial land surface condition of a catchment prior to the event. Hydrological data assimilation, a method that combines observations and model estimations to update the model predictions, has been the most common approach used to reduce the uncertainty of the model states (Vrugt et al., 2005) .

Importantly, the accuracy of hydrological models is strongly dependent on precipitation input data. Observed precipitation information, known as quantitative precipitation estimation (QPE), can be derived from gauge networks, weather radars or satellite images, and plays an important role in now- and hindcasting of catchment runoff (Gourley and Vieux, 2005). Rain gauge networks are the most common and reliable source of observational data on precipitation. However, rain gauges are usually spatially limited, with interpolation commonly required. Therefore the uncertainty of derived precipitation estimates increased with distance between the gauges. In contrast, weather radars present the opportunity to measure precipitation data with good spatial and temporal resolution. However, weather radars require continuous calibration using a gauge network due to variations in raindrop size (Harrison et al., 2000). Furthermore, the accuracy of the rainfall estimate declines with distance from the radar, because the radar scans are too high to see low-level precipitation at far range (Smith et al., 1996). Given that precipitation is highly variable in space and time and weather radar coverage is limited, satellite-based rainfall information can overcome some of the deficiencies of conventional gauge and radar measurements (Behrangi et al., 2014). However, independent verification of satellite-based data against gauges or radar estimations is required before the application in hydrological modelling (Kidd and Levizzani, 2011).

In order to predict future estimates of streamflow, it is necessary to rely upon precipitation forecasts. Such precipitation information, known as quantitative precipitation forecasts (QPFs), can come in various forms, including deterministic and probabilistic. Numerical Weather Prediction (NWP) models have been used since the 1940's to provide forecast precipitation and other atmospheric variables (Muluye, 2011). They are based on mathematical models of the atmosphere and oceans and can predict the precipitation based on current weather conditions. However, forecasting of precipitation is challenging because such a variable is discontinuous and varies rapidly in space and time (Shrestha et al., 2013). Nonetheless , the NWP models are becoming increasingly more accurate at predicting precipitation with lead times of 2-10 days ahead, making it an important source of precipitation data for short to medium term flood forecasting (Cuo et al., 2011).

2.2 Hydrological Models

The models available for hydrological prediction range from simple conceptual lumped models to comprehensive physically based distributed models. Lumped modelling uses an integrated description of parameters over the entire catchment as a single area, while distributed models break the watershed down into many small subareas based on a grid or physical characteristics. Conceptual models are the most effective in flood forecasting systems but represent the major physical processes of the hydrologic cycles in a simplistic way (Aubert et al., 2003). They consist of storages with parameters controlling store sizes and rate of the outflows. Most conceptual models can be used on the basis of event-based simulation or continuous simulation. An event-based model estimates the runoff from an individual storm, while continuous models which include more hydrological process allow for simulation of both rainfall events and interstorm conditions.

During the past 50 years, many lumped models have been developed, including the Soil Moisture Accounting Runoff model (SMAR; O'Connell et al., 1970), Sacramento Soil Moisture Accounting model (SAC-SMA; Burnash et al., 1973), Simplified HYDROLOG model (SimHYD; Chiew and Siriwardena, 2005), Génie Rural 4 paramètres Journalier (GR4J; Perrin et al., 2003), Génie Rural avec simulation de l'HUMidité (GRHUM; Loumagne et al., 1996), Probability Distributed Model (PDM; Moore, 2007), and Time-area Topographic Extension (TATE; Calver, 1996), Identification of unit Hydrographs and Component flows from Rainfall, Evaporation and Streamflow data (IHACRES; Jakeman et al., 1990). During the past decade, some researchers have focused on developing distributed models such as Hydrologiska Byrans Vattenavdelning (HBV; Lindström, 1997), Soil and Water Assessment Tool (SWAT; Arnold et al., 1998), MIKE System Hydrologique European (MIKE-SHE; DHI, 2000), TopNet (Bandaragoda et al., 2004) and TOPographic Kinematic APproximation, Integration (TOPKAPI; Ciarapica and Todini, 2002), and LISFLOOD (Thielen et al., 2008). Operational flood forecasting within the Australian Bureau of Meteorology (BoM) has been based on the Unified River Basin Simulator (URBS; Carroll, 1994), which is a semi-distributed conceptual rainfall-runoff and routing model. URBS is an event-based model, using a “best-guess” approach for estimation of initial losses and forecast precipitation data. There have been some recent developments in the BoM modelling, with continuous modelling of catchments over Australia being introduced using a Short-Term Water Information Forecasting Tool (SWIFT; Pagano et al., 2010). This tool is a collection of rainfall-runoff models and utilities aimed for operational applications in the flood forecasting system of Australia.

While hydrologic models are used extensively in the simulation of catchments, the performance of the models is highly dependent on the model structure, parameter values (Moradkhani et al., 2005), forcing data, and the initial conditions (Grayson and Blöschl, 2000). During the past decades, many researchers have focused on comparing streamflow modelling results from a wide range of rainfall-runoff models with different structures, and some efforts have been undertaken to adopt a calibration procedure for parameter estimation of models (Conti et al., 2002; Kay et al., 2006; Goswami and O'Connor, 2007; Gibbs et al., 2008; Zakermoshfegh et al., 2008; Abushandi and Merkel, 2011; Dakhlaoui et al., 2012). For example , Kay et al. (2006) compared three different approaches to the spatial generalization of parameters in two continuous rainfall–runoff models, PDM and TATE to obtain best performance of the models for use in flood frequency estimation. Abushandi and Merkel (2011) calibrated and applied the metric conceptual IHACRES model to the Wadi Dhuliel arid catchment in north-east Jordan. Based on their results, the best performance of the IHACRES model on a daily basis was poor, but the performance on storm events scale showed a good agreement between observed and simulated streamflow.

In addition, Dakhlaoui et al. (2012) adopted three efficiency-improving techniques including i) estimation of the objective function by *K*-Nearest Neighbour (KNN) method, ii) parameter space transformation, and iii) modification of SCE-UA (Shuffled Complex Evolution developed at the University of Arizona) to improve the efficiency of the SCE-UA optimisation method for calibration of the HBV model. They showed that the differences between the techniques were not detectable on the basis of objective function and parameters sample distributions. However, the implementation of the KNN technique improved the efficiency from 25% to 50% compared to the initial SCE-U, that logarithmic transformation of the HBV leads to 20% improvement of the convergence speed, and the modification of the SCE-UA algorithm made an improvement of the convergence speed of about 30%.

Limited attempt has been made to take the advantage of soil moisture observations in calibration of models. For example, Parajka et al. (2009) used both runoff and satellite-based top soil moisture data in Austria to calibrate the HBV model by minimizing a multi-objective function, and showed that use of both runoff and soil moisture data for model calibration provided more robust parameters than using either of these observational data in calibration. In Europe, Wanders et al. (2014a) utilised satellite soil moisture data from AMSR-E, ASCAT and SMOS to calibrate LISFLOOD physically-based model using a dual EnKF approach and demonstrated that the calibration to both discharge and soil moisture data resulted in a reduction by 10-30% in RMSE for discharge simulations. Silvestro et al (2015) used soil moisture data from European Organisation for the Exploitation of Meteorological Satellites (EUMETSAT) in Italy to calibrate Continuum distributed hydrological model and found that use of both ground-based and satellite data additionally constrained the independent parameters in the calibration process and improved the model predictions. In addition, Sutadujaja et al. (2014) explored the use of discharge observations and SCAT/ERS data for calibration of a coupled groundwater-land surface model and found that the joint calibration was successful in discharge, soil moisture and groundwater head estimations with acceptable accuracy.

There are only a small number of studies specific to Australia. Chiew et al. (1993) compared 5 different models including simple and complex conceptual rainfall-runoff models in 8 catchments in Australia and concluded that a complex conceptual model (MODHYDROLOG; Chiew and McMahon, 1991) was the best for simulating high and low daily flows, while a simple model (SFB; Boughton,1984) was adequate for estimating monthly and annual flows in wetter catchments. Some studies have focused on the impact of rainfall accuracy on flow predictions in Australian catchments. For example, Vaze et al. (2011) investigated improvement in performance of 4 different conceptual rainfall runoff models, with improved spatial representation of rainfall in 240 catchments across Australia.

Some other studies have taken the benefit of different type of observations such as evapotranspiration or leaf area index in Australia. Zhang et al. (2009) have investigated the use of a MODerate-resolution Imaging Spectrometer (MODIS) remote sensing evapotranspiration product in a modified SimHYD model, a daily conceptual rainfall-runoff model, for a test catchment in southeast Australia. They have shown that SimHYD calibration against both observed streamflow and evapotranspiration provided a better prediction of streamflow compared to calibration against the observed streamflow data alone. They also showed that runoff simulations were further improved for the modified SimHYD model that used the MODIS leaf area index (LAI) data directly. They indicated that it is likely that the use of other remotely sensed data, such as soil moisture, will further improve the prediction of runoff in ungauged catchments providing the rainfall-runoff models are modified to use remotely sensed data directly. Zhang et al. (2011) investigated the effect of incorporation of NOAA LAI time series data and land cover types into a modified SimHYD model with daily runoff estimation for ungauged catchments and daily soil moisture estimation for gauged and ungauged catchments in 470 catchments in Australia. Their modelling results indicated that the daily runoff series and total runoff volume modelled by the modified SimHYD model were similar or only very marginally better than those simulated by the original SimHYD model. However, the modified model simulated soil moisture noticeably better than the original model for both gauged and ungauged catchments.

The studies mentioned above, have mainly focused on the effect of model structure or parameter estimation and forcing data, on hydrological modelling. Limited effort has been made to account for impact of soil moisture storage estimation accuracy in the models through calibration and validation procedures. It should be noted that the accurate representation of soil moisture in such models offers the opportunities for data assimilation, which has been demonstrated in recent years to yield the best estimate of soil moisture states in land surface models. The success of data assimilation relies on accurate model state prediction, which is largely dependent on the accuracy of parameter estimation.

2.3 Importance of Precipitation

Major floods typically occur as a result of extreme precipitation events, meaning that flood forecasting is very dependent on the accuracy of precipitation input , which is a highly stochastic phenomenon (Thirel et al., 2010a). In many instances, input precipitation uncertainty outweighs hydrological model uncertainty (Krzysztofowicz, 1999). For years, researchers have produced QPEs for use in streamflow prediction, by spatially interpolating gauge rainfall, but the accuracy of this estimation decreases with distance between the gauges. By contrast, weather radar and satellite precipitation has the potential to provide much better spatial characterisation of precipitation, but the accuracy of these measurements needs to be evaluated against ground-based observations. Kim et al. (2008) concluded that conditional merging of gauge and weather radar rainfall can best represent the spatial and temporal characteristics of rainfall and thus improve flood estimations, but this only provides rainfall input up to near real time and not into the future. Tramblay et al. (2011) used uniform and spatial rainfall data derived from rain gauge and radar for an event-based rainfall-runoff model. They showed that on average use of spatial rainfall data increased Nash-Sutcliffe Efficiency (NSE) coefficient of streamflow modelling from 0.77 to 0.86 for gauge-based data, and from 0.76 to 0.81 for radar data.

For hydrologic forecasting, a Quantitative Precipitation Forecast (QPF) from Numerical Weather Prediction (NWP) models remains the primary source of rainfall data for input into hydrologic forecasting models, other than a forecaster's intuition. However, the performance of flood forecasts from such hydrological models is highly dependent on the accuracy of the rainfall distribution. While a large number of studies have assessed NWP precipitation forecasts, most of the long-term evaluations have relied upon observations from rain gauges. For example, Damrath et al. (2000) evaluated the QPF from the German Weather Service (DWD) using long-time verification statistics against 240 gauge stations over seven years in Germany and Switzerland, including the Frequency Bias Index (FBI) and the True Skill Statistics (TSS), and presented examples of application to flood events. They identified a problem in the parameterisation of convective precipitation, which was expected to lead to comparatively poor QPF input to hydrologic models in the case of summertime flash floods. Moreover, Clark and Hay (2004) examined forty years of 8 day ahead precipitation forecasts from the National Centres for Environmental Prediction (NCEP) against a dense gauge network in the US and showed that there were systematic precipitation biases exceeding 100% of the mean.

A small number of studies have used gauge observations for evaluation of the forecasts for individual events. Richard et al. (2003) assessed precipitation output from four different forecasting models including the global model (GM), Europa-Modell (EM), the Deutschland-Modell (DM) and Lokal-Modell (LM) against a high-density gauge station network for several events in Italy and Germany on an hourly and a daily basis. They showed that all models were able to produce the occurrence of the events, but the amount of forecast was poorly predicted with no specific trend in over- or under-estimation. They also indicated that with the high-resolution DM and LM, specific patterns of the precipitation field could be simulated well. More recently, Roberts et al. (2009) showed improved forecast performance from the Met Office Unified Model (UM) for an event in 2005 in the north-west of England when using the model with 1 and 4 km resolution, compared to the forecasts with 12 km resolution. In this work, the 12 km model had 30-50% underestimation over the highest areas, while the 4 km model had 20% underestimation to 50% overestimation, and the 1 km model overestimated the rain from 10 to 50% compared with 24 hour accumulations from rain gauges over the area.

There are only a few studies that have assessed the forecast precipitation in Australia. McBride and Ebert (2000) verified 24-hour precipitation forecasts from 7 NWP models including Global Assimilation and Prediction System (GASP) and Limited Area and Prediction System (LAPS) against an 1° resolution operational daily rainfall analysis for 12 months in Australia. They used categorical scores including bias score, probability of detection and false alarm ratio, and showed that the models overestimated rainfall in summer and underestimated it in winter. Ebert et al. (2003) reported the Working Group of Numerical Experimentation (WGNE) assessment of 24-hour precipitation forecasts from several NWP models against gridded rain gauge analysis with 1° resolution from 1997 to 2000 in different areas including Australia. They presented the bias as the ratio of the frequency of the forecast rain to the frequency of observed rain and showed that the Australian models consistently overestimated rain frequency in south-eastern Australia. Shrestha et al. (2013) evaluated the quality of four NWP models from the Australian Community Climate Earth-System Simulator (ACCESS) including ACCESS-VT (Victoria-Tasmania region), ACCESS-R (Regional model), ACCESS-A (Australian domain) and ACCESS-G (Global domain) against rain gauges from 31 March 2010 to 30 March 2011. This evaluation was at point and catchment scale in the Ovens catchment, located in south-east Australia. They showed that the skill of the models varied across the gauges and with forecast lead time. They also showed that the ACCESS-VT and ACCESS-A models overestimated rainfall by up to 60% in low rainfall areas (low elevation) and underestimated rainfall by up to 30% in high rainfall areas (high elevation); ACCESS-R had a similar pattern but with much greater bias while ACCESS-G had a systematic bias with underestimation up to 70% across all stations and increasing with altitude.

Although gauge observations have been the most common benchmark used for assessment of model rainfall forecasts, they are based on point measurements which suffer from inaccuracies in spatial representation when used in verification of forecasts averaged over a large area (Tustison et al., 2001). Furthermore, a dense gauge network is usually required to achieve proper evaluation of forecast rainfall over an area, and there can be large discrepancies between rain gauge measurements even when co-located (Wood et al., 2000; Ciach, 2003). In contrast, weather radar provides an alternative means of determining QPE with a fine spatial and temporal resolution over a large area. Advances in radar technology and its processing have brought about opportunities for hydrological applications. For example, Bowler et al. (2006) developed a Short-Term Ensemble Prediction System (STEPS) for use in flash flood modelling through real-time correction of numerical weather prediction model forecasts using extrapolation-based radar nowcasts. Ebert et al. (2004) verified the performance of the short-term forecasts from the Forecast Demonstration Project (FDP) nowcast algorithms using radar reflectivity and rainfall analysis and a rain gauge network.

Because of its large spatial coverage relative to rain gauges, and area-averaged response, radar is a useful source of data for verification of QPF, provided that the errors in radar-based precipitation estimates are corrected. Radar is an active sensor that emits short pulses of microwave energy, and measures the power scattered back by raindrops as a reflectivity factor (Z). This reflectivity is then usually converted to a rain rate (R) through calibration of an empirical Z-R relationship such as

$$Z = aR^b, \tag{2.1}$$

where Z is radar reflectivity ($mm^6\,m^{-3}$), R is the rainfall rate (mm/h), and a and b are the radar parameters estimated using rain gauge observations. The Z-R relationship requires the specification of parameters a and b, which are functions of both radar and rainfall characteristics (Battan, 1973; Collier, 1989; Rinehart, 1991). Alfieri et al. (2010) tried to produce an accurate radar-based estimate of rainfall intensity by using different Z-R relationships derived from 1 to 24 hour calibration time windows, as well as event-based readjustment for 19 rain events in north-western Italy. They obtained the best performance from calibration windows of 2-5 hours, with the error 28% lower than calibration to the whole sample of the rainfall pairs which uses the climatological Z-R relationship. Chumchean et al. (2006) used an integrated method to correct the rainfall estimations from radar by removing the range-dependent bias from the radar reflectivities, using different Z-R relationships for different types of rainfall and removing the mean field bias from the radar rainfall estimates.

While there have been some efforts by researchers to use radar-based rainfall estimates for NWP forecast rainfall verification (Colle and Mass, 1996; Yu et al., 1998; Casati et al., 2004; Davis et al., 2006; Rezacova et al., 2007;

Roberts, 2008; Roberts and Lean, 2008), this approach has not yet been conducted for evaluation of forecasts from Australian models. In addition, radar-based verifications have been mostly used for specific events rather than long-time assessment. For example, Rezacova et al. (2007) applied the area-related RMSE (Root Mean Square Error) verification method for two local convective events in the Czech Republic using the Lokall Model of the COSMO consortium (LM COSMO) and adjusted radar data. This adjustment included combining daily radar precipitation with rain gauge data. The model RMSE ranged from 0 to 5.8 mm/h over the whole verification domain with averages of 0.9 and 0.7 mm/h for the first and second event respectively compared with adjusted radar precipitation.

While traditional methods of statistics are useful for indicating the overall performance of model predictions in each grid , especially over a long period, new methods have been used recently for spatial verifications. These new methods are especially useful in representing the skill of mesoscale forecasts or event-based evaluations. Ebert and McBride (2000), Marzban and Sandgathe (2006) and Davis et al. (2006) developed object-based techniques that associate the error to the displacement, intensity, and structure of precipitation forecasts. These methods indicate an approach for correcting the forecast of specific events by verifying to what extent the forecast matches the observed location, shape and magnitude. However, these objective methods require sufficiently skilful forecast, such that the corresponding observed and forecast objects can be matched. Ebert and McBride (2000) applied this objective-based method using 24-hour forecast from the LAPS NWP model over a four-year period in Australia, but against operational daily rain analysis.

There is also a wide range of neighbourhood verifications (Fuzzy methods) looking for approximate agreement between the model and observation within different time and/or space windows (Casati et al., 2004; Ebert, 2008; Roberts and Lean, 2008). For example, Casati et al. (2004) used an intensity-scale approach to evaluate the NIMROD forecast skill against radar data analysis for six events in the UK as a function of precipitation intensity and spatial scale of the error. These methods provide the temporal or spatial scale at which the forecasts reach a specific accuracy. Moreover, Roberts and Lean (2008) introduced and applied the Fractions Skill Score (FSS) method to compare the forecast rainfall from the Met Office Unified Model (UM) and radar rain fractional occurrences of exceeding a given threshold. Roberts (2008) used spatial and temporal verification with the FSS to compare operational forecasts from the Met Office UM in the UK (grid spacing of 12 km) with radar observations for the whole 2003. They found that the smallest useful scale for the very-localized rain for a 0-1 hour was around 140 km and for 2-24 hour was 230 km, while for widespread rain the smallest useful scale was around 40 km for 0-1 hour increasing to 85 km for 2-24 hour lead times. Methods such as upscaling (Weygandt et al., 2004; Yates et al., 2006), multi-event contingency table (Atger, 2001) and Fuzzy logic (Damrath, 2004) are other approaches defined for fuzzy verifications. Importantly, it was found that the neighbour method may not indicate perfect performance when applied to a perfect forecast, due to the influence of nearby pixels.

2.4 Remote Sensing of Soil Moisture

Soil moisture is a key hydrological state variable that plays an essential role in the exchange of energy and water within the soil-vegetation-atmosphere continuum (Chen et al., 2011). Correct initialisation of soil moisture states in hydrological models are expected to yield improved flood predictions within the models. The observations used for estimation of initial soil water content range from direct ground-based measurement of soil moisture to indirectly measured data such as backscattered and emitted microwave radiances through remote sensing technology. The ground-based measurements include both surface and root-zone soil moisture observations. However, these measurements are not widely available and such point-based measurements do not represent the high spatial and temporal variation in soil moisture (Engman, 1991). Many advances in remote sensing have provided a variety of opportunities for measuring soil moisture at regular time intervals over time and across large areas (Engman, 1990; Pratola et al., 2015).

Microwave remote sensing has been used as the most effective technique in characterizing near-surface soil moisture due to its all-weather capabilities and effective penetration depth at long wavelengths (Njoku and Entekhabi, 1996; Wagner et al., 1999; Wagner et al., 2007). The wavelength of electromagnetic energy in the microwave region is between 1 and 100 cm. For soil moisture retrieval, the most important bands have been X (wavelength λ = 2.5-3.8 cm), C (λ = 3.8-7.5 cm) and L (λ = 15-30 cm). Soil moisture is inferred from variation in the microwave observations caused by large differences in the dielectric constant of dry soil and water. The dielectric constant of water is 80, while it is only 3 for dry soil (Njoku and Entekhabi, 1996). An electromagnetic model, such as a radiative transfer model in the case of naturally emitted microwave energy, or a backscattering model in the case of transmitted-reflected microwave energy, is used to relate satellite observations to soil dielectric constant. A dielectric mixing model is then used to translate the dielectric constant value to soil moisture content.

The naturally emitted microwave energy approach is referred to as passive microwave (Njoku and Entekhabi, 1996), while the transmitted-reflected microwave energy approach is referred to as active microwave (Walker et al., 2004). Recently, ESA’s Water Cycle Multi-mission Observation Strategy and Climate Change Initiative (ESA CCI) has focused on creating a merged soil moisture product based on six active/passive microwave products including the first and second European Remote Sensing Satellites (ERS-1 and ERS-2), Meteorological Operational (MetOp) platform Advanced Scatterometer, the Scanning Multichannel Microwave Radiometer (SMMR), the Special Sensor Microwave Imager (SSM/I), the Tropical rainfall measuring mission Microwave Imager (TMI), Advanced Microwave Scanning Radiometer on Earth Observing System (AMSR-E), and Windsat radiometers (Liu et al., 2011; Wagner et al., 2012). ESA CCI aims to produce the most complete and consistent global soil moisture dataset based on active and passive microwave sensors. The first version of the product was released in June 2012 by the Vienna University of Technology, TUWIEN, covering the 32-year period from 1978 to 2010 and was extended to the end of 2013. Apart from the microwave sensors, other approaches such as optical or thermal infrared have been used but these are limited by the presence of cloud cover and the more tenuous relationship between the observed quantity (surface colour or temperature) and the soil moisture of interest. Consequently, only the microwave remote sensing products are described below.

2.4.1 Passive Microwave Remote Sensing

Passive microwave sensors measure the naturally emitted electromagnetic radiation, which is proportional to the product of the surface temperature and the surface emissivity (which in turn is affected by the soil dielectric constant), referred to as brightness temperature (Engman and Chauhan, 1995). Different microwave radiative transfer models are used to retrieve soil moisture from passive microwave brightness temperature (Owe et al., 2001; Njoku et al., 2003). For soil moisture retrieval, passive microwave remote sensing has been considered to be superior due to its ability to penetrate cloud, and the low sensitivity to land surface roughness, vegetation cover and topographic features (Walker et al., 2004). Despite its high sensitivity to near-surface soil moisture, current passive microwave systems have low spatial resolutions due to limitations on the maximum antenna size that can be operated in space.

Operational satellite-based passive microwave sensors have been available since 1978 including the Scanning Multichannel Microwave Radiometer (SMMR; Gloersen and Barath, 1977), the Special Sensor Microwave Imager (SSM/I; Jun et al., 2005), the microwave imager from Tropical Rainfall Measuring Mission (TRMM; Gao et al., 2006), the Advanced Microwave Scanning Radiometer on Earth Observing System (AMSR-E; Njoku et al., 2003), WindSat (Li and Gaiser, 2007), Soil Moisture and Ocean Salinity (SMOS; Kerr et al., 2001), and Soil Moiature Active Passive (SMAP; Entekhabi et al., 2010). However, only the SMOS and SMAP satellites were dedicated to the task of soil moisture remote sensing. SMMR measured radiation at five frequencies, from 6.63 GHz to 37 GHz. The instrument began transmitting data on October 1978 and was eventually deactivated in August 1987. The spatial resolution of SMMR was rather coarse (from approximately 25 km at 37 GHz to 150 km at 6.6 GHz). SSM/I is a seven-channel four-frequency passive microwave radiometric system launched on July 1987 and it is flown on board Defense Meteorological Satellite Program (DMSP). The instrument generates surface brightness temperature with a daily acquisition time at a spatial resolution of 25 km for lower frequencies (19.35, 22.235, 37.0 GHz) and 12.5 km for the higher frequency (85.5 GHz) (Robinson et al., 1992). TRMM is the first satellite Earth observation mission to monitor tropical rainfall which has been flying aboard the US DMSP satellites since November 1987. One of the primary sensors flying on TRMM is the TRMM Microwave Imager (TMI) operating at frequencies between 10.65 to 85.5 GHz from December 1997 to April 2015. TMI is a nine-channel radiometer and makes measurements of near-surface soil moisture at 25 to 50 km spatial resolutions with a revisit time of 1-3 days (Bindlish et al., 2003).

AMSR-E on the AQUA satellite provided a global soil moisture product with repeat coverage every 2 days or less. AMSR-E provided global soil moisture products at both C-band and X-band with frequencies of 6.9 and 10.7 GHz respectively. The data were reported on the 25 km Equal Area Scalable Earth (EASE) global grid spacing. The C-band observations are sensitive to soil moisture in the top ~1 cm of the Earth surface (Njoku et al., 2003) while the higher frequency X-band AMSR-E data has less penetration depth and are therefore considered to be less appropriate for soil moisture sensing. AMSR-E was launched in May 2002 and ceased operations on October 2011. It was replaced with AMSR2 in May 2012 (Wu et al., 2016). WindSat is a microwave radiometer flown on board of the Department of Defense Coriolis satellite. It was launched on January 2003 and comprises 22 channels operating at five frequencies ranging from 6.8 to 37.0 GHz (Li and Gaiser, 2007). The VUA-NASA (Vrije Universiteit Amsterdam and NASA) Land Parameter Retrieval Model (LPRM) software package has been used to retrieve soil moisture data from a wide range of X- and C-band passive systems including SMMR, AMSR-E, WindSat and TRMM (Owe et al., 2008).

Recently, the SMOS satellite of the European Space Agency (ESA) was launched in November 2009. SMOS is the first mission dedicated to soil moisture and measures near-surface (top 5 cm) soil moisture and ocean salinity. It is based on a Microwave Imaging Radiometer with Aperture Synthesis (MIRAS); a two-dimensional radiometer operating at L-band. SMOS provides global maps of soil moisture with a ground resolution of about 40 km and 3 days revisit time (Kerr et al., 2001; Kerr et al., 2010). The SMOS retrieval algorithm is designed to use SMOS Level 1c product which is processed maps of brightness temperature (TB). The main component of the SMOS Level 2 retrieval algorithm is the L-band Microwave Emission of the Biosphere (L-MEB) model which simulates the microwave emission at L-band from the soil-vegetation layer. The retrieval algorithm is based on minimizing a cost function which accounts for the squared weighted differences between measured and modelled TB data, for a collection of incidence angles. This is achieved by finding the best set of the parameters, e.g., soil moisture and vegetation characteristics (Panciera et al., 2009; Kerr et al., 2012). SMOS Level 3 and 4 products are the provision of the level 2 data and include the product from Center Aval de Traitemnet des Donnees SMOS (CATDS; http://www.catds.fr) and Centro de Producción de datos SMOS de niveles 3 y 4 (CP34; http://cp34-bec.cmima.csic.es/bec-officially-broadens-its-scope/#content). The Level 3 CATDS data are based on the best estimation of soil moisture when several multi-orbit retrievals are available for a given day and provide 1 day, 3 days and 10 days global maps of soil moisture values. The level 3/4 SMOS CP34 is designed and validated by the Barcelona Expert Centre (BEC). More recently, the National Aeronautics and Space Administration (NASA) has developed SMAP, the Soil Moisture Active Passive mission (Entekhabi et al., 2010) launched in January 2015. The SMAP soil moisture data have not been explained in details as they have become available recently and thus the data are not applicable in this research.

2.4.2 Active Microwave Remote Sensing

Active microwave remote sensors measure the electromagnetic radiation that is emitted toward the earth surface and then returned to the sensor, known as the backscatter radiation (Woodhouse, 2005). The magnitude of the backscatter coefficient obtained in active systems is related to soil moisture through the contrast of soil and water dielectric constants. The most common active microwave configurations are known as scatterometers and synthetic aperture radars (SAR). SAR is a coherent radar system, where high resolution images are generated from the backscatter signals using a synthetic antenna aperture, while a scatterometer is microwave radar sensor that measures the backscatter of the surface using real aperture. The sensitivity of the radar backscatter signal to soil moisture is significantly higher at lower frequencies, while at higher frequencies the signal is more sensitive to vegetation. However, the signal is heavily affected by surface roughness at all frequencies, making interpretation extremely difficult.

Soil moisture estimates using active microwave observations have been made from several space-borne systems, including the first and second European Remote Sensing SAR (ERS-1 and ERS-2; Wagner et al., 2007) of the European Space Agency (ESA), ESA’s ENVISAT (ERS-3) Advanced SAR (ASAR; Pathe et al., 2009), the Advanced Scatterometer (ASCAT) on the ESA’s meteorological operational (MetOp) platform, Canadian RADARSAT-1 (Mohamed Abou et al., 2012) and RADARSAT-2 (Cable et al., 2014), the Phased Array type SAR (PALSAR; Shimada et al., 2009) on the Japanese Advance Land Observing Satellite (ALOS), and German TerraSAR (Werninghaus and R. Buckreuss, 2010). The ERS-1 and ERS-2 were launched in 1991 and 1995 and were retired in 2000 and 2011 respectively. They carried an Active Microwave Instrument (AMI) which is a combination of a SAR and a Scatterometer. The AMI was a C-band radar (5.3 GHz) which has acquired data with a spatial resolution of 50 km at vertical polarization and a temporal resolution of 3-4 days. ASAR was launched in 2002, on board ENVISAT as the successor to ERS, and operates at C-band with five polarization modes (VV, HH, VV/HH, HV/HH, or VH/VV), a revisit time of 35 days and different spatial resolutions, a couple of meters in the image mode to 1 km in the global mode. In addition, ASCAT was launched on board the MetOp-A satellite in October 2006 as the successor instrument of ERS-1 and ERS-2. It operates in the C-band (5.3 GHz) in vertical polarization with a spatial resolution of 25 or 50 km (Wagner et al., 2007) and temporal resolution of 1-2 days. The TUWIEN change detection algorithm was used to estimate soil moisture from the ERS, ASCAT and ASAR data (Wagner et al., 1999; Bartalis et al., 2007).

RADARSAT-1 C-band SAR was launched in 1995 by the Canadian Space Agency. The sensor captured swaths of 45 to 500 km, with resolutions from 8 to 100 m. RADRASAT-1 had a repeat cycle of 24 days, but it covered the Arctic daily and most of Canada within three days. RADARSAT-2 was expanded on the RADARSAT-1 which was decommissioned in 2013. RADARSAT-2 has improved spatial resolution, more imaging modes and the ability to provide images either to the right or to the left of the satellite (Livingstone et al., 2006). Operational soil moisture products have been only obtained from ASCAT, ASAR, ERS-1 and ERS-2 instruments on global scales while other remote sensing soil moisture data from active systems such as RADARSAT-1/2 and PALSAR have been available for local applications. Recently, Sentinel-1 was launched on April 2014 as a part of the Global Monitoring for Environment and Security (GMES) program of ESA and the European Commission (EC). The mission is intended to provide a global near-real-time surface soil moisture retrieval service at 1 km resolution through the C-band SAR measurements (Hornacek et al., 2012).

2.4.3 Intercomparision Studies

Evaluation of satellite-based soil moisture products is needed to estimate the errors of the observations for optimal correction of state predictions in data assimilation within the hydrological models. Several studies have evaluated surface soil moisture products based on passive microwave sensors against in situ measurements and modelled data either on a regional scale, for example in the US (Al Bitar et al., 2012; Collow et al., 2012; Wagner et al., 2014), Europe

(Albergel et al., 2009; Brocca et al., 2011; Lacava et al., 2012; Griesfeller et al., 2016), Australia (Walker et al., 2004; Draper et al., 2009b; Mladenova et al., 2010; Doubková et al., 2012; Su et al., 2013; Yee, 2016), Africa (Gruhier et al., 2010; Louvet et al., 2015) and China (Jian et al., 2015) or at the global scale (Albergel et al., 2012; Albergel et al., 2013; Al-Yaari et al., 2014; Dorigo et al., 2015; Kim et al., 2015).

Specifically in Australia, Walker et al. (2004) evaluated backscattering data from C-band SAR instrument on board the ERS-2 satellite against field observations and predicted backscattering from several backscattering models. Draper et al. (2009b) compared VUA NASA AMSR-E near-surface soil moisture product to the in-situ observations from Murrumbidgee and Goulburn Monitoring Networks in southeast Australia. They showed that the AMSR-E soil moisture has a strong association to ground-based data, with correlations of greater than 0.8 and RMSD less than 0.03 m^3/m^3 when the satellite data were first filtered to reduce the noise using a 5-day moving average and then linearly rescaled to have the same mean and variance as the in-situ data. In addition, Mladenova et al. (2010) evaluated the spatial sensitivity of the ASAR surface soil moisture product developed from TUWIEN change detection algorithm against data from the National Airborne Field Experiment (NAFE) 2005 in southeast Australia. They showed the ASAR data had RMSD of 0.12 m^3/m^3 at 1 km resolution and it remained high up to 20-km resolution while it decreased to 0.07 m^3/m^3 at 25 km resolution. In addition, Doubkova et al. (2012) assessed directly estimated errors against the predicted errors calculated by ASAR Global Mode error estimate using independent top soil moisture from the grid-based landscape hydrological model (AWRA-L). Before the evaluation, the modelled data were rescaled to satellite data using linear rescaling method. They showed that both direct and predicted RMSD values are between 10% and 40% of saturated soil moisture and errors above 30% were mostly seen in steep slopes, rock outcrops and along the eastern coast.

Table 2.1: Comparison of major characteristics of passive and active microwave sensors.

Sensor	Satellite	Data availability	Spatial resolution	Revisit time (days)
Passive				
SMMR	Nimbus 7	1978-1987	25, 150 km	2-3
SMM/I	DMSP	1987-present	25, 12.5 km	1
TMI	TRMM	1997-present	25, 50 km	1-3
AMSR-E	Aqua	2002-2011	25 km	1-2
WindSat	Coriolis	2003-present	25, 50 km	1-2
MIRAS	SMOS	2009-present	40 km	1-3
AMSR2	GCOM-W1	2012-present	10, 25 km	1-2
Radiometer	SMAP	2015-present	40 km	1-3
Active				
SCAT	ERS-1/2	1991-2000 /1995-2011	25, 50 km	3-4
SAR	ERS-1/2	1991-2000 /1995-2011	6-30 m	35
SAR	RADARSAT-1/2	1995-2013 /2007-present	8-100 m	24
ASAR	ENVISAT	2002-2012	30-1000 m	35
PALSAR	ALOS-1/2	2006-2011 /2014-present	10-100 m	46
ASCAT	MetOp	2006-present	25, 50 km	1-2
SAR	TerraSAR	2007-present	5-150 m	11
SAR	Sentinel-1	2014-present	1 km	1-6

Recently, Su et al. (2013) showed that three soil moisture products from AMSR-E, ASCAT and SMOS in southeast Australia yielded correlations of 0.63-0.71 and a similar RMSD in the order of 0.1 m^3/m^3 against in-situ observations while after using three correction methods, minimum maximum correction, linear rescaling and CDF-matching, RMSD decreased to 0.04-0.06 m^3/m^3 and the CDF method produces only marginal further improvements to correlations (0.67-0.75) and RMSDs compared to the linear rescaling method. More recently, Yee (2016) evaluated AMSR2 Level 3 soil moisture products retrieved from the Japanese Aerospace exploration Agency (JAXA) and LPRM algorithm together with the SMOS Level 3 product against in-situ data in southeast Australia and found that in applications where information regarding the temporal variability of soil moisture is needed, X-band products of LPRM algorithm from evening observations were recommended (RMSD of 0.05-0.08 m^3/m^3), while both morning and evening retrievals from SMOS can be used to capture both temporal and absolute variability (RMSD of 0.06-0.08 m^3/m^3).

As a summary, major characteristics of the passive and active microwave sensors explained in sections 2.4.1 and 2.4.2 are compared in Table 2.1. As presented in Table 2.1, the active SAR systems have the capabilities to provide a much higher spatial resolution (~3 km or better). However, the measurements are confounded by the effect of surface roughness, topographic features and vegetation cover (Walker et al., 2004). In addition, they generally suffer from lower temporal resolution as compared to the passive sensors. As stated before, the highest sensitivity of microwave brightness temperatures to soil moisture is achieved at L-band and the signals become more dominated by vegetation characteristics at higher frequencies. The use of long-wave L-band also allows a larger penetration depth into the surface soil layer than shorter wavelengths. SMOS and SMAP are the first spaceborne missions specifically dedicated to soil moisture monitoring, operating at L-band frequencies. For the SMOS retrievals, vegetation and soil contributions to the signal can be easily separated, as MIRAS created images of any point of the surface at several angles. The SMAP soil moisture data cannot be used in this research as the satellite was launched in

January 2015 which is not within the focus study period of this research (2007-2012). In addition, the application of soil moisture data from some other satellites (e.g., SMMR, AMSR-E, AMSR2 and ERS-1/2) in this work is not also possible due to the unavailability of the data during the whole or part of the study period of this research. Consequently, for application of remote sensing soil moisture retrievals in catchments such as Murrumbidgee with some dense vegetation coverages, SMOS products are the most appropriate data to be used.

2.5 Hydrological Data Assimilation

Data assimilation techniques have the potential to combine the model predictions with observational data to obtain the best possible estimate of the current status of the hydrological system. Basically, there are four methods commonly used for model updating in data assimilation: input updating, parameter updating, error correction and state updating (Houser et al., 2012). The first category improves the model accuracy by improving the input to the model. Parameter updating adjusts the model parameters to better match the observed and predicted state values, while in error correction the deviation between modelled and observed output is used to forecast the future values of the errors by means of time series models like ARMA models. If the model suffers from a bad state initialization then the state of the model can be corrected using state updating so that the difference between the predicted and observed state is decreased. In this chapter, state updating has been fully discussed in the literature as one of the most effective approaches used in streamflow forecasting (Clark et al., 2008; Seo et al., 2009).

According to the choice of assimilation algorithm used, data assimilation can be classified as i) sequential (direct observer) such as direct insertion, statistical interpolation, nudging, Particle Filter (PF), Extended Kalman Filter (EKF) and Ensemble Kalman Filter (EnKF) and ii) variational (dynamic observer) such as adjoint method (Kalman, 1960; Talagrand, 1987). Figure 2.1 illustrates schematically the differences between sequential and variational approaches.

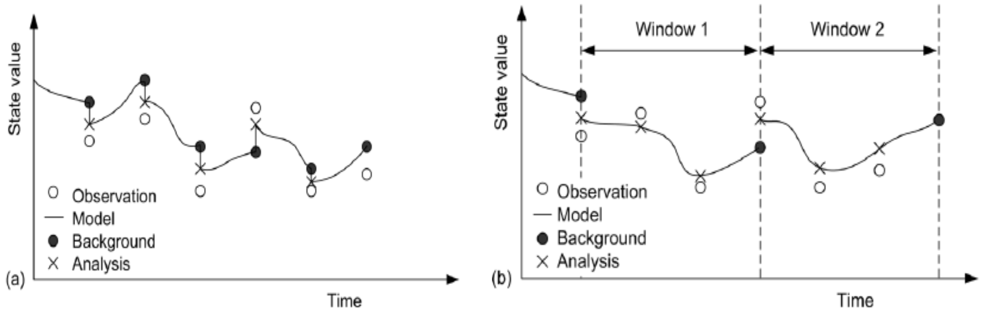

Figure 2.1: Schematic of sequential (a) and variational (b) data assimilation approaches (Houser et al., 2012).

The direct observer technique sequentially updates the model forecast, using the difference between observation and model prediction whenever an observation is available (Walker and Houser, 2005). The estimated state vector ($\hat{X}_k^a$) is known as analysis, indicated by superscript a, and calculated by (Nichols, 2003):

$$\hat{X}_k^a = X_k^b + K_k(Z_k - \hat{Z}_k), \tag{2.2}$$

where X_k^b is the model initial state or background indicated by superscript b, and subscript k refers to the time of the update. K is the weighting factor or gain given by:

$$K = BH^T\,(HBH^T + R)^{-1}, \tag{2.3}$$

where B and R are background and observation covariance matrices respectively, and H is the observation operator matrix.

The Kalman Filter is based on the assumption that the error terms are uncorrelated and have a Gaussian distribution. The family of Kalman filter approaches directly update the background covariance matrix to calculate the gain matrix in equation (2.3). In the standard Kalman filter (KF; Kalman, 1960) this is achieved by application of standard error propagation theory on a linear model used for forecasting the system state vector. The state covariance update is based on:

$$B^a = (I - KH)\,B^b\,(I - KH)^T + KRK^T\,, \tag{2.4}$$

where I is the identity matrix. The updated state covariance are then propagated by the model until the next update step by adding an error term Q to the model error covariance forecast as:

$$B_{k+1}^{b} = M_k B_k^{a} M_k^{T} + Q_k \,, \tag{2.5}$$

where M_k is the model operator matrix. The Kalman filter approach can be adapted for near-real-time application by running only the forward Kalman Filter loop. However, it can be computationally demanding unless simplifying assumptions are made, has only limited capability to deal with model errors, and the necessary linearization can lead to unstable solutions. The linearized version of the Kalman Filter is called the EKF, in which the forecast error covariance is calculated through a Taylor series linearization of the model (Plaza et al., 2012). In the EnKF (Evensen, 1994), the model error covariance is calculated using the information of an ensemble of model simulations. The EnKF has received significant attention in hydrological data assimilation since it is not limited by the need for a linearized model for the purpose of error estimation. Another form is the Ensemble Kalman Smoother (EnKS) where all model states are updated within a fixed lag of time (Evensen and van Leeuwen, 2000). The Ensemble Square Root Filter (EnSRF) was also introduced by Whitaker and Hamill (2002) which does not require observation perturbation which has the advantage of not needing observation perturbation, and thus eliminating the errors induced by sampling the observation in EnKF. In addition, PF, also known as sequential Monte Carlo (SMC) method, is a nonlinear non-Gaussian approach which adopts a set of randomly chosen states, often called particles, without any assumptions about the nature of the distributions.

The variational method uses all past and future observations over an assimilation window to estimate the unknown variables by repeatedly integrating forwards and backwards through the model (Walker and Houser, 2005; Lai et al., 2014), by minimizing over space and time an objective or penalty function J, including a background and observation penalty term, such a (Walker and Houser, 2005; Lai et al., 2014):

$$J = {}^{1}\!/_{2}\ (X_0 - X_0^b)^T {B_0^b}^{-1} (X_0 - X_0^b) + {}^{1}\!/_{2} \sum_{k=0}^{n-1} (Z_k - \hat{Z}_k)^T\, {R_k}^{-1}\, (Z_{k-} \hat{Z}_k)\,, \qquad (2.6)$$

where X_0^b and X_0 are the initial state vector before and after analysis, Z is observation and $\hat{Z}$ refers to model prediction, B_0^b and R are the background and observation covariance matrices respectively, the superscript b refers to the background estimate of the state vector, the subscript k refers to time, and n is the number of time steps. Variational methods use complex optimization algorithms that adjust initial state to obtain a good fit to observations (Talagrand, 1987). Use of the adjoint model for the inverse constraining needs an extensive programming effort and adds to the complexity of the method. Another alternative data assimilation method is Evolutionary Data Assimilation (EDA; Dumedah and Coulibaly, 2013) which uses multi-objective evolutionary strategy method to continuously evolve ensemble model states and parameter sets where it determines the model error and the penalty function for different assimilation time steps.

The selection of an appropriate data assimilation approach depends on the choice between computational efficiency, making the best use of available information, flexibility and robustness, and operational feasibility. The variational approaches and EDA method deal with more complexity compared to the filtering approaches. The PF updating is based on the particle weights instead of state variables (Liu and Gupta, 2007), which reduces numerical instability, especially in physically based or process-based models (Gordon et al., 1993; Arulampalam et al., 2002). Approaches like direct insertion, statistical interpolation, and nudging which are computationally efficient and easy to implement, do not account for observation uncertainty in estimating model background state uncertainty. In enhanced approaches such as EnKF, a correct estimation of forecast and observation error covariance is crucial for the high quality of data assimilation (Zheng, 2009). Unfortunately, it is difficult to have exact error estimations since the true states are never known (Sénégas et al., 2001) and thus tuning algorithms are usually required to compensate for the impact of the errors (Liang et al., 2012). Therefore, initial rigor of the use of formal uncertainty framework defined in sophisticated approaches is usually missed. Moreover, the power of complex approaches is to extend corrections from observations to unobserved states. However, since the current operational models typically have a single-layer corresponded to soil moisture state, complex data assimilation approaches are not warranted in operational systems. Consequently, given the significant challenges in tuning uncertainties, there is considerable value in assessing the use of more simplistic approaches for application in operational hydrological modelling and therefore, the nudging approach is selected to be used as the data assimilation technique in this research. In the context of streamflow forecasting, there are three main types of observation that can be used in an assimilation context: discharge assimilation, soil moisture assimilation and snow assimilation. These are discussed in the next sections.

2.5.1 Discharge Assimilation

Many researchers have investigated the application of discharge assimilation. This is not only the most commonly used approach to improving flood forecasting, but is also the oldest approach such as the study performed by Yang and Michel (2000). There are a few studies on error correction, where the predicted streamflow was corrected using observed discharge without changing the inputs, states, or parameters of the model (Shamseldin and O Connor, 2001; Anctil et al., 2003; Goswami et al., 2005; Pagano et al., 2011). For example, Goswami et al. (2005) compared the standard linear Auto-Regressive model, Neural Network Updating and Linear Transfer Function in the River Brosna catchment in Ireland. In relation to the peak flows and time to peak, none of the tested methods were suitable for correcting the streamflow in that study. Pagano et al. (2011) proposed a dual-pass method of error correction in the GR4J model for 330 Australian and 183 United States catchments and found that in most catchments, the use of the long-memory error-correction did not improve model performance significantly , while short-memory error correction was responsible for the vast majority of skill improvements seen.

The oldest approach has been to simply correct the trajectory of streamflow forecasts using the error correction method. However, there has been a much larger focus on state updating using the discharge observations, mostly with a particular focus on application of the EnKF (Vrugt et al., 2005; Pauwels and De Lannoy, 2006; Weerts and El Serafy, 2006; Clark et al., 2008; Komma et al., 2008; Pauwels and De Lannoy, 2009; Li et al., 2013). Komma et al. (2008) assimilated runoff observations to update soil moisture in the Kamp catchment in Austria using the Ensemble Kalman Filter (EnKF) in a semi distributed model. They showed that the peak flow errors decreased from 25% to 12% and 25% to 19% for 3 and 48 hour lead times respectively. Clark et al. (2008) demonstrated that application of EnKF for state updating was not appropriate for increasing the efficiency of the streamflow simulation in a distributed model, but found that using a variant of EnKF without observation perturbation through the EnSRF yielded an improvement in streamflow predictions. Pauwels and Lannoy (2006) synthetically assimilated observed discharge using the EnKF to correct model results obtained with erroneous initial conditions and strongly over- and underestimated precipitation data in a lumped water and energy balance model (TOPMODEL-Based Land-Atmosphere Transfer Scheme; TOPLATS). Their results suggested that the assimilation of observed discharge can correct erroneous model initial conditions and can also reduce the bias in the modelled turbulent fluxes when the precipitation used to force the model is underestimated, while the improvement in the modelled wetness conditions after data assimilation did not lead to a significant improvement in the modelled energy balance.

Furthermore, Li et al. (2011) showed that updating soil moisture states using EnKF in the Ovens catchment in Australia resulted in a poorer PDM model performance due to a lagged response in discharge, but also led to slower degradation of the forecast accuracy. Li et al. (2013) compared the EnKF with EnKS for discharge assimilation in the Ovens catchment in Australia using PDM and GR4J models to investigate the utility of an ensemble Kalman smoother (EnKS) for addressing the time-lag issue between soil moisture and discharge in EnKF. They showed that the EnKS was superior to the EnKF when only soil moisture was updated, while the EnKS and the EnKF have similar results when both soil moisture and routing storages are updated. This result suggests that the EnKS can better improve the streamflow forecasting for models that do not have storage-based routing schemes (e.g., unit-hydrograph-based routing). There are also implementations of EKF, such as Aubert et al. (2003), where they used EKF in the GR4J model and showed that assimilation of streamflow observations was effective for low flow predictions, while assimilation of both streamflow and soil moisture improved the entire forecasting period .

There are a limited number of studies that have tended to use other methods such as variational assimilation (Seo et al., 2003; Rüdiger, 2006; Seo et al., 2009) or EDA (Dumedah and Coulibaly, 2013). Seo et al. (2003; 2009) applied variational assimilation of streamflow, precipitation and potential evaporation into the SAC-SMA model in a lumped fashion for different basins in the US and found that this approach has better performance than assimilation based on just state space-based state updating. Rüdiger (2006) also investigated the improvement in soil moisture estimations by assimilating streamflow observations using the variational approach but in a land surface model. He found that assimilation of streamflow had a significant improvement in streamflow predictions after modifications to infiltration mechanism of the model and catchment disaggregation. In addition, Dumedah and Coulibaly (2013) incorporated EDA into the Soil and Water Assessment Tool (SWAT) to assimilate streamflow in the Spencer Creek watershed in southern Ontario, Canada. Their approach was based on updated model states and its parameterizations and the assimilation was determined by applying the penalty function to merge background information with perturbed observation data. Their results showed improvement in both streamflow and soil moisture estimates when compared to open-loop simulation.

The literature reviewed above demonstrates that there have been comprehensive studies on discharge assimilation during the past decade, with discharge assimilation for soil moisture state updating having an overall positive impact. However, discharge assimilation has not been implemented in operational forecasting applications due to the uncertainties resulting from the time lag between soil moisture and runoff at the catchment outlet.

2.5.2 Soil Moisture Assimilation

Data assimilation is one of the most commonly used approaches in recent years for incorporating observations into models to obtain the best estimate of the system. However, a number of issues arise when assimilating remote sensing observations into hydrological models, including the spatial scale mismatch between the satellite observations and model simulations. For example, passive microwave satellite soil moisture products, such as from AMSR-E and SMOS, have spatial resolution of around 50 km, whereas the hydrological models are often run at a much higher spatial resolution. Conversely, active sensors such as ASCAT and ERS-1/2 are capable of providing higher spatial resolution, but due to their sensitivity to surface roughness and vegetation canopy, lack the accuracy of passive microwave remotely sensed data. Many studies have investigated approaches to partition the coarse scale spatial observations to the fine scale model grid cells (Reichle et al., 2001; Bindlish and Barros, 2002; Kim and Barros, 2002; Chauhan et al., 2003; Merlin et al., 2008; Piles et al., 2011; Merlin et al., 2012; Piles et al., 2014; Wu et al., 2015). However, evaluation of the downscaling approaches against dense soil moisture observational networks and for different types of land use and vegetation cover is still required. The best practice approaches adopted for downscaling remote sensing data are based on a combination of passive microwave data with high spatial resolution active microwave data (Bindlish and Barros, 2002; Zhan et al., 2006) or optical data such as surface temperature and vegetation index (Chauhan et al., 2003; Merlin et al., 2012), and the use of topography and soil depth information (Pellenq et al., 2003).

A further issue on application of satellite observations in hydrological models is the vertical disagreement between the satellite observations and model predictions. Current remote sensing technology can only provide soil moisture data at the top 5 cm of the soil rather than the entire profile, while the moisture condition in both root-zone and subsurface layers is more critical for simulating hydrologic processes. Therefore, it is difficult to assimilate satellite data into hydrological or meteorological models (Brocca et al. 2010a, 2012a; Dharssi et al. 2011). Hence, filtering approaches, e.g., moving average filter (Draper et al., 2009b) and exponential filter (Wagner et al., 1999), have been used to smooth surface soil moisture and estimate profile soil moisture, prior the application within hydrological models (Scipal et al., 2008).

For example, Albergel et al. (2008) assessed application of the exponential filter to estimate profile soil moisture using both in-situ and modelled surface soil moisture from the Safran-Isba-Modcou (SIM) model in France. They found that overall the soil wetness indices derived from the surface soil moisture observations and simulations agree well with the reference root-zone soil moisture. Because of the limited sensing depth and temporal repeat, assimilation methods can be coupled with land surface models to estimate the profile soil moisture from the near-surface data (Entekhabi et al., 1994; Houser et al., 1998; Walker et al., 2001; Heathman et al., 2003; Merlin et al., 2006; Kumar et al., 2009; Draper et al., 2012; Plaza et al., 2012; Dumedah and Walker, 2014; Reichle et al., 2014; Yin et al., 2014; Dumedah et al., 2015). This approach has been mainly focused on estimating the soil moisture for weather forecasting and agricultural application rather than improving streamflow prediction.

Further, even though the temporal patterns are similar, there are often systematic differences between the observed and simulated soil moisture, as the models often differ from reality, with soil moisture being a “tuning” parameter, whereas remote sensing techniques seek to provide real soil moisture content. Many modelers have sought to overcome this shortcoming of their models by fudging the remotely sensed data to take on the dynamics of their model, rather than calibrate or fix their model (Draper et al., 2009a). Consequently, rescaling approaches such as minimum maximum correction (Su et al., 2013), linear rescaling (Draper et al., 2009b; Brocca et al., 2010b), linear regression correction (Jackson et al., 2010; Brocca et al., 2011), Cumulative Density Function (CDF) matching (Reichle and Koster, 2004; Drusch et al., 2005; Brocca et al., 2011), and triple collocation based method (Yilmaz and Crow, 2013; Chen et al., 2014) have been used.

In the minimum maximum correction method, the maximum and minimum values of in situ data are chosen to define the upper and lower values of satellite time series. In the linear rescaling approach, satellite time series are forced to have the same mean μ and standard deviation σ of the in situ or modelled time series. The linear regression method fits a linear equation to the satellite data by minimizing the difference between estimated satellite data and the in-situ measurements and in the CDF-matching, the satellite data is rescaled in a such way that its CDF matches the CDF of the reference data. The recent adoption of methods such as the CDF-matching, to make observations look like the deficient model, does not mean that the these are the only or accepted approach needed for pre-processing of all observational data. For example, Pauwels et al. (2015) showed this quite dramatically in a synthetic assimilation case, when assimilating a CDF-matched ground water storage to improve discharge.

There are a few studies which have been focused on application of in-situ soil moisture data in hydrological modelling (Aubert et al., 2003; Brocca et al., 2009b; Tramblay et al., 2010; Chen et al., 2011). Aubert et al. (2003) showed that assimilation of soil moisture using the EKF in GR4J improved flood events prediction, and dual assimilation of both streamflow and soil moisture provided more accurate prediction for the entire forecasting period. Brocca et al. (2009b) showed that assimilation of observed soil moisture into an event-based rainfall-runoff model improved runoff volume and peak discharge for 5 catchments in Central Italy. They estimated the relationship between the Soil Potential Maximum Retention parameter of the Soil Conservation Service-Curve Number (SCS-CN) and in-situ saturation degree to improve initial soil moisture estimation in the model. Similarly, Trembely et al. (2010) used this approach to estimate the Soil Potential Maximum Retention parameter of the SCS-CN in the Valescure catchment in southern France, focusing on assessment of initial soil moisture condition in the event-based modelling approach rather than assimilation of the soil moisture. Chen et al. (2011) assimilated in-situ soil moisture into the Soil and Water Assessment Tool (SWAT) model for the Cobb Creek watershed in Oklahoma using the EnKF and demonstrated that application of soil moisture observations had limited success in correcting the upper-layer soil moisture of the model, and was unsuccessful in updating the deep soil moisture and in improving streamflow prediction due to the lack of vertical soil water coupling in the model.

There are, however, some studies that have demonstrated the potential of satellite soil moisture observations to improve streamflow prediction. Pauwels et al. (2002) and Matgen et al. (2006) assimilated ERS-based soil moisture retrievals with high spatial resolution for streamflow forecasting. But the low revisit time (monthly scale) of these observations makes them unsuitable for operational hydrological modelling. Brocca et al. (2009a) used remotely sensed soil moisture measurements from the European Remote Sensing satellites (ERS), in upper Tiber river catchment in Central Italy, using the same approach as Brocca et al. (2009b) and Trembely et al. (2010). Beck et al. (2009) also used observations from Advanced Microwave Scanning Radiometer-EOS (AMSR-E) in 186 Australian catchments with the similar approach as Brocca et al. (2009a). In both studies performed by Brocca et al. (2009) and Beck et al. (2009) it was found that incorporation of the remote sensing data was quite effective in estimating the runoff. They found that incorporation of the remote sensing data was quite effective in estimating the runoff. Parajka et al. (2006) used ERS based data, but for calibration of a semi-distributed conceptual rainfall-runoff model (HBV; Lindstrom et al 1997) in Austria. They used an exponential filtering method to estimate root-zone soil moisture and found that data assimilation during the calibration phase improved the soil moisture estimations in gauged catchments without any significant decrease in the runoff model accuracy while it decreased the runoff prediction accuracy in ungauged catchments.

In addition, Crow and Ryu (2009) implemented a new sequential assimilation system to simultaneously update both internal soil moisture states and external rainfall input to the SAC-SMA model, using EnKS and EnKF. They showed that for a wide range of climatic conditions, the approach can enhance the value of remotely sensed soil moisture data for runoff prediction applications. Their study used synthetic data with the aim of verifying the results with real remotely sensed data. By using a simplified nudging scheme, Brocca et al. (2010b) investigated the impact of profile soil wetness assimilation from the Advanced SCATterometer (ASCAT) on flood estimation in a one-layer continuous rainfall-runoff model, MISDC (Modello Idrologico SemiDistribuito in Continuo) in five subcatchments in Central Italy. This model has two components. The first part is an external Soil Water Balance (SWB) model which simulates the saturation degree temporal pattern as the initial condition for the second component, which is an event-based model using SCS-CN method. They used the exponential filtering method based on the Albergel (2009) formulation to linearly rescaled the ASCAT based SWI to modelled saturation degree to estimate profile soil moisture, and showed that the rescaled SWI matched the range of variability of modelled data. Their results revealed that the Soil Wetness Index (SWI) derived from the ASCAT sensor can be adopted to improve the runoff predictions, mainly if the initial condition of the soil wetness is unknown.

Recently, Brocca et al. (2012) analysed the performance of a continuous two-layer rainfall-runoff model (MISDC-2L) using EnKF to assimilate both surface and root-zone products derived from the ASCAT in the Niccone catchment in Central Italy. The exponential filtering method was used in this work to infer the root-zone soil moisture data. They showed that assimilation of root-zone soil moisture provided a significant improvement in discharge modelling while assimilation of a surface product had only a small effect. Massari et al. (2014) introduced the Simplified Continuous Rainfall–Runoff model (SCRRM), which uses globally available soil moisture observations to identify the initial wetness condition in the model. They directly used ASCAT soil wetness index and normalised soil moisture data from AMSR-E and ECMWF products in the modelling over a catchment in Greece and found that the proposed modelling approach was suitable for runoff prediction in poorly gauged areas. Chen et al. (2014) assimilated satellite data from ASCAT and SMOS into SAC-SMA model over the central US using EnKF and EnKS and showed that soil moisture state correction was more efficient in improving the base flow component of streamflow while both the high and low-flow components of streamflow were improved when rainfall and soil moisture state corrections were combined. Wanders et al. (2014b) evaluated the value of assimilation of three soil moisture products; AMSR-E, ASCAT and SMOS; for the European Flood Awareness System (EFAS) using a distributed hydrological model (LISFLOOD) for flood predictions. Their results showed that the overall discharge forecast skill was improved, with a 10 % reduction in the MAE.

In addition, Ridler et al. (2014) found that assimilation of SMOS Level 3 CATDS data into integrated hydrological and soil-vegetation-atmosphere transfer (MIKE SHE SW-ET) model improved soil moisture simulations but had little impact on streamflow estimations. Alvarez-Garreton et al. (2014) assimilated the surface soil moisture and the soil wetness index derived from the AMSR-E in a lumped PDM model using EnKF. They used exponential filtering, linear regression and anomaly-based CDF-matching to scale satellite data to the model soil moisture predictions. They found that the ensemble mean of the root mean square difference between discharge predictions and the observations was reduced by 25% after assimilation, and even though there was improvement in streamflow prediction, the assimilation of soil moisture showed limited capability in error correction when there was a large bias in the peak flow prediction. More recently, Alvarez-Garreton et al. (2015) expanded the latter study by improving the representation of model error and correcting the soil moisture and streamflow biases using AMSR-E and ASCAT soil moisture data in a semi-distributed scheme. They demonstrated that the efficacy of soil moisture assimilation was enhanced when the spatial distribution in forcing data and routing processes are taken into account and adequately processed satellite soil moisture can reduce errors in the model soil moisture predictions. Lievens et al. (2015) showed that assimilation of SMOS Level 3 CATDS product with the mean bias correction improved soil moisture and runoff peaks simulated by Variable Infiltration Capacity (VIC) land surface model over the Murray Darling basin in Australia. Leroux et al. (2016) showed that assimilation of SMOS data into Distributed

Hydrology Soil Vegetation Model (DHSVM) reduced the errors due to the use of satellite precipitation data and improved the streamflow predictions.

In all studies above, sequential data assimilation has been used as the most effective approach. The number of studies that applied variational approaches is limited, due to the extensive computational effort required for them. For example, Rüdiger (2006) assimilated both streamflow and soil moisture data from AMSR-E into the catchment-based land surface model (CLSM) for streamflow forecasting purposes using the variational approach and the method resulted in a significant improvement of the streamflow, but soil moisture conditions in only 2 out of the 12 monitored subcatchments were improved. Some other studies have used the variational approach only for soil moisture retrieval in land surface models (Calvet et al., 1998; Reichle et al., 2000; Xiangjun et al., 2009; Li et al., 2010) without any focus on streamflow validation.

According to the literature reviewed above, research during the past decade has mainly been dedicated to the use of in-situ soil moisture measurements or synthetic experiments when applied in the context of streamlow modelling; other sources of soil moisture data have been more widely used in broader contexts. The limited application of soil moisture data from satellites in rainfall-runoff modelling is due in part to the mismatches between satellite data and hydrological models, including the difference in depth of satellite data (2-5 cm) and the model bulk storage. Recent studies have tended to demonstrate the value of real satellite data applications. Only a few studies (Brocca et al., 2010b; Brocca et al., 2012; Alvarez-Garreton et al., 2014; Wanders et al., 2014b; Alvarez-Garreton et al., 2015; Lievens et al., 2015) have demonstrated the potential improvement in streamflow prediction capability through better estimates of antecedent soil moisture condition. In particular, application of soil moisture in hydrological modelling of Australian catchments has received limited consideration in the literature. Furthermore, many of the previous studies did not have in-situ soil moisture observations available to assess why the assimilation of remote sensing data improved the modelling performance. Consequently, assimilation of remotely sensed soil moisture data still has huge challenges to be overcome in order to improve hydrological modelling, especially in Australia.

2.5.3 Snow Assimilation

Snow observations can be used for state updating of the models in two forms: Snow Water Equivalent (SWE) and Snow Covered Area (SCA). SCA provides information about the presence or absence of snow while SWE includes the depth of liquid water that would result from melting the snow. Snow height and water equivalent observations are available from meteorological stations, but these data are very dependent on the local conditions (wind, vegetation, slope, sun exposure) and cannot represent the accurate spatial variability of the snow cover (Thirel et al., 2013). Therefore, satellite observation of snow has become an important alternative source of data for hydrological process modelling, with observations usually available every one day to two days over large areas (Thirel et al., 2011).

SCA products are currently produced through optical remote sensing sensors with good spatial resolutions and retrieval frequency, such as the Advanced Very High Resolution Radiometer (AVHRR), Geostationary Operational Environmental Satellites (GOES) and MODIS (Hall et al., 2002; Maurer et al., 2003). The MODIS satellite sensors are particularly appealing due to their high temporal resolution of a day and relatively high spatial resolution of about 500 m. However , the optical sensors cannot see through the clouds leading to discontinuous snow cover data (Gao et al., 2010). To overcome this problem, techniques, such as use of cloud-free data from other days or from neighbouring pixels, can be applied (Parajka and Bloschl, 2008; Gafurov and Bardossy, 2009). In addition, optical sensors cannot provide any information about snow depth or SWE, which is most useful for hydrological applications. On the other hand, passive microwave remote sensing sensors, such as Advanced Microwave Scanning Radiometer-EOS (AMSR-E), Scanning Multichannel Microwave Radiometer (SMMR) and Special Sensor Microwave/Imager (SSM/I), do not suffer from cloud issues and can retrieve SWE (Thirel et al., 2013). However, the coarse resolution (e.g., 25 km for AMSR-E SWE) and the reduced temporal frequency (more than a day) limit their application for assimilation into models.

A large amount of research for estimation of snowpack has been undertaken over the last two decades (e.g., Barnett et al., 1989; Boone and Etchevers, 2001; Decker et al., 2003), but there is still a great need for developing the capability of snow data assimilation in streamflow forecasting modelling. Among these studies, most efforts have been dedicated to the application of SCA data (Rodell and Houser, 2004; Clark et al., 2006; Roy et al., 2010; Tang and Lettenmaier, 2010; Thirel et al., 2013). Rodell and Houser (2004) implemented satellite information of SCA from MODIS to update the modelled snow water equivalent in the Mosaic land surface model using a new adding/removal scheme for three regions in the US. They added 5 mm of snow if the model had no snow and if MODIS showed more than 40% of SCA, and removed the snow if the MODIS SCA was lower than 10%. They showed a more accurate snow coverage and water equivalent estimate relative to in situ snow time series than for the control (not updated) simulation. Clark et al. (2006) assimilated synthetic SCA information to update snow in a hydrological model using the EnKF and found that while the snow prediction was improved , there was only minor improvements in the streamflow simulations.

More recently, Roy et al. (2010) integrated MODIS data with NOAA Ice Mapping System (IMS) products and examined the application of these data into the MOHYSE hydrological model for two study areas in Canada with a “direct-insertion” method using a SWE threshold. This means that if snow was observed by the satellite but the model had less snow than the SWE threshold, the model snow was fixed to this threshold. On the other hand, if the satellite observed no snow and model had more snow than the threshold, the snow was fixed to the threshold in the model. This method improved the simulation of discharge peaks (NSE and RMSE) when using both MODIS data and the NOAA IMS products, but improved only the RMSE of discharges when only MODIS was used. This method is simple to implement, but the method is case-dependent and its application may not improve the results in all cases. Tang and Lettenmaier (2010) used the MOD10A1 data from MODIS to update the snow cover variable in the VIC model for the western US and showed that the MODIS updating generally reduced the simulated streamflow, but did not necessarily reduce simulation errors. Moreover, Thirel et al. (2013) assimilated MODIS SCA data into a distributed hydrological model (LISFLOOD) using the particle filter the Morava River basin (Czech Republic) and evaluated the effects of the method on the simulation of snow and discharge. Their assimilation results showed some improvements in discharge simulation in the small upstream areas but a poor efficiency for the entire basin.

There are a few studies on application of SWE in land surface or hydrological models. Slater and Clark (2006) assimilated SWE measurements from a telemetry network in the Upper Colorado River basin using EnKF into a conceptual model (SNOW-17) and showed an improvement of the simulated SWE. Dong et al. (2007) assimilated remotely sensed SWE data from SMMR into a land surface model and showed SWE prediction improvement when evaluated against in situ SWE observations. He et al. (2012) used a parameter uncertainty analysis algorithm (ISURF) formulated into EnKF for assimilation of SWE to generate updated snow states in a coupled SNOW17/SAC-SMA model in Sierra Nevada Mountains in northern California. Their findings indicated that the assimilation scheme has the potential to supplement the current operational (deterministic) forecasting method in terms of providing improved single valued (e.g., ensemble mean) streamflow predictions as well as meaningful ensemble predictions. More specifically, Schreider et al. (1997) applied IHACRES rainfall-runoff model (Jakeman et al., 1990) in Australia to Kiewa and Mitta-Mitta catchments in the upper Murray-Darling Basin. These catchments are located in the highest parts of the Australian alpine region where the snow melt-accumulation prominently affects in the hydrological regime of these catchments. They used an empirical snow melt-accumulation model to calculate time series of equivalent precipitation as the input into the rainfall-runoff model without any attempt for application of snow observations in the modelling.

It can be seen from the above that most of the research on snow assimilation has been based on the application of remotely sensed snow cover observations with relatively few using SWE. Moreover, most have used in situ observations of SWE rather than remotely sensed SWE due to the coarse resolution (25-50 km). Most importantly, there has been no investigation on the impact of snow observation application in streamflow modelling in Australia, and the operational flood forecasting models used in Australia do not include any snow component. Therefore, there is a need to further investigate the application of remotely sensed snow with hydrological modelling for applicable areas in Australia.

2.6 Hydrological Models and Study Site

According to the literature review, there are an extensive number of hydrological models. However, in the context of this thesis, only those models used within the Australian operational forecasting system are considered as candidates for the research of this thesis. Two continuous conceptual rainfall-runoff models, Génie Rural 4 paramètres Horaire (GR4H) and Probability Distributed Model (PDM), have been selected from the collection of hydrological models in the operational SWIFT modelling framework (Pagano et al., 2010). In addition, these two models have been selected as they are Soil Moisture Accounting (SMA) models which are often used in operational flood forecasting requirements (Leahy et al., 2008).

The focus study area is the Murrumbidgee catchment in south-eastern Australia. This study area has been selected due to the extensive in-situ soil moisture observations in its subcatchments. Such observations are from the OzNet monitoring stations (Smith et al., 2012). The total size of the Murrumbidgee catchment is 84,000 km^2 with elevations ranging from 50 to 2200 m, and represents 8.2 percent of the total area of the Murray Darling Basin (MDB) in south-eastern Australia. The land use in the Murrumbidgee catchment includes dryland and irrigated agriculture, native vegetation, plantation forests and urban areas (CSIRO, 2008). The streamflow in the upper Murrumbidgee including the tributaries upstream of the Burrinjuck and Blowering dams is highly regulated (see Figure 4.1). To simplify the modelling, the upper Murrumbidgee and the regulated areas are not included in the simulations. This means that the area located between the gauging stations just downstream of the Burrinjuck and Blowering dams and the Wagga Wagga station has been selected as the focus of this study, and the observed streamflow downstream of the dams has been used to provide the inflow at the upstream boundary of the study area.

Based on stream gauge observations from New South Wales office of Water (http://www.water.nsw.gov.au/realtime-data/default.aspx), the average of median and maximum flows at the Wagga Wagga station, during the period of 2007 to 2012, are respectively 5 and 70 m3/sec over the dry years and 25 and 1450 m3/sec over the wet years. These flow values are generated in the tributaries from the two dams down to the Wagga Wagga station, with an area of about 10886 km^2.

Due to snow fall in the mountainous parts of the Murrumbidgee, the existence of snow, and thus the effect of snow melt in streamflow generation, is investigated in this thesis to determine the need for its further consideration in this research. Snow cover data from the MOD-MADI product (Bormann et al., 2012) has been used for this purpose. This investigation indicated that the area covered by snow is located upstream of the dams, and so the snow impacts on the study area are already captured through the use of gauging station at the upstream boundary. Therefore, the snow has no direct impact on modelling the runoff generation in the selected study site, and thus no snow component is included in the modelling conducted in this research.

2.7 Proposed Algorithm for Streamflow Forecasting

Based on the literature review, the key findings are as follows:

- There are many studies on application of soil moisture observations in hydrological or land surface modelling, but most of them have focused on improved estimation of the soil moisture state themselves, rather than improving the streamflow forecasting.

- Discharge assimilation has been the oldest approach in streamflow forecasting with only a few recent studies demonstrating the improvement in streamflow from the use of satellite-based soil moisture.
- There is a mismatch between the satellite penetration depth and the model soil water store that is currently hindering satellite retrieval application.
- There is limited incorporation of remote sensing soil moisture or forecast precipitation data within the flood forecasting system of Australia.

Based on these key findings and the shortcomings outlined in previous sections, an algorithm to enhance the current Australian flood forecasting system is proposed. A schematic of the proposed algorithm is presented in Figure 2.2. While snow has impact on the streamflow in part of the Murrumbidgee catchment, snow physics in the model and updating snow states via assimilating remotely sensed snow observations into the model is not included in the proposed algorithm. For soil moisture application, the hypothesis here is that the model physics simulates the soil moisture in such a way that the model soil water content is consistent with the soil moisture observations, and that the profile storage in the model will be effectively updated through the application of satellite-based profile soil moisture, leading to improved streamflow forecasts. In this research, two different calibration methods are used for parameter estimation: traditional calibration to streamflow and joint-calibration to both streamflow and in-situ soil moisture data from OzNet monitoring stations (see Figure 2.2(a)). Shuffled Complex Evolution method is adopted as a calibration algorithm.

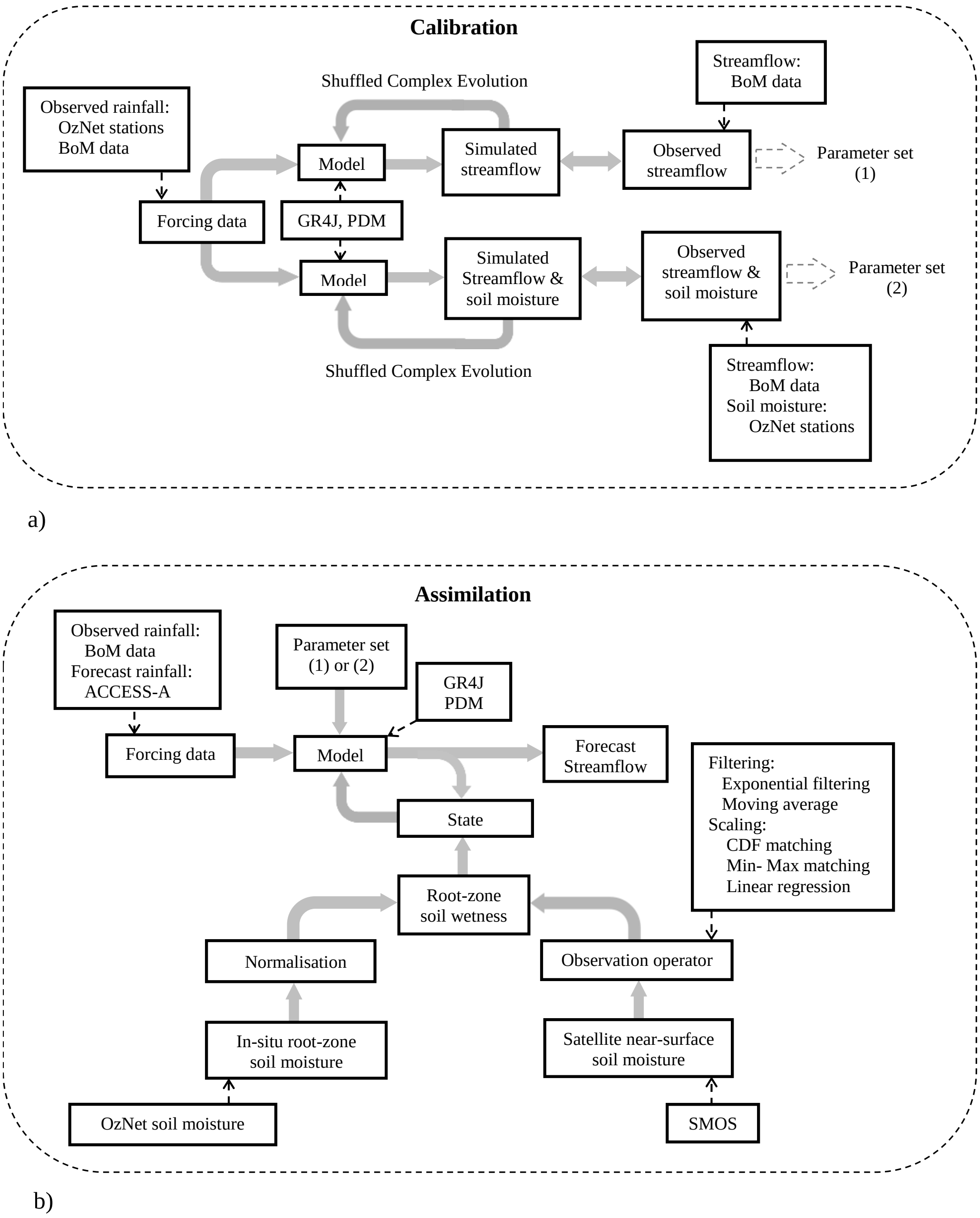

Figure 2.2: Schematic of the proposed algorithm for streamflow forecasting for (a) calibration and (b) assimilation steps.

The possible advantage of soil moisture assimilation is investigated with application of satellite-based soil moisture in the modelling. The best parameter set obtained from the calibration step is used in the evaluation and assimilation step (see Figure 2.2(b)). To update model soil moisture prediction, a rescaling/filtering approach is first used to estimate satellite root-zone soil moisture in a way that is consistent with the in-situ soil moisture data. The soil water state of the model is then updated with the best root-zone estimate using observed\forecast rainfall input data. For comparison, in-situ soil moisture observations have been also used for model constraint where ground-based observations are available. Further details on the methodology are given in Chapter 4 to 6.

Based on the proposed algorithm, the following key research tasks will be conducted to address the objective of the research: (i) assessment of forecast rainfall for application in streamflow forecasting, (ii) assessment of model calibration with and without constraint to in-situ root-zone soil moisture observation, (ii) estimation of satellite root-zone soil wetness from the near-surface data, (iii) dynamic assimilation of the streamflow modelling with in-situ /satellite-based root-zone soil moisture, (v) assessment of streamflow forecasting using forecast rainfall with and without satellite-based soil moisture constraint.

2.8 Chapter Summary

The rainfall-runoff models typically used for streamflow modelling, the challenges for forecast rainfall assessment, and the value of discharge, soil moisture and snow assimilation in rainfall-runoff modelling have been presented. Following a comprehensive study of the literature and current shortcomings, it has been shown that data assimilation into rainfall-runoff modelling for flood forecasting still has huge challenges to overcome. Most importantly, there is no significant effort for operational application of satellite-based soil moisture information for flood forecasting in Australia. Limitations include the disparity between the depth of satellite observations and the layer thickness of the hydrological models, and the spatial and temporal resolution of the satellite observations. Therefore, an appropriate observation operator to deal with the mismatch is crucial. According to the challenges above, an algorithm for this research has been proposed for improving streamflow forecasting in an

Australian catchment, through a hydrological model constrained with remotely-sensed soil moisture observations, coupled with rainfall forecasts for streamflow forecasting.

Chapter 3
Evaluation of Numerical Weather Prediction Rainfall Forecasts

This chapter presents the evaluation of Quantitative Precipitation Forecast (QPF) data from an operational numerical weather prediction model (NWP) used in Australia. The forecast rainfall data are subsequently used in an operational streamflow forecasting scenario in Chapter 6. The evaluation in this chapter gives an understanding of the uncertainties in the forecast rainfall which would likely be transferred to the streamflow forecast model. First, data from a weather radar and the NWP forecasts are compared to independent point-measurements from in-situ rainfall data from research monitoring stations over a short period of time. The forecast is then assessed against the spatially distributed radar data over a long period. In order to remove bias in the radar data, the radar observations are first calibrated to the in-situ rainfall data. These adopted radar rain intensities were then used for evaluating the quality of rainfall forecasts for an area of coincident radar coverage, based on the comprehensive review of methods commonly used in Chapter 2. Parts of the results presented in this chapter have been published as a peer reviewed conference paper (Shahrban et al., 2011), while other parts have been published in Hydrological Sciences Journal (Shahrban et al., 2016).

3.1 Study Site and Data Sets

The area of Yarrawonga weather radar coverage including part of the Murrumbidgee catchment has been selected for forecast rainfall evaluation in this chapter (see Figure 3.1) while the streamflow modelling presented in other chapters focuses on an adjacent area in this catchment. This area has been chosen for evaluation of the forecast rainfall data due to the availability of rainfall observations from the OzNet monitoring stations (Smith et al., 2012; see also www.oznet.org.au) covered by the weather radar, on the assumption that the evaluation results will be representative of the neighbouring area. This assumption is based on the close proximity, meaning that meteorological characteristics of both areas are similar.

Based on the Yarrawonga radar observations, stratiform rainfall with long duration and low to medium intensities (below 15 mm/h) is the dominant rain system in the study area in 2010 and 2011, with convective systems occurring only during the warm seasons. According to a review by Green et al. (2011), the average annual rainfall from 1898 to 2010 on the focus area in this work ranges from 350 mm on the western plains to 1100 mm in the higher elevations on the eastern part. Elevations in the Murrumbidgee catchment varies from over 2,200 m in the eastern parts to less than 50 m on the western plains (Green et al., 2011), while the elevation in the study area ranges from about 80 m in the north-western region to about 330 m in the south-eastern region of the northern part of the radar coverage area. Typical hourly radar rain maps over the entire radar coverage are shown in Figure 3.2. Based on the radar observations, the annual rainfall across the study area in the northern part of the radar coverage area ranges from 350 to 800 mm in 2010 and from 410 to 940 mm in 2011.

Five rain gauges from OzNet monitoring stations in the Yanco region (Y9, Y10, Y11, Y12 and Y13) are located within the radar coverage. However, Y13 is not included in this work because of a large gap (March 2010 to May 2011) in the data due to the instrument failure. These gauges provide rainfall data in 6-minute intervals and have been used for primary evaluation of radar and ACCESS data during January to August 2010. The OzNet rainfall data have also been used for calibrating the radar observations from January 2010 to December 2011. The selection of different time periods for these analyses is due to availability of the rain gauge data at the time of undertaking the tasks. On the other hand, calibrated data from the Yarrawonga radar of the Australian weather radar network is used for verification of the NWP forecast rainfall.

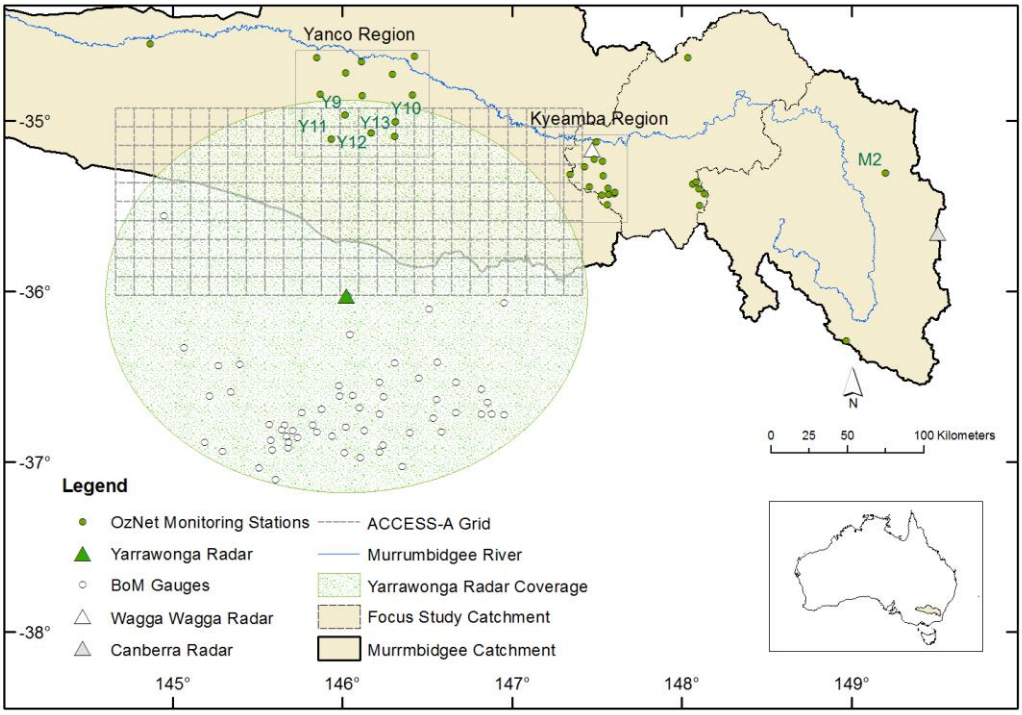

Figure 3.1: Location of Yarrawonga radar, radar coverage, OzNet rain gauges and ACCESS-A grids coinciding with radar coverage in the study area.

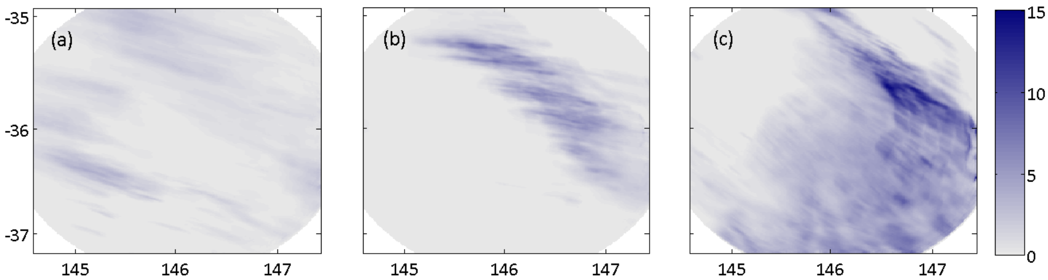

Figure 3.2: Typical hourly radar rain maps seen over the entire radar coverage area shown in the figure above. The rain maps have been shown from events on 24 April 2010 (a), 4 July 2011 (b) and 28 September 2011 (c). Note that the white areas on the top and bottom corners of the images are NA radar data. The rainfall values in mm are given on the colour bar and the horizontal and vertical axis labels are degrees of longitude and latitude, respectively.

Table 3.1: The spatial and temporal characteristics of radar and ACCESS-A data and the period of study used for two evaluations.

Data	Grid spacing	Temporal resolution	Evaluation of radar and ACCESS-A against Y10 station			Evaluation of ACCESS-A against radar		
			Spatial aggregation	Temporal aggregation	Period	Spatial aggregation	Temporal aggregation	Period
Radar	1 km	10 min	1 km	1 h	Jan 2010 - Aug 2010	12 km	1 h	Jan 2010 - Dec 2011
ACCESS-A	~12 km	1 h	~12 km	1 h		~12 km	1 h	

This C-band Doppler radar, operated by the Bureau of Meteorology (BoM), scans rainfall every 10 minutes with 1 km resolution and a range of 128 km. It has a partial coverage of the OzNet stations in the Yanco region as shown in Figure 3.1. The radar scans over 14 elevations (0.5º, 0.9º, 1.3º, 1.8º, 2.4º, 3.1º, 4.2º, 5.6º, 7.4º, 10º, 13.3º, 17.9º, 23.9º and 32º) with the same range (Rennie, 2012) and operated properly during the entire study period of this work. The radar 10-minute rainfall data were accumulated to hourly time steps, by adding six consecutive 10-minute accumulations. There are two other radars in the Murrumbidgee catchment, being the Wagga Wagga radar (C-band) located in the Kyeamba region and the Canberra radar (S-band). However, there is only one independent monitoring station (M2) in the Canberra radar coverage, and the Wagga Wagga radar is an old radar that was installed for qualitative radar observations and is not suitable for use in quantitative precipitation estimation.

The accuracy of radar-based rainfall estimates depends on i) the reflectivity measurements from the radar and ii) the parameters used for conversion of the reflectivity (Z) to rain rate (R). The estimation of rainfall from radar has been very challenging due to factors such as radar calibration (Joss and Lee, 1995), measurement error and sampling uncertainty (Jordan et al., 2000; Jordan et al., 2003; Piccolo and Chirico, 2005), attenuation (Hildebrand, 1978), range effects (Chumchean et al., 2006; Gabella et al., 2006), and variability of raindrop size distributions on the Z-R relationship (Lee et al., 2009; Alfieri et al., 2010). The procedure used by the Australian BoM for estimating real time radar rainfall consists of three main steps: i) measurement of reflectivity and removal of measurement errors from ground clutter, beam blocking, bright band, hail and range dependent bias, ii) conversion of the reflectivity to a rainfall rate, and iii) mean field bias adjustment using the available real-time rain gauge network. In the second step, radar rainfall of each pixel is estimated based on the Z-R relationship developed separately for stratiform or convective rainfall types. In the last step, based on a Kalman filtering approach, a spatially uniform bias adjustment factor is used to correct the initial radar rainfall estimates on hourly time steps (Chumchean et al., 2006; Chumchean et al., 2008). The rain gauges within the radar coverage used operationally by the BoM for radar rainfall estimation from the Yarrawonga radar are shown in Figure 3.1. The BoM rain gauges are mostly located in the southern part of the radar coverage due to high rainfall amounts and the flood warning priorities in this area. Therefore, even though the errors in the Z-R conversion and mean field bias have been mainly reduced in the three steps of the rainfall estimation procedure, there is still likely to be a bias in the radar data due to the lack of sufficient rain gauges in the northern part of the radar coverage area. It should be mentioned that the focused study area of this work is approximately flat, so the effect of topography in the radar data used in this study is not significant.

ACCESS-A (BoM, 2010; Puri et al., 2013) forecast rainfall data from the Australian Community Climate and Earth-System Simulator (ACCESS) is used over the years 2010 and 2011, due to the effective resolution (12 km) and coverage of the study area. The new operational ACCESS NWP systems from the Australian BoM replace the GASP, LAPS, TXLAPS and MESOLAPS NWP systems in Australia. ACCESS became operational for NWP application in 2010 and includes several models with different domains, resolutions, and forecast lead times. These models include ACCESS-G (global, 80 km), ACCESS-R (regional, 37.5 km), ACCESS-T (tropical, 37.5 m), ACCESS-A (Australia, 12 km), ACCESS-C (cities, 5 km) and ACCESS-TC (tropical cyclone, 12 km). The ACCESS system uses a four dimensional variational data assimilation (4DVAR) scheme which takes into account various observations with different times or locations for initialising the model in a dynamically consistent way. All models except ACCESS-G use boundary conditions that are provided by a coarser resolution ACCESS mode. For example, ACCESS-R and ACCESS-T are nested inside the previous run of ACCESS-G, while ACCESS-A and ACCESS-C are nested inside the concurrent run of ACCESS-R. ACCESS-A has four runs per day with base times of 00:00, 06:00, 12:00 and 18:00 UTC and forecast duration of 48 hours. The OzNet rain gauges, the radar coverage, and ACCESS-A grid in the study area are presented in Figure 3.1. To compare the characteristics of the datasets used in this work, the spatial and temporal resolution of the data and the study periods in this work are presented in Table 3.1.

3.2 Methodology

3.2.1 Evaluation of Radar and ACCESS-A against In-situ Rainfall Data

This subsection describes the primary evaluation of radar and ACCESS data carried out against single gauge station. In this study, rainfall estimates from weather radar observations and ACCESS-A NWP model were evaluated against independent rain gauge measurements. Station Y10 in the Yanco region was arbitrarily selected as the representative station for an 8-month comparative study from January to August 2010. The first 8 months of 2010 were chosen for the analysis as the OzNet rain gauge data were not available for September 2010 to December 2011 at the time of undertaking this analysis. Four different time series of hourly NWP data were obtained from forecasts using lead times of 1-12, 13-24, 25-36 and 37-48 hours. Each of the hourly time series were accumulated to daily precipitation and individually compared with hourly and daily gauge observations on the basis of the nearest neighbour.

Two types of comparison including categorical and continuous statistics were made (McPhee et al., 2005). Probability of detection (POD) and false alarm ratio (FAR) were computed as the categorical statistics estimating the accuracy score of the data. Additionally, mean error (bias) and root mean square error (RMSE) were the continuous statistics calculated in this study. The details of the evaluation metrics are presented in section 3.2.3. Bias and RMSE were computed as the average of differences between the precipitation values from the gauge station and the corresponding radar/ACCESS grid containing the station. Bias and RMSE is based only on those cases in which non-zero precipitation was observed by at least one of the data sources compared. This prevents the error statistics from being unduly influenced by the large number of non-raining periods.

3.2.2 Evaluation of ACCESS-A against Radar Observations

In this study, the ACCESS-A rainfall forecast was evaluated against the radar rainfall estimates from January 2010 to December 2011 over the area common to these two data sets. Understanding of radar rainfall uncertainties and rainfall processes is dependent on the availability of a dense rain gauge network for the accurate estimation of the parameters for Z-R relationship used for radar rainfall estimates (Krajewski et al., 2010; Peleg et al., 2013). Since the rain gauges used by the BoM for estimation of radar rainfall intensities are mainly located in the southern part of the radar coverage where orographic enhancement is important (see Figure 3.1), radar rain rate adjustment in the northern part of the radar domain was needed to decrease the errors brought by calibration to the BoM rain gauges alone. Thus, before using radar observations for evaluation of the ACCESS-A forecast rainfall, the radar rainfall intensities were adjusted to rain gauges using a new power-law relationship for each event over the entire northern part of the radar coverage. The adjusted radar rain intensities were then used for evaluating the rainfall forecasts for a coincident area in the northern radar coverage. The Z-R relationship is influenced by the raindrop size distribution, which can vary greatly within a given event, and from one rainfall event to another (Doelling et al., 1998; Atlas et al., 1999; Steiner and Smith, 2000). Therefore, any correction of this relationship required for accurate radar rainfall estimates should be done for individual events rather than over long periods (Alfieri et al., 2010).

For adjusting radar rainfall rates, new power-law relationships between radar hourly rain intensities and independent gauge rainfall rates from four available rain gauges (Y9, Y10, Y11 and Y12) were calibrated for each event by estimating the parameter α and β according to

$$R' = \alpha R^{\beta}, \tag{3.1}$$

where R' is the gauge rainfall rate intensities (mm/h) and R is the radar rainfall rate (mm/h) in the corresponding radar pixel. This new relationship is based on the power-law relationship typically used in the initial conversion of radar reflectivity measurements to rainfall intensity (Battan, 1973; Collier, 1989; Rinehart, 1991). In the adjustment process, the radar rain rates were brought as close as possible to the gauge rates at hourly time steps by minimizing the error between radar and rain gauge estimates. Each parameter set (α and β), which was estimated for each event, was used to calculate the new radar rain rates for the individual event over the entire northern part of the radar coverage using the power-law relationship in equation (3.1). This event-dependent calibration method accounts for the dependency of the Z-R relationship on rainfall characteristics such as rainfall drop size distribution, which varies in both space and time (Atlas et al., 1999; Mapiam et al., 2009). The methodology for adjusting radar rainfall rates was based on the algorithm proposed by Fields et al. (2004). Similarly, Mapiam and Sriwongsitanon (2008) used this method for adjusting the Z-R relationship using a linear regression between the radar rainfall and the observed gauge rainfall in the Ping river basin in northern Thailand, but the exponent in the equation was fixed, assuming that it is less sensitive than the other parameter.

For verification of NWP forecast rainfall against radar data, the average of adjusted rainfall rates over the nearest radar pixels which were within the ACCESS grid spacing was calculated. Based on expert judgment, a minimum value of 5 mm/d was used as a threshold for both observation and forecast over the entire study area for separating rain storms from drizzle. It means that all daily rain maps containing at least one pixel with 5 mm/d in the radar observations and/or forecasts were used in the evaluation. RMSE, RE (relative error, or in other words bias) and ME (mean error) were used as traditional verification metrics to identify the pixel by pixel differences between the model and the average of radar adjusted rates in all 12 km × 12 km ACCESS-A grids over the northern range of the radar coverage where the radar adjustment was implemented. RMSE was calculated for hourly and daily time scales to test the improvement in daily accumulations, due to expected decreases in possible timing and location errors in longer term accumulations. As such, the useful timescale of NWP rainfall forecasts could be assessed. The evaluation metrics are presented in section 3.2.3.

Moreover, the contingency table of Ebert and McBride (2000), as described in Table 3.2, was calculated at hourly and daily timescales to better relate the rainfall forecast errors to factors such as wrong timing, wrong location, and error in rain amount. This contingency table is different from the traditional contingency table with standard verifications using categorical statistics such as bias score, probability of detection and false alarm ratio (Doswell et al., 1990; Wilks, 1995). The method in Table 3.2 compares the observed and forecast location and magnitude over the entire study domain, and calculates the categorical scores based on the overall rain map in the study area. To identify whether the location of the forecasts was adequately predicted, the distance (D_c) separating the centroids of observed and forecast rain objects should be such that $D_c<R_{eff}$ and R_{eff} is the effective radius of observed rain object. This approach is based on the method used by Ebert and McBride (2000) and Davis et al. (2006) for diagnosing forecast location errors. All rain maps from hourly and daily accumulations, with D_c smaller than R_{eff} are accepted as a good forecast location and categorised as "close" in Table 3.2.

Table 3.2: Schematic explanation of contingency table for rain events.

	Too Little	Approx. Correct	Too Much
Close	Underestimate	Hit	Overestimate
Far	Missed Event	Missed Location	False alarm

To decide whether the magnitude of the forecast is correctly predicted or not, several categories have been defined for both hourly and daily intensities. The categories are: 0.5-1, 1-2, 2-5, 5-10, 10-20, and >20 mm/h for hourly rates, and 5-10, 10-20, 20-50, 50-100, and >100 mm/d for daily rates. The categories for daily rates are quite similar to those used by Ebert and McBride (2000). However, a minimum value of 5 mm/d was used as a threshold for at least one pixel over the study area, to include a rain map on hourly or daily calculations. For hourly timescale the categories were approximately derived from the daily categories by converting the ranges to hourly rates with some changes in the values. In a time step with a "close" forecast location, if the forecast maximum intensity was within the same category as the maximum observed value, then the magnitude of the rain in the whole domain was assumed as well predicted for that time step, making it a "hit". Otherwise, if the maximum forecast rate was more than one category greater than the maximum observed rate the forecast was defined as an "overestimate", while if it was more than one category less than the observation the forecast was defined as an "underestimate". If D was equal or larger than R_{eff}, the location was not correctly predicted and the forecast was defined to be in the "far" category. If the predicted maximum intensity was approximately similar to the maximum observed value it was defined as a "missed location", but if the maximum intensity was categorised in a group smaller than the maximum observed value it was defined as a "missed event". Otherwise, if it was greater than the observed category it was defined as a "false alarm". This methodology for comparing rain magnitude is based on the approach used in Ebert and McBride (2000) for daily events.

3.2.3 Evaluation Metrics

The continuous evaluation metrics consist of RMSE, ME and RE (or bias) given by:

$$\mathrm{RMSE} = \sqrt{\frac{1}{N}\sum_{i=1}^{N}(Y_i - X_i)^2}\ , \tag{3.2}$$

$$\mathrm{ME} = \frac{1}{N}\sum_{i=1}^{N}(Y_i - X_i)\ , \tag{3.3}$$

$$\mathrm{RE} = \frac{\sum_{i=1}^{N}(Y_i - X_i)}{\sum_{i=1}^{N}(X_i)}\ , \tag{3.4}$$

where Y_i is the forecast value, X_i is the corresponding observed value, and N is the number of forecast-observation pairs. RMSE is one of the most common methods of verification and represents the average magnitude of forecast errors. RE is the total difference between forecasts and observations over the time interval divided by total observation, and ME is the average of differences between observations and forecasts over the same time interval. The ME can be used to identify the arithmetic average of the forecast errors, while the RE is useful to assess the performance of the forecasts compared with the total observations. In addition, the categorical scores, POD and FAR, are calculated by:

$$\mathrm{POD} = \frac{H}{H + M}\ , \tag{3.5}$$

$$\mathrm{FAR} = \frac{H}{H + F}\ , \tag{3.6}$$

where H (hits) is the number of actual rain events predicted by the radar/model, M (misses) is the number of actual rainfall events missed by them, F (false alarm) is the non-observed rain predicted by the radar/model, and R is the number of correct non-forecast cases. Both POD and FAR have a range of 0 to 1. For POD, a perfect score is 1 while 0 represents the perfect forecast for FAR.

3.3 Results

3.3.1 Evaluation of Radar and ACCESS-A against In-situ Data

The results of the contingency table are presented in Table 3.3. Threshold values of 0.1 to 5 mm/d are typically used in many studies to separate rain from no-rain events. In this study, the thresholds 0.1 mm/hr and 1 mm/d were used at hourly and daily scales respectively. It can be seen from Table 3.3 that the POD and FAR have been improved for daily as compared to hourly results, especially for ACCESS-A. There was no significant change between ACCESS-A estimates with different lead times, and the average over the 4 time series is presented in the table. As presented in Table 3.3, 75 percent of the daily gauge rainfall is detected by the radar, while there is only 9 percent false rain in the daily radar data. In contrast, on average 90 percent of the daily gauge measurement is predicted by the ACCESS model, and the false alarm ratio is 32 percent.

The Bias and RMSE for daily and hourly radar and NWP data during each month and the 8-month period are listed in Tables 3.4 and 3.5. The number of hourly data missed by the radar is 743 in 8 months (13%) with a mean of 3 missed hours per day and a median of 1 missed hour per day. It can be seen from Tables 3.4 and 3.5 that there is no clear trend in monthly Bias and RMSE during the 8 months for radar and NWP. However, most hourly and daily forecasts from ACCESS-A tended to have a positive bias, indicating that ACCESS typically overestimates the precipitation, while the radar on average underestimated the rainfall. These bias estimates differ from those derived from BoM verification studies for the period November 2009 to March 2010, with an underestimation of -2.5 to -3.2 mm/d (BoM, 2010).

Table 3.3: The POD and FAR for radar and ACCESS-A.

	POD		FAR	
	Hourly	Daily	Hourly	Daily
Radar	0.68	0.75	0.26	0.09
ACCESS	0.62	0.90	0.74	0.32

The poorest results in radar data can be seen in March where the RMSE reached its maximum value. This can be related to the particular weather events in this month; the total rainfall measured by the gauge in March is 47 mm with an average intensity of 2 mm/h, which is high relative to other months. Similar conditions with intense rainfall can be seen in February and May (total rainfall values of 54 and 53 mm) where the errors in radar data were also relatively high. This suggests that radar errors increased with rainfall intensity. Additionally, the distribution of BoM gauges in the Yanco area for calibration of radar data is not uniform, with a particular bias to the south (see Figure 3.1). Therefore, radar calibration factors are likely not representing any special weather conditions in the Yanco area. Furthermore, the study gauge is located a large distance from the radar (more than 100 km), and it is well known that the error of radar precipitation measurement increases with distance (Sebastianelli et al., 2010). The results in Table 3.4 showed that the forecast with lead times of 1-12 hours had the largest bias on hourly and daily time steps. The RMSE for the forecasts with lead times of 37-48 and 1-12 hours were larger on hourly and daily time scales respectively compared to the errors obtained for the two other forecasts.

To evaluate the relative importance of the error arising from comparing a NWP grid against a single gauge observation, the standard deviation of the gauge observations from 3 adjacent stations (Y10, Y12 and Y13) was calculated and compared with the RMSE of the forecasts on daily and hourly time scales. The standard deviations, 1.12 mm/h and 3 mm/d, were a significant fraction of the RMSE, indicating that the gauge sampling error may be significantly contributing to the RMSE statistic when comparing at this scale.

Table 3.4: Average of bias (mm/h and mm/d) between radar/ACCESS-A and gauge rainfall.

Month	Radar		Access 1-12hr forecast		Access 13-24hr forecast		Access 25-36hr forecast		Access 37-48hr forecast	
	Hourly	Daily*	Hourly	Daily	Hourly	Daily	Hourly	Daily	Hourly	Daily
Jan.	0.03	0.10	0.09	0.43	0.14	0.92	0.18	1.30	0.22	1.69
Feb.	-0.26	-1.48	0.02	0.14	0.02	-0.49	0.15	1.26	-0.07	-0.75
Mar.	-0.78	-3.44	-0.01	-0.07	0.16	1.56	0.11	0.79	0.40	3.62
Apr.	0.03	0.15	0.39	2.83	0.27	1.61	0.09	0.58	0.25	2.00
May.	0.12	0.68	0.01	0.09	-0.07	-0.81	0.02	0.32	0.09	0.93
Jun.	0.00	0.01	0.03	0.25	0.08	0.69	0.05	0.39	0.06	0.62
Jul.	-0.06	-0.20	0.07	0.77	0.05	0.57	0.00	0.04	-0.02	-0.26
Aug.	0.02	0.06	0.14	1.86	0.07	0.89	0.14	1.75	0.03	0.35
All months	-0.16	-0.65	0.09	0.89	0.07	0.64	0.08	0.79	0.08	0.81

Table 3.5: Average of RMSE (mm/h and mm/d) between radar/ACCESS and gauge rainfall.

Month	Radar		Access 1-12hr forecast		Access 13-24hr forecast		Access 25-36hr forecast		Access 37-48hr forecast	
	Hourly	Daily*	Hourly	Daily	Hourly	Daily	Hourly	Daily	Hourly	Daily
Jan.	0.12	0.10	0.34	1.37	0.38	2.46	0.51	3.30	0.45	3.50
Feb.	1.72	4.91	1.43	5.10	1.58	6.80	1.79	6.72	1.56	6.21
Mar.	2.48	9.16	1.56	6.62	1.19	3.55	2.40	2.56	2.96	10.52
Apr.	0.58	1.31	2.15	11.52	1.86	6.41	0.68	2.96	0.92	6.03
May.	1.25	3.57	0.82	1.46	0.80	2.12	0.77	1.44	0.94	2.95
Jun.	0.44	0.62	0.14	0.47	0.30	2.05	0.25	1.62	0.29	2.26
Jul.	0.93	1.19	0.76	2.03	0.79	2.52	0.70	1.57	0.73	1.95
Aug.	0.52	1.90	0.45	3.45	0.37	2.05	0.56	4.06	0.32	1.24
All months	1.38	4.17	1.08	5.38	0.97	3.83	1.04	3.39	1.15	4.74

* Note: 743 hours of hourly data is missed by the radar in 8 months. The mean of missing data is 3 hours per day and the median is 1 hour per day. The daily accumulated radar rainfall is computed under the assumption that the hourly radar missing values should be zero where the values before and after the missing hours are zero in both the radar and gauge records. Then, all remaining non-value radar data and their corresponding gauge values were removed from the daily analysis.

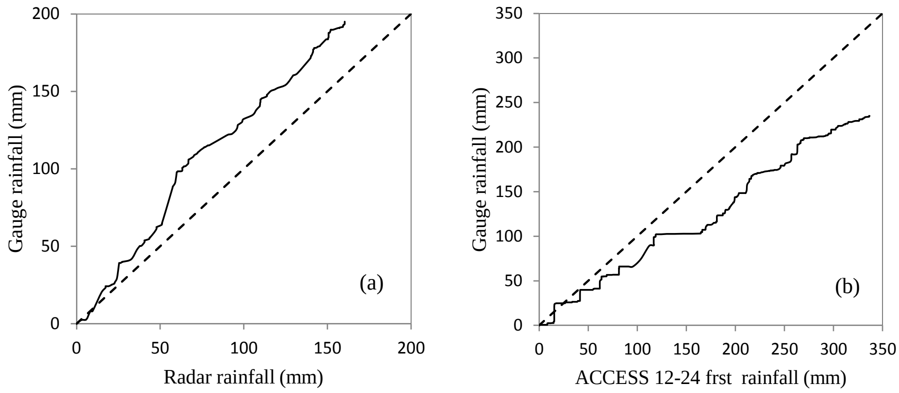

Figure 3.3: Comparison of hourly cumulative rainfall between gauge and a) radar and b) ACCESS.

The cumulative plot has been calculated in order to characterize the consistency of the rainfall data. Figure 3.3 illustrates the cumulative plots for hourly values of radar and the ACCESS 13-24 hr forecast rainfall against gauge data. The observed slope should be compared with the dashed line. The radar data had significant difference with the gauge observations in March, where the gauge cumulative value increased up to 98 mm as compared to only 60 mm for radar, but subsequently continued in a more consistent manner as compared with gauge data, where the plot is parallel to the dashed line. In this figure the ACCESS 13-24 hour forecast demonstrated a better trend in comparison with the three other forecast lead times (not shown here), but timing errors are quite obvious in many instances. Moreover, several events were forecast but were not observed. The ratio of total sum of gauge measurements to total rainfall estimates for radar is 1.22, while for ACCESS it is 0.63, 0.70, 0.67 and 0.68 for the four different forecast periods.

The NWP model outputs used in the study have relatively coarse resolution (12 km), with significant errors expected from using a single gauge to estimate the mean hourly rainfall over the pixel. Therefore, comparison between a large area rainfall prediction and a single rain gauge may be significantly impacting the NWP statistics due to the relatively coarse resolution of the ACCESS grid. Consequently, for the application of ACCESS-A data in hydrological modelling, further study of the forecast rainfall estimates is recommended be carried out with more independent rain gauges over a large experimental area.

3.3.2 Calibration of Radar Rainfall

For calibrating radar rain rates during the study period of January 2010 to December 2011, hourly accumulations were calculated for rainfall rates from four Yanco gauges as well as coincident radar pixels in the northern part of the radar coverage. New spatially uniform parameters α and β were estimated for 87 separate events over the two year study period, using the average hourly rainfall for the four radar grid cells (1 km x 1 km) and the four corresponding gauges. The parameters were selected to yield the best power-law fit between the radar and gauge rainfall rates across the four gauges. The non-linear least squares method was used for fitting the rates to the new relationships. Before fitting, the outliers for each event were excluded from the fitting. The outliers for each event were identified as the pairs with gauge-based rain rate less than the 10th percentile of gauge rain rates whilst the radar-based rate was greater than the 90th percentile of radar rates in an event, or vice versa.

The new parameters were applied to the entire northern domain of the radar coverage for each event, in order to derive calibrated radar hourly rates. The parameters α and β had a temporal range between 0.05 to 5.18 and 0.05 to 3.27 respectively for the events, with no specific seasonal trend seen in the values of the parameters. In the study by Mapiam and Sriwongsitanon (2008), the parameter α was estimated to be equal to 1.868 which is consistent with the range obtained here, while they used a fixed exponent β (equal to 1). Figure 3.4 shows the cumulative rainfall for the four rain gauge locations and a scatter plot of radar rainfall compared with gauge observations before and after calibration. In the cumulative rainfall plot, created by summing the hourly rainfall rates from the January 2010 to December 2011, the time steps with missing gauge and/or radar values were removed from the calculations. The figure shows data for the full two-year period. The scatter plot has been shown for the four Yanco gauges used for radar calibration. It can be seen from the cumulative rainfall plots that the bias in the radar rainfall estimates was reduced by the calibration. In the scatter plot, apart from some points of overestimation, most of the radar rates (mainly underestimations) were improved, showing that the bias in the overall radar estimates were removed through the calibration process. The bias and RMSE between gauge and radar rainfall rates were decreased from -14% and 2 mm/h to 3% and 1.7 mm/h respectively after radar calibration in four grids containing Yanco stations for the whole study period.

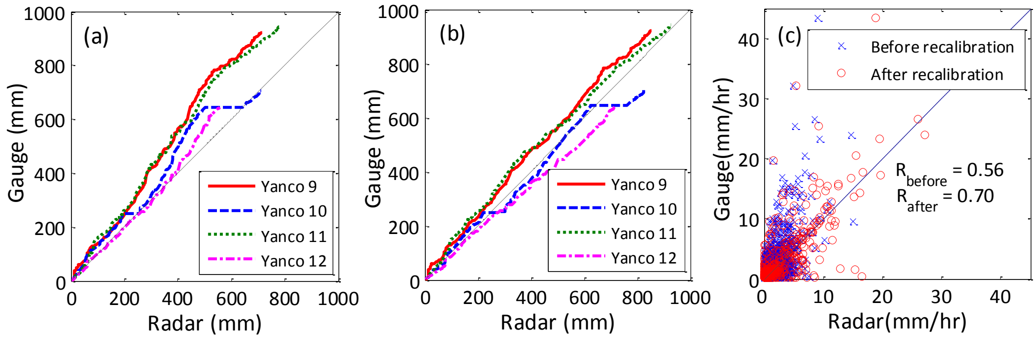

Figure 3.4: Cumulative rainfall plots for radar before calibration (a) and after calibration (b); scatter plot for radar rainfall rates compared with gauge observations before and after radar calibration (c). Data is from January 2010 to December 2011.

3.3.3 Evaluation of ACCESS-A Using Continuous Metrics

After calibrating the radar rainfall rates, the radar hourly rainfall accumulations with 1 km grid spacing were aggregated to the ACCESS-A 12 km grid spacing (as explained in section 3.2.2) for verification of the forecast rainfall in the northern half of the radar domain. Based on the evaluation of the forecast rainfall against in-situ rainfall data in this chapter, the average RMSE and mean error of ACCESS-A on an hourly time step was found to be the lowest for lead times of 13-24 hours among other possible lead times (1-12, 25-36 and 37-48 hours). Therefore, the forecast data for lead times of 13 to 24 hours and from base times of 00:00 and 12:00 are used to produce the continuous forecast time series in this work. The use of 13-24 hours lead time avoids the model initialisation and spin-up problems in the shorter lead times as well as the forecast uncertainties that usually increase for the longer lead times. In order to compare the forecasts with gauge or radar observations, cumulative rainfall from ACCESS-A are shown against cumulative gauge point measurements and cumulative adjusted radar rainfall in Figures 3.5(a) and (b), and a scatter plot of ACCESS-A is presented against the radar adjusted rates in Figure 3.5(c) for the entire two-year period. Here, radar and ACCESS-A are both rainfall over the 12km ×12km pixels containing the rain gauges. From the cumulative plots, ACCESS-A mostly overestimated rainfall compared to the gauges and radar with the ME and RMSE of 12% and 1.3 mm/h respectively, when compared to the radar data. According to Figures 3.5(c), there is poor agreement between Radar and ACESSS with correlation coefficient of 0.25, which could be related to the timing errors.

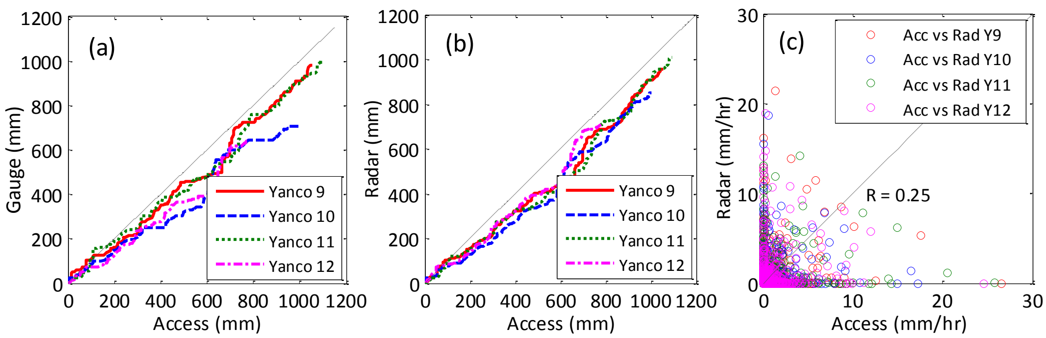

Figure 3.5: Cumulative rainfall plots for ACCESS-A compared with gauge (a) and calibrated radar (b); scatter plot for ACCESS-A rainfall rates compared with calibrated radar observations (c). Data is from January 2010 to December 2011.

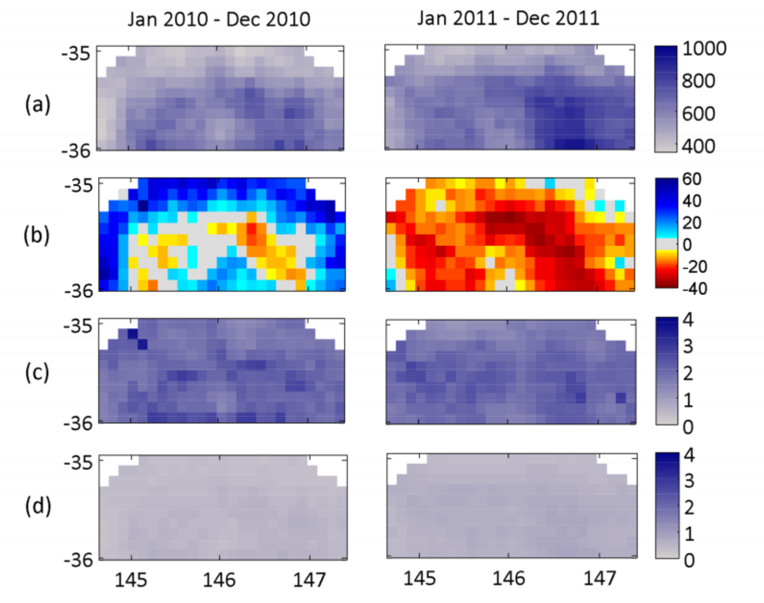

Figure 3.6: Total calibrated radar observations (mm) (a); relative error (%) between hourly ACCESS-A and calibrated radar (b); and RMSE (mm/h) between hourly (c) and daily (d) ACCESS-A and calibrated Radar. Data is for 2010 (left) and 2011 (right). Note that the white pixels on the top corners of the images are NA radar data. A consistent colour scale has been used to permit easy cross comparison. The horizontal and vertical axis labels are degrees of longitude and latitude, respectively.

The total annual radar adjusted observations across all 12 km ×12 km ACCESS-A pixels over the northern part of the radar coverage is shown for 2010 and 2011 in Figure 3.6(a), varying from 350 to 800 mm in 2010 and from 410 to 940 mm in 2011 across the area. From the figures, it can be seen that there is a similar pattern in the annual rainfall observations over the area in 2010 and 2011. In these figures, there could be possible underestimation of the rainfall near the edge of the radar range, associated to residual bias due to the vertical profile of reflectivity, while radar clutter might be a reason for the decrease of the rainfall near the radar location in the central-lower part of the image.

Figures 3.6(b) and (c) depict the spatial variation of annual RE (%) and RMSE (mm/h) for each year across all ACCESS-A pixels in the study area. The

RE varied between −22% to +59% in 2010 and −38% to 14% in 2011 across the pixels in the study area, as shown in Figure 3.6(b). It can also be seen from this figure that ACCESS-A performance changed across the pixels in the study area, and had a very different response in 2010 to that in 2011. It mainly overestimated rainfall in 2010 (errors are shown in blue colour), with very small relative errors in the middle parts (grey colour) in this year. However, it underestimated rainfall in most of the central parts (yellow to red colour) in 2011. Comparing Figure 3.6(a) with Figure 3.6(b), it is revealed that ACCESS-A overestimated the areas with low rainfall observations in 2010 and underestimated the areas with high rainfall observations in 2011, while the error was nearly zero in the areas with moderate rainfall. The range of RE obtained here is similar to the errors estimated by Shrestha et al. (2013) from March 2010 to March 2011 in the Ovens catchment in south-eastern Australia using gauge data alone. They showed that ACCESS-A overestimated precipitation in dry, low elevation areas by up to 60% and underestimated it in wet, high elevation areas by up to 30%. However, the study area here is nearly flat with an average slope between 0% and 1.8%. Therefore, this study shows that the error is more likely to be dependent on observed rain magnitude through time than on elevation, as was proposed by Shrestha et al. (2013). In Figure 3.6(c), RMSE was not very different between 2010 and 2011, varying between 1.4 to 3.7 mm/h in 2010 and 1.2 to 2.9 mm/h in 2011 across the pixels in the study area. The range of RMSE across the area on daily accumulations here agrees with the RMSE found in the study by Shrestha et al. (2013) with values from 6.4 to 14.6 mm/d for ACCESS-A model.

To account for the difference in the errors through the months, the hourly RE, ME and RMSE were investigated separately for 3-monthly periods as shown in Figures 3.7-3.9, with the total radar observation across the pixels presented for each period in Figure 3.10. Figures 3.7 and 3.8 show that there is no consistent error in ACCESS-A forecasts across the study area through the 3-monthly periods. The variations in the errors seen between the 3-monthly periods in Figure 3.7 are mainly related to the dependency of the model skill on actual rainfall observations, which varied considerably across the study area. This means that the model underestimated rainfall during the periods with heavy rain rates and overestimated light rainfall events. From Figure 3.7, it was also revealed that ACCESS-A strongly underestimated rainfall amounts in January to March 2011 due to the inability of the model to predict heavy rainfall events from convective storms during the summer. In addition, from Figures 3.7 and 3.8, it was found that the ME varied between -1 to 1 mm for each 3-monthly period, while the range of RE was very high for each period across all pixels. For example, in April to June 2010 the ME ranged from -0.22 to 0.87 mm across the pixels while RE varied from -32% to 270% of total observed rainfall across the pixels. Indeed, in some periods of the year RE was as high as 60% across the study area with ACCESS-A underestimating rainfall or it was as much as 270%, with ACCESS-A overestimating rainfall. The RE was more than 100% in January to March and July to September 2010, and was more than 200% in April to June 2010 and 2011. Since the model overestimated low rainfall values, the RE was very high where it was positive.

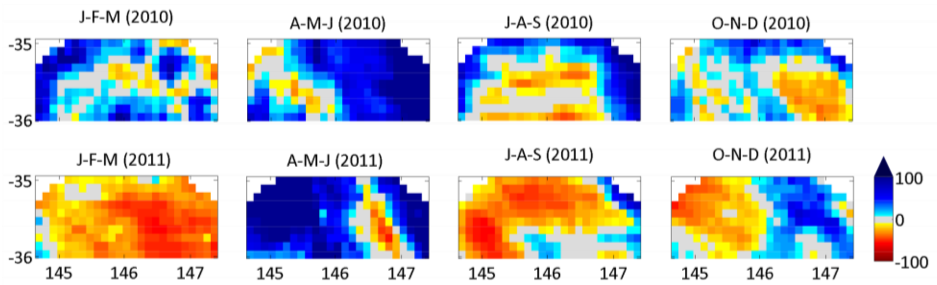

Figure 3.7: Relative error (%) between hourly ACCESS-A and calibrated radar over 3-monthly periods for 2010 and 2011. Note that the white pixels on the top corners of the images are NA radar data. A consistent colour scale has been used to permit easy cross comparison; however the maximum errors for J-F-M, A-M-J and J-A-S 2010 and A-M-J 2011 are off the scale in the figure, as indicated by the arrow. The horizontal and vertical axis labels are degrees of longitude and latitude, respectively.

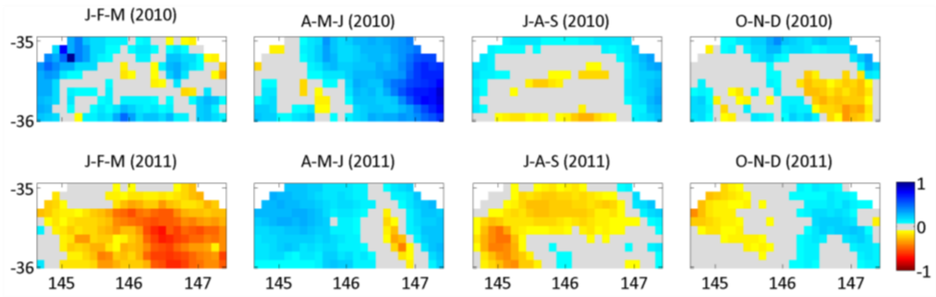

Figure 3.8: Mean error (mm/h) between hourly ACCESS-A and calibrated radar over 3-monthly periods for 2010 and 2011. Note that the white pixels on the top corners of the images are NA radar data. A consistent colour scale has been used to permit easy cross comparison. The horizontal and vertical axis labels are degrees of longitude and latitude, respectively.

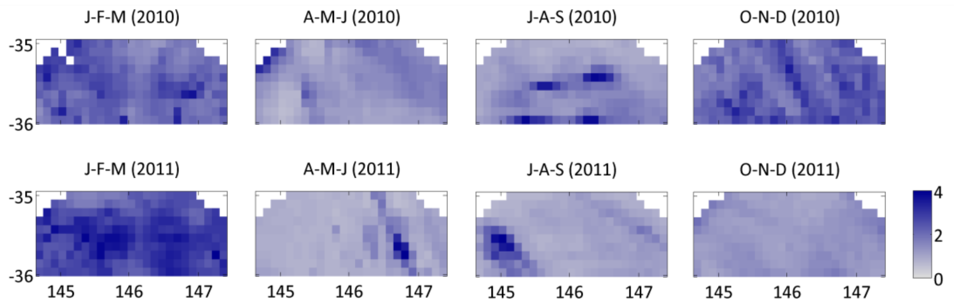

Figure 3.9: RMSE (mm/h) between hourly ACCESS-A and calibrated radar over 3-monthly periods for 2010 and 2011. Note that the white pixels on the top corners of the images are NA radar data. A consistent colour scale has been used to permit easy cross comparison. The horizontal and vertical axis labels are degrees of longitude and latitude, respectively.

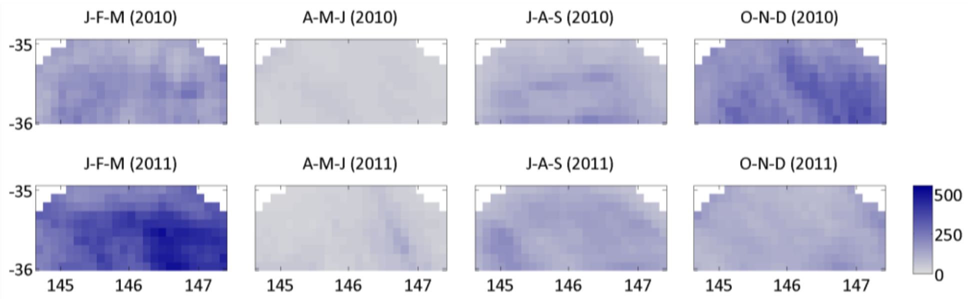

Figure 3.10: Total calibrated radar rainfall (mm) over 3-month periods for 2010 and 2011. Note that the white pixels on the top corners of the images are NA radar data. A consistent colour scale has been used to permit easy cross comparison. The horizontal and vertical axis labels are degrees of longitude and latitude, respectively.

By comparing the RMSE in Figure 3.9 with total observed rainfall in Figure 3.10, it is clear that RMSE was high in periods with medium to high rainfall observations over the periods. For example, maximum RMSE was in the periods October to December 2010 and January to March 2011, with total observed rainfall over 3-monthly period varying from 1.4 to 3.4 mm/h and 1.6 to 4.6 mm/h respectively. In order to investigate the extent to which the error decreases with accumulation periods, the RMSE was also calculated on daily accumulations with results shown in Figure 3.6(d) for 2010 and 2011 respectively. The daily RMSE ranged from 0.3 to 0.7 mm/h (7.2 to 16.8 mm/d) in 2010 and from 0.4 to 0.9 mm/h (9.6 to 21.6 mm/d) in 2011 across the pixels. From these results, the areal averages of RME were decreased by 78% and 68% for 2010 and 2011 respectively in daily time steps. However, the range of RMSE on the daily time scale was still high (7.2 to 16.8 mm/d for 2010 and 9.6 to 21.6 mm/d for 2011).

3.3.4 Evaluation of ACCESS-A Using Contingency Table

To evaluate the importance of timing as a source of error in the forecasts, relative to errors in the rainfall volume and location over the entire study domain, the contingency table in Table 3.2 was calculated for hourly and daily accumulations. This approach allowed for an approximate evaluation of forecast location assuming that the rain forecast object initially matches the observed object. To produce this table, the rain events that did not contain at least one observed and/or forecast pixel with more than 5 mm/d rainfall were removed, and thresholds of 0.1 mm/h and 1.0 mm/d were used to distinguish between rain and no-rain pixels for hourly and daily analysis respectively. All hourly and daily rainfall amounts below these thresholds were considered zero. To distinguish whether the forecast location was sufficiently good or not, the effective radius of the observed rain object and the distance between centroids of observed and forecast rain objects were calculated for each time steps (see section 3.2.2). The effective radius was estimated as the radius of a circular region having the same area as the observed rain area, and the centroid of observed (or forecast) rain object was calculated as the arithmetic mean location of all observed (or forecast) rain pixels in a rain map. For comparing forecast magnitude and radar rain rates, the categories for hourly and daily timescales defined in section 3 were used.

The results for the contingency table are presented in Table 3.6 as a percentage, being the number of hours/days for each event type as defined in Table 3.2, divided by the total hours/days (excluding no rain observations and forecasts). This table indicates that 53% of the hours had wrong location with fractions of 14%, 24% and 15% for missed location, missed events and false alarms, while 47% of the forecasts were within the correct location. However, only 13% of the forecasts were identified as a “hit”. The results from the contingency table showed that the deficiency in ACCESS-A forecast on hourly time scale is related to both imperfect location and wrong magnitude. The large effect of displacement error in forecast uncertainties obtained here is consistent with the results from Ebert et al. (2004), which indicated that 1-h forecasts from nowcast algorithms may have position errors of up to 80 km with a mean error of about 15-30 km.

For daily accumulations, the fractions of wrong locations decreased to 6% for missed location, missed events and false alarms, and consequently the total fraction of forecasts with correct locations increased to 82%, due to reducing the timing errors by using longer accumulation time. However, only 21% of these days were well forecast (hits), showing that a large fraction of daily rain images (79%) had forecasts with wrong magnitude and/or location. Velasco-Forero et al. (2009) have shown previously that the spatial correlation of radar rainfall fields could be as small as 0.3 over distances as short as 20 km. Therefore, for the study area here (100×250 km^2), it is expected that forecasts with wrong location would have similarly low correlations with observations. The moderate improvement from hourly to daily accumulation indicated that the location deficiency on hourly scale, which was mainly related to the timing errors, was reduced on daily accumulations, while wrong magnitude was still the main source of errors on daily time scale. Moreover, Kobold and Sušelj (2005) showed that 15% deviation in rainfall input into rainfall-runoff models led to 20% error in peak discharge predictions. Consequently the errors obtained in this study indicate that the raw ACCESS-A forecasts may not be sufficiently accurate to be used in hydrological forecasting, since a large fraction of the study area had relative errors more than 15% (Figure 3.7).

Table 3.6: Contingency table for hourly and daily rainfall over the entire area from January 2010 to December 2011.

	Hits (%)	Underestimates (%)	Overestimates (%)	Missed-locations (%)	Missed-events (%)	False alarms (%)
Hourly	13	25	9	14	24	15
Daily	21	28	33	6	6	6

3.4 Chapter Summary

Assessment of the forecast precipitation was required before it could be used as input to hydrological models. In this chapter, forecast rainfall from the Australian Community Climate Earth-System Simulator (ACCESS) was evaluated on hourly and daily timescales, using radar observations in south-eastern Australia. The radar observations and ACCESS-A forecasts were first evaluated against gauge measurements from research monitoring stations. Radar rain intensities were then calibrated to these gauge rainfall data at hourly time steps, located in the northern part of the radar coverage where no operational rain gauge data were available for the initial radar calibration. It was shown that the ACCESS-A model errors were significant and varied from -40% to +60% across the study area. The errors were dependent on the rainfall magnitude, and the model overestimated rainfall in low precipitation areas and underestimated rainfall in high rainfall areas. Since the cumulative rainfall observations varied across the area and through the year, the relative error in the forecasts varied considerably with space and time, such that there was no consistent bias across the study area. Moreover, further analysis indicated that both location and magnitude errors were the main sources of forecast uncertainties on hourly accumulations, while magnitude was the dominant error on daily time scale. Consequently, the precipitation output from ACCESS-A may not be useful for direct application in hydrological modelling on hourly or daily time scales, and significant uncertainty is expected to be transferred to streamflow forecast model.

Chapter 4

Importance of Soil Moisture in Rainfall-runoff Model Calibration

This chapter evaluates the impact of using soil moisture observations in rainfall-runoff model calibration. A joint-calibration which used both in-situ soil wetness and streamflow observations in the parameter optimization is applied and compared with results from calibration to streamflow alone in two different lumped conceptual models, GR4H and PDM. The models are evaluated for their ability to accurately represent the soil moisture and its impact on the streamflow prediction, by comparing the simulated soil moisture with field observations from a research monitoring network. This assessment is aimed at the application of soil moisture data in improving streamflow modelling. Two subcatchments, Kyeamba and Adelong Creek, where the in-situ data from monitoring stations are available, were selected for investigation in this chapter. For each subcatchment, average in-situ root-zone soil wetness is estimated from several stations and used for calibration and evaluation of the models. The work discussed in this chapter has been submitted to the Hydrological Processes Journal.

4.1 Experimental Data Sets

The flow in the Murrumbidgee catchment is highly regulated to support irrigated agriculture. Therefore, to simplify modelling of the effect of regulations, the streamflow model performance was assessed in the unregulated area located between the gauging stations downstream of Burrinjuck and Blowering dams and the township of Wagga Wagga. The work presented in this chapter focuses on two subcatchments within the unregulated study area: the upper Kyeamba Creek and

Adelong Creek subcatchments (Figure 4.1). These two subcatchments were selected based on the availability of streamflow and ground-based soil moisture observations. Several OzNet monitoring stations (http://www.oznet.org.au; Smith *et al*., 2012) are located in the Kyeamba (K1, K2, K3, K4, K5 and K7) and Adelong subcatchments (A1, A2, A3, A4 and A5) with soil moisture and rainfall observations spanning the period of interest. The OzNet monitoring stations, operational rain gauges and stream gauges are shown in Figure 4.1.

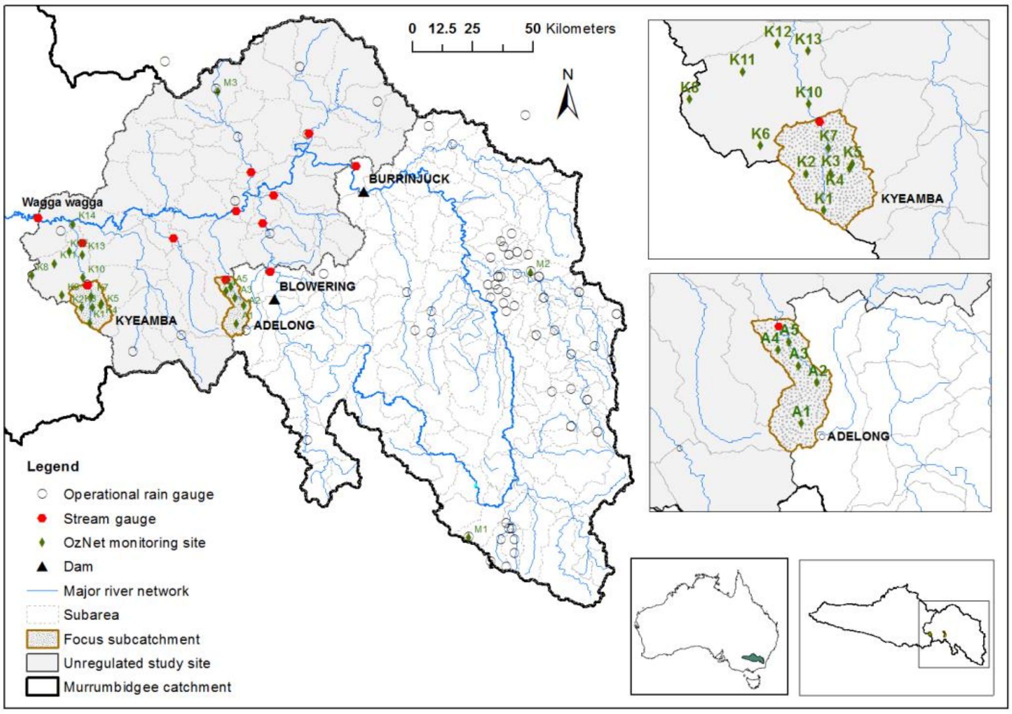

Figure 4.1: Location of operational rain gauges, OzNet monitoring stations, stream gauges and the two focus subcatchments (Kyeamba and Adelong) in the Murrumbidgee catchment that are used in this study.

The Kyeamba and Adelong Creek subcatchments are in topographically different locations in the mid-Murrumbidgee catchment with approximate areas of 190 and 157 km^2, respectively. The elevation ranges from 300 to 600 m in the Kyeamba area, and from 300 to 1000 m in the Adelong area. The average slopes in these subcatchments are about 0.67% and 1.12%, respectively. The land use in both areas is dominated by dryland grazing, but native forest is also present in the Adelong subcatchment (Green et al., 2011). Over a 10-year period from 2003-2012, average annual rainfall was 641 mm/yr for the upper Kyeamba Creek subcatchment and 846 mm/yr for the Adelong Creek subcatchment, with average flows of 35 mm/yr (total flow of 66×10^6 m^3) and 137 mm/yr (total flow of 215×10^6 m^3), respectively. Average values of annual potential evapotranspiration (PET) in the subcatchments for the corresponding period are 1430 mm/yr (P/PET = 0.45) and 1380 mm/yr (P/PET = 0.61), respectively. Semi-arid catchments are defined as having P/PET between 0.2 to 0.5 (Wheater et al., 2007), so the Kyeamba subcatchment can be identified to have characteristics close to semi-arid areas.

At the OzNet stations, rainfall observations are available with 6 minute temporal resolution for six stations in the upper Kyeamba and five stations in Adelong Creek subcatchment. The data have been aggregated to hourly time steps to be used in this study. The OzNet rainfall data were not continuously available for all stations. Thus, an interpolation approach such as Thiessen polygons was not used for areal rainfall estimation of each subcatchment, because of the limited number of stations with available data over some periods. Therefore, after comparing the cumulative rainfall plots of different OzNet stations from January 2007 to December 2010 for each subcatchment, the gauge station that had the smallest difference from most of the stations was selected as the most representative rainfall station for the subcatchment, being K7 and A4 for Kyeamba and Adelong respectively. In addition, the representative rain gauge station was selected among the gauges with long time series of rainfall data measured. For Kyeamba, station K1 was excluded from the analysis as the cumulative rainfall in this station was very different from the other K stations.

Operational rainfall real-time data, which are used for flood forecasting, are also available on hourly time steps (see Figure 4.1). The operational gauges are sparsely located and often far away from the subcatchment of interest, while the OzNet rainfall data are available from multiple stations within the subcatchments. Therefore, it is expected that the OzNet rainfall data are more likely to be closer to the subcatchment true rainfall than the operational real-time data. Thus, the rainfall data from the most representative OzNet station during January 2007 to December 2010 have been used for the calibration period, as representing the best available data.

Nevertheless, the OzNet rainfall data are not continuously available for all stations during the validation period (January 2011 to December 2012), meaning that OzNet rainfall data for the validation period are not as good as the data used during the calibration period. Therefore, the different rainfall data sets used include; OzNet rainfall data from 2007 to 2010 for calibration, and both OzNet rainfall observations from 2011 to 2012 and operational rainfall data from 2007 to 2012 for validation of the modelling. The validation with operational data in 2007-2010 was to understand how the difference between OzNet and operational rainfall data would affect the validation results in 2011-2012. In addition, there are no available OzNet rainfall data in the other subcatchments of the Murrumbidgee catchment. Hence, operational rainfall data have also been used here with the aim of demonstrating the impact on broader application. The OzNet rainfall observations from the M3 station were not used for the Muttama creek subcatchment as the data was missing due to the instrument breakdown during many months of the selected study period.

It should be noted that there was no major streamflow in the catchment from 2001 to 2009 while there were significant events in 2010 and relatively mild events in 2011 and 2012 (see Figures 4.4 and 4.5). On the other hand, there have been some events prior to 2001. However, rainfall data from the OzNet stations or BoM are not available or accurate enough for the period before 2001. Therefore, four year period of 2007 to 2010 was chosen for the calibration and the period of 2011 to 2012 was chosen for the validation as the most appropriate periods for this work. For this research, the operational rainfall data have been interpolated into all subareas including the upper Kyeamba and Adelong subcatchments (see Figure 4.1) using inverse distance squared weighting approach. The data have been used on hourly time steps. To have an overview of the difference between OzNet data and the operational data, cumulative rainfall observations from OzNet stations are compared with cumulative operational rainfall for each subcatchment during 2007 to 2010 in Figure 4.2. In this figure, except for the big difference in the early stages in the Kyeamba data, all K stations showed good agreement with operational data with correlation coefficients from 0.47 to 0.5, while among A stations, A2 was closer to the operational data than other A stations within the Adelong subcatchment with correlation coefficients from 0.42 to 0.54.

Subcatchment average soil wetness data were derived from OzNet stations for the application of soil moisture observations in the modelling of these two areas. Volumetric soil moisture data were available at either 20 or 30 minute time intervals for three soil layers, being 0-30, 30-60 and 60-90 cm depths. The data were collected by Campbell Scientific probes (CS615 or CS616) for the six K stations (K1, K2, K3, K4, K5 and K7) in Upper Kyeamba and the five A stations (A1, A2, A3, A4 and A5) in Adelong. The average volumetric soil moisture over an equivalent depth of soil as that used in the model was first calculated for each OzNet station using the data for these three depths (0-30, 30-60 and 60-90 cm), and then aggregated to hourly time steps to be used for soil wetness estimation for each station. At each time step, the arithmetic average of the soil wetness was then calculated over the stations for each subcatchment. The soil moisture data were available from stations K1, K2, K3, K4, K5 and K7 in Kyeamba and from A1, A2, A3, A4 and A5 in Adelong during the calibration period (2007-2010), while the data were missing for stations K1, K2, K5, A4 and A5 during the validation period (2011-2012). Thus, the average soil wetness data were estimated using the data from K3, K4 and K7 for Kyeamba and A1, A2 and A3 for the Adelong subcatchment. Soil wetness values from the stations had quite a large range at each time step, so the use of a limited number of stations in calculating the subcatchment average soil wetness could result in some uncertainties. Hence, it is expected that the subcatchment average soil wetness observations during the validation period would have lower accuracy compared to the calibration period.

The details of the approach used for estimation of the subcatchment average soil wetness are given in section 4.2. Average monthly PET data were derived from the gridded Australian Water Availability Project data set (AWAP; Raupach *et al*., 2009) interpolated to the study subcatchments. The real-time streamflow observations for the 6 year period 2007 to 2012 were obtained from the New South Wales office of Water (http://www.water.nsw.gov.au/realtime-data/default.aspx) for stream gauges at the subcatchment outlets.

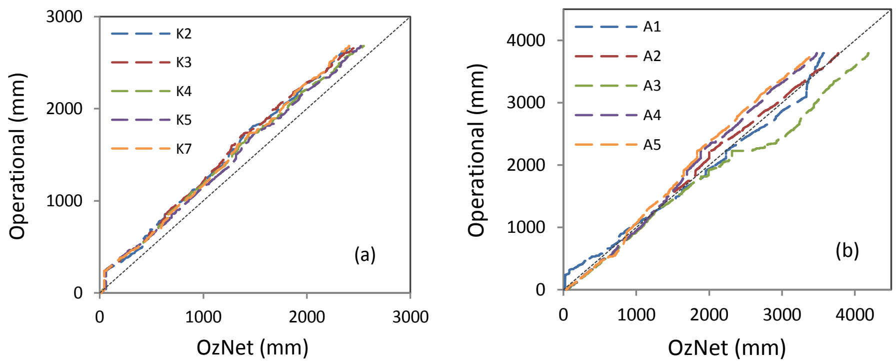

Figure 4.2: Cumulative rainfall from OzNet stations in the Kyeamba (a) and Adelong (b) subcatchments compared with cumulative interpolated operational rainfall in the subcatchment. Comparison is for 2007 to 2010 period.

4.2 Descriptions of the Rainfall-runoff Models

The continuous conceptual rainfall-runoff models used for this study include GR4H (Génie Rural 4 paramètres Horaire; Mathevet, 2005) and PDM (Probability Distributed Model; Moore, 2007). The structure of the models is shown in Figure 4.3. These models have been selected based on i) the available models in the SWIFT modelling toolkit designed for operational flood forecasting in Australia, ii) the aims for using soil moisture observations, and iii) availability of the input data required for the models. Consequently, the models implemented in the SWIFT framework (Pagano et al., 2010) have been used for testing in the study catchment, to investigate their applicability to flood forecasting of Australian catchments. The two models transform rainfall and potential evaporation input to streamflow at the catchment outlet. In this study, the models were applied at hourly time steps in a lumped configuration for each subcatchment separately, with unique rainfall and potential evaporation over each subcatchment. The lumped modelling approach adopted here is suitable for the small- to medium-sized catchments used in this work (Blackie and Eeles, 1985).

The GR4H model is derived from the daily GR4J model (Perrin et al., 2003), which is a lumped unit hydrograph model , being an evolution of the Génie Rural 3 paramètres Journalier (GR3J) model originally proposed by Edijatno and Michel (1989) and then improved by Nascimento (1995) and Edijatno et al. (1999). The GR4H structure is similar to GR4J, but with several adjustments to make the model more efficient at time steps shorter than one day (Bennett et al., 2014). GR4H consists of a production SMA store and a routing store. The model has four parameters: the maximum capacity of production store, a groundwater exchange coefficient, the maximum capacity of routing store, and the time base of the unit hydrograph (see Figure 4.3(a)). The rainfall (P) and Potential Evaporation (PE) are subtracted after interception to estimate the net rainfall (P_n) or evapotranspiration (E_n). In Figure 4.3(a), if P >= E; then P_n = P-E and E_n = 0, otherwise P_n = 0 and E_n = E-P. In the case that P_n is not zero, the infiltration to the production store (P_s) is defined by a function of level S in the production store by:

$$P_s = \frac{x_1\left(1-\left(\frac{S}{x_1}\right)^2\right)\tanh\left(\frac{P_n}{x_1}\right)}{1+\frac{S}{x_1}\tanh\left(\frac{P_n}{x_1}\right)} \tag{4.1}$$

where x_1 (mm) is the maximum capacity of the SMA store. When E_n is not zero, the actual evaporation rate (E_s) is calculated by a function of the level in the production store given by:

$$E_s = \frac{S\left(2-\frac{S}{x_1}\right)\tanh\left(\frac{E_n}{x_1}\right)}{1+\left(1-\frac{S}{x_1}\right)\tanh\left(\frac{E_n}{x_1}\right)} \tag{4.2}$$

P_n is divided to direct runoff and infiltration into the production SMA store (P_s). The percolation leakage (Perc) from the production store is then calculated as a power function of the reservoir content by:

$$\mathrm{Perc} = S\left\{1-\left[1+\left(\frac{4}{9}\frac{S}{x_1}\right)^4\right]^{-1/4}\right\} \tag{4.3}$$

Total runoff (P_r) is the sum of the direct runoff and the percolation leakage from the production store. Two unit hydrographs are used to simulate the time lag between rainfall and the streamflow. Ninety percent of total runoff is routed by the unit hydrograph UH1 and then a non-linear routing store, while 10% of the runoff is routed by the second unit hydrograph (UH2). A function F is applied to both flow components to represent groundwater exchanges calculated as:

$$F = x_2\left(\frac{R}{x_3}\right)^{7/2} \tag{4.4}$$

where R is the level in the routing store, x_3 is the maximum routing store capacity and x_2 is the groundwater exchange coefficient. Table 4.1 summarises the parameters for GR4H and their optimised values used in this research.

Perrin et al. (2003) tested the GR4J model in 429 river basins with climates ranging from semi-arid to temperate and tropical humid, and showed that the results of the model were satisfactory compared to other models of the same type, such as IHACRES, HBV, SMAR and TOPMODEL. In addition, based on the study by Vaze et al. (2010), GR4J had similar or better performance compared to other models (SACRAMENTO, IHACRES, SimHYDE, AWBM and SMARG) in 232 catchments in south-eastern Australia.

The PDM model has eight parameters and partitions the rainfall into direct runoff, soil moisture storage (S_1) and groundwater recharge as shown in Figure 4.3. The model assumes that different points in the catchment have a different storage capacity, with spatial variation of the capacity over the catchment described by a probability distribution. In this research, a Pareto distribution, which is the most widely used distribution in practice, has been used with the probability density function f(c) and the cumulative distribution function $F_{pdm}(c)$ given by:

$$f(c) = \frac{b}{c_{max} - c_{min}} \left(\frac{c_{max} - c}{c_{max} - c_{min}} \right)^{b-1}, \qquad (4.5)$$

$$F_{pdm}(c) = 1 - \left(\frac{c_{max} - c}{c_{max} - c_{min}} \right)^{b}, \qquad (4.6)$$

where c is the storage capacity, c_{min} and c_{max} are the minimum and maximum soil moisture storage capacities (mm), and b is the exponent of the Pareto distribution controlling the degree of spatial variability of storage capacity. The effective rainfall is equal to the soil moisture excess calculated at each time step and a function is used to relate the relative saturation of the catchment to the ratio of actual to potential evaporation ($\frac{E_i'}{E_i}$) as:

$$\frac{E_i'}{E_i} = 1 - \left\{ \frac{\left(S_{max} - S(t)\right)}{S_{max}} \right\}^{b_e} \qquad (4.7)$$

where S_{max} is mean storage capacity and S(t) is the total water in storage over the basin. The PDM model used here employs a cascade of two linear reservoirs (S_{21} and S_{22}), with time constant k_1 and k_2, to route surface storage flow (q_s) as:

$$q_{s,t} = -\delta_1 q_{s,t-1} - \delta_2 q_{s,t-2} + \omega_0 u_t + \omega_1 u_{t-1} \qquad (4.8)$$

with

$$\delta_1 = -(\delta_1^* + \delta_2^*),\ \delta_2 = \delta_1^*\,\delta_2^*,\ \delta_1^* = \exp(-\Delta t/k_1),\quad \delta_2^* = \exp(-\Delta t/k_2)$$

$$\omega_0 = \frac{k_1(\delta_1^* - 1) - k_2(\delta_2^* - 1)}{k_2 - k_1},\qquad k_1 \neq k_2$$

$$\omega_1 = \frac{k_2(\delta_2^* - 1)\delta_1^* - k_1(\delta_1^* - 1)\delta_2^*}{k_2 - k_1},\qquad k_1 \neq k_2$$

$$\omega_0 = 1 - \left(1 + {}^{\Delta t}/_{k_1}\right)\delta_1^*,\qquad k_1 = k_2$$

$$\omega_1 = \left(\delta_1^* - 1 + {}^{\Delta t}/_{k_1}\right)\delta_1^*,\qquad k_1 = k_2\,.$$

A standard groundwater recharge function linearly relates the rate of the drainage (d_i) to the basin soil moisture content as:

$$d_i = k_g^{-1}(S(t) - S_t)^{b_g} \tag{4.9}$$

where k_g is the recharge time constant, b_g is the exponent of recharge function and S_t is the soil tension storage capacity below which there is no drainage. A nonlinear storage (S_3) is used to route subsurface flow (q_b) with the rate of outflow proportional to some power, m, of the volume of water held in the storage per unit area as:

$$q_b = k\,S^m\,,\ k > 0, m > 0 \tag{4.10}$$

where k is the storage rate coefficient and m is the store exponent. A cubic form (m=3) is used here and an approximate recursive solution using a method by Smith (1977) gives the following equation for the storage:

$$S(t + \Delta t) = S(t) - \frac{1}{3kS^2(t)}\{\exp(-3kS^2(t)\Delta t) - 1\}\left(u - kS^3(t)\right) \tag{4.11}$$

The parameterisation $k_b = k^{-1}$ with unit h mm^{m-1} is used. The model outflow is formed from the surface runoff and subsurface flow. The summary of the parameters for the PDM model and the optimised values of them are presented in Table 4.1. This model has been widely used both for operational and design flow predictions purposes in the UK and Belgium (Moore, 1999; Cabus, 2008; Pechlivanidis et al., 2010).

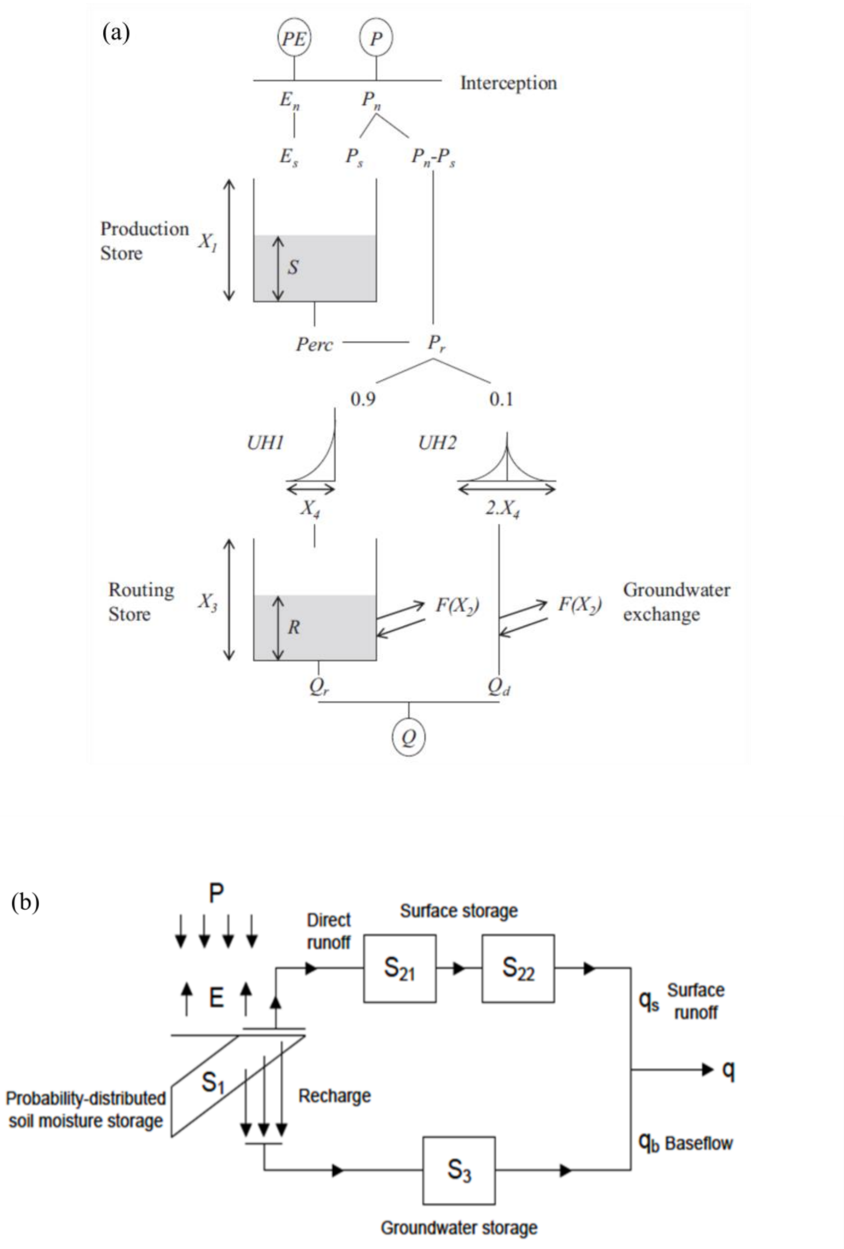

Figure 4.3: The structure of GR4H (a) and PDM (b) models.

4.3 Methods

4.3.1 Calibration and Validation of Models

The hydrological models were first calibrated to streamflow observations at the Kyeamba and Adelong subcatchment outlets using hourly data for the period 2007-2010. The models were also calibrated jointly to streamflow and soil moisture observations as a joint-calibration in both subcatchments, to additionally achieve the best match between observed and modelled soil wetness. The Shuffled Complex Evolution algorithm (SCE; Duan *et al*., 1994) was used to automatically calibrate the parameters by minimizing an objective function. The adopted objective function for calibrating to streamflow only (F_{SF}) is the mean squared error (MSE) of simulated streamflow:

$$F_{SF}= \frac{1}{n}\sum_{i=1}^{n} (Q_{obs,i} - Q_{sim,i})^2 , \qquad (4.12)$$

where $Q_{obs,i}$ and $Q_{sim,i}$ are the observed and simulated streamflow respectively at the i^{th} time step, and n is the number of time steps available for calibration. This objective function has been adopted because it is sensitive to error in high flows, which are more important for flood modelling than low flows.

The objective function adopted to calibrate the model jointly to streamflow and soil moisture observations (F_{joint}) is also based on the average sum of squared errors:

$$F_{joint} = \frac{1}{2}\left(\frac{\frac{1}{n}\sum_{i=1}^{n}(Q_{obs,i}-Q_{sim,i})^2}{\frac{1}{n}\sum_{i=1}^{n}(Q_{obs,i}-\overline{Q}_{obs})^2} + \frac{\frac{1}{n}\sum_{i=1}^{n}(SW_{obs,i}-SW_{sim,i})^2}{\frac{1}{n}\sum_{i=1}^{n}(SW_{obs,i}-\overline{SW}_{obs})^2} \right) , \qquad (4.13)$$

where $SW_{obs,i}$ and $SW_{sim,i}$ are the observed and simulated soil wetness respectively at the i^{th} time step, and $\overline{Q}_{obs}$ and $\overline{SW}_{obs}$ are the average of streamflow and soil wetness observations respectively over the entire calibration period (see next section for soil wetness estimations). To allow for scale differences between the streamflow and soil moisture simulation errors, the sum of square errors for each component are normalised by the variance of the corresponding observations.

The model performance for streamflow modelling in the calibration and validation periods is assessed using the Nash-Sutcliffe Efficiency (NSE; Nash and Sutcliffe, 1970) coefficient based on observed and simulated streamflow as:

$$\mathrm{NSE} = 1 - \frac{\sum_{i=1}^{n}\left(Q_{obs,i} - Q_{sim,i}\right)^2}{\sum_{i=1}^{n}\left(Q_{obs,i} - \bar{Q}_{obs,i}\right)^2} \;, \tag{4.14}$$

where NSE ranges from $-\infty$ to 1. An efficiency of 1 represents a perfect match of simulated flow to the observed data.

4.3.2 Estimation of Observed and Modelled Soil Wetness

Modelled soil wetness at each time step has been estimated from the conceptual soil water store of the model using:

$$SW_{sim,i}(\%) = \frac{SM_{sim,i}\ (mm)}{C_{max}(mm)} \times 100 \;, \tag{4.15}$$

where $SM_{sim,i}$ is the simulated soil moisture at the i^{th} time step and C_{max} is the maximum soil water content of the model, being the maximum capacity of the production store in GR4H model or the average capacity of soil moisture storage over the catchment in PDM. Equation (4.15) is based on the assumption that the model soil water content will reach to the maximum storage capacity at least once during the six year study period. This means that it is assumed that C_{max} represents the actual upper bound of the soil moisture content. The observed soil wetness used in this study is the average of OzNet soil wetness over the monitoring stations for each subcatchment, where the soil wetness for each station has been calculated as:

$$SW_{obs,i}(\%) = \frac{\theta_i - \theta_{min}}{\theta_{max} - \theta_{min}} \times 100 \;, \tag{4.16}$$

Here θ_i is the average volumetric soil moisture (m^3/m^3) at the i^{th} time step, and θ_{min} and θ_{max} are the minimum and maximum of the volumetric soil moisture (m^3/m^3) at each OzNet station for an equivalent soil depth, as implied by the size of the conceptual soil water store in the model defined by:

$$\text{Equivalent Depth} = \frac{C_{max}}{\text{Soil Porosity}} \quad . \tag{4.17}$$

Equation (4.16) effectively scales the soil moisture observation at each time step to a value between 0 and 100, representing the degree of saturation of a soil column with equivalent soil depth. Volumetric soil moisture data (θ) were available over the soil layers 0-30, 30-60 and 60-90 cm for each of the six K stations in the Upper Kyeamba subcatchment, and the five A stations in the Adelong subcatchment (shown in Figure 4.1). The average of the volumetric soil moisture over the equivalent depth of the soil has been calculated for each station using the available data for these three different depths. The θ_{min} and θ_{max} have been obtained from six years of soil moisture record (2007-2012) for each station separately, taking into account the variation of soil moisture over the catchment during this long period. The average of the soil wetness was then calculated over different stations for each of the subcatchments. Since all stations were not operating continuously for 2011-2012, the average soil wetness was taken from only 2 or 3 stations rather than all stations within the subcatchment in these instances.

After calibration of the models, the model soil wetness was assessed against soil wetness observations using the same soil wetness observations for the calibration and validation periods. The difference between observed and modelled soil wetness is presented as the root mean square error (RMSE) and mean error (ME) for calibration and validation periods. The mean error is the average of differences over the calibration or validation period. This comparison gives a view of the accuracy of the models in estimation of the antecedent soil moisture prior to a runoff event.

4.4 Results

4.4.1 Evaluation of Streamflow Predictions

A warm-up period during which the state variable of the model evolves from 0 (default value) to an appropriate value is used for the calibration to avoid the effect of initialisation on the calibration results. After calibration, the initial state value at the end of the simulation during calibration period is used as the model initialisation for the validation. The optimized values for the parameters of the GR4H and PDM models are presented in Tables 4.1. In order to contextualise the modelling results, the observed rainfall, observed and simulated streamflow, and the NSE scores for the calibration and validation periods of the two models for the Kyeamba and Adelong subcatchments are illustrated in Figures 4.4 and 4.5, respectively. In these figures, the results for calibration to only streamflow (SF-calibration) (Figures 4.4(a), 4.4(b), 4.5(a) and 4.5(b)) are compared with the results for calibration to both streamflow and soil moisture (joint-calibration) (Figures 4.4(c), 4.4(d), 4.5(c) and 4.5(d)). The validation results in these figures are from operational rainfall data. Table 4.2 presents in more detail the NSE scores for calibration in 2007 to 2010 (Cal.), validation using OzNet rainfall data in 2011 to 2012 (Val.1), operational rainfall data in 2007 to 2010 (Val.2), and 2011 to 2012 (Val.3). In this table, the RMSE between observed and simulated soil wetness is also presented in the second column for calibration and validation (Val.3).

It is clear from Table 4.2 that calibration NSE of PDM is better than GR4H for both calibration schemes in both study subcatchments, but the validation skill score for GR4H is mostly better than PDM for both subcatchments. There are big differences between the NSE scores in calibration and validation with operational rainfall data (Val.2) due to the lower spatial resolution of the operational rain gauges compared to the OzNet stations. However, there was no significant difference between the validation skill scores when using OzNet and operational rainfall data in 2011-2012 (Val.1 and Val.3) for the Kyeamba subcatchment, and the scores for Val.3 were even better than Val.1 for the Adelong subcatchment. Because the same validation scores were achieved from OzNet and operational rainfall data in 2011-2012 for Kyeamba (Val.1 and Val.3) and better skill obtained in validation from operational data for the Adelong area (Val.3), it is assumed that use of operational rainfall data with low spatial resolution should not adversely affect the modelling results. Thus, in the following the results from using operational rainfall data (Val.3) will be focused for both subcatchments for the validation period.

After joint-calibration in the Kyeamba area, the NSE scores of the GR4H models in both calibration and validation (Val.3) decreased, from 0.71 to 0.68 and from 0.63 to 0.58 respectively. In this subcatchment, the PDM model skill during the calibration period did not change (0.75 for both calibration schemes), while it showed slightly increased skill scores in the validation (Val.3), increasing from 0.59 to 0.61. In the Adelong subcatchment, the skill score during the calibration decreased slightly, from 0.80 to 0.79 in GR4H and from 0.83 to 0.81 in PDM, while the Val.3 score increased slightly (from 0.80 to 0.83) for GR4H and significantly (from 0.2 to 0.35) for PDM after joint-calibration. Therefore, a small degradation was seen in the calibration scores when using soil moisture in addition to streamflow, but apart from GR4H in the upper Kyeamba subcatchment, the validation scores improved after joint-calibration, especially in cases with very low skill (e.g., PDM for the Adelong subcatchment). This result indicates that overall the soil moisture constraint in the calibration procedure has improved the model skill in streamflow prediction over the whole validation period. In addition, the results showed that although the PDM model with more parameters had better SF prediction skill in both calibration methods, the model was outperformed in the validation period by the GR4H model in most cases, despite it having a simple structure and fewer parameters. It is also shown that despite the semi-arid characteristics of the Kyeamba area, the performance of both models was acceptable in this catchment with calibration and validation NSE scores mostly greater than 0.60.

Table 4.1: The optimised parameters for GR4H and PDM models for calibration to streamflow (SF-cali) and joint-calibration with normalised soil moisture (Joint-cali) or CDF-matched soil moisture in the Kyeamba and Adelong catchments.

Parameter	Description	Kyeamba		Adelong	
		SF-cali	Joint-cali	SF-cali	Joint-cali
GR4H					
x_1 (mm)	Maximum production store capacity	286.0	193.9	108.3	167.0
x_2 (mm)	Groundwater exchange coefficient	-0.6	-3.0	-3.17	-1.99
x_3 (mm)	Maximum routing store capacity	6.27	7.29	18.59	16.15
x_4 (h)	Time base of unit hydrograph UH1	3.55	3.6	4.97	5.0
PDM					
c_{max} (mm)	Maximum storage capacity	245.0	247.4	358.6	309.9
b (-)	Exponent of Pareto distribution for spatial variability of store capacity	0.13	0.15	0.27	0.11
b_e (-)	Exponent in actual evaporation function	1.97	1.74	5.83	1.38
b_g (-)	Exponent of recharge function	3.28	2.76	3.72	1.90
k_b (h mm^2)	Baseflow time constant	1180.8	1999.9	3000.0	2999.8
k_g (h mm$^{bg-1)}$	Groundwater recharge time constant	7318	59991.1	69999.6	48173.2
c_{minrat} (-)	The ratio of C_{min} to C_{max}	0.07	0.12	0.56	0.45
St_{ratio} (-)	The ratio of soil tension storage capacity to C_{max}	0.83	0.72	0.81	0.59
k_1 (h)	Time constant of cascade of linear reservoirs	1.0	1.0	3.14	2.71
k_2 (h)	Time constant of cascade of linear reservoirs	2.84	3.01	1.0	1.0

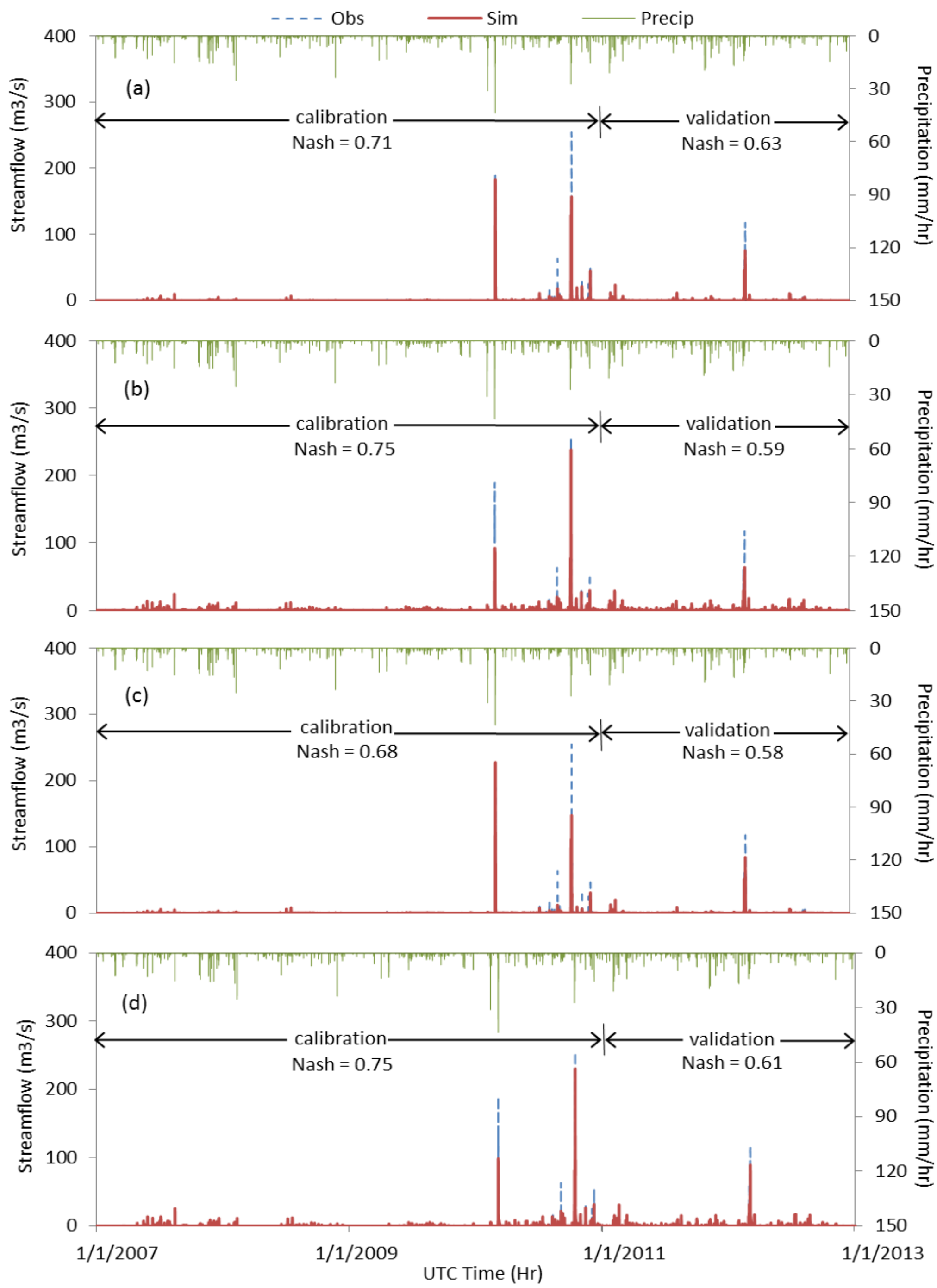

Figure 4.4: Observed OzNet (calibration period) and operational (validation period) rainfall, and observed and simulated streamflow for calibration to streamflow from GR4H (a) and PDM (b), and calibration to both streamflow and soil moisture from GR4H (c) and PDM (d), for the upper Kyeamba subcatchment.

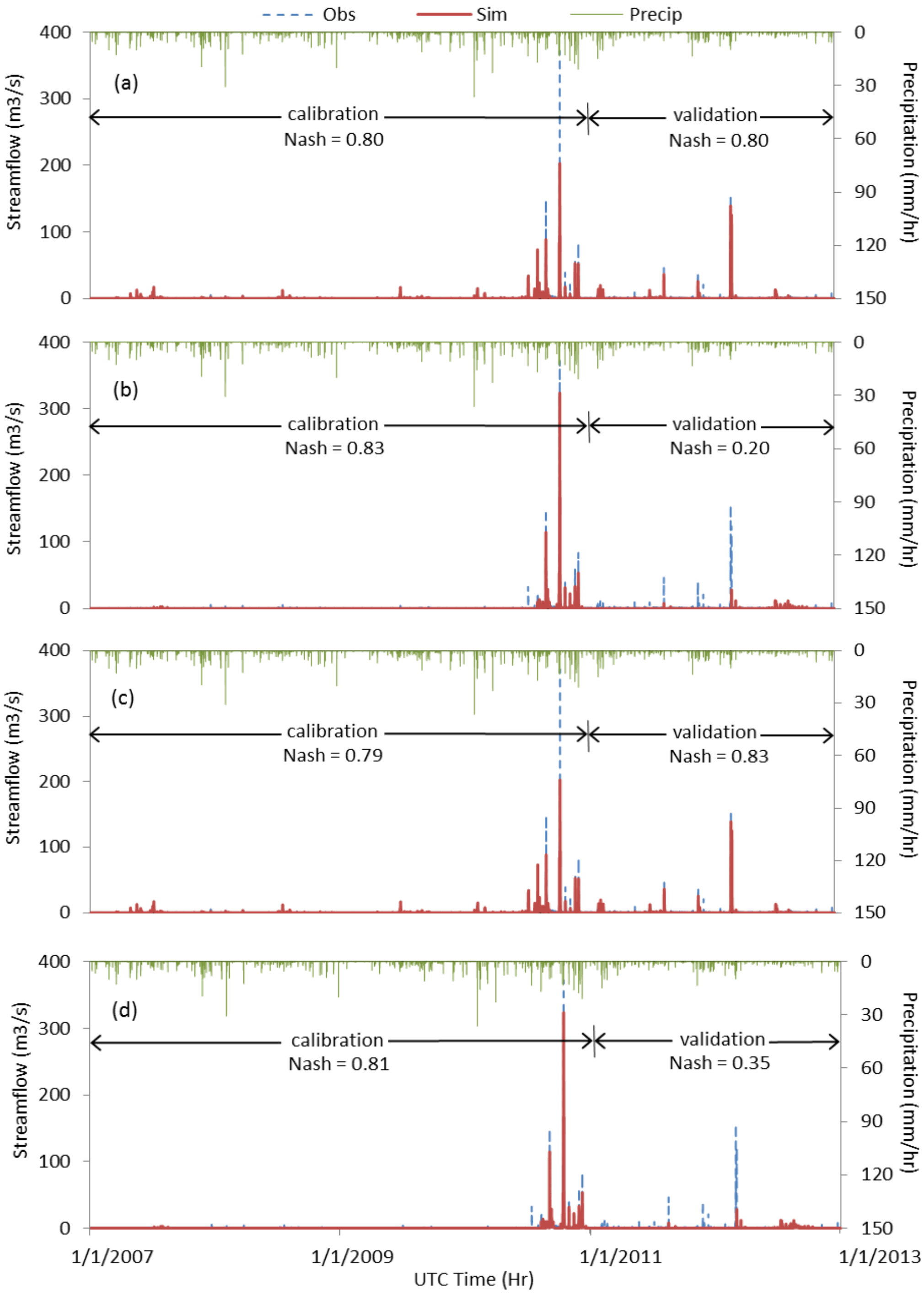

Figure 4.5: Same as Figure 4.4 but for the Adelong Creek subcatchment.

Table 4.2: NSE scores of streamflow modelling and RMSE (%) between observed and predicted soil wetness from calibration to streamflow alone (SF-cal.), and calibration to both streamflow and soil moisture (Joint-cal.) in the Kyeamba (K) and Adelong (A) subcatchments for the GR4H and PDM models. The NSE scores are shown for calibration with OzNet rainfall (2007-2010, Cal.), validation with OzNet rainfall (2011-2012, Val.1,), validation with operational rainfall (2007-2010, Val.2 and 2011-2012, Val.3); the RMSE results are shown for Cal. and Val.3 in the right hand column.

Sub. Catch	Model	SF-cal.						Joint-cal.					
		Cal.		Val.1	Val.2	Val.3		Cal.		Val.1	Val.2	Val.3	
K	GR4H	0.71	9.7	0.63	0.51	0.63	10.6	0.68	9.6	0.58	0.46	0.58	11.4
	PDM	0.75	10.1	0.59	0.39	0.59	11.4	0.75	9.5	0.61	0.39	0.61	10.3
A	GR4H	0.80	20.7	0.70	0.59	0.80	18.4	0.79	17.9	0.66	0.57	0.83	15.3
	PDM	0.83	26.6	0.10	0.42	0.20	22.4	0.81	11.9	0.17	0.38	0.35	16.3

The degradation in the calibration and validation skills of the GR4H model for the Kyeamba subcatchment, and also the degradation in skills of both models for the calibration in the Adelong subcatchment after joint-calibration, should be investigated in more detail for specific events to see how the performance of the models changed after joint-calibration. Significant improvements in streamflow prediction were seen in PDM after joint-calibration in the Adelong area, as compared to calibration to streamflow alone. While significant improvement was not achieved in the streamflow predictions after joint-calibration of the GR4H model in both subcatchments and the PDM model in the Kyeamba subcatchment, the model maximum soil store capacity has been changed dramatically in GR4H and slightly in PDM in both study areas compared to SF-calibration alone (see Table 4.1). The change in this parameter shows that with small change in the calibration skill, the joint-calibration has adjusted the soil moisture parameter in a way which is more consistent with soil moisture observations.

4.4.2 Evaluation of Modelled Soil Wetness

Figures 4.6 and 4.7 depict soil wetness estimation in the models, evaluated against the average of the soil wetness observations from OzNet stations during the calibration period for the Kyeamba and Adelong subcatchments respectively. Similar plots in Figures 4.8 and 4.9 illustrate how the soil water content was simulated for the validation period from 2011 to 2012 (Val.3). In these figures, RMSE and ME between soil wetness observations and model soil wetness estimations have been shown after using the parameters from SF-calibration and joint-calibration. The comparison allows for investigation of the difference in the soil moisture simulation before and after joint-calibration in the models.

The models performed differently in soil wetness estimation over the catchments, and this different performance of the models can be associated to the structure of the models and the hydrological processes they use for soil moisture estimation. The PDM model saturated at some points, meaning that the catchment average soil moisture storage was saturated during some periods. However, in

GR4H, for both catchments, the model total saturation was not achieved in either the calibration or validation period, with the maximum water level in the storages for SF-calibration and joint-calibration being 204 and 161 mm in Kyeamba and 105 and 154 mmm in Adelong respectively. Therefore, to be consistent with the observations, which were scaled to 0 to 100, the simulated soil wetness shown in Figures 4.6(a), 4.7(a), 4.8(a) and 4.9(a) for the GR4H has been calculated by scaling the modelled soil water level to a value between 0 and 100 using the maximum and minimum values of modelled soil water storage obtained from the entire six year study period. It should also be mentioned that because the observed subcatchment soil wetness was the average of stations, the maximum soil wetness result shown is a value that is slightly smaller than 100%. Likewise, the minimum soil wetness did not reach zero as the minimum saturation did not occur at the same time for all stations in the subcatchment. For joint-calibration, the models were initialised with the soil wetness observations at the beginning of the calibration as shown in Figures 4.6 and 4.7, but the results indicated that the initialisation had no impact on the model skill during the following time intervals.

As seen in Figures 4.6 and 4.7, the RMSE and ME mostly decreased after joint-calibration, when compared to SF-calibration alone, but there were still differences between the simulations and observations. In these figures, it is clear that the variation of soil wetness observations through time have been simulated correctly by the models in both subcatchments. However, apart from some periods, the models mostly underestimated the soil moisture and could not reach the high value of saturation during the wet periods. Moreover, Figures 4.6(a) and (b) show that both models underestimated soil wetness in both calibration approaches in Kyeamba with approximately the same RMSE, 9.7% and 9.6% in GR4H and 10.1% and 9.5% in PDM for SF-calibration and joint-calibration respectively. The ME increased from -0.4% to -4.4% in GR4H after joint-calibration while the error decreased from -3.1% to -1.3% in PDM.

Figures 4.7(a) and (b) show that in the Adelong area, apart from some periods in 2010, both models underestimated soil moisture for SF-calibration with a much higher RMSE and ME seen in the PDM model (26.6% and -22.2% respectively) compared to RMSE (20.7%) and ME (-15%) for GR4H. However, after joint-calibration, the errors in PDM declined significantly, to 11.9% (RMSE) and -3.8% (ME), which were much lower than the RMSE and ME for GR4H (17.9% and -13.5% respectively). This improvement in the modelled soil wetness is clear in Figure 4.7(b). From the results in Figures 4.6 and 4.7, it is seen that there is only a small change in the soil moisture simulations after joint-calibration where the model already had relatively good performance in the streamflow modelling (e.g., GR4H model in both catchments and PDM model in the Kyeamba area). However, in the Adelong subcatchment, the errors between the modelled and observed soil wetness improved significantly in the PDM model, which had the worst skill in streamflow and soil wetness estimations in SF-calibration.

In Figures 4.8 and 4.9, there were no significant changes in RMSE errors in the soil moisture simulations compared to the observations after joint-calibration for Kyeamba (10.6% and 11.4% in GR4H and 11.4% and 10.3% in PDM), while the error improved from 18.4% and 22.4% to 15.3% and 16.3% in GR4H and PDM for the Adelong subcatchment. The ME increased slightly in GR4H from 2.2% to -4.8% while it decreased slightly from -1.4% to 0.3% in PDM in the Kyeamba subcatchment. In the Adelong area, ME improved from -11.1% to -7.2% in GR4H after joint-calibration. However, ME degraded from -4.2 to 11.8% in PDM after the joint-calibration. Moreover, it is clear from Figures 4.8(a) and (b) that in Kyeamba there is no significant change in the soil wetness simulations after joint-calibration in both models, with better soil moisture simulations seen in the GR4H after joint-calibration. According to soil wetness estimations presented in Figures 4.6 to 4.9, it was shown that the errors between observed and predicted soil wetness were reduced or did not change significantly in most cases, except for the mean error obtained for PDM in the Adelong subcatchment during the validation period. This indicates that the joint-calibration has improved modelled soil wetness in a way which is more consistent with observations. Indeed, the simulation with the parameters obtained from joint-calibration is much more consistent with the real condition in the catchment in terms of the soil water storage.

From the Figure 4.9(a), there was no significant change in the Adelong catchment in the soil moisture simulations for GR4H. However, PDM showed some improvements in soil moisture simulation in mid-2011, but the huge differences in early 2012 were not reduced after joint-calibration. It should be highlighted here that, as explained in section 5.1, there were less continuous data available from the OzNet stations during the validation period. The use of a limited number of stations in calculating the subcatchment average soil wetness would result in greater uncertainties during the validation period compared to the calibration period. Therefore, the difference between soil wetness observations and simulations being higher in the validation than the calibration period is no surprise. The GR4H and PDM models were also jointly calibrated to stream flow and OzNet soil moisture observations when the OzNet observations have been rescaled to the model soil water content using CDF-matching approach. This allows for evaluation of the effect of CDF-matching rescaling approach on the joint-calibration. The results of the joint-calibration after CDF-matching soil moisture observation to model predictions are presented in Appendix A1. These results showed that the use of CDF-matched observations in joint-calibration did not add any enhancement to the calibration results as compared to the joint-calibration results presented in this chapter.

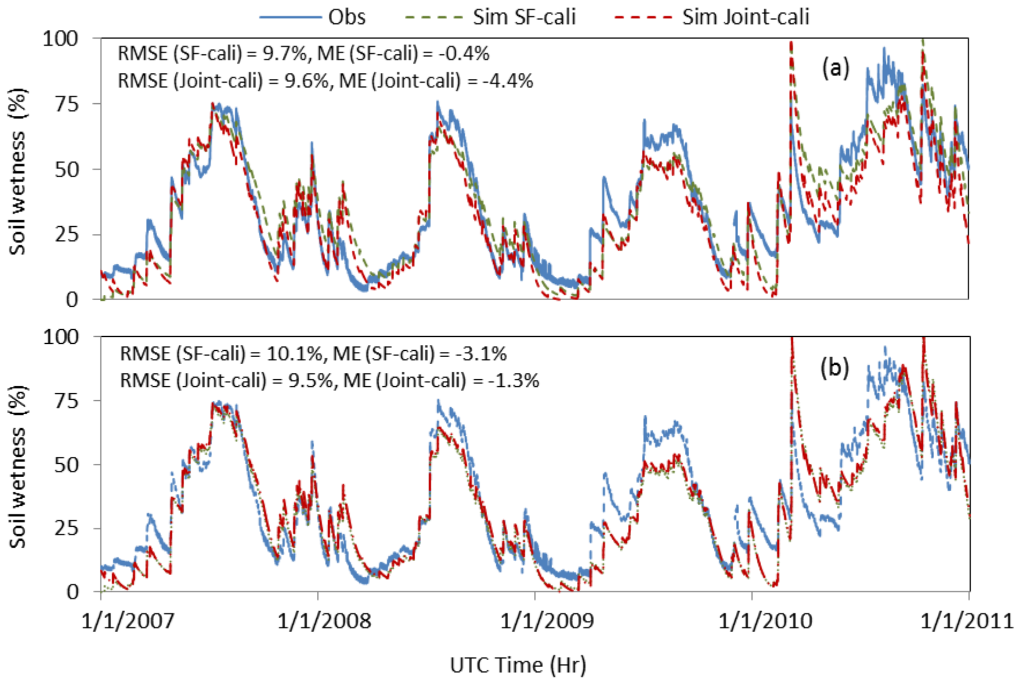

Figure 4.6: Observed and simulated soil wetness for GR4H (a) and PDM (b) for the calibration period in the upper Kyeamba subcatchment; Calibration is to streamflow alone (SF-cali) and to streamflow and soil moisture jointly (Joint-cali). OzNet rainfall data are used for the calibration.

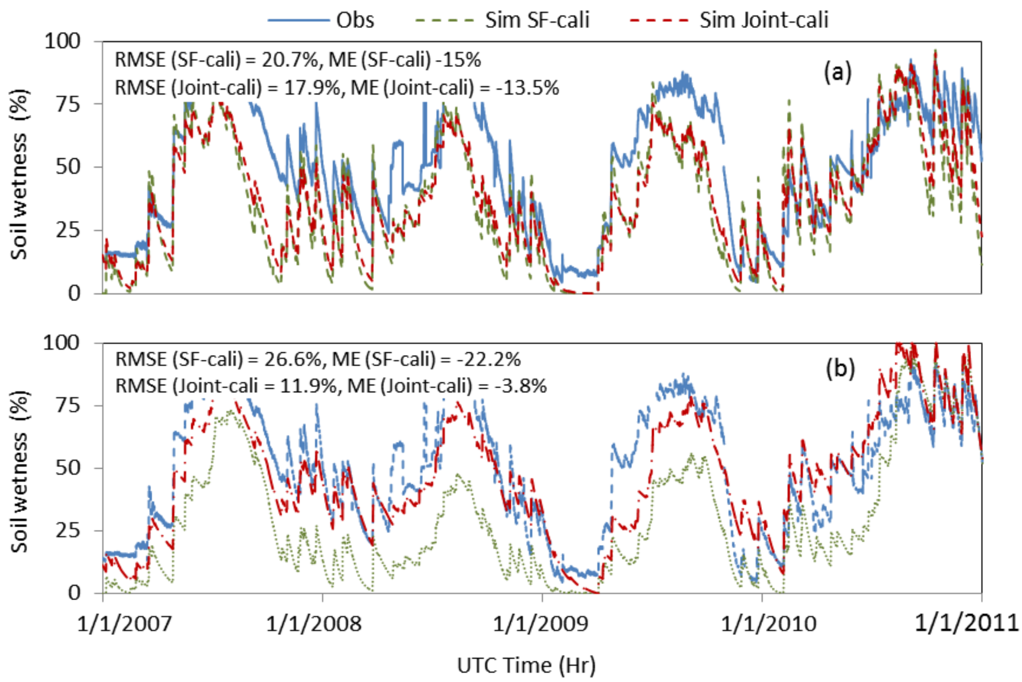

Figure 4.7: Same as Figure 4.6 but for the Adelong Creek subcatchment.

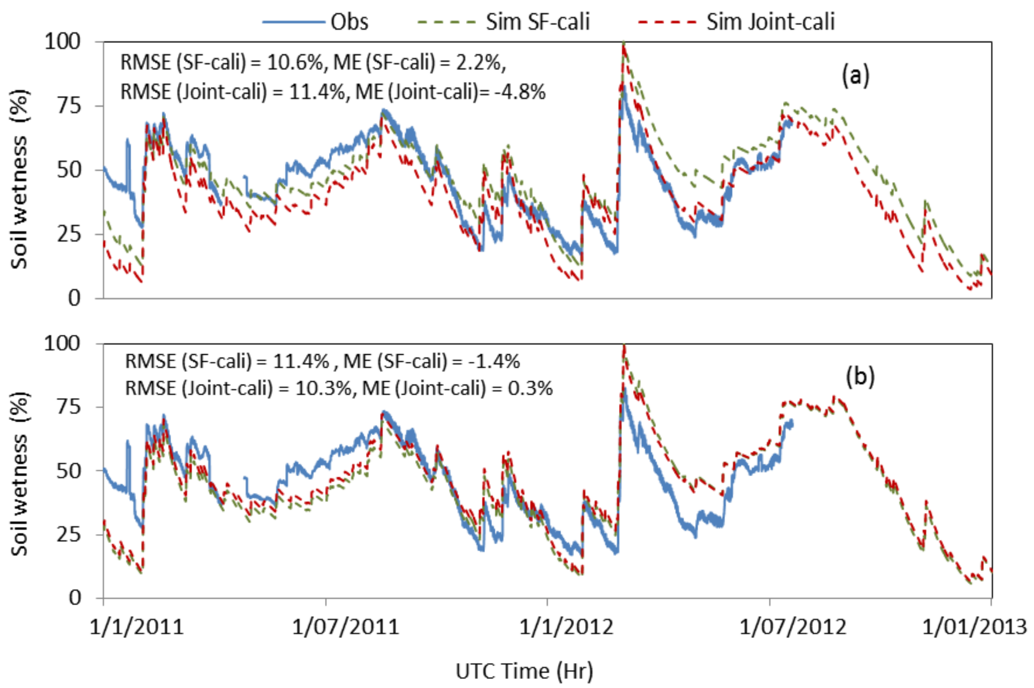

Figure 4.8: Observed and simulated soil wetness for GR4H (a) and PDM (b) for the validation period in the upper Kyeamba subcatchment; Calibration is to streamflow alone (SF-cali) and to streamflow and soil moisture jointly (Joint-cali). Operational rainfall data are used for the validation.

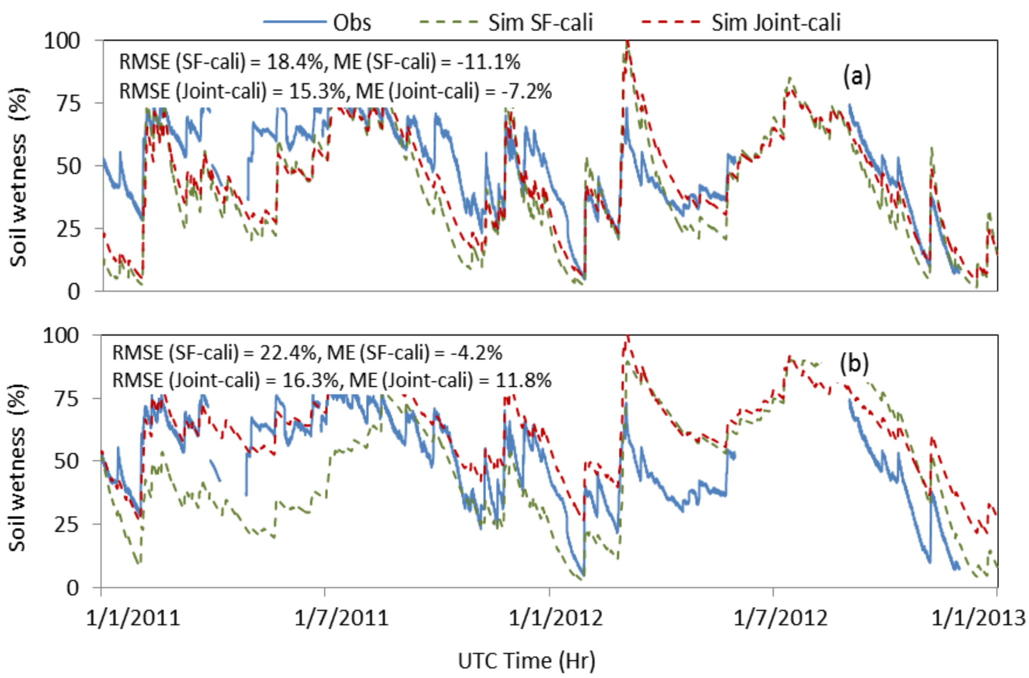

Figure 4.9: Same as Figure 4.8 but for the Adelong Creek subcatchment.

It is important to recognise that possible uncertainties in the observational data, including streamflow, rainfall and soil moisture observations, will have an influence on the modelling skill scores and the errors in the calibration and validation period. While the joint-calibration scheme buffers the uncertainties in the rainfall and streamflow observations in the calibration, this could also bring some other uncertainties into the modelling due to errors in the soil wetness observation estimations. For example, the average of the volumetric soil moisture has been calculated over the equivalent depth, as implied by the size of the soil water store in the model. The value of the equivalent depth was estimated based an approximate soil porosity value assumed to be 0.4 for the study subcatchments, based on Australian Soil Resource Information System (http://www.asris.csiro.au/themes/Atlas.html). Furthermore, some investigations on the accuracy of the soil moisture observations from the field measurements are required for application of this calibration method as the estimated soil wetness observation is very sensitive to the changes in the volumetric soil moisture data.

4.4.3 Event-based Evaluation of Streamflow

There were some big runoff events in 2010 and 2012 in the Murrumbidgee catchment resulting in floods. Here, the focus is on the streamflow and soil moisture predictions in the two focus subcatchments during these periods. To evaluate the model streamflow and soil moisture prediction skill, Figure 4.10 compares observed flow and soil wetness in Kyeamba subcatchment with simulated flow and soil wetness using parameters from SF-calibration and joint-calibration for the two events, October 2010 (calibration) and March 2012 (validation). The same plots are presented in Figure 4.11 for the Adelong subcatchment. In Figures 4.10(a) and (c), there were small differences in streamflow simulation in October 2010 (calibration) between SF-calibration and joint-calibration for the Kyeamba area. However, in March 2012 (validation), the magnitude of the peak flows between the two calibration approaches was not very different in GR4H, but was slightly improved in PDM for the second flow in this subcatchment. In these figures, both models had poor performance in terms of the peak value, shape and timing of the flow for the event in 2012. GR4H had better shape in flow for the second flow but with a bigger timing error than PDM. Therefore, despite the small degradations from GR4H in Cal.1 and Val.3 scores in Table 4.2, the performance of GR4H did not change significantly after joint-calibration.

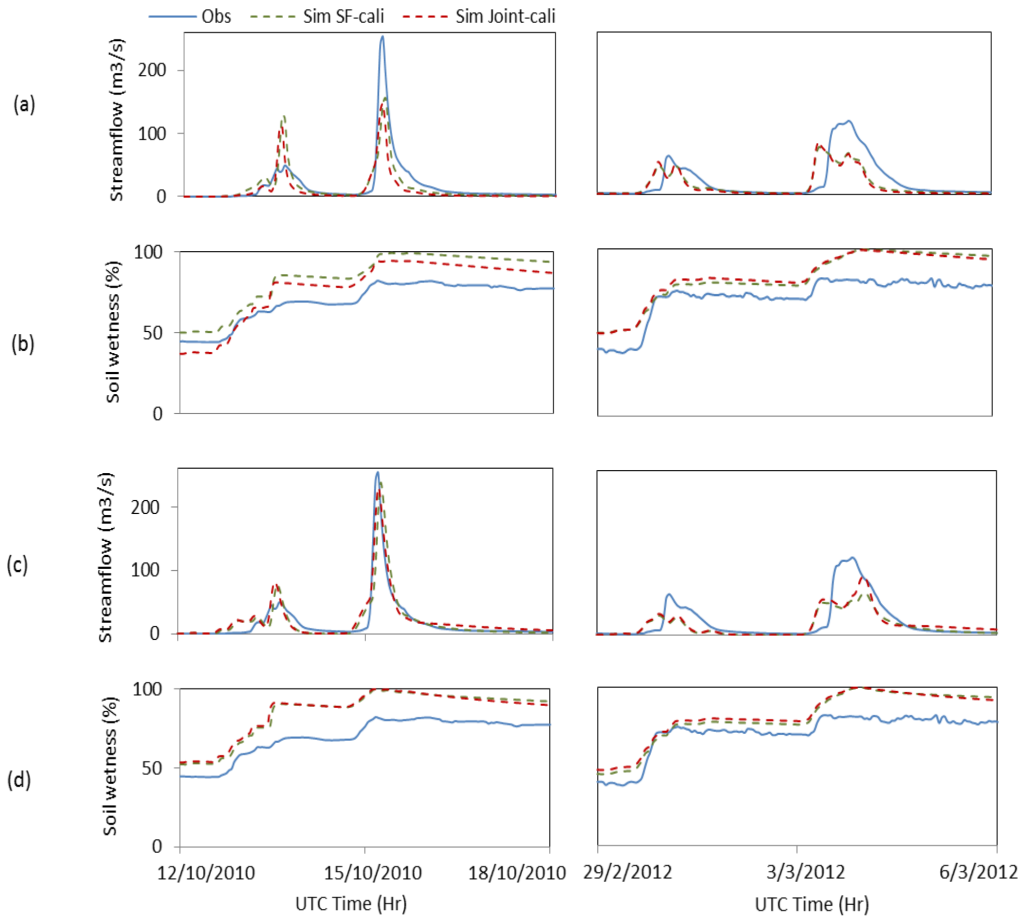

Figure 4.10: Comparison of observed and simulated streamflow and soil wetness from GR4H (a and b) and PDM (c and d) models for a calibration event (left) using OzNet rainfall data, and a validation event (right) using operational rainfall data, after calibration to only streamflow (SF-cali) and calibration to both streamflow and soil moisture (Joint-cali) in the upper Kyeamba Creek catchment.

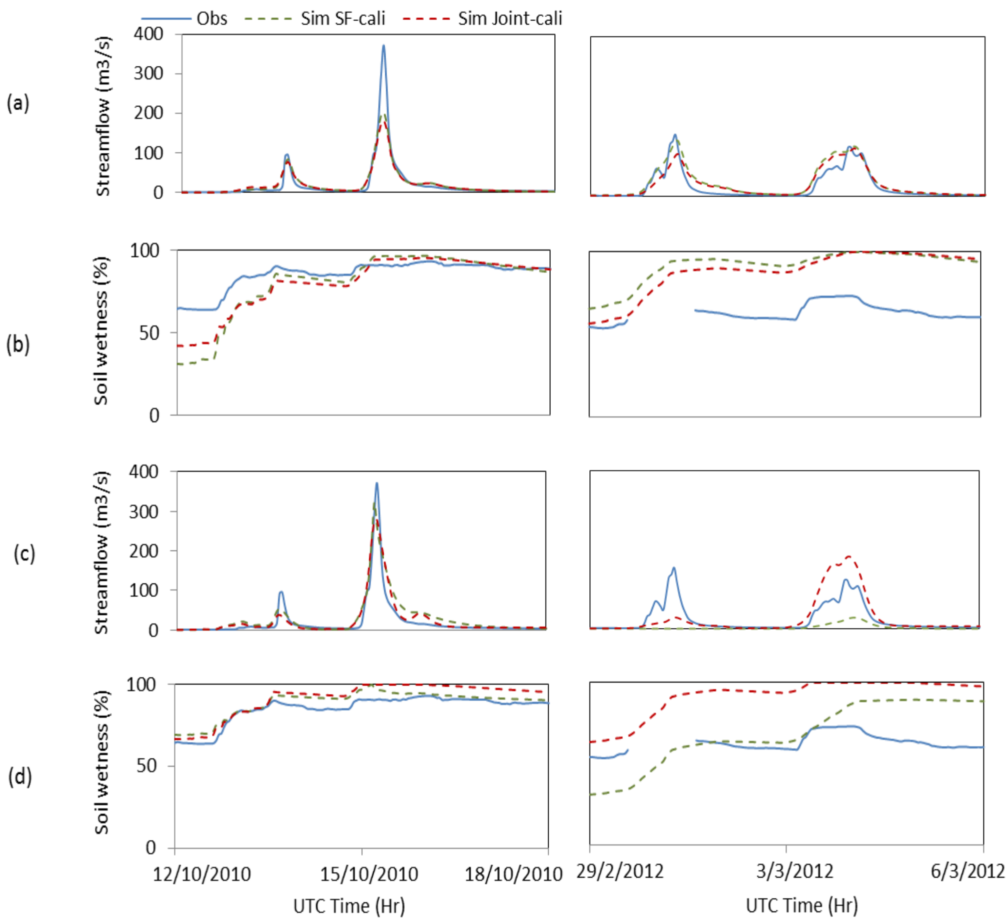

Figure 4.11: Same as Figure 4.10 but for the Adelong Creek catchment.

Figures 4.11(a) and (c) show that there are some small degradations in flow simulations in October 2010 in the Adelong area for both models after joint-calibration compared to SF-calibration alone. In March 2012, GR4H underestimated the first flow after joint-calibration, while it was well predicted using parameters from SF-calibration. However, there was no change in the second flow prediction. PDM strongly underestimated both events in 2012 for SF-calibration, while it performed slightly better in the first event and overestimated the second event. As shown in Figures 4.10(d) and 4.11(d), PDM showed 100% saturation for both calibration approaches in Kyeamba and for joint-calibration in the Adelong area. GR4H did not reach 100% saturation for joint-calibration in

Kyeamba and for both calibration schemes in the Adelong area in October 2010, as seen in Figures 4.10(b) and 4.11(b). From the event-based evaluation shown in Figures 4.10 and 4.11, it was found that PDM had better performance than GR4H in the calibration period, while it did not outperform GR4H in the validation.

4.5 Chapter Summary

This chapter evaluated streamflow modelling results from the GR4H and PDM hydrological models in two Australian subcatchments, using calibration to streamflow and joint-calibration to streamflow and soil moisture observations. Soil moisture storage in the models has been evaluated against soil moisture observations from field measurements. Results from the calibration and validation indicated that the GR4H and PDM models had a different streamflow and soil moisture simulation performance in the same study subcatchments depending on the event and calibration approach. The PDM model had the best performance in terms of both streamflow and soil moisture estimations during the calibration period, but was outperformed by the GR4H model during the validation period. It was also shown that the soil moisture estimation was improved significantly by joint-calibration to streamflow and soil moisture for the case where streamflow and soil moisture estimations were poor. In other cases, addition of the soil moisture constraint did not degrade the results.

Chapter 5

Satellite-based Soil Moisture Impact on Streamflow Prediction

This chapter demonstrates the impact of remotely sensed soil moisture observations on streamflow prediction in two rainfall-runoff models, GR4H and PDM, when soil moisture state in the models is updated through a nudging approach. Several subcatchments in the study area are calibrated using streamflow observations alone, while two of the subcatchments have been jointly calibrated to streamflow and soil moisture observations in Chapter 4. Based on the model joint calibration to streamflow and soil moisture, the model predictions are further constrained with root-zone soil moisture observations by a nudging approach, and evaluated in terms of improved soil moisture and streamflow prediction skill. Since the satellite measurements only give an estimate of soil moisture for the near-surface layer, root-zone satellite soil moisture are estimated for one example subcatchment, Kyeamba Creek, using CDF-matching, and two filtering methods (exponential filtering and moving average) and benchmarked against in-situ data. The best approach for estimating root-zone satellite soil moisture is then used for the entire study site. For comparison, the models are also constrained with root-zone in-situ soil moisture observations in two subcatchments, Kyeamba and Adelong Creek, where monitoring stations are available.

5.1 Study Site and Data Sets

The study site is located between the gauging stations downstream of the Burrinjuck and Blowering dams and the township of Wagga Wagga. This area is selected to simplify modelling of the effect of regulated flows due to Burrinjuck and Blowering dams. The study site consists of 10 subcatchments that include 63 subareas, with a total area of about 10,886 km^2. Based on topography and river network information, the entire study catchment was delineated into several subcatchments which were divided into subareas. Therefore, the hydrological models were run using a semi-distributed approach for the entire area, and a lumped approach for the subcatchments with single subareas (e.g., Kyeamba Creek) using unique rainfall and potential evaporation input data for the subareas and spatially uniform hydrologic model parameters over each subcatchment. The GR4H (Mathevet, 2005) and PDM (Moore, 2007) hydrological models were used for this study, to understand the impact of satellite-based soil moisture constraint on streamflow modelling in the Murrumbidgee catchment. Full descriptions of the models were given in Chapter 4. Runoff routing between subareas was presented by a linear Muskingum channel routing method which has two parameters, k and x (Gill, 1978):

$$S_m = k[Ix-(1-x)O] \ , \tag{5.1}$$

where S_m is the storage within the routing reach, I and O are the inflow and outflow the reach, respectively, k is the storage time constant parameter and x is a weighting factor parameter.

OzNet monitoring stations are available for three of the subcatchments; Kyeamba, Adelong and Muttama Creek. The location of the study site, subcatchments and OzNet monitoring stations are shown in Figure 5.1. The OzNet rainfall and soil moisture observations (Smith et al., 2012) from monitoring stations in the Kyeamba and Adelong subcatchments (K1, K2, K3, K4, K5, K7, A1, A2, A3, A4 and A5) are used from January 2007 to December 2012. The OzNet observations (rainfall and soil moisture) from the M3 station were not used for the Muttama creek subcatchment in this study as the data was missing due to the instrument breakdown during many months of the selected study period. The rainfall observations from the most representative OzNet stations among the five rain gauges within each of the Kyeamba and Adelong subcatchments (K2, K3, K4, K5, K7, A1, A2, A3, A4 and A5) were aggregated to hourly time scale for use in the model calibration from 2007 to 2010, as the most accurate rainfall data available in these two subcatchments. The station K1 was excluded from the analysis as the rainfall in this rain gauge was very different from other the other K stations.

Since the OzNet data is not continuously available for all the stations during the validation/testing period (January 2011 to December 2012), operational real-time rainfall observations used in flood forecasting by Australian BoM in Australia were used on hourly time steps for validation of these subcatchments over January 2011 to December 2012. Operational rainfall data was also used for calibration and validation of all other subcatchments over the periods of 2007 to 2010 and 2011 to 2012 respectively. The operational data was interpolated to all subareas in the entire study site using inverse distance squared weighting method. Six years of real-time streamflow observations (2007-2012) from 10 stream gauges (locations shown in Figure 5.1) are used for evaluation of the model outputs. These were obtained from the New South Wales office of Water database (See http://www.water.nsw.gov.au/realtime-data). The PET data is derived from the Australian Water Availability Project (AWAP) gridded monthly analysis data (AWAP; Raupach et al., 2009) with about 5 km spatial resolution. This was interpolated to all subareas within the study site using inverse distance squared weighting method for application in this work. The monthly PET values were then disaggregated to hourly data by dividing the monthly values by the number of hours in the months.

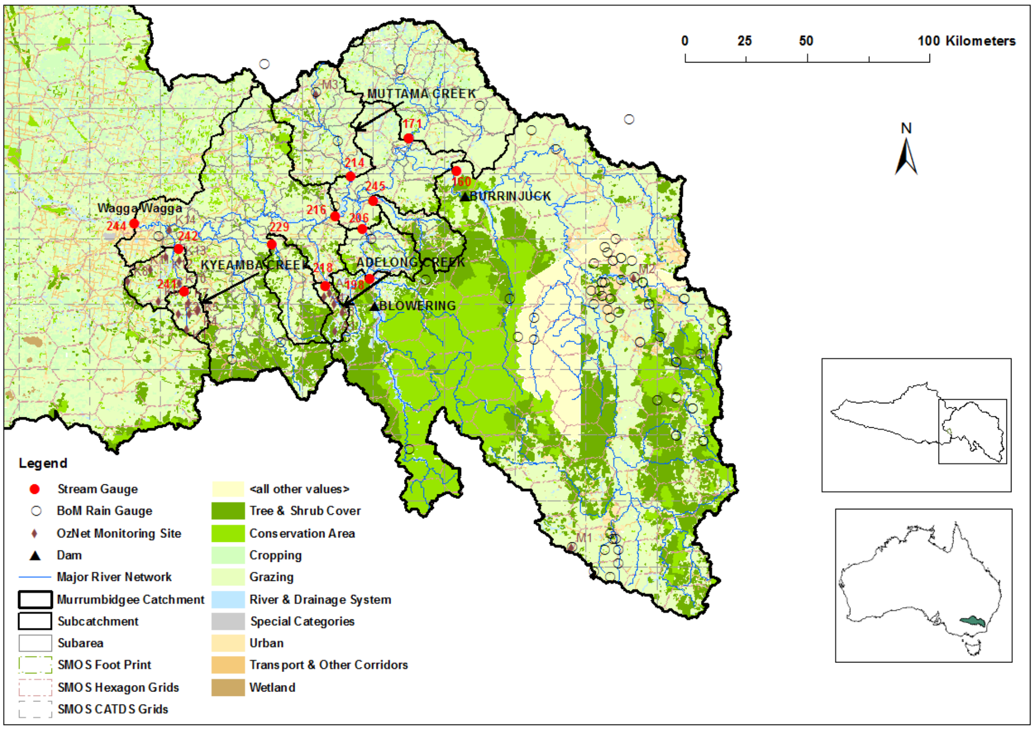

Figure 5.1: Location of BoM operational rain gauges, OzNet monitoring stations, stream gauges, Kyeamba Creek, Adelong Creek and Muttama Creek subcatchments in the Murrumbidgee catchment.

Volumetric soil moisture observations from the stations in the Kyeamba Creek and Adelong Creek subcatchments are available on either 20 or 30 min time intervals at depths of 0-8, 0-30, 30-60 and 60-90 cm. The data were aggregated and analysed on hourly time steps to estimate the best average soil moisture in these two subcatchments. The detail of this analysis has been explained in Chapter 4. These two subcatchments were jointly-calibrated to both streamflow data and subcatchment average root-zone soil moisture observations from OzNet monitoring stations. The method used for soil moisture estimation and the effectiveness of the calibration approach as compared to the calibration to streamflow alone has been also presented in Chapter 4. The other subcatchments within the study area here were calibrated to only streamflow as there were no in-situ soil moisture data available in this area. The satellite soil moisture observations were not available from 2007 to 2009 to be used for the model calibration purposes. The in-situ soil moisture observations were used as the reference data for estimation of satellite-based root-zone soil moisture in the Kyeamba subcatchment, and also for direct insertion into the models and comparison with the satellite-based model constraint results in both Kyeamba and Adelong subcatchments.

In this study, the Level 3 daily soil moisture product from SMOS generated by Center Aval de Traitemnet des Donnees, known as SMOS CATDS, has been used as the satellite near-surface observations (See http://www.catds.fr). The Level 3 CATDS data is available as volumetric soil moisture with a temporal repeat of two to four days and is processed from the ESA Level 1B brightness temperature product. The algorithm is based on the level 2 soil moisture retrieval which is done by a standard iterative minimization of a cost function (Kerr et al., 2012). For the Level 3 product, several overpasses of multiangular observations over a 7-day window is considered (Jacquette et al., 2010; Al-Yaari et al., 2014) and the data is presented on the EASE (Equal Area Scalable Earth) gridding system with a spatial resolution of 25 km (rectangular grey grids with dashed lines in Figure 5.1). While the SMOS mission provides continuous radiometric measurements over the Earth surface at 42 km footprint resolution, different ESA products have been reported on a 15 km hexagonal Discrete Global Grid (DGG). According to the study performed by Dumedah et al. (2014), the SMOS data can be used directly on the DGG, or any regular grid of equivalent spatial resolution, without significant downgrading the accuracy. Thus, there is expected to be little difference between using the SMOS observations with 42 km resolution or on the DDG or CATDS grids. The SMOS footprints, ESA rectangular grids and the DGG are shown in Figure 5.1.

5.2 Methodology

5.2.1 Estimation of Satellite Root-zone Soil Moisture

The satellite-based soil moisture data represent the soil moisture in the top few centimetres of soil only. While the root-zone soil moisture values have been found to have strong correlation with surface soil moisture values, because both are affected by the weather pattern during the preceding few days to weeks (eg., Albergel et al., 2008), the root-zone layers typically have a smaller temporal variation and a lag in time (Bisselink et al., 2011). Consequently, a filtering approach has often been used to smooth and lag the surface soil moisture to better represent the root-zone soil water content needed for hydrological model application (Wagner et al., 1999).

The two CATDS soil moisture pixels overlaying the Kyeamba catchment were selected for potential use in this study. To have the most accurate estimation of soil moisture in this subcatchment, the near-surface soil moisture from the northern pixel with less tree cover was used (see Figure 5.1). The near-surface satellite soil moisture was similarly estimated for each of the 63 subareas in the entire study site, being between Wagga Wagga and the Blowering and Burrnjuck dam outlets. To run on a semi-distributed mode, the forcing data information (rainfall, evapotranspiration and soil moisture data) was interpolated onto each subarea within the subcatchments.

Since the satellite surface soil moisture observations contain fluctuations larger than those naturally occurring, the data was first de-noised by calculating a 3-day central moving average of the satellite data according to a study by Draper et al. (2009b). While Draper et al. (2009b) used a 5-day moving average for de-noising, a smaller time window with 3-day length was chosen here based on the lower frequency noises in the SMOS data as compared to AMSR-E. To retrieve root-zone estimation of soil moisture, three methods were tested; a Cumulative Density Function (CDF) matching, exponential filtering and moving average filtering. The CDF-matching was used to rescale the CDF of the near-surface satellite soil moisture retrievals to the CDF of the in-situ root-zone soil moisture observations in the Kyeamba subcatchment, by fitting a degree 5 Polynomial function (Brocca et al., 2011) to the difference between the two soil moisture data sets. The three methods were first applied for the Kyeamba subcatchment as an example site, to estimate the parameters required for CDF-matching or the two filtering approaches, and select the best approach. To account for direct application of rescaling or filtering for root-zone soil moisture estimation in subcatchments where there are no ground-based soil moisture observations, the best approach, which was chosen based on comparison with in-situ data in the Kyeamba area, has been used for all other subcatchments in the study site.

The exponential filter described by Wagner et al. (1999) is a simple method to approximate root-zone soil moisture values from near-surface observations, which assumes that the time variation of the soil moisture profile is linearly related to the difference between the surface and the profile values. In this study, the recursive formulation of the method is used (Albergel et al., 2009):

$$SWI_n = SWI_{n-1} + K_n(SSM_{tn} - SWI_{n-1}), \tag{5.2}$$

$$K_n = \frac{K_{n-1}}{K_{n-1} + e^{-\left(\frac{T_n - T_{n-1}}{T}\right)}}, \tag{5.3}$$

where SWI is the profile Soil Wetness Index, SSM is the satellite near-surface soil moisture retrieval and T is a parameter called the characteristic time length, representing the temporal variation of soil moisture within the root-zone profile; the gain K_n ranges between 0 and 1. For initialisation, K_1=1 and SWI_1=SSM_{t1}.

The second filtering method is based on a backward moving average (Draper et al., 2009b). This simple method was used for comparison with the former filtering method. For the moving average approach the average of soil moisture was calculated at each time step by averaging over a specific number of days in the past using:

$$\mathrm{SWI}_{\mathrm{root,n}} = \frac{\sum_{\mathrm{i=n\text{-}d}}^{\mathrm{i=n}} (\mathrm{w_i} \times \mathrm{SWI}_{\mathrm{surf,i}})}{\sum_{\mathrm{i=n\text{-}d}}^{\mathrm{i=n}} \mathrm{w_i}} \ , \qquad (5.4)$$

where w_i is the multiplicative weight representing the recency of the observations, and d is the number of days used to define the time window for observations to be used in the calculation.

The parameter T in the exponential filter used in equation (5.3), the parameter d and the multiplicative weights in the moving average in equation (5.4) were calibrated by minimising the root mean square error between average of OzNet in-situ soil moisture data over the depth 0-90 cm using six K stations in the Kyeamba subcatchment and root-zone satellite-based estimations in this area. Both SMOS and in-situ data are expressed in volumetric terms (m^3/m^3) while the modelled data are in terms of soil wetness. Consequently, the SMOS and in-situ root-zone data were scaled to a value between 0 and 1 using the minimum and maximum soil moisture for each individual dataset. This normalisation allows for a consistent comparison of the satellite-based root-zone soil wetness estimations, the in-situ soil wetness observations, and the modelled soil wetness.

5.2.2 Data Assimilation Technique

A nudging scheme was used to update the modelled soil wetness ($SW_{sim,i}$), whenever a soil wetness observation ($SW_{obs,i}$) becomes available (Dharssi et al., 2011; Brocca et al., 2013):

$$\mathrm{SW}_{\mathrm{ass,i}} = \mathrm{SW}_{\mathrm{sim,i}} + \mathrm{G}\left(\mathrm{SW}_{\mathrm{obs,i}} - \mathrm{SW}_{\mathrm{sim,i}}\right), \qquad (5.5)$$

where i is time, $SW_{ass,i}$ is the updated modelled soil wetness and G is a constant weighting parameter. G represents the relative weight of the uncertainties of the model estimation against the observation:

$$\mathrm{G} = \frac{\sigma_{\mathrm{sim}}^2}{\sigma_{\mathrm{sim}}^2 + \sigma_{\mathrm{obs}}^2} \ , \qquad (5.5)$$

where σ^2_{obs} and σ^2_{sim} are the error variance of observed and modelled soil wetness respectively. For G equal to 1 the observations are assumed perfect (direct insertion), and for G equals to 1 the model estimations are assumed with no error (open loop). In this work, for SMOS data assimilation the values of the errors utilized in equation (5.6) were determined based on the error estimates of satellite and modelled root-zone soil wetness which were obtained against OzNet soil wetness observations.

5.2.3 Evaluation of Models

The two rainfall-runoff models, GR4H and PDM, were calibrated jointly to both streamflow and OzNet root-zone soil wetness observations for Kyeamba and Adelong subcatchments for the period of January 2007 to December 2010 based on the multi-objective function described in Chapter 4, section 4.3.1. In all other subcatchments, the models were calibrated to streamflow observations alone using mean squared error (MSE) as the objective function (see Chapter 4, section 4.3.1). In both calibration approaches, the Shuffled Complex Evolution (SCE) method was used to automatically calibrate the models. Nash-Sutcliffe Efficiency (NSE; Nash and Sutcliffe, 1970) coefficient was used to evaluate the performance of the models based on observed and simulated streamflow according to:

$$NS=1-\frac{\sum_{i=1}^{n}\left(Q_{obs,i}-Q_{sim,i}\right)^2}{\sum_{i=1}^{n}\left(Q_{obs,i}-\overline{Q}_{obs,i}\right)^2}\ . \tag{5.6}$$

The model performance was evaluated during the validation period January 2011-December 2012 for both with and without the application of satellite-based root-zone soil moisture data. To update the soil moisture state in the models, the nudging approach was chosen. This is a simple data assimilation approach as a trade-off between computationally efficiency, ease of implementation, and relevance to the single soil water store in the models used here, and not accounting for the observation uncertainty/model uncertainty.

5.3 Results

5.3.1 Assessment of SMOS Surface Soil Moisture

Near-surface soil moisture from L3-daily CATDS has been assessed against near-surface soil wetness obtained from in-situ OzNet stations at depth 0-8 cm, using data from the Kyeamba subcatchment at the time of the SMOS satellite overpass. The near-surface soil moisture retrievals from SMOS before and after de-noising is compared against the average of in-situ observations from six OzNet stations in the Kyeamba catchment for the depth of 0-8 cm in Figure 5.2 and the scatter plots of the data have been compared in Figures 5.3(a) and (b). The RMSD and correlation coefficient (R) between the datasets are shown in Figure 5.3. In Figure 5.2, the range of soil moisture from six Kyeamba stations (K1, K2, K3, K4, K5 and K7 shown in Figure 5.1) has been shown in grey colour. The comparison is for data from January 2010 to July 2012, as this was the overlap period with the most available data. RMSD and bias between the in-situ and SMOS near-surface observations did not change after de-noising being 0.06 and -0.02 m^3/m^3, while R increased slightly from 0.74 to 0.77.

The RMSD and bias found between SMOS and in-situ observations here are in agreement with the ranges estimated by Ridler et al. (2014) for SMOS retrievals against average in-situ network over western Denmark (0.049 to 0.14 and -0.02 to -0.13 m^3/m^3 respectively). RMSD, bias and correlation estimated in this work are slightly different from those found by Lievens et al. (2015) with average values of 0.091, -0.019 and 0.69 respectively for SMOS near-surface observations, but against 49 OzNet stations across a larger area of south-eastern Australia. Other researchers have also had consistent ranges of error estimation with those of this thesis (Rüdiger et al., 2011; Al Bitar et al., 2012).

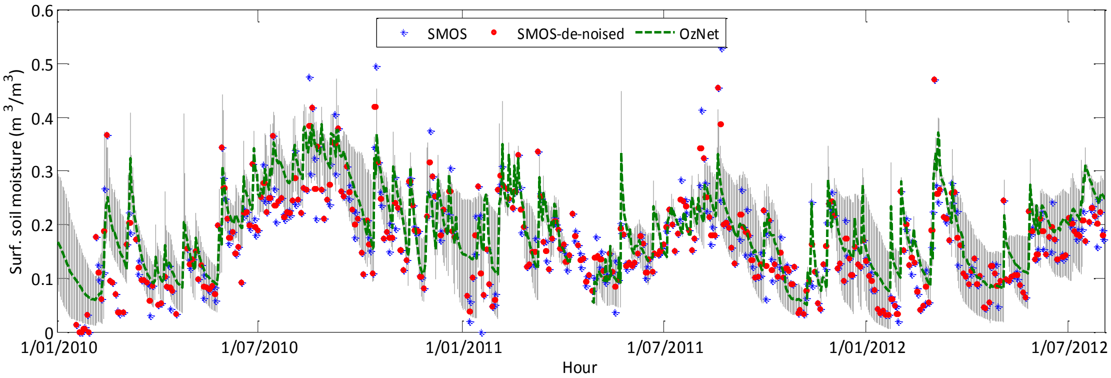

Figure 5.2: Comparison between OzNet soil moisture measurements at depth 0-8 cm and SMOS near-surface soil moisture observations before and after removing the noise in the Kyeamba subcatchment; data are from January 2010 to July 2012.

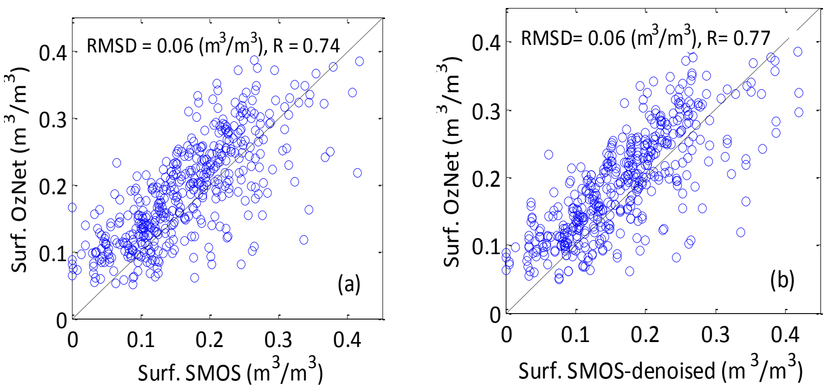

Figure 5.3: Scatter plots of OzNet soil moisture at depth 0-8 cm and SMOS near-surface soil moisture observations before (a) and after de-noising (b) in the Kyeamba subcatchment; data are from January 2010 to July 2012.

5.3.2 Estimation of SMOS Root-zone Soil Wetness

The root-zone SMOS soil wetness has been estimated from the near-surface de-noised data in the Kyeamba subcatchment using CDF-matching and exponential and moving average filtering methods in this catchment. The CDF of the OzNet data and near-surface SMOS observations, before and after CDF-matching, and the polynomial function used to correct the SMOS data by fitting the SMOS to the corresponding differences between the data sets, are illustrated in Figure 5.4. The parameters for this function were calibrated using in-situ data from January 2010 to July 2012. As shown in Figure 5.4(a), the CDF of SMOS matches the CDF of the OzNet data completely after applying the method. The parameter of characteristic time length (T) in the exponential filter was optimised to a value of 12 days, which was estimated by minimising the RMSD between the average of observed root-zone in-situ soil moisture from the six OzNet stations in the Kyeamba subcatchment and the root-zone soil moisture estimated from SMOS over the period January to December 2010.

The optimal parameter T obtained here is slightly lower than the optimal values of this parameter found by Wagner et al. (1999), who indicated that for soil layer depths of 0-20 and 0-100 cm any choice of T between 15 to 30 days produced reasonable results. However, it is consistent with the optimum value of T in other studies, such as that by Alvarez-Garreton et al. (2014) who found a value of 9 days for a soil layer of 180 cm. The optimum value of T is no doubt dependent on the depth of soil layer as well as soil characteristics of the study area, such as hydraulic conductivity, slope, depth to groundwater and underlying material. For the moving average method, the parameter d, which is the number of days in the smoothing time window, was optimised to a value of 26 days using the in-situ data for the same period as the exponential filtering. The optimised weights in equation (5.4) varied from 0.04 to 1.9 and showed that from the most recent days to the early ones, on average, there is a descending trend in the weights within the moving average window. This showed that the moving averaged profile estimations are more dependent on the surface soil moisture values from the latest days rather than the early days with long lags on the time window.

After rescaling or filtering the data, both root-zone in-situ and SMOS-based soil moisture were normalised to values between 0 and 1 using the maximum and minimum values of each datasets from January 2010 to July 2012. This normalisation allowed direct comparison between the datasets. To assess the robustness of the methods in estimating profile soil wetness, the root-zone SMOS-based soil wetness was compared to root-zone in-situ soil wetness data from January 2010 to July 2012. The time series of root-zone soil wetness from satellite and in-situ measurements are presented from the CDF-matching, exponential filtering and moving average in Figure 5.5.

The scatter plots of the datasets and the RMSD and R between them are also shown in Figures 5.6(a) to (c). The results before normalising the data (not presented here) showed that the RMSD between root-zone soil moisture estimations and in-situ soil moisture data for January 2010 to December 2012 was 0.03, 0.09 and 0.1 m^3/m^3 for CDF-matching, exponential filtering and moving average filtering respectively and the correlation coefficient (R) equals to 0.70, 0.93 and 0.92 for the methods respectively. Wagner et al. (1999) found smaller average RMSE between ERS scatterometer root-zone soil moisture and in-situ root-zone soil moisture at soil layer with depth 0-100 cm being equal to 0.04 m^3/m^3 on average when using exponential filtering, with smaller average R between 0.33 to 0.49. As presented in Figures 5.6, after converting the data into to soil wetness, the RMSD between the CDF-matched SMOS estimates and the in-situ data was large and the R was small as compared to the two other methods. While qualitatively there was no significant difference between exponential filtering and moving average results in Figure 5.6, the smallest RMSD and maximum R were obtained from exponential filtering. Consequently, the exponential filtering method was selected for the remainder of this study with a characteristic time length of 12 days.

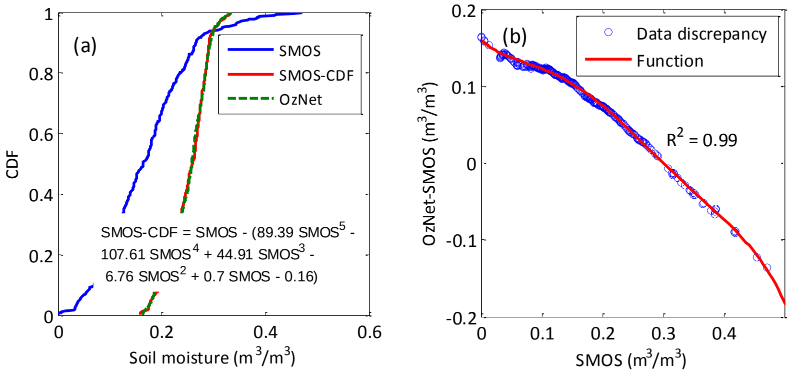

Figure 5.4: Cumulative density function for OzNet soil moisture at depth 0-90 cm, near-surface SMOS data (SMOS) and root-zone SMOS data (SMOS-CDF) obtained from CDF-matching approach (a) and the difference between the root-zone OzNet and near-surface SMOS data prior to CDF-matching (b) in the Kyeamba subcatchment; data are from January 2010 to July 2012.

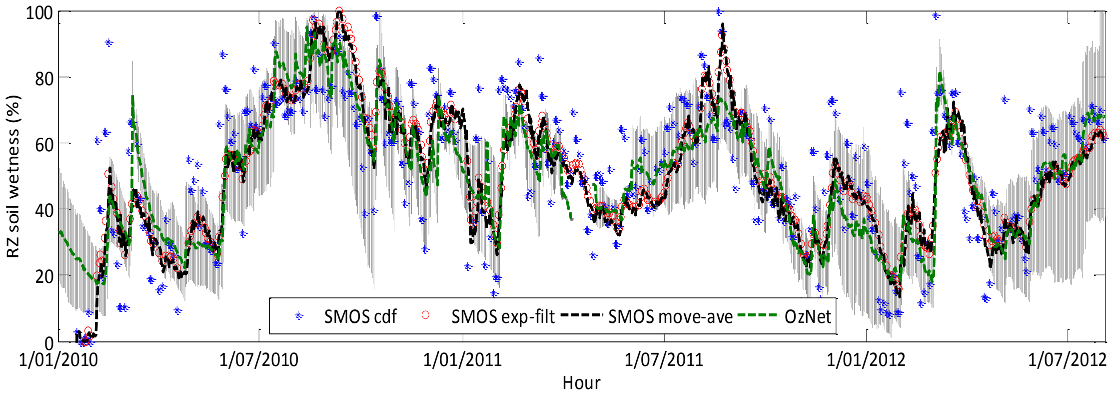

Figure 5.5: Comparison between SMOS-based root-zone estimations and average of OzNet soil wetness observations over the depth 0-90 cm for CDF-matching, exponential filtering and moving average approaches in the Kyeamba subcatchment; data are from January 2010 to July 2012 and the OzNet observation range has been shown in grey colour.

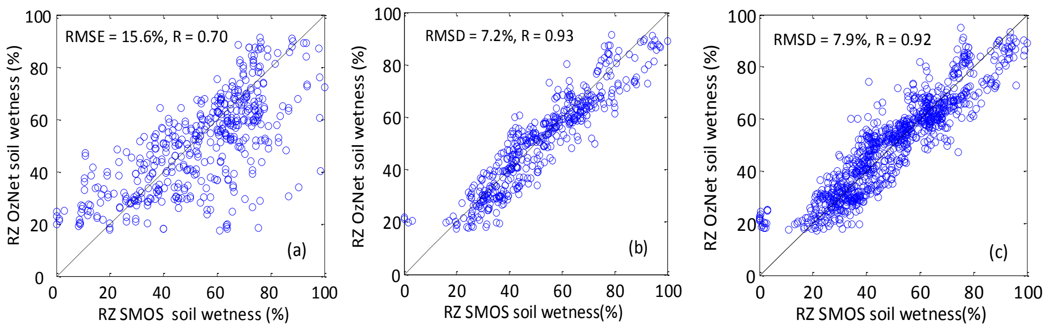

Figure 5.6: Scatter plots of mean OzNet soil wetness over depth 0-90 cm and SMOS-based root-zone estimations from CDF-matching (a), exponential filtering (b) and moving average (c) approaches in the Kyeamba catchment; data are from January 2010 to July 2012.

It should be mentioned that the exponential filtered/moving averaged satellite-based estimations have been alternatively rescaled to either OzNet root-zone volumetric soil moisture data or modelled soil water predictions using CDF-matching, to investigate the effect of different approaches on the SMOS estimates. The SMOS root-zone estimates from the alternatives have been evaluated against both OzNet data and model predictions. The results for this evaluation have been presented in Appendix A2. Based on the evaluation of SMOS estimations against OzNet in-situ data which is the reference data, CDF-matching to OzNet data showed better skill scores than CDF-matching to model predictions when they were evaluated against the OzNet data, and there is small difference between the skill scores form exponential filtering alone and exponential filtering followed by CDF-matching to the OzNet data.

5.3.3 Application of SMOS in the Kyeamba Subcatchment

The root-zone soil wetness derived from SMOS was assimilated into the prediction models for the Kyeamba subcatchment (January 2011 to December 2012) using the nudging approach to investigate the possible improvement in the model performance. The models were also separately constrained by direct insertion of in-situ root-zone soil wetness observations from OzNet stations as the reference data, to investigate the difference between using satellite or ground measurements. This is important to understand for the later application in the other subcatchments where only SMOS data are available.

The operational rainfall observations and the observed streamflow in the Kyeamba subcatchment that were used in this validation are shown in Figure 5.7(a). Two events for which the in-situ and satellite-based soil wetness were tested in this subcatchment are shown. In Figures 5.7(b) and (c), the root-zone soil wetness data from OzNet stations and SMOS are compared to model soil wetness predictions before and after assimilation during the validation period (2011-2012) for the GR4H and PDM models respectively. The scatter plots, RMSD and R of the data sets are presented in Figure 5.8(a) to (d). Figures 5.7(b) and (c) show that there was typically a bigger difference between model predicted and observed streamflow during the peak flows when using SMOS derived root-zone soil moisture as compared to OzNet observations. As presented in Figure 5.8, the RMSD and R of SMOS for GR4H were16% and 0.82 which were quite similar as PDM (15%, 0.81). The RMSD and R between the OzNet data and predicted soil wetness from either model was 16% and 0.85.

According to the error estimations in sections 5.3.2 and 5.3.3 in this thesis, RMSD between the SMOS root-zone estimations and the in-situ data was 7.2%, and RMSD between the GR4H and PDM models and in-situ OzNet soil wetness was 15% and 16% respectively. Thus, based on RMSD between OzNet data and either the model or SMOS, which may be considered equivalent to standard deviation of the data, the parameter G in equation (5.6) was expected to be approximately 0.8. The observed and simulated streamflow and root-zone soil wetness before and after the insertion of OzNet and after assimilation of SMOS root-zone soil wetness with G equal to 0.8 and 1 in the models are compared for a small event in February 2011 and a major event in February/March 2012 for the Kyeamba subcatchment in Figures 5.9 and 5.10 respectively. It is clear from these figures that the models underpredicted the soil wetness at the time of the small peak flows and overpredicted the soil wetness during the moderate or major peak flows as compared to the OzNet or SMOS observations.

Figure 5.7: Input precipitation data and observed streamflow (a) and comparison between OzNet average soil wetness observation (OzNet), SMOS-based profile soil wetness obtained from exponential filtering (SMOS exp-filt), modelled soil wetness with insertion of the SMOS data (DI-SMOS) and open simulation (Sim) from GR4H (b) and PDM (c) in the Kyeamba subcatchment from January 2011 to December 2012.

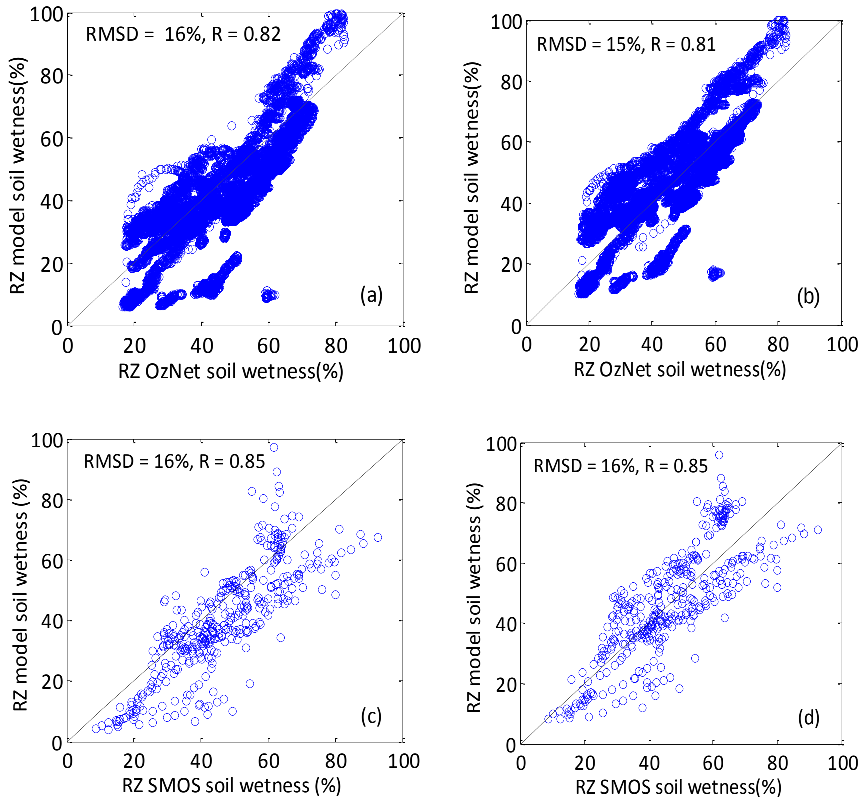

Figure 5.8: Scatter plots of OzNet root-zone soil wetness (a and b) and SMOS-based root-zone soil wetness obtained from exponential filtering (c and d) against modelled soil wetness from GR4H (a and c) and PDM (b and d) in the Kyeamba subcatchment; the OzNet data vs modelled data is hourly from January 2011 to July 2012 due to availability of observations, and the SMOS data vs modelled data is every 2 to 3 days from January 2011 to December 2012.

As presented in Figures 5.9(a) to (d), after assimilation (nudging with G equal to 0.8 or direct insertion) of OzNet or SMOS data into the models, the increased soil wetness in the models increased streamflow for the peaks in both models, whereas reductions in the simulated streamflow were actually needed for improving streamflow predictions. Similarly, Figures 5.10(a) to (d) show that after the assimilation the skill of the models in streamflow prediction was degraded for the second peak, as the soil moisture values in the models were decreased resulting in a reduction of streamflow, whereas an increase in streamflow was required, while the prediction of the first peak was not changed significantly. These results highlight the deficiency of the models to translate soil moisture and rainfall to correct values of runoff.

To evaluate root-zone soil moisture estimates obtained from different rescaling approaches, assimilation results from SMOS estimations obtained by exponential filtering alone, CDF-matching to OzNet data after exponential filtering, and CDF-matching to model predictions after exponential filtering have been compared for the Kyeamba subcatchment as illustrated in Appendix A2. It is clear from the comparison that for both events in 2011 and 2012, no improvement was provided by the application of any of the SMOS estimations as compared to the open loop simulation. Nash-Sutcliffe Efficiency (NSE), RMSD and volumetric error (Vol E) between observed and modelled streamflow for open loop simulation (Sim), for direct insertion of OzNet data, and for assimilation of SMOS soil wetness estimations with weighting parameter equal to 0.8 and 1.0 in GR4H and PDM models are presented for Kyeamba in Table 5.1. The volumetric error is the sum of differences between observed and modelled flow divided by the sum of the observations. These skill scores have been presented for two events illustrated in Figures 5.9 and 5.10. As shown in this table, streamflow prediction performance did not improve after assimilation of SMOS data into either model.

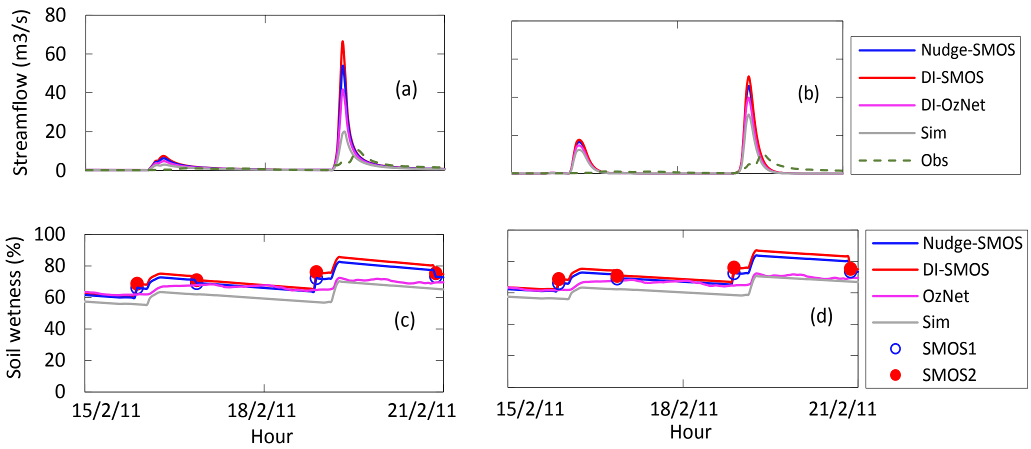

Figure 5.9: Comparison of observed and modelled streamflow and root-zone soil wetness before (sim), after direct insertion of OzNet root-zone data (DI-OzNet), and after assimilation (direct insertion and nudging with G equal to 0.8) of estimated root-zone soil wetness from SMOS using exponential filter (DI-SMOS, Nudge-SMOS) for GR4J (a and c) and PDM (b and d) models in the Kyeamba subcatchment for a small event in 2011. SMOS1 and SMOS2 in the second panel are estimated SMOS soil wetness for G equal to 0.8 and 1.0 respectively.

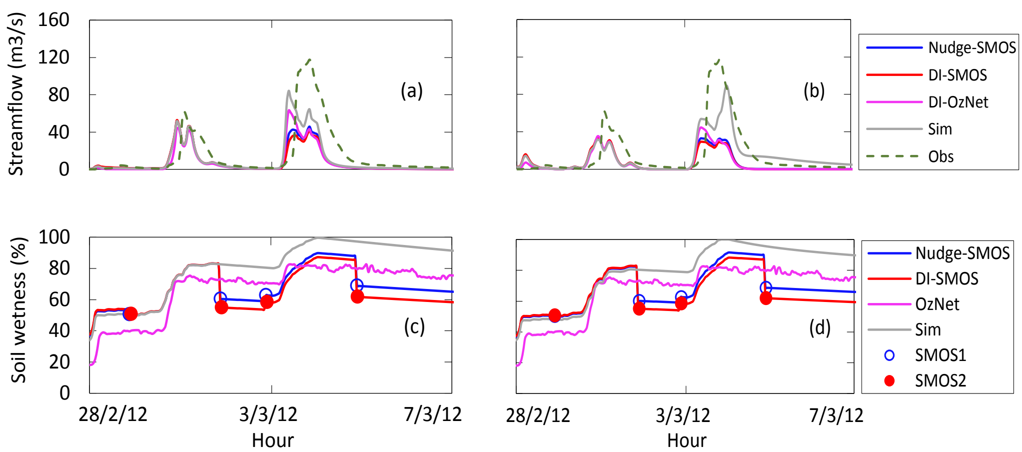

Figure 5.10: Same as Figure 5.9 but for a major event in 2012.

Table 5.1: NSE, RMSD (m^3/s) and Vol E (%) between observed and modelled streamflow for open simulation (Sim), for direct insertion of OzNet (DI OzNet), and for assimilation of SMOS soil wetness estimations with G equal to 0.8 (Nudge) or 1.0 (DI) for the Kyeamba subcatchment during a small event in February 2011 (event 1), a major event in February and March 2012 (event 2).

Model	Event	NSE				RMSD				Vol E			
		Sim	DI OzNet	Nudge SMOS	DI SMOS	Sim	DI OzNet	Nudge SMOS	DI SMOS	Sim	DI OzNet	Nudge SMOS	DI SMOS
GR4H	1	-0.54	-5.30	-9.48	-14.61	2.4	4.9	6.4	7.8	6.3	56.0	84.6	109.2
	2	0.45	0.34	0.39	0.36	20.7	22.6	21.7	22.3	-35.5	-51.8	-49.7	-52.5
PDM	1	-5.0	-8.76	-11.95	-14.93	4.8	6.2	7.1	7.9	23.7	54.3	76.3	93.5
	2	0.6	0.24	0.27	0.23	17.6	24.2	23.8	24.5	-17.0	-60.0	-58.4	-60.8

5.3.4 Application of SMOS in the Entire Study Site

Table 5.2 presents the calibration and validation NSE values for streamflow simulations from the GR4H and PDM models for 10 subcatchments within the entire study site down to Wagga Wagga station. In this subsection, the impact of assimilation of satellite-based soil wetness data on the streamflow prediction performance for all subcatchments and thus the streamflow prediction at the city of Wagga Wagga was assessed. Consequently, the root-zone soil wetness estimates from SMOS were used to update soil water state of the models using direct insertion or nudging with G equal to 0.8 for all subareas within the subcatchments located downstream of Blowering and Burrinjuck dams to Wagga Wagga. Here, it was assumed that the errors between OzNet observations and model or satellite data over the entire study site were similar to those estimated for the Kyeamba subcatchment in sections 5.3.2 and 5.3.3, Therefore, the parameter G used in the nudging approach here was assumed to be the same as the value used for Kyeamba (equal to 0.8).

Table 5.2: NSE between observed and modelled streamflow from the GR4H and PDM models for open loop simulation during the calibration and validation periods at 10 stream gauges in the entire study site.

Stream Gauge		171	206	214	245	216	218	229	241	242	244
GR4H	Cal.	0.29	0.97	0.68	0.75	0.98	0.79	0.65	0.68	0.55	0.70
	Val.	0.26	0.90	0.79	0.73	0.96	0.80	0.73	0.63	0.64	0.61
PDM	Cal.	0.59	0.98	0.82	0.74	0.99	0.81	0.85	0.75	0.57	0.97
	Val.	0.49	0.91	0.30	0.69	0.96	0.20	0.25	0.59	0.48	0.71

The exponential filter was applied to the interpolated and de-noised SMOS soil moisture data for each subarea, followed by conversion to soil wetness by normalisation to 0 and 1. The observed and modelled streamflow and root-zone soil wetness data are illustrated for two moderate events in August and November 2011 in the Adelong Creek subcatchment, and February and August 2011 in the Muttama Creek subcatchment (see Figure 5.1 for locations), in Figures 5.11 and 5.12 respectively. In addition, NSE, RMSD and Vol E between the observed and modelled streamflow for open loop simulation, after direct insertion of OzNet data, and after SMOS soil wetness direct insertion and nudging with G equal to 0.8 are presented for the events in Tables 5.3 and 5.4 respectively.

In Figure 5.11, the streamflow and soil wetness predictions from direct insertion of the OzNet data are also shown for Adelong subcatchment. In this figure, the soil wetness prediction is nearly same as OzNet observations (purple line in the second row). The peak flows in Figure 5.11(a) and (b) improved by 10% and 35% of the observed peak flows after direct insertion of OzNet observations in the GR4H model while the SMOS constraint degraded the modelled streamflow predictions in terms of the peak flows. However, according to the results presented in Table 5.3 the model skill scores improved for the event in August 2011 (event 2) after either SMOS assimilation (G equals to 0.8 or 1) for this subcatchment as a result of improved low flows, while no score improvement was seen for the event in November 2011. It is clear that there was no significant difference between the model performances for the assimilation of SMOS data when G changed from 0.8 to 1. In Figures 5.11(c) and (d), the PDM model skill degraded after assimilation of either the OzNet or SMOS data.

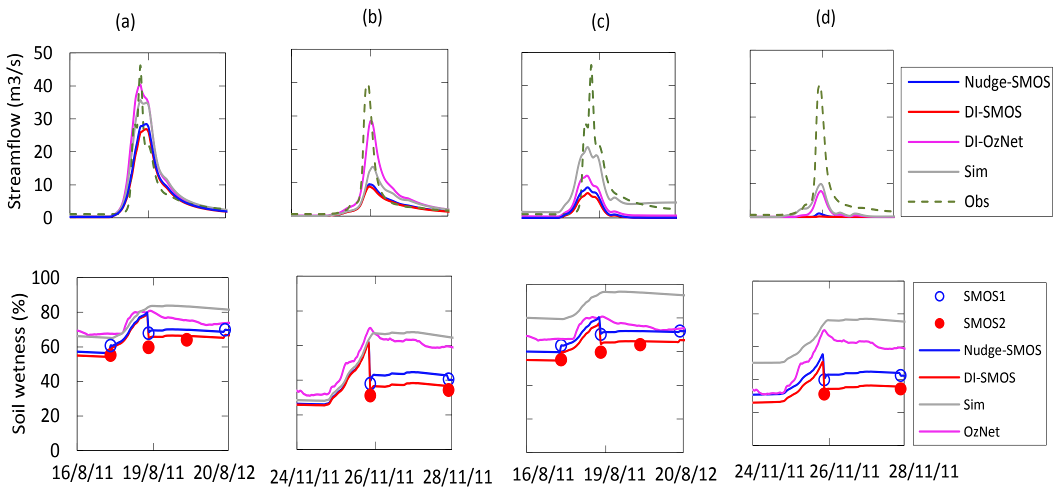

Figure 5.11: Comparison of observed and modelled streamflow and root-zone soil wetness for open loop simulation (sim), after direct insertion of observed root-zone soil wetness from OzNet (DI-OzNet), and after assimilation of SMOS data with G equal to 0.8 (Nudge-SMOS) or direct insertion (DI-SMOS) for GR4J (a and b) and PDM (c and d) models in the Adelong subcatchment for two moderate events in August and November 2011.SMOS1 and SMOS2 in the second panel are estimated SMOS soil wetness for G equal to 0.8 and 1 respectively.

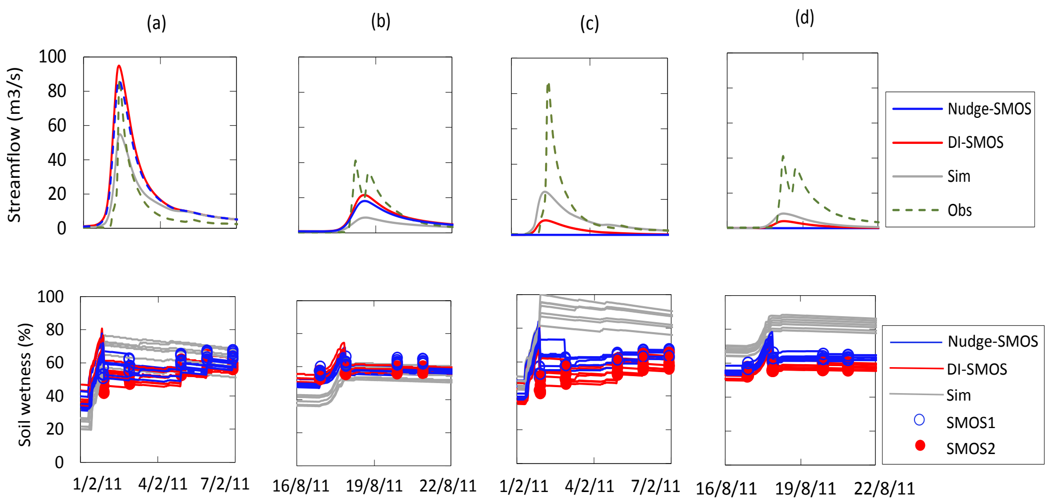

Figure 5.12: Same as Figure 5.11 but for the Muttama subcatchment and two moderate events in February and August 2011. Note: The SMOS data and soil moisture outputs from the models are shown for the seven subareas within this subcatchment, and no OzNet data comparison is shown for M3 station as no continuous data set from M3 station is available.

The peak flow predictions in GR4H were improved by 30% and 23% of the observed peak flow values in Figures 5.12(a) and (b) respectively after SMOS nudging for GR4H, while in PDM the model prediction was again degraded. In Table 5.3, it is indicated that the NSE skill of the GR4H model decreased after assimilation for the event in February 2011 due to the overprediction of the low flows. From Tables 5.3 and 5.4, it was also found that the performance of streamflow prediction from the nudging changed marginally for GR4H as compared to direct insertion while it degraded more for PDM. The skill degradation in the PDM model seen in Figures 5.11 and 5.12 is due to the high soil wetness overprediction by the model which could not be corrected by the observational data constraint. The better streamflow and soil moisture prediction results from GR4J as compared to PDM is consistent with the results found in the previous chapter. It should be noted that there were a few other small to moderate events in these two subcatchments. For all these events, model performance in streamflow prediction did not change or degraded in either model for the entire validation period (2011-2012) when applying the soil wetness constraint.

There was a single major event during the validation period in each of the Adelong and Muttama subcatchments, which occurred in early March 2012. To investigate the effect of observation constraint on model streamflow prediction skill for big streamflow values, the observed and modelled streamflow and soil wetness data are also shown for this major event in Figures 5.13(a) to (d). In this case the streamflow peak was improved by 9% for the first peak in the GR4H model after either SMOS assimilation in the Adelong subcatchment, and with no change in the predictions from using the in-situ data constraint. However, the second peak prediction degraded by 6% and 40% for SMOS and OzNet data constraint respectively. In the Muttama subcatchment, peak flow prediction skills were degraded after assimilation of SMOS data. As shown in Table 5.3, NSE and RMSD were improved for Adelong for this event in GR4H with no significant change in Vol E, while all skill scores were degraded for the Muttama subcatchment. The skill scores in Table 5.4 showed the NSE and RMSD values improved for PDM in both Adelong and Muttama, while the peak flow predictions in Figures 5.13(c) and (d) indicated great discrepancy when using the observation constraint for both subcatchments, again suggesting that the GR4H model is much better suited to the conditions of this study site than PDM.

The limited success from application of SMOS data for major event prediction using the GR4H model is mainly associated to the model deficiency in relating soil moisture state to the runoff generation as well as uncertainties in the soil moisture observations for this type of events. The model reached higher profile saturation level as compared to the observations in high flows. In this case, the model was not able to simulate runoff mechanism properly, which is probably dominated by surface runoff in the study area. In addition, the use of medium to high value for parameter T in the filtering method here (12 days) leads to a higher degree of smoothing. This resulted in very low soil wetness estimation from SMOS for high flows. Consequently sudden changes in soil moisture which are mostly seen in the high flow peaks here are not reflected properly by the SMOS observations. Moreover, the number of days with available data within the filtering time window is crucial for the accuracy of root-zone soil moisture estimates; especially during the peak flows. Since, the satellite observations used here were usually available every 2 to 4 days; it was clear that the availability of the data affected the results in this study especially during the high flows.

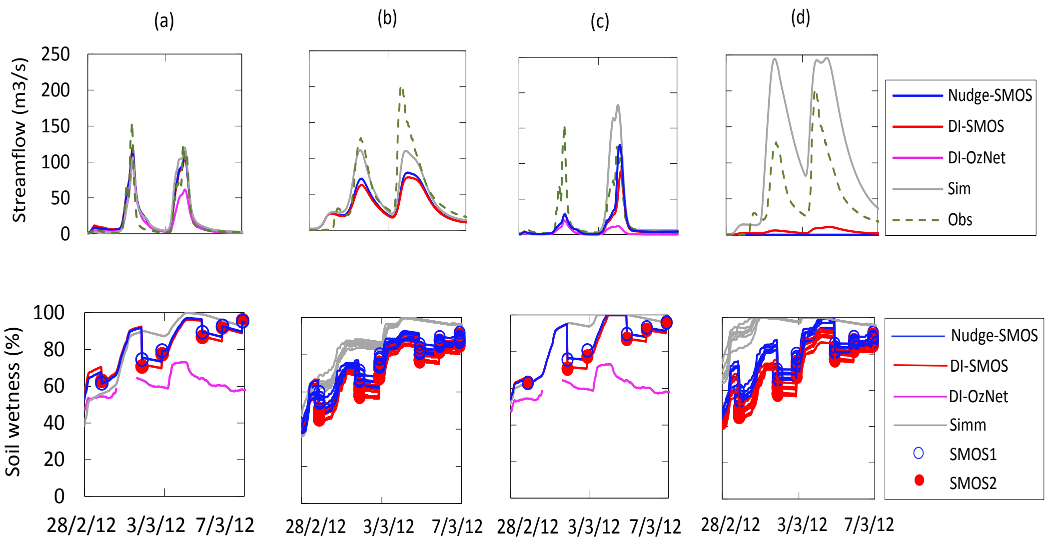

Figure 5.13: Same as Figure 5.11 but for the Adelong (a and c) and Muttama (b and d) subcatchments for a major event in February and March 2012. Note: The soil moisture outputs from the models are shown for seven subareas within Muttama subcatchment and no OzNet comparison is available for this subcatchment.

The streamflow predictions at Wagga Wagga outlet before and after assimilation of satellite-based root-zone soil wetness estimations over the entire study site for a moderate event in 2011 and a major event in 2012 are presented in Figures 5.14(a) and (c) for the GR4H model and Figures 5.14(b) and (d) for the PDM model. In Figure 5.14(a), there is a small improvement (7% of the observed peak flow) in the moderate flow prediction after application of SMOS observations in the GR4H model, with no difference between nudging results with G equal to 0.8 and 1. The flow predictions did not change for the PDM model for this event as shown in Figure 5.14(b). In Table 5.3, the NSE and RMSD improved from 0.72 to 0.79 (0.80) and from 53.1 to 45.9 (44.7) m^3/s after SMOS nudging (or direct insertion) in GR4H at Wagga Wagga station with no significant change in Vol E. For the major event in Figure 5.14(c) and (d), the streamflow values remained underestimated for both models without any improvement in the time lags compared to the observed flow. However in Table 5.3, the NSE and RMSD skill scores improved in GR4H for this event. The improved skill here is mainly due to the time lag in predicted flows which resulted in a decreased difference between observed and predicted flow at each time step while the peak flow was degraded. Conversely, the skill scores degraded for PDM for both events as shown in Table 5.4. It should be mentioned that no noticeable difference was seen in the models for the entire validation period after soil wetness constraint with some degradation of the prediction skill.

The method used here for updating the soil water state of the models was nudging, which simply accounts for observation and model errors by using a constant weighting parameter G with the observations assumed perfect when G was equal to 1. However, this method gave us an insight into the effect of incorporation of observational data in the modelling in a simple way as compared to application of sophisticated data assimilation methods. Brocca et al. (2010b) showed in a synthetic experience that use of a direct insertion method was as effective as a nudging data assimilation approach in improving discharge predictions when gain parameter (the relative weight of the model prediction error variance against that of observations) was smaller than 1 in the nudging, unless the model error was equal or less than half of the observation error. Similarly in the study here, taking into account the observation/model uncertainties did not affect the overall results since the model error was approximately twice the SMOS error when the data sets were assessed again in-situ root-zone observation in the Kyeamba subcatchment (see RMSD in Figures 5.6(b) and 5.8(c) for SMOS and model errors respectively).

The assimilation results of alternative root-zone soil moisture estimates obtained from different rescaling approach (CDF-matching to OzNet data after exponential filtering and CDF-matching to model predictions after exponential filtering) have been compared with the results from exponential filtering with normalization alone for Wagga Wagga station as illustrated in Appendix A2. NSE and the volumetric error between the observed and predicted flows have also been presented in Table A2.3 for several subcatchments within the entire study area down to Wagga Wagga station. In this Table it is shown that the root-zone SMOS data which were estimated from exponential filtering followed by normalization is the best approach particularly for the subcatchments in the entire study site with no OzNet data available to be used for accurate estimation of the function of CDF-matching to in-situ data.

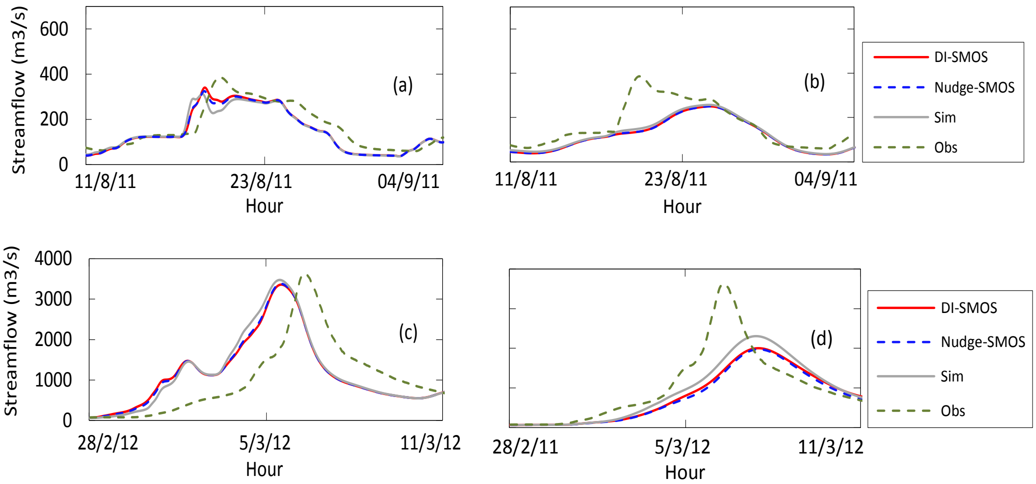

Figure 5.14: Comparison of observed and modelled streamflow for open loop simulation (sim) and after assimilation of observed SMOS soil wetness using nudging approach with G equal 0.8 (Nudge-SMOS) or 1 (DI-SMOS) for GR4J (a and c) and PDM (b and d) models at Wagga Wagga station for a moderate event in 2011 and a major event in 2012.

Table 5.3: NSE, RMSD (m3/s) and Vol E (%) between observed and modelled streamflow for open simulation (Sim), after direct insertion of OzNet data (DI OzNet), and after assimilation of SMOS soil wetness estimations with G equal to 0.8 (Nudge SMOS) or 1.0 (DI SMOS) for GR4H in Adelong Creek (A) and Muttama Creek (M) subcatchments, and at Wagga Wagga station (W) during different events; three moderate events in February 2011 (event 1), August 2011 (event 2) and November 2011(event 3), and a major event (February and March 2012 (4)). Note that OzNet data are available only for Adelong Creek subcatchment.

Subcat.	Event	NSE				RMSD				Vol E			
		Sim	DI OzNet	Nudge SMOS	DI SMOS	Sim	DI OzNet	Nudge SMOS	DI SMOS	Sim	DI OzNet	Nudge SMOS	DI SMOS
A	2	0.79	0.76	0.85	0.82	4.2	4.4	3.5	3.7	22.9	29.5	-3.2	-8.8
	3	0.45	0.73	0.33	0.30	6.1	4.2	6.7	6.9	-25.5	9.7	-46.7	-50.4
	4	0.85	0.76	0.90	0.90	12.5	15.4	10.1	10.0	19.4	-18.9	20.2	20.8
M	1	0.81	-	0.37	0.10	7.2	-	13.3	15.9	31.0	-	83.4	97.3
	2	0.07	-	0.62	0.74	9.9	-	6.3	5.2	-64.8	-	-32.8	-22.3
	4	0.74	-	0.46	0.37	25.0	-	36.0	38.9	-13.4	-	-34.7	-39.4
W	2	0.72	-	0.79	0.80	53.1	-	45.9	44.7	-12.5	-	-11.8	-11.0
	4	0.23	-	0.29	0.30	712.7	-	683.6	680.0	11.1	-	9.8	9.9

Table 5.4: Same as Table 5.3, but for the PDM model.

Subcat.	Event	NSE				RMSD				Vol E			
		Sim	DI OzNet	Nudge SMOS	DI SMOS	Sim	DI OzNet	Nudge SMOS	DI SMOS	Sim	DI OzNet	Nudge SMOS	DI SMOS
A	2	0.66	0.28	-0.09	-0.01	5.3	7.7	8.7	9.2	-4.1	-60.8	-76.2	-81.3
	3	0.29	0.15	-0.28	-0.34	6.9	7.6	9.3	9.4	-69.6	-82.2	-98.4	-99.7
	4	0.19	-0.1	0.52	0.44	28.6	32.1	22.0	23.7	14.8	-85.2	-37.2	-49.6
M	1	0.43	-	-0.41	-0.1	12.6	-	19.9	17.2	-29.5	-	-99.9	-78.8
	2	-0.1	-	-0.8	-0.42	10.5	-	13.7	12.2	-71.5	-	-100.0	-86.9
	4	-1.4	-	-1.17	-0.89	76.3	-	72.5	67.6	115.0	-	-100.0	-91.8
W	2	0.48	-	0.39	0.40	71.7	-	77.6	77.5	-25.2	-	-28.7	-28.7
	4	0.65	-	0.52	0.55	478.0	-	562.0	546.6	-10.4	-	-21.9	-17.6

5.3.5 Sensitivity Analysis for observation and model errors

A sensitivity analysis was undertaken to realize how the assimilation outcome would change when different weighting parameter (G in equation (5.6)) was varied from 0 to 1. The streamflow prediction results from open loop simulation (no assimilation, G=0) and direct insertion (G=1) are compared to the prediction results obtained from the nudging approach when the G parameter changed from 0.1 to 0.9. The NSE and Vol E, which were calculated between modelled and observed streamflow for the two events in 2011 and 2012 at Wagga Wagga are presented for GR4H in Figure 5.15. NSE and Vol E were also calculated at 10 stream gauges over the whole period of 2011 and 2012, which are presented in Figure 5.16. The location of these stream gauges are shown in Figure 5.1. The stream gauges in Figure 5.16 were categorized to three groups according to the NSE and Vol E values. The sensitivity analysis has been carried out for the GR4H model since this model outperformed the PDM model in terms of streamflow and soil moisture predictions in Chapter 4 and sections 5.3.3 and 5.3.4.

In Figure 5.15, the NSE score increased slightly from 0.23 to 0.30 and from 0.72 to 0.80 for the first and second event and the Vol E value improved from -12.5% to -11% and from 11.1% to 9.9% for the events respectively when G increased up to 1. Based on NSE shown in Figure 5.16, the model performance did not change significantly for five stream gauges (218, 229, 216, 206 and 244) by using different weighting parameter as compared to direct insertion results. In addition, the NSE score decreased when the weighting parameter increased from 0 to 1 for 5 stream gauges (171, 214, 245, 241 and 242); but there were marginal increases in NSE scores when G equaled to 0.8 as compared to direct insertion for these stream gauges. However, the streamflow predictions were degraded for the latter 5 stream gauges when either weighting parameter was used. The Vol E values decreased for 4 stream gauges (214, 229, 241 and 242) with weighting parameter increase, while it increased dramatically for two gauges (171 and 218).

However it did not change significantly for four other gauges (206, 216, 245 and 244).

The NSE scores obtained in the sensitivity analysis here showed that the use of different weighting parameter G did not make any significant difference in the model performance where the SMOS data assimilation provided improvements in the streamflow prediction results. Conversely, where the data assimilation degraded the model performance, significant changes were seen in the NSE score, but no improvement was achieved for data assimilation when G changed from 0.1 to 1 as compared to the open loop simulations. These results indicated that the use of different assumed errors in the nudging scheme did not significantly affect the assimilation performance. However, Brocca et al. (2013) showed that the improvement or degradation occurrence of the NSE coefficient in a real data nudging assimilation into a rainfall-runoff model did not depend on the choice of the gain parameter value, while the degree of the improvement (or degradation) depends on the weights used. Similar to the findings in this thesis, Alvarez-Garreton et al. (2014) showed that different assumed observation error structures did not have significant effect on data assimilation results.

The small sensitivity of the assimilation results to the assumed observation and model errors can be associated to the model deficiency in relating soil moisture states to runoff generation, and poor rainfall data as well as the uncertainties arising from filtering and rescaling approaches used for root-zone satellite-based soil moisture estimations. Since streamflow performance is directly related to the model quality before soil moisture assimilation and the overall water available in the system due to rainfall, soil moisture data assimilation alone does not address the systematic issues found in the model prior to assimilation (Alvarez-Garreton et al., 2015). Hence, quality assurance of the modelling in terms of parameter optimization and the structure used for relating soil water state and runoff generation is strongly recommended prior to data assimilation.

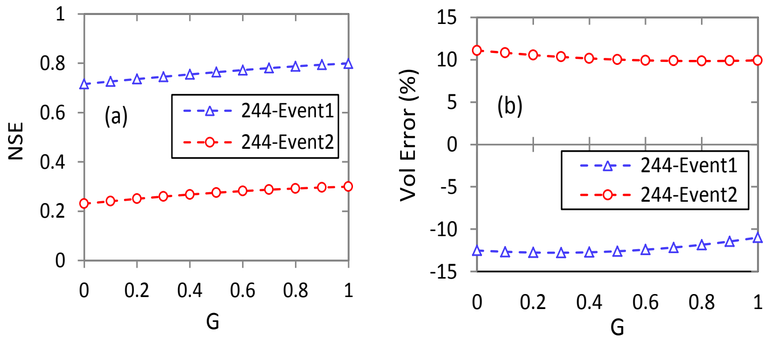

Figure 5.15: NSE score and Vol E (%) between observed and predicted streamflow for the nudging approach with different G at Wagga Wagga station for the event in August 2011 (event 1) and the event in February and March 2012 (event 2).

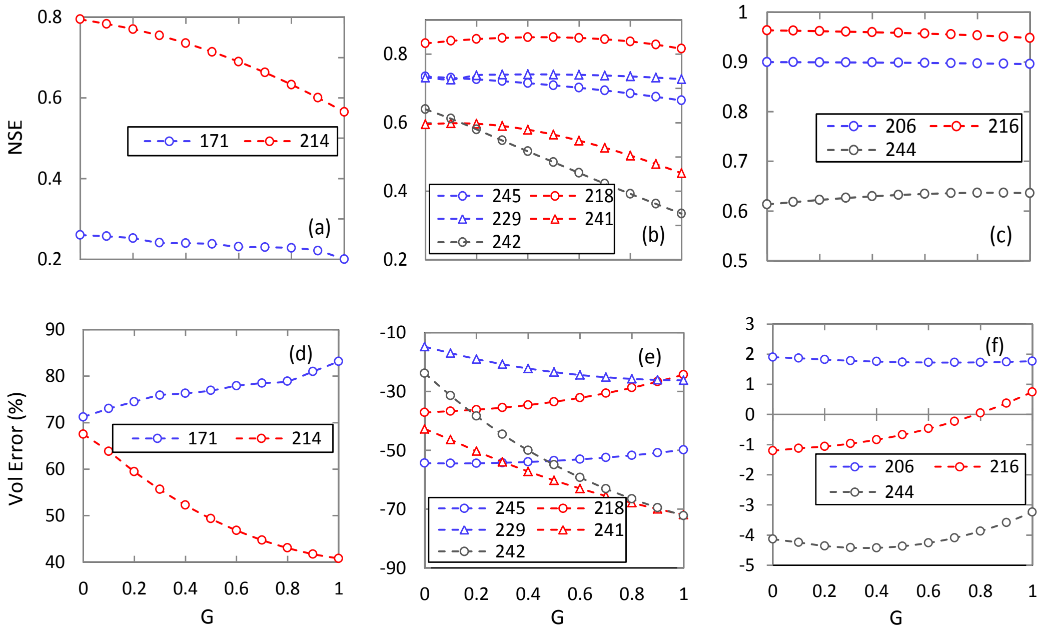

Figure 5.16: NSE score and Vol E (%) between observed and predicted streamflow for the nudging approach with different G at 10 stream gauges in the entire study area down to Wagga Wagga station for January 2011 to December 2012.

5.4 Chapter Summary

This chapter presented a study on incorporating soil moisture observations from the Soil Moisture and Ocean Salinity (SMOS) satellite into two operational streamflow prediction models, PDM and GR4H. The impact on streamflow prediction performance when the soil water state of the model was updated by soil moisture assimilation was demonstrated for several subcatchments in the Mid-Murrumbidgee catchment in southeast Australia. The CDF-matching, exponential filtering and moving average methods were applied to near-surface SMOS observations to approximate the model root-zone soil water store. The estimates from these methods were evaluated against in-situ root-zone observations from the OzNet monitoring network. Based on the error estimates, exponential filtering with a characteristic time length of 12 days was chosen among the three methods used, and thus subsequently applied in this study. The SMOS-based root-zone soil wetness was then used to constrain the models by using the nudging approach. The results showed that the PDM streamflow prediction performance was degraded after the assimilation of soil moisture data. However, for GR4H the results generally showed some improvements for moderate events, but no effect for major events, indicating an overall improvement in the robustness of the GR4H model. This highlights the potential for using soil moisture data to improve streamflow prediction, and the accompanying need to improve the relationship between soil moisture and runoff generation representation in operational streamflow forecasting models.

Chapter 6
Satellite-based Soil Moisture Impact on Real-time Streamflow Forecasting

This chapter presents the results of rainfall-runoff modelling for streamflow forecasting using the system presented in Chapter 5, calibrated according to Chapter 4, and forced with the QPF (Quantitative Precipitation Forecasting) data from the Australian NWP (Numerical Weather Prediction) system evaluated in Chapter 3. The impact of satellite-based soil moisture estimate on the constrained streamflow modelling was demonstrated in Chapter 5. Thus, in this chapter the impact of the soil moisture estimate on hydrological model initialisation is tested for streamflow forecasting under real-time conditions. Accordingly, the model soil water state is updated by direct insertion of satellite-derived root-zone soil moisture prior to a forecast being made with the QPF. The results from streamflow forecasting are assessed using actual streamflow observations, and compared with those using actual observed rainfall, and both with and without satellite soil moisture as a model initialisation constraint.

6.1 Study Site and Data Sets

The study site includes 10 subcatchments including 63 subareas down to the Wagga Wagga outlet, as shown in Figure 6.1. Real-time operational rainfall observations from the Australian Bureau of Meteorology (BoM), interpolated to the subareas, were used for running the model up to real-time during the initialisation of the model prior to the streamflow forecasting, together with monthly PET data from Australian Water Availability Project (AWAP; Raupach et al., 2009). As in previous chapters, the real-time streamflow observations for 10 stream gauges at subcatchment outlets (shown in Figure 6.1), obtained from the New South Wales Office of Water database (see http://www.water.nsw.gov.au/realtime-data), are used for evaluation of the model forecasts.

The ACCESS-A (BoM, 2010; Puri et al., 2013) forecast rainfall from the Australian Community Climate and Earth-System Simulator (ACCESS; BoM, 2010; Puri et al., 2013) are used as the forecast data to test the proposed system for two events in 2011 and one event in 2012. The ACCESS-A grids with 12 km resolution are shown in Figure 6.1. ACCESS-A is run four times per day with base times of 00:00, 06:00, 12:00 and 18:00 UTC and a forecast duration of 48 hours. In this work, the forecast from base times of 00:00 and 12:00 are used for the sake of simplicity. Moreover, since the hourly forecast data were shown to have larger bias for lead times of 1 to 12 hours when compared to gauge observations in chapter 3, the first 12 hours are excluded and the continuous 36-hour forecasts from the lead times of 13 to 48 hours are used in this chapter. Root-zone soil wetness data from the SMOS CATDS (Center Aval de Traitemnet des Donnees; See http://www.catds.fr) product, which was estimated for all subareas in the study site, have been used for the application of soil moisture observations in the forecasting. The SMOS root-zone soil wetness has been estimated using exponential filtering method to smooth and lag the near-surface satellite data, and then benchmarked against in-situ observations. The detail of the satellite data and the approach used for estimation of the soil wetness from the satellite data have been given in Chapter 5, section 5.2.1.

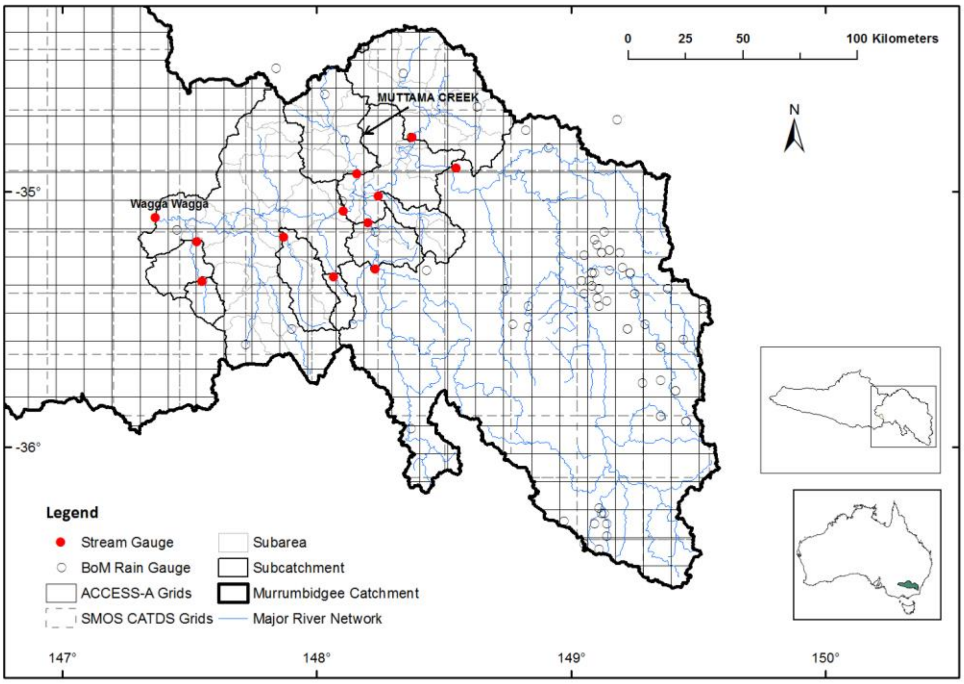

Figure 6.1: The location of subcatchments, stream gauges, and BoM rain gauges, SMOS grids and ACCESS-A grids in the study area.

6.2 Methodology

Real-time streamflow forecasting from the GR4H model has been investigated with and without constraining the model initial condition with satellite-based root-zone soil wetness observations. This model has been chosen as the modelling results from this model were better than those obtained from the PDM model in chapter 5. For this purpose, the GR4H model was initialised in two different ways: i) using the modelled soil water content at one time step before the model runs for streamflow forecasting, and ii) direct insertion of satellite-based root-zone soil wetness in the models whenever the soil moisture data is available from January 2011 to one hour time step before the forecasting. In both initialisation approaches for with and without soil moisture observation constraint, actual observed rainfall forcing was used from January 2011 up to the point of the initialisation of the forecast period. In order to predict the streamflow, a model forecast was made every 12 hours, upon "issue" of the forecast rainfall, out to 36-

hour lead time. This means that 36-hour forecast rainfall data were used to generate the streamflow forecast with lead times of 1 to 36 hours after each forecast started, being 12 hours after the rainfall forecast was first issued.

All subareas within the 10 subcatchments were initialised for soil moisture during the initialisation period. The model defines soil moisture as the soil water level (mm) in the production store. These soil wetness observations were converted to soil water storage level to be used in the model by multiplying the soil wetness observations by the maximum simulated soil moisture obtained during the 6 year period, rather than the model production store capacity since the GR4H model did not show 100% saturation during the six year of calibration and validation period (2007 to 2012). The model performance in streamflow forecasting for different lead times is evaluated based on mean absolute error (MAE) which is the average of absolute value of differences between observed and forecast flow.

6.3 Results

The streamflow forecasting results with and without soil moisture observation constraint initialisation were evaluated against streamflow observations for a medium event in August 2011 and a large event in February and March 2012 for Muttama Creek subcatchment in Figure 6.2. For comparison, the streamflow predictions using observed rainfall data with and without direct insertion of soil moisture observations are also shown. The same results are illustrated for a medium event in August 2011 and a large event in March 2012 in Figure 6.3 for Wagga Wagga outlet. In Figures 6.2 (a) and (b), the 11 and 12 forecasts with lead time from 1 hour to 36 hours are shown respectively.

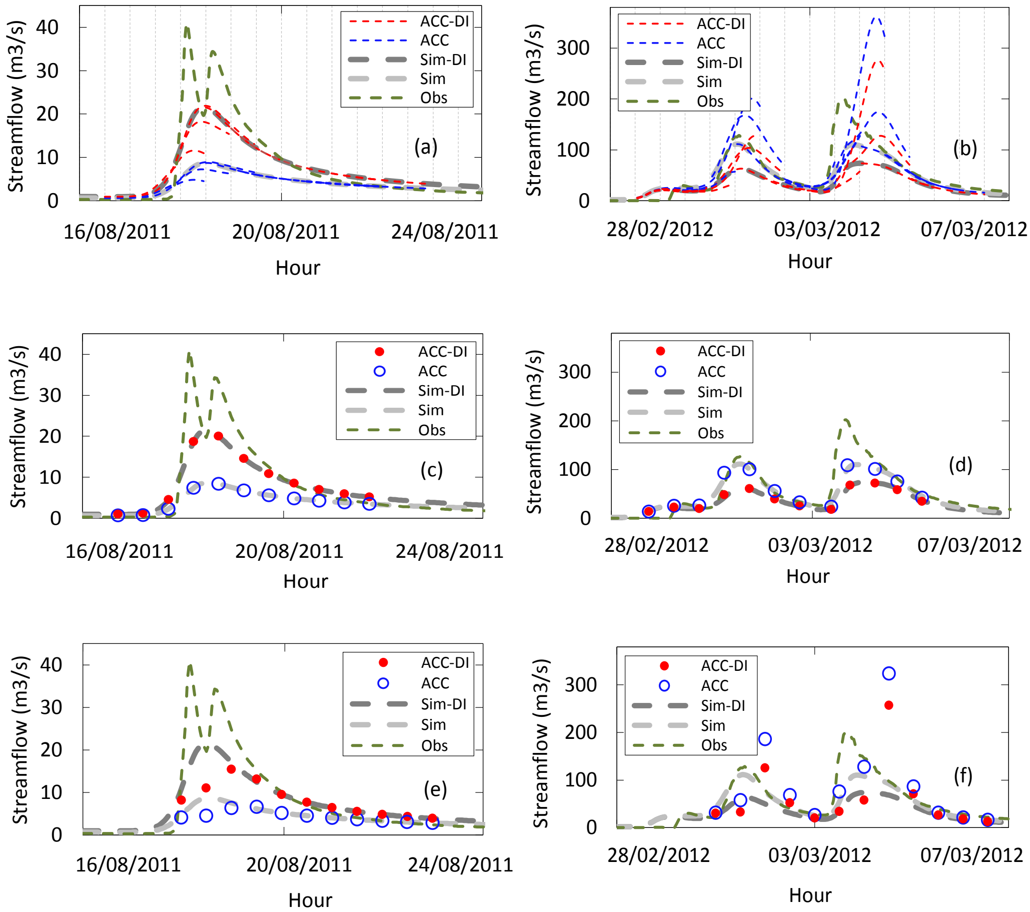

Figure 6.2: Comparison of streamflow forecasts (blue dots) and forecasts (red dots) for lead time of up to 36 hours (a and b) and 6-hour lead time (c and d) and 36-hour lead time (e and f) for events in August 2011 (16/8/2011 to 23/8/2011; left), and February and March 2012 (28/2/2012 to 6/3/2012; right) in the Muttama Creek subcatchment. The gray dashed lines with 12-hour intervals in figures 6.2 (a) and (b) indicate the start time of the forecasts.

In order to investigate the effect of direct insertion in more detail, the streamflow results are also presented for lead times of 6-hour and 36-hour in Figures 6.2 (c) and (e) for the first event, and in Figures 6.2 (d) and (f) for the second event, respectively. In Figures 6.2 (c) and (e), the difference between observed and forecast streamflow decreased when the soil moisture observations were used before the forecast for the initialisation, as compared to the forecast results without soil moisture observations constraint. However, the streamflow peak and timing degraded for the 36-hour lead time compared to the result from 6-hour lead time. In Figure 6.2 (d), the forecast results with 6-hour lead time without soil moisture observation constraint was better than the results with soil moisture observation constraint used before the event, while the streamflow peak results with 36-hour lead time improved after the soil moisture constraint compared to the results with no observation constraint with time lag to the flow observations existed for the peaks in this figure. In Figures 6.2 (c) and (d), there is no difference between forecasts with 6-hour lead time and the model prediction with observed rainfall when direct insertion was used for the initialisation. Similarly, the forecast were the same as the prediction when no insertion was used. This suggested that only the model initialisation had impact on the model performance. However, the forecasts with 36-hour lead time shown in Figures 6.2 (e) and (f) were degraded for both with and without soil moisture observation constraint as opposed to the model prediction with observed rainfall when they are compared to the streamflow observation. In this case, both rainfall and initialisation had impact on the model forecasts.

In Figures 6.3 (a) and (b), there are 14 and 11 events for the first and second events respectively. As shown in Figures 6.3 (c) and (e), the streamflow forecast after initialisation with soil moisture observations improved in terms of shape, peak value and timing for both 6-hour and 36-hour lead times. In Figures 6.3 (d) and (f), the forecasts with soil moisture observation constraint improved slightly in terms of the shape, while the flow peak degraded slightly as compared to the observation. In Figures 6.2 (c) to (f) and 6.3 (c) to (f), there are a limited number of forecasts for each lead time as the rainfall forecast issued every 12 hours was used in this work. Despite the high relative bias ranges estimated for the forecast rainfall data in Chapter 3 (-40% to +60% of total observation), Figure 6.3 indicates that use of forecast rainfall with 6-hour lead time did not change the model performance for both with and without soil moisture observation constraint as compared to the predictions with actual-rainfall-forced model. However, for 36-hour lead time the model performance was degraded by the use of forecast rainfall as opposed to model predictions with rainfall observation. This means that the only initial condition had impact on the forecasting results for shorter lead times while both rainfall and initialisation influences the forecast for 36-hour lead time.

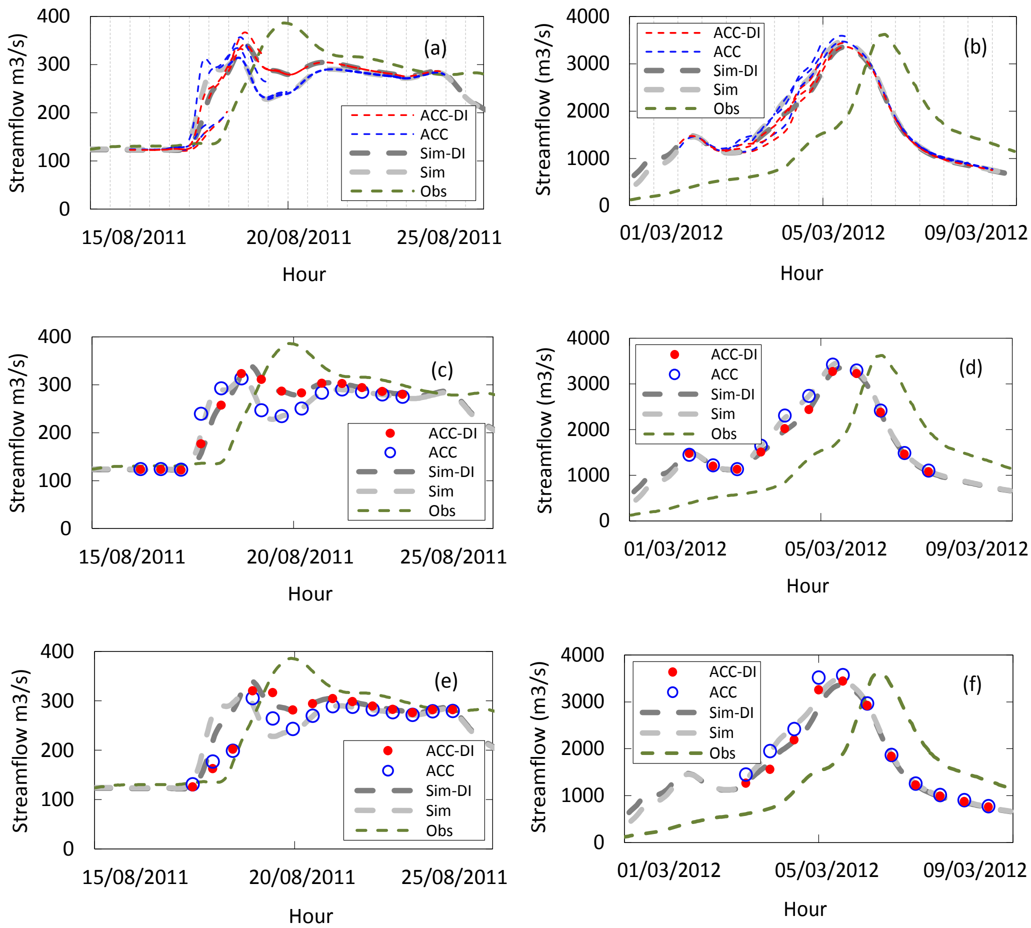

Figure 6.3: Same as figure 6.2 but for the Wagga Wagga outlet.

A limited improvement was achieved in the forecasts at Wagga Wagga outlet when the soil moisture observations were used for model initialisation. In fact, the direct insertion results at the outlet were strongly influenced by the effect of soil moisture constraint on the forecasting for all 10 subcatchments upstream of the outlet. For example, as shown in the Muttama Creek subcatchment, one subcatchment upstream of the Wagga Wagga outlet, the application of soil moisture observations have resulted in an improvement of the prediction of peak flow for the medium event at the subcatchment outlet. But the forecasting results at Wagga Wagga did not show the same level of improvement in predicting the streamflow peak for that event. On the other hand, despite the simplicity of the data assimilation method used, and the simplicity of the approach to translating satellite observed near-surface soil moisture to root-zone estimates, the potential benefit of the data assimilation approach was clearly demonstrated. The possible positive effect of dual assimilation of both streamflow and soil moisture observations into the forecast model is required to be investigated.

In order to evaluate how the forecast results changed with different lead times, when the model were initialised with soil moisture observations prior to a forecast, the mean absolute error (MAE) between forecast and observed streamflow has been calculated for lead times of 1 to 36 hours. The variations in MAE have been shown in Figures 6.4 (a) and (b) for Muttama Creek subcatchment and at Wagga Wagga respectively. It is clear that based on the MAE, the model performance improved for the first event in Muttama Creek subcatchment and for the two events at Wagga Wagga outlet, when initialising the model with observed soil moisture prior to the events. However, for the second event in Muttama Creek subcatchment, the MAE increased for lead time of up to 22 hours, while the model constrained with observations performed better than the forecast with no observation constraint for the lead times of 23 to 36 hours. The benefit of soil moisture observation constraint in forecasting for longer lead time in this subcatchment was already shown in Figure 6.2 (f) for the second event, while the model skill was degraded for the shorter lead time (6-hour) in Figure 6.2 (d).

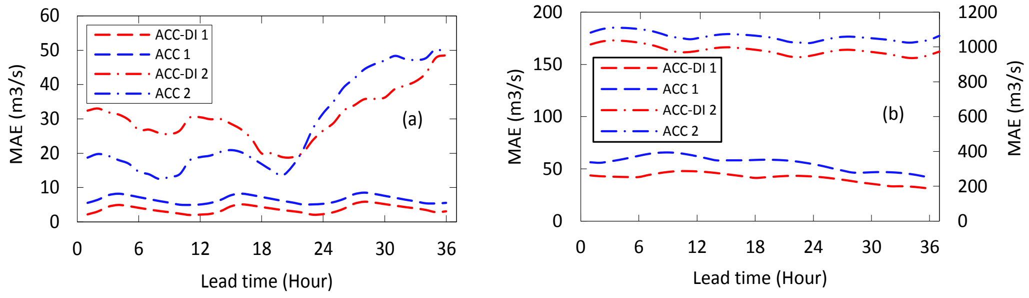

Figure 6.4: The MAE between observed and forecast streamflow for the events in August 2011 (1) and February/March 2012 (2) in Muttama Creek subcatchment (a) and at Wagga Wagga (b). The errors for with and without direct insertion are shown in red and blue lines respectively and the MAE for the second event at Wagga Wagga has been presented on the secondary vertical axis.

It was expected that the model skill in streamflow forecasting would degrade with increased lead time due to the propagation of rainfall forecast errors in to the forecast model. However, there is no clear change in the MAE over different lead times for the event in August 2011 in the Muttama Creek subcatchment and at Wagga Wagga, or the event in March 2012 only at Wagga Wagga. The event in February/March 2012 for Muttama Creek showed an increase in MAE for lead times of more than 23 hours. In these figures, there is a clear cyclic trend in the MAE. This trend is probably due to the cyclic nature of biases in the NWP rainfall predictions associated to the limited ability of NWP models to display the diurnal cycle of rainfall (Robertson et al., 2013). The effect of diurnal cycle in the forecast rainfall, however, has not been investigated in Chapter 3. Moreover, Li et al. (2014) showed increased biases with increasing lead time in real-time forecasting using the PDM model and regional version of ACCESS (ACCESS-R) in the Ovens catchment in Australia. The bias in their study varied from nearly 0 to 5 m^3/s in the open loop simulation, which decreased to 0 to 2 m^3/s after discharge assimilation using the EnKF or EnKS. Bennett et al.

(2014) showed that the relative bias in streamflow forecasts from the GR4H model changed mostly from -25% to +50% of the mean observed flow in south-eastern Australia for lead times up to 2 days when using raw ACCESS-G forecast rainfall, while the biases with post-processed forecast rainfall were similar to the errors obtained from perfect-rainfall-forced forecasts.

6.4 Chapter Summary

This study incorporated soil moisture observations from the SMOS satellite together with ACCESS-A forecast rainfall data into the GR4H model to assess the potential improvement in real-time streamflow forecasting in the Murrumbidgee catchment. The effectiveness of direct insertion of these observations was assessed for the catchment area upstream of Wagga Wagga. Forecasts were made with and without direct insertion of soil moisture observations into the model. Variations in mean absolute error between forecasts and observed streamflow were calculated for different lead times. The results in this work showed that streamflow forecasting with soil moisture constraint typically improved predictions for lead times out to 36 hours, while for one event there was improved forecasting only for lead times of 23 to 36 hours. It was also shown that the initial condition had impact on the forecasting results for lead time of 6 hours while both rainfall and initialisation influenced the forecast for 36-hour lead time.

Chapter 7
Conclusions and Future Work

This thesis has investigated the potential for operational streamflow forecasting to benefit from use of remotely sensed soil moisture observations and NWP forecast rainfall in Australian catchments. The main focus was on a study site where rainfall and soil moisture observations from several research monitoring stations were available. Catchment-based soil wetness from the monitoring stations were used to evaluate hydrological model soil wetness predictions, and the subsequent effect on streamflow predictions, which has never before been taken into consideration for operational flood forecasting in Australia. Satellite-based soil moisture data were assimilated into the hydrological model using a nudging approach. To do this, the satellite-derived soil moisture was first converted to a root-zone soil wetness estimate, which was later used in hydrological modelling. Different filtering/scaling methods including CDF-matching, exponential filtering and moving average, were tested for this purpose. The root-zone estimates were benchmarked against in-situ data for one subcatchment, and subsequently the best approach was selected and applied for assimilation into the model over the entire study site. Moreover, the uncertainty in forecast rainfall was assessed against weather radar coverage and available rain gauge observations in an area adjacent to the key study site, prior to its application to streamflow forecasting. This chapter reports the main findings arising from Chapters 3 to 6 of this thesis and discusses the limitations and their impact on future work.

7.1 Conclusions

The conclusions of this thesis are based on four investigations: i) evaluation of uncertainty in the NWP based rainfall forecasts, ii) the importance of soil moisture in calibration of rainfall-runoff modelling iii) application of satellite-based soil moisture estimation to streamflow prediction, and iv) soil moisture impact on real-time streamflow forecasting.

7.1.1 Evaluation of Numerical Weather Prediction Rainfall

Evaluation of precipitation from NWP models has been an important subject during the past decade, but most have focussed on individual events. The goal of this work was therefore to assess the errors in operational NWP rainfall forecasts from an Australian-domain model, ACCESS-A, across a multi-year time frame in the vicinity of the study site for streamflow modelling. This assessment was important for understanding the impacts on flood forecasting when using NWP rainfall forecasts as input. Specifically, a study was undertaken to evaluate rainfall estimates from Yarrawonga weather radar and the ACCESS-A NWP model using independent rain gauge measurements from the OzNet monitoring stations. Then, the ACCESS-A forecast data were evaluated against the recalibrated radar observations over a large area.

When compared directly against rain gauge data, it was found that the radar mostly underestimated rainfall, with the most considerable difference from gauge measurements being in March, which had the heaviest rainfalls. In contrast, the ACCESS-A NWP model mostly overestimated the rainfall, with the forecasts with lead times of 13-24 and 25-36 hours outperforming the 1-12 and 37-48 hour lead times. Since the ACCESS-A model outputs used in the study had a spatial resolution of 12 km, significant errors were expected from direct comparison with single gauge. Therefore, ACCESS-A rainfall forecasts with lead times of 13-24 hours were evaluated against de-biased weather radar data according to the independent rain gauges. The evaluation of NWP data was based on RE (relative error), ME (mean error), RMSE and a contingency table, which were calculated over the two years spanning from January 2010 to December 2011. For this purpose, radar rainfall intensities were adjusted to independent rain gauges by estimating a new relationship between radar and gauge rates. The results revealed that the skill of the NWP rainfall forecasts varied across the study area and through time, being highly dependent on the rainfall observations over the study area. Use of daily accumulation of ACCESS-A resulted in decreased errors compared with hourly time scale, but the forecast skill was still not appropriate for hydrological modelling applications.

In addition, based on a contingency table, both location and magnitude errors were the main sources of forecast uncertainties on hourly accumulations, while wrong magnitude was the dominant source of error on daily time scale. Consequently, the results from this work suggested that without error correction i) the raw hourly forecasts may not be sufficiently accurate to be used for flood forecasting at the scale of ACCESS-A and ii) the improvement in daily forecast accumulations is still not enough to allow for hydrological applications at the spatial scale of the NWP forecast model. It is therefore concluded that the NWP model uncertainty is expected to be propagated into the streamflow forecasting in this research. This hypothesis was further tested in Chapter 6 of this thesis.

7.1.2 Rainfall-runoff Model Calibration

Two rainfall-runoff models, GR4H and PDM, were selected for use in this research, among the models included for operational flood forecasting in Australia. The hypothesis here was that the model physics simulates the soil water content in such a way that the model soil water content is consistent with the soil moisture observations, and therefore, the profile storage in the model will be effectively updated through the application of satellite-based profile soil moisture, leading to improved streamflow forecasts. Hence, the effect of soil moisture incorporation in calibration of the models has been investigated.

Two calibration methods were used and evaluated in two subcatchments, Kyeamba and Adelong Creek, where in-situ rainfall and soil moisture observations were available from several monitoring stations. For the first calibration method, the objective function was based on minimising only the difference between observed and modelled streamflow, as the most common method used in calibration of hydrological models. In the second calibration method, the difference between observed and simulated soil wetness was coupled with streamflow differences to account for the effect of accuracy of soil water storage simulation in the modelling, with the aim of future application of ground-based/remote sensing observations for model calibration in operational flood forecasting in Australia. Soil moisture estimated with and without joint-calibration in the models was evaluated against soil moisture observations from field measurements from the OzNet monitoring stations. The models had different performance in soil wetness estimation, and this is associated to the structure of the models and the hydrological processes they use for soil moisture estimation.

Rainfall observations from the OzNet monitoring stations were used in the calibration process and operational rainfall data were used for validation, with the aim of demonstrating the impact on broader application in the entire study site. It was shown that use of operational rainfall data from sparsely distributed gauges did not adversely affect the modelling results. Despite the semi-arid characteristics of the Kyeamba area, the performance of both models was acceptable in this catchment with calibration and validation NSE scores mostly greater than 0.60. The performance of the models in flow estimation mostly did not change significantly after joint-calibration in the calibration period. However, in the validation period, the PDM model had much better predictions of the flows as opposed to calibration to streamflow alone, especially in the subcatchment where it had low streamflow prediction skill from the initial calibration.

This study indicated that while the soil moisture constraint in the calibration procedure did not improve the model skill in streamflow prediction for the calibration period, the streamflow prediction for the validation period was more robust. Moreover, while PDM had better streamflow and soil moisture estimation over the joint calibration period, the improved prediction skill did not translate into the validation period, where GR4H showed much better prediction. Consequently, it is recommended that the GR4H model be used in Australia, in preference to PDM, and that soil moisture data be used in the calibration process.

7.1.3 Use of Soil Moisture to Constrain Streamflow Prediction

The GR4H and PDM models have been constrained with SMOS-based satellite estimates of root-zone soil wetness using the nudging method to investigate the possible improvement in streamflow prediction. For comparison, the models were also constrained with in-situ based root-zone soil wetness data in two subcatchments, Kyeamba and Adelong Creek subcatchments, due to the availability of OzNet monitoring stations, allowing the satellite data constraint to be benchmarked against the use of in-situ data. In all other subcatchments, including the Muttama Creek subcatchment, only SMOS root-zone estimates could be inserted.

Since current remote sensing technology can only provide soil moisture data in the top 5 cm of the soil, rather than the entire profile, a CDF-matching and two filtering methods (exponential filter and moving average) were applied to the near-surface satellite soil moisture data for estimating the root-zone soil wetness, and benchmarked against the in-situ data. The root-zone soil moisture estimates were converted to soil wetness by normalising the data between 0 and 1 using maximum and minimum soil moisture values over a representative time period. The results showed that the CDF-matching was not effective in estimation of root-zone soil wetness, with the root-zone soil wetness estimation from exponential filtering giving a slightly better result (RMSD of 7.2% and R of 0.93) than the moving average filter when compared with in-situ data. Thus, the exponential filter can be effectively applied to SMOS data for estimating root-zone soil wetness for areas where in-situ data is not available.

The results also indicate that streamflow predictions did not improve for either model after application of either OzNet or SMOS data in the Kyeamba subcatchment. This is believed to be related to a deficiency in the model coupling of streamflow simulation with soil wetness observations. In contrast, the GR4H model skill was improved slightly after direct insertion of OzNet soil wetness for two moderate events in the Adelong subcatchment, while assimilation of SMOS degraded the streamflow prediction. Furthermore, GR4H showed improved streamflow prediction after SMOS insertion for two moderate events in the Muttama subcatchment. The better performance of GR4H here is consistent with the earlier finding from using soil moisture data to constrain model calibration.

At Wagga Wagga, apart from a very small improvement in GR4H for the moderate event in August 2011, most of the predictions did not change or were degraded slightly after SMOS-based data applications in the entire study site. The limited improvement at Wagga Wagga, which was highly influenced by the performance of the model in the upstream subcatchments, indicated that insertion of soil wetness data in GR4H did not result in improvement in all upstream subcatchments. The PDM model prediction was degraded in all events for the subcatchments and at Wagga Wagga. This again highlights the systematic issue of PDM to correctly simulate the relationship between soil wetness, precipitation and runoff generation.

As a conclusion, the results in this study indicate that the effectiveness of data assimilation depended on both catchment characteristics and the selected model for coupling soil moisture and runoff generation. The limited success in application of both the satellite and in-situ soil moisture observations for streamflow prediction from the GR4H model was mainly due to the model structure deficiency in soil moisture prediction and observation uncertainties.

7.1.4 Soil Moisture Impact on Streamflow Forecasting

The impact of the satellite-based root-zone soil moisture constrain on the GR4H model was further investigated when the model was forced with operational QPFs from ACESS-A for the 10 subcatchments in the study site. ACCESS-A forecast rainfall with the lead time from 13 to 48 hours was used to generate forecast streamflow with lead times of 1-36 hours. The soil water state of the model was updated by assimilation of satellite-based root-zone soil wetness in the models utilizing all the soil moisture data available up to one hour before the forecast. The streamflow forecasts with and without the soil moisture observation constraint were compared to the model predictions using observed rainfall.

It was revealed that the initial soil moisture condition had the greatest impact on the forecasting results for shorter lead times (e.g., 1 to 12 hours), while both rainfall and soil moisture initialisation influenced the forecasts for longer lead times (e.g., 24 to 36 hours). This indicated that the ACCESS-A forcing data were sufficiently accurate in predicting rainfall for shorter lead times, while forecast uncertainties are significant for longer lead times. As a main conclusion, the streamflow forecasting with soil moisture constraint typically improved predictions for lead times out to 36 hours, especially for moderate events, while for one major event there was improved forecasting only for long lead times (e.g., 24 to 36 hours).

7.2 Future Work

The applicability of using remotely sensed soil moisture observations in operational streamflow forecasting has been investigated in this thesis. The limitations of the research and some important aspects that are required to be addressed in future work are discussed here.

7.2.1 Limitations in Application of Numerical Weather Prediction

Radar-rainfall estimates can provide the broad-scale observations required for verifying model precipitation forecasts, provided the errors in radar-based rainfall are corrected. The evaluation of ACCESS-A QPFs in Chapter 3 of this thesis was based on the assumption that after adjusting the radar, the error in the radar estimate has been sufficiently minimized to be useful in evaluation of forecast rainfall data. Nevertheless, there might be residual bias in the radar estimates due to some factors such as vertical profile of reflectivity. In addition, the QPFs uncertainty estimated showed that the errors in ACCESS-A data varied considerably with space (-40% to +60%). However, in the study site of this research, significant uncertainty was not transferred to the streamflow forecasting, especially for shorter lead times. For other catchments where rainfall error has significant impact on streamflow forecasts, it is beneficial to use post-processing methods such as probability modelling or exceedance probability correction to remove biases in the forecast rainfall. For example, using exceedance probability of observational data, the forecasts could possibly be corrected so that their probabilities match those observed. In addition, post-processed ensemble forecast rainfall with quantified uncertainties could be adopted for a reliable ensemble streamflow forecasting.

7.2.2 Use of Satellite-based Soil moisture in Model Calibration

In this thesis, the usability of ground-based root-zone soil moisture observations in model calibration process was demonstrated for subcatchments where in-situ data were available. For operational flood forecasting, therefore, use of satellite-based soil moisture observations is recommended for model calibration process. It is obvious that an appropriate pre-processing method such as exponential filtering is required prior to the application in a single-layer model. In areas, where ground-based soil moisture measurements are not available to be used for evaluation of root-zone estimates, the pre-processing and calibration approach could be assessed by evaluating the model streamflow predictions against observed streamflow.

7.2.3 Impact of Observation and Model Uncertainties

The nudging approach used in this research for constraining the models with satellite-based data simply take into consideration the observation or model background uncertainty, and the observations are assumed “perfect” for direct insertion. To investigate the effect of observation and model uncertainties on data assimilation efficiency, more attention should focus on quantifying the observation and model errors to be included in data assimilation approaches such as the EnKF or EnKS. The model error can be represented in the EnKF by perturbing the forcing data inputs, model parameters or state. For satellite-derived soil moisture observations, the error could be estimated based on the difference between satellite-based observations and in-situ measurements.

7.2.4 Joint Assimilation of Streamflow and Soil Moisture

In this research, there have been some improvements in streamflow forecasting from the soil moisture constraint, especially for medium events. Joint assimilation of both streamflow and soil moisture observations, which takes the advantage of both types of observations, warrants investigation. This could be especially useful for better prediction of major events, in which the effect of extreme rainfall on runoff generation is more prominent than soil moisture initial condition.

7.2.5 Application of a Model with Two-layer Soil Moisture Store

The proposed algorithm for streamflow forecasting was tested using a model with single layer soil moisture store. This restricts the direct application of satellite data, and so some uncertainties associated with estimating the root-zone soil moisture using the exponential filtering approach are introduced to the streamflow forecasting. It is thus recommended that a two-layer model which simulates both near-surface and root-zone layers, such as SAC-SMA or GRHUM models, be tested for incorporation of near-surface observations directly.

References

ABUSHANDI, E. H. and MERKEL, B. J. 2011. Application of IHACRES rainfall-runoff model to the wadi Dhuliel arid catchment, Jordan. *Journal of Water and Climate Change,* 2**,** 56-71.

AL-YAARI, A., WIGNERON, J. P., DUCHARNE, A., KERR, Y., DE ROSNAY, P., DE JEU, R., GOVIND, A., AL BITAR, A., ALBERGEL, C., MUÑOZ-SABATER, J., RICHAUME, P. and MIALON, A. 2014. Global-scale evaluation of two satellite-based passive microwave soil moisture datasets (SMOS and AMSR-E) with respect to Land Data Assimilation System estimates. *Remote Sensing of Environment,* 149**,** 181-195.

AL BITAR, A., LEROUX, D., KERR, Y. H., MERLIN, O., RICHAUME, P., SAHOO, A. and WOOD, E. F. 2012. Evaluation of SMOS Soil Moisture Products Over Continental U.S. Using the SCAN/SNOTEL Network. *IEEE Transactions on Geoscience and Remote Sensing,* 50**,** 1572-1586.

ALBERGEL, C., RUDIGER, C., PELLARIN, T., CALVET, J. C., FRITZ, N., FROISSARD, F., SUQUIA, D., PETITPA, A., PIGUET, B. and MARTIN, E. 2008. From near-surface to root-zone soil moisture using an exponential filter: An assessment of the method based on in-situ observations and model simulations. *Hydrology and Earth System Sciences Discussions,* 5**,** 1603-1640.

ALBERGEL, C., RUDIGER, C., CARRER, D., CALVET, J. C., FRITZ, N., NAEIMI, V., BARTALIS, Z. and HASENAUER, S. 2009. An evaluation of ASCAT surface soil moisture products with in-situ observations in Southwestern France. *Hydrology and Earth System Sciences,* 13**,** 115-124.

ALBERGEL, C., DE ROSNAY, P., GRUHIER, C., MUÑOZ-SABATER, J., HASENAUER, S., ISAKSEN, L., KERR, Y. and WAGNER, W. 2012. Evaluation of remotely sensed and modelled soil moisture products using global ground-based in situ observations. *Remote Sensing of Environment,* 118**,** 215-226.

ALBERGEL, C., DORIGO, W., REICHLE, R. H., BALSAMO, G., DE ROSNAY, P., MUÑOZ-SABATER, J., ISAKSEN, L., DE JEU, R. and WAGNER, W. 2013. Skill and Global Trend Analysis of Soil Moisture from Reanalyses and Microwave Remote Sensing. *Journal of Hydrometeorology,* 14**,** 1259-1277.

ALFIERI, L., CLAPS, P. and LAIO, F. 2010. Time-dependent Z-R relationships for estimating rainfall fields from radar measurements. *Natural Hazards and Earth System Science,* 10**,** 149-158.

ALVAREZ-GARRETON, C., RYU, D., WESTERN, A. W., CROW, W. T. and ROBERTSON, D. E. 2014. The impacts of assimilating satellite soil moisture into a rainfall-runoff model in a semi-arid catchment. *Journal of Hydrology,* 519**,** 2763-2774.

ALVAREZ-GARRETON, C., RYU, D., WESTERN, A. W., SU, C. H., CROW, W. T., ROBERTSON, D. E. and LEAHY, C. 2015. Improving operational flood ensemble prediction by the assimilation of satellite soil moisture: comparison between lumped and semi-distributed schemes. *Hydrology & Earth System Sciences,* 19**,** 1659-1676.

ANCTIL, F., PERRIN, C. and ANDREASSIAN, V. 2003. ANN OUTPUT UPDATING OF LUMPED CONCEPTUAL RAINFALL/RUNOFF FORECASTING MODELS. *Journal of the American Water Resources Association,* 39**,** 1269.

ARNOLD, J. G., SRINIVASAN, R., MUTTIAH, R. S. and WILLIAMS, J. R. 1998. LARGE AREA HYDROLOGIC MODELING AND ASSESSMENT PART I: MODEL DEVELOPMENT1. *JAWRA Journal of the American Water Resources Association,* 34**,** 73-89.

ARULAMPALAM, M. S., MASKELL, S., GORDON, N. and CLAPP, T. 2002. A tutorial on particle filters for online nonlinear/non-Gaussian Bayesian tracking. *IEEE Transactions on Signal Processing,* 50**,** 174-188.

ATGER, F. 2001. Verification of intense precipitation forecasts from single models and ensemble prediction systems. *Nonlinear Processes in Geophysics,* 8**,** 401-417.

ATLAS, D., ULBRICH, C. W., MARKS, F. D., AMITAI, E. and WILLIAMS, C. R. 1999. Systematic variation of drop size and radar-rainfall relations. *Journal of Geophysical Research: Atmospheres,* 104**,** 6155-6169.

AUBERT, D., LOUMAGNE, C. and OUDIN, L. 2003. Sequential assimilation of soil moisture and streamflow data in a conceptual rainfall-runoff model. *Journal of Hydrology,* 280**,** 145-161.

BANDARAGODA, C., TARBOTON, D. G. and WOODS, R. Application of TOPNET in the distributed model intercomparison project. 2004. Elsevier, 178-201.

BARTALIS, Z., WAGNER, W., NAEIMI, V., HASENAUER, S., SCIPAL, K., BONEKAMP, H., FIGA, J. and ANDERSON, C. 2007. Initial soil moisture retrievals from the METOP-A Advanced Scatterometer (ASCAT). *Geophysical Research Letters,* 34**,** n/a-n/a.

BASHA, E. A., RAVELA, S. and RUS, D. 2008. Model-based monitoring for early warning flood detection. *Proceedings of the 6th ACM conference on Embedded network sensor systems.* Raleigh, NC, USA: ACM.

BATTAN, L., J. 1973. Radar observation of the atmosphere. L. J. Battan (The University of Chicago Press) 1973. PP X, 324; 125 figures, 21 tables. £7·15. *Quarterly Journal of the Royal Meteorological Society,* 99**,** 793-793.

BECK, H. E., DE JEU, R. A. M., SCHELLEKENS, J., VAN DIJK, A. I. J. M. and BRUIJNZEEL, L. A. 2009. Improving curve number based storm runoff estimates using soil moisture proxies. *IEEE Journal of Selected Topics In Applied Earth Observations And Remote Sensing,* 2**,** 250-9.

BEHRANGI, A., ANDREADIS, K., FISHER, J. B., TURK, F. J., GRANGER, S., PAINTER, T. and DAS, N. 2014. Satellite-Based Precipitation Estimation and Its Application for Streamflow Prediction over Mountainous Western U.S. Basins. *Journal of Applied Meteorology & Climatology,* 53**,** 2823-2842.

BENNETT, J. C., ROBERTSON, D. E., SHRESTHA, D. L., WANG, Q. J., ENEVER, D., HAPUARACHCHI, P. and TUTEJA, N. K. 2014. A System for Continuous Hydrological Ensemble Forecasting (SCHEF) to lead times of 9days. *Journal of Hydrology,* 519**,** 2832-2846.

BEVEN, K. 1989. Changing ideas in hydrology - the case of physically-based models. *Journal of Hydrology,* 105**,** 157-172.

BINDLISH, R. and BARROS, A. P. 2002. Subpixel variability of remotely sensed soil moisture: an inter-comparison study of SAR and ESTAR. *Geoscience and Remote Sensing, IEEE Transactions on,* 40**,** 326-337.

BINDLISH, R., JACKSON, T. J., WOOD, E., GAO, H., STARKS, P., BOSCH, D. and LAKSHMI, V. 2003. Soil moisture estimates from TRMM Microwave Imager observations over the Southern United States. *Remote Sensing of Environment,* 85**,** 507-515.

BINDLISH, R., CROW, W. T. and JACKSON, T. J. 2009. Role of passive microwave remote sensing in improving flood forecasts. *IEEE Geoscience and Remote Sensing Letters,* 6**,** 112-116.

BIONDI, D. and DE LUCA, D. L. 2013. Performance assessment of a Bayesian Forecasting System (BFS) for real-time flood forecasting. *Journal of Hydrology,* 479**,** 51-63.

BISSELINK, B., VAN MEIJGAARD, E., DOLMAN, A. J. and DE JEU, R. A. M. 2011. Initializing a regional climate model with satellite-derived soil moisture. 116**,** D02121 (13 pp.).

BLACKIE, J. R. and EELES, C. W. O. 1985. LUMPED CATCHMENT MODELS. Chichester, Engl: John Wiley & Sons.

BOM 2010. Operational implementation of the ACCESS numerinumerical weather prediction systems. *NMOC Operations Bulletin,* 83**,** Melbourne, Australia.

BORMANN, K. J., MCCABE, M. F. and EVANS, J. P. 2012. Satellite based observations for seasonal snow cover detection and characterisation in Australia. *Remote Sensing of Environment,* 123**,** 57-71.

BOUGHTON, W. C. 1984. A simple model for estimating the water yield of ungauged catchments. *Transactions of the Institution of Engineers, Australia, Civil Engineering,* CE26**,** 83-8.

BOWLER, N. E., PIERCE, C. E. and SEED, A. W. 2006. STEPS: A probabilistic precipitation forecasting scheme which merges an extrapolation nowcast with downscaled NWP. *Quarterly Journal of the Royal Meteorological Society,* 132**,** 2127-2155.

BRAVO, J. M., PAZ, A. R., COLLISCHONN, W., UVO, C. B., PEDROLLO, O. C. and CHOU, S. C. 2009. Incorporating forecasts of rainfall in two hydrologic models used for medium-range streamflow forecasting. *Journal of Hydrologic Engineering,* 14**,** 435-445.

BROCCA, L., MELONE, F., MORAMARCO, T. and MORBIDELLI, R. 2009a. Antecedent wetness conditions based on ERS scatterometer data. *Journal of Hydrology,* 364**,** 73-87.

BROCCA, L., MELONE, F., MORAMARCO, T. and SINGH, V. P. 2009b. Assimilation of observed soil moisture data in storm rainfall-runoff modeling. *Journal of Hydrologic Engineering,* 14**,** 153-165.

BROCCA, L., MELONE, F., MORAMARCO, T. and MORBIDELLI, R. 2010a. Spatial-temporal variability of soil moisture and its estimation across scales. *Water Resources Research,* 46**,** W02516.

BROCCA, L., MELONE, F., MORAMARCO, T., WAGNER, W., NAEIMI, V., BARTALIS, Z. and HASENAUER, S. 2010b. Improving runoff prediction through the assimilation of the ASCAT soil moisture product. *Hydrology and Earth System Sciences,* 14**,** 1881-1893.

BROCCA, L., HASENAUER, S., LACAVA, T., MELONE, F., MORAMARCO, T., WAGNER, W., DORIGO, W., MATGEN, P., MARTÍNEZ-FERNÁNDEZ, J., LLORENS, P., LATRON, J., MARTIN, C. and BITTELLI, M. 2011. Soil moisture estimation through ASCAT and AMSR-E sensors: An intercomparison and validation study across Europe. *Remote Sensing of Environment*, 115**,** 3390-3408.

BROCCA, L., MORAMARCO, T., MELONE, F., WAGNER, W., HASENAUER, S. and HAHN, S. 2012. Assimilation of surface- and root-zone ASCAT soil moisture products into rainfall-runoff modeling. *IEEE Transactions on Geoscience and Remote Sensing,* 50**,** 2542-55.

BROCCA, L., MORAMARCO, T., DORIGO, W. and WAGNER, W. Assimilation of satellite soil moisture data into rainfall-runoff modelling for several catchments worldwide. 2013 IEEE International Geoscience and Remote Sensing Symposium (IGARSS), 21-26 July 2013, 2013 Piscataway, NJ, USA. IEEE, 2281-4.

BURNASH, R. J. C., FERRAL, R. L., MCGUIRE, R. A. and CENTER, J. F.-S. R. F. 1973. *A generalized streamflow simulation system: conceptual modeling for digital computers*, U. S. Dept. of Commerce, National Weather Service.

CABLE, J. W., KOVACS, J. M., JIALI, S. and XIANFENG, J. 2014. Multi-Temporal Polarimetric RADARSAT-2 for Land Cover Monitoring in Northeastern Ontario, Canada. *Remote Sensing,* 6**,** 2372-2392.

CABUS, P. 2008. River flow prediction through rainfall-runoff modelling with a probability-distributed model (PDM) in Flanders, Belgium. *Agricultural Water Management,* 95**,** 859-868.

CALVER, A. 1996. Development and experience of the TATE rainfall runoff model. *Proceedings of the Institution of Civil Engineers: Water, Maritime and Energy,* 118**,** 168-176.

CALVET, J. C., NOILHAN, J. and BESSEMOULIN, P. 1998. Retrieving the root-zone soil moisture from surface soil moisture or temperature estimates: a feasibility study based on field measurements. *Journal of Applied Meteorology,* 37**,** 371-86.

CARROLL, D. G. Aspects of the URBS runoff routing model. Proceedings of the Water Down Under 1994 Conference. Part 3 (of 3), November 21, 1994 - November 25, 1994, 1994 Adelaide, Aust. IE Aust, 169-176.

CASATI, B., ROSS, G. and STEPHENSON, D. B. 2004. A new intensity-scale approach for the verification of spatial precipitation forecasts. *Meteorological Applications*, 11**,** 141-154.

CHAUHAN, N. S., MILLER, S. and ARDANUY, P. 2003. Spaceborne soil moisture estimation at high resolution: a microwave-optical/IR synergistic approach. *International Journal of Remote Sensing,* 24**,** 4599-4622.

CHEN, F., CROW, W. T., STARKS, P. J. and MORIASI, D. N. 2011. Improving hydrologic predictions of a catchment model via assimilation of surface soil moisture. *Advances in Water Resources,* 34**,** 526-536.

CHEN, F., CROW, W. T. and RYU, D. 2014. Dual Forcing and State Correction via Soil Moisture Assimilation for Improved Rainfall-Runoff Modeling. *Journal of Hydrometeorology,* 15**,** 1832-1848.

CHIEW, F. H. S., STEWARDSON, M. J. and MCMAHON, T. A. 1993. Comparison of six rainfall-runoff modelling approaches. *Journal of Hydrology,* 147**,** 1-36.

CHIEW, F. H. S. and SIRIWARDENA, L. Estimation of SIMHYD parameter values for application in ungauged catchments. *In:* ZERGER, A. & ARGENT, R. M., eds. MODSIM05; international congress on Modelling and simulation advances and applications for management and decision making; proceedings, 2005. Modelling and Simulation Society of Australia and New Zealand Inc., Canberra, A.C.T., Australia, 2883-2889.

CHUMCHEAN, S., SHARMA, A. and SEED, A. 2006. An Integrated Approach to Error Correction for Real-Time Radar-Rainfall Estimation. *Journal of Atmospheric and Oceanic Technology,* 23**,** 67-79.

CHUMCHEAN, S., SEED, A. and SHARMA, A. 2008. An operational approach for classifying storms in real-time radar rainfall estimation. *Journal of Hydrology,* 363**,** 1-17.

CIACH, G. J. 2003. Local random errors in tipping-bucket rain gauge measurements. *Journal of Atmospheric and Oceanic Technology,* 20**,** 752-9.

CIARAPICA, L. and TODINI, E. 2002. TOPKAPI: A model for the representation of the rainfall-runoff process at different scales. *Hydrological Processes,* 16**,** 207-229.

CLARK, M. P. and HAY, L. E. 2004. Use of Medium-Range Numerical Weather Prediction Model Output to Produce Forecasts of Streamflow. *Journal of Hydrometeorology,* 5**,** 15-32.

CLARK, M. P., SLATER, A. G., BARRETT, A. P., HAY, L. E., MCCABE, G. J., RAJAGOPALAN, B. and LEAVESLEY, G. H. 2006. Assimilation of snow covered area information into hydrologic and land-surface models. *Advances in Water Resources,* 29**,** 1209-1221.

CLARK, M. P., RUPP, D. E., WOODS, R. A., ZHENG, X., IBBITT, R. P., SLATER, A. G., SCHMIDT, J. and UDDSTROM, M. J. 2008. Hydrological data assimilation with the ensemble Kalman filter: Use of streamflow observations to update states in a distributed hydrological model. *Advances in Water Resources,* 31**,** 1309-1324.

CLOKE, H. L. and PAPPENBERGER, F. 2009. Ensemble flood forecasting: A review. *Journal of Hydrology,* 375**,** 613-626.

COLLE, B. A. and MASS, C. F. 1996. An Observational and Modeling Study of the Interaction of Low-Level Southwesterly Flow with the Olympic Mountains during COAST IOP 4. *Monthly Weather Review,* 124**,** 2152-2175.

COLLIER, C. G. 1989. *Applications of weather radar systems a guide to uses of radar data in meteorology and hydrology,* Ellis Horwood.

COLLOW, T. W., ROBOCK, A., BASARA, J. B. and ILLSTON, B. G. 2012. Evaluation of SMOS retrievals of soil moisture over the central United States with currently available in situ observations. *JOURNAL OF GEOPHYSICAL RESEARCH -ALL SERIES-,* 117**,** D09113.

CONTI, M., FERRANTE, M. and SAVI, F. A genetic algorithm to calibrate the rainfall-runoff model of Tiber catchment. ASM 2002 IASTED International Conference on Applied Simulation and Modeling, 25-28 June 2002, 2002 Anaheim, CA, USA. ACTA Press, 524-9.

CROW, W. T. and RYU, D. 2009. A new data assimilation approach for improving runoff prediction using remotely-sensed soil moisture retrievals. *Hydrology and Earth System Sciences,* 13**,** 1-16.

CSIRO 2008. Water availability in the Murrumbidgee: a report to the Australian Government from the CSIRO Murray-Darling Basin sustainable yields project, CSIRO, Australia. 155 pp.

CUO, L., PAGANO, T. C. and WANG, Q. J. 2011. A review of quantitative precipitation forecasts and their use in short- to medium-range streamflow forecasting. *Journal of Hydrometeorology,* 12**,** 713-728.

DAKHLAOUI, H., BARGAOUI, Z. and BARDOSSY, A. 2012. Toward a more efficient calibration schema for HBV rainfall-runoff model. *Journal of Hydrology,* 444-445**,** 161-179.

DAMRATH, U., DOMS, G., FRUHWALD, D., HEISE, E., RICHTER, B. and STEPPELER, J. 2000. Operational quantitative precipitation forecasting at the German Weather Service. *Journal of Hydrology,* 239**,** 260-285.

DAMRATH, U. 2004. Verification against precipitation observations of a high density network – what did we learn? . *International Verification Methods Workshop, Montreal, 15–17 September 2004*.

DAVIS, C., BROWN, B. and BULLOCK, R. 2006. Object-Based Verification of Precipitation Forecasts. Part I: Methodology and Application to Mesoscale Rain Areas. *Monthly Weather Review,* 134**,** 1772-1784.

DHARSSI, I., BOVIS, K. J., MACPHERSON, B. and JONES, C. P. 2011. Operational assimilation of ASCAT surface soil wetness at the Met Office. *Hydrol. Earth Syst. Sci.,* 15**,** 2729-2746.

DHI. 2000. MIKE SHE Water Movement User Manual. *DHI Water and Environment,* Hørsholm, Denmark.

DOELLING, I. G., JOSS, J. and RIEDL, J. 1998. Systematic variations of Z–R-relationships from drop size distributions measured in northern Germany during seven years. *Atmospheric Research,* 47–48**,** 635-649.

DONG, J., WALKER, J. P., HOUSER, P. R. and SUN CHAOJIAO, C. 2007. Scanning multichannel microwave radiometer snow water equivalent assimilation. *Journal of Geophysical Research-Part D-Atmospheres,* 112**,** 75-90.

DONG, X., DOHMEN-JANSSEN, C. M., BOOIJ, M. and HULSCHER, S. 2006. Effect of flow forecasting quality on benefits of reservoir operation - A case study for the Geheyan reservoir (China). *Hydrology and Earth System Sciences Discussions,* 3**,** 3771-3814.

DORIGO, W. A., GRUBER, A., DE JEU, R. A. M., WAGNER, W., STACKE, T., LOEW, A., ALBERGEL, C., BROCCA, L., CHUNG, D., PARINUSSA, R. M. and KIDD, R. 2015. Evaluation of the ESA CCI soil moisture product using ground-based observations. *Remote Sensing of Environment,* 162**,** 380-395.

DOSWELL, C. A., DAVIES-JONES, R. and KELLER, D. L. 1990. On Summary Measures of Skill in Rare Event Forecasting Based on Contingency Tables. *Weather and Forecasting,* 5**,** 576-585.

DOUBKOVÁ, M., VAN DIJK, A. I. J. M., SABEL, D., WAGNER, W. and BLÖSCHL, G. 2012. Evaluation of the predicted error of the soil moisture retrieval from C-band SAR by comparison against modelled soil moisture estimates over Australia. *Remote Sensing of Environment,* 120**,** 188-196.

DRAPER, C. S., MAHFOUF, J. F. and WALKER, J. P. 2009a. An EKF assimilation of AMSR-E soil moisture into the ISBA land surface scheme.

Journal of Geophysical Research - Part D - Atmospheres, 114**,** D20104 (13 pp.).

DRAPER, C. S., WALKER, J. P., STEINLE, P. J., DE JEU, R. A. M. and HOLMES, T. R. H. 2009b. An evaluation of AMSR-E derived soil moisture over Australia. *Remote Sensing of Environment,* 113**,** 703-710.

DRAPER, C. S., REICHLE, R. H., DE LANNOY, G. J. M. and LIU, Q. 2012. Assimilation of passive and active microwave soil moisture retrievals. *Geophysical Research Letters,* 39**,** n/a-n/a.

DRUSCH, M., WOOD, E. F. and GAO, H. 2005. Observation operators for the direct assimilation of TRMM microwave imager retrieved soil moisture. *Geophysical Research Letters,* 32**,** L15403.

DUAN, Q., SOROOSHIAN, S. and GUPTA, V. K. 1994. Optimal use of the SCE-UA global optimization method for calibrating watershed models. *Journal of Hydrology,* 158**,** 265-284.

DUMEDAH, G. and COULIBALY, P. 2013. Evolutionary assimilation of streamflow in distributed hydrologic modeling using in-situ soil moisture data. *Advances in Water Resources,* 53**,** 231-241.

DUMEDAH, G. and WALKER, J. P. 2014. Intercomparison of the JULES and CABLE land surface models through assimilation of remotely sensed soil moisture in southeast Australia. *Advances in Water Resources,* 74**,** 231-244.

DUMEDAH, G., WALKER, J. P. and RUDIGER, C. 2014. Can SMOS data be used directly on the 15-km discrete global grid? *IEEE Transactions on Geoscience and Remote Sensing***,** 2538.

DUMEDAH, G., P. WALKER, J. and MERLIN, O. 2015. Root-zone soil moisture estimation from assimilation of downscaled Soil Moisture and Ocean Salinity data. *Advances in Water Resources,* 84**,** 14-22.

EBERT, E. E. and MCBRIDE, J. L. 2000. Verification of precipitation in weather systems; determination of systematic errors. *Journal of Hydrology,* 239**,** 179-202.

EBERT, E. E., WILSON, L. J., BROWN, B. G., NURMI, P., BROOKS, H. E., BALLY, J. and JAENEKE, M. 2004. Verification of nowcasts from the WWRP Sydney 2000 Forecast Demonstration Project. *Weather and Forecasting,* 19**,** 73-96.

EBERT, E. E. 2008. Fuzzy verification of high-resolution gridded forecasts: a review and proposed framework. *Meteorological Applications,* 15**,** 51-64.

EDIJATNO and MICHEL, C. 1989. Un modèle pluie-débit journalier à trois paramètres. *La Houille Blanche* 2**,** 113-121.

EDIJATNO, DE OLIVEIRA NASCIMENTO, N., YANG, X., MAKHLOUF, Z. and MICHEL, C. 1999. GR3J: A daily watershed model with three free parameters. *Hydrological Sciences Journal,* 44**,** 263-277.

ENGMAN, E. T. 1990. Progress in Microwave Remote Sensing of Soil Moisture. *Canadian Journal of Remote Sensing,* 16**,** 6-14.

ENGMAN, E. T. 1991. Applications of microwave remote sensing of soil moisture for water resources and agriculture. *Remote sensing of environment (USA)***,** 213.

ENGMAN, E. T. and CHAUHAN, N. 1995. Status of microwave soil moisture measurements with remote sensing. *Remote Sensing of Environment,* 51**,** 189-198.

ENTEKHABI, D., NAKAMURA, H. and NJOKU, E. G. 1994. Solving the inverse problem for soil moisture and temperature profiles by sequential assimilation of multifrequency remotely sensed observations. *IEEE Transactions on Geoscience and Remote Sensing***,** 438.

ENTEKHABI, D., NJOKU, E. G., O'NEILL, P. E., KELLOGG, K. H., CROW, W. T., EDELSTEIN, W. N., ENTIN, J. K., GOODMAN, S. D., JACKSON, T. J., JOHNSON, J., KIMBALL, J., PIEPMEIER, J. R., KOSTER, R. D., MARTIN, N., MCDONALD, K. C., MOGHADDAM, M., MORAN, S., REICHLE, R., SHI, J. C., SPENCER, M. W., THURMAN, S. W., LEUNG, T. and VAN ZYL, J. 2010. The Soil Moisture Active Passive (SMAP) Mission. *Proceedings of the IEEE,* 98**,** 704-716.

EVENSEN, G. 1994. Sequential data assimilation with a nonlinear quasi-geostrophic model using Monte Carlo methods to forecast error statistics. *Journal of Geophysical Research: Oceans,* 99**,** 10143-10162.

EVENSEN, G. and VAN LEEUWEN, P. J. 2000. An Ensemble Kalman Smoother for Nonlinear Dynamics. *Monthly Weather Review,* 128**,** 1852-1867.

FIELDS, G., SEED, A., YU, B. and MALONE, T. 2004. Calibration of weather radar in South East Queensland. *Sixth international symposium on hydrological applications of weather radar, Melbourne, Australia*.

GABELLA, M., JOSS, J., PERONA, G. and MICHAELIDES, S. 2006. Range adjustment for ground-based radar, derived with the spaceborne TRMM precipitation radar. *IEEE Transactions on Geoscience and Remote Sensing,* 44**,** 126-33.

GAFUROV, A. and BARDOSSY, A. 2009. Cloud removal methodology from MODIS snow cover product. *Hydrology and Earth System Sciences,* 13**,** 1361-1373.

GAO, H., WOOD, E. F., JACKSON, T. J., DRUSCH, M. and BINDLISH, R. 2006. Using TRMM/TMI to Retrieve Surface Soil Moisture over the Southern United States from 1998 to 2002. *Journal of Hydrometeorology,* 7**,** 23-38.

GAO, Y., XIE, H., LU, N., YAO, T. and LIANG, T. 2010. Toward advanced daily cloud-free snow cover and snow water equivalent products from Terra-Aqua MODIS and Aqua AMSR-E measurements. *Journal of Hydrology,* 385**,** 23-35.

GIBBS, M. S., DANDY, G. C. and MAIER, H. R. Calibration of rainfall runoff models in ungauged catchments: Regionalization relationships for a rainfall runoff model. World Environmental and Water Resources Congress 2008: Ahupua'a, May 12, 2008 - May 16, 2008, 2008 Honolulu, HI, United states. American Society of Civil Engineers, Environmental and Water Resources Institute of ASCE.

GILL, M. A. 1978. Flood routing by the Muskingum method. *Journal of Hydrology,* 36**,** 353-363.

GLANTZ, M. H. 2004. *Early Warning Systems: Do's and Don'ts*, The Center.

GLOERSEN, P. and BARATH, F. 1977. A scanning multichannel microwave radiometer for Nimbus-G and SeaSat-A. *Oceanic Engineering, IEEE Journal of,* 2**,** 172-178.

GORDON, N. J., SALMOND, D. J. and SMITH, A. F. M. 1993. Novel approach to nonlinear/non-Gaussian Bayesian state estimation. *Radar and Signal Processing, IEE Proceedings F,* 140**,** 107-113.

GOSWAMI, M., O'CONNOR, K. M., BHATTARAI, K. P. and SHAMSELDIN, A. Y. 2005. Assessing the performance of eight real-time updating models and procedures for the Brosna River. *Hydrology and Earth System Sciences,* 9**,** 394-411.

GOSWAMI, M. and O'CONNOR, K. M. 2007. Comparative assessment of six automatic optimization techniques for calibration of a conceptual rainfall-runoff model. *Hydrological Sciences Journal*, 52**,** 432-449.

GOURLEY, J. J. and VIEUX, B. E. 2005. A Method for Evaluating the Accuracy of Quantitative Precipitation Estimates from a Hydrologic Modeling Perspective. *Journal of Hydrometeorology,* 6**,** 115-133.

GRAYSON, R. and BLÖSCHL, G. 2000. Spatial modelling of catchment dynamics, in: Grayson, R. and Blöschl,G. (Eds.). *Spatial Patterns in Catchment Hydrology: Observations and Modelling,***,** Cambridge University Press, Cambridge, UK, 51-81.

GREEN, D., PETROVIC, J., MOSS, P. and BURRELL, M. 2011. Water resources and management overview: Murrumbidgee catchment, . NSW Office of Water, Sydney.

GRIESFELLER, A., LAHOZ, W. A., JEU, R. A. M. D., DORIGO, W., HAUGEN, L. E., SVENDBY, T. M. and WAGNER, W. 2016. Evaluation of satellite soil moisture products over Norway using ground-based observations. *International Journal of Applied Earth Observation and Geoinformation,* 45, Part B**,** 155-164.

GRUHIER, C., DE ROSNAY, P., HASENAUER, S., HOLMES, T., DE JEU, R., KERR, Y., MOUGIN, E., NJOKU, E., TIMOUK, F., WAGNER, W. and ZRIBI, M. 2010. Soil moisture active and passive microwave products: intercomparison and evaluation over a Sahelian site. *Hydrol. Earth Syst. Sci.,* 14**,** 141-156.

HAMLET, A., HUPPERT, D. and LETTENMAIER, D. 2002. Economic Value of Long-Lead Streamflow Forecasts for Columbia River Hydropower. *Journal of Water Resources Planning and Management,* 128**,** 91-101.

HAPUARACHCHI, H. A. P., WANG, Q. J. and PAGANO, T. C. 2011. A review of advances in flash flood forecasting. *Hydrological Processes,* 25**,** 2771-2784.

HARRISON, D. L., DRISCOLL, S. J. and KITCHEN, M. 2000. Improving precipitation estimates from weather radar using quality control and correction techniques. *Meteorological Applications,* 7**,** 135.

HE, M., HOGUE, T. S., MARGULIS, S. A. and FRANZ, K. J. 2012. An integrated uncertainty and ensemble-based data assimilation approach for improved operational streamflow predictions. *Hydrol. Earth Syst. Sci.,* 16**,** 815-831.

HEATHMAN, G. C., STARKS, P. J., AHUJA, L. R. and JACKSON, T. J. 2003. Assimilation of surface soil moisture to estimate profile soil water content. *Journal of Hydrology,* 279**,** 1-17.

HILDEBRAND, P. H. 1978. Iterative correction for attenuation of 5 cm radar in rain. *Journal of Applied Meteorology,* 17**,** 508-14.

HORNACEK, M., WAGNER, W., SABEL, D., TRUONG, H. L., SNOEIJ, P., HAHMANN, T., DIEDRICH, E. and DOUBKOVA, M. 2012. Potential for High Resolution Systematic Global Surface Soil Moisture Retrieval via Change Detection Using Sentinel-1. *IEEE Journal of Selected Topics In Applied Earth Observations And Remote Sensing,* 5**,** 1303-1311.

HOUSER, P. R., SHUTTLEWORTH, W. J., FAMIGLIETTI, J. S., GUPTA, H. V., SYED, K. H. and GOODRICH, D. C. 1998. Integration of soil moisture remote sensing and hydrologic modeling using data assimilation. *Water Resources Research,* 34**,** 3405-3420.

HOUSER, P. R., DE LANNOY, G. and WALKER, J. P. 2012. Hydrologic Data Assimilation. *In:* P., T. J. (ed.) *Approaches to Managing Disaster - Assessing Hazards, Emergencies and Disaster Impacts.* InTech.

JACKSON, T. J., COSH, M. H., BINDLISH, R., STARKS, P. J., BOSCH, D. D., SEYFRIED, M., GOODRICH, D. C., MORAN, M. S. and DU, J. 2010. Validation of advanced microwave scanning radiometer soil moisture products. *IEEE Transactions on Geoscience and Remote Sensing,* 48**,** 4256-4272.

JACQUETTE, E., BITAR, A. A., MIALON, A., KERR, Y., QUESNEY, A., CABOT, F. and RICHAUME, P. 2010. SMOS CATDS level 3 global products over land [7824 0K]. *PROCEEDINGS- SPIE THE INTERNATIONAL SOCIETY FOR OPTICAL ENGINEERING,* 7826**,** xxxii.

JAKEMAN, A. J., LITTLEWOOD, I. G. and WHITEHEAD, P. G. 1990. Computation of the instantaneous unit hydrograph and identifiable component flows with application to two small upland catchments. *Journal of Hydrology,* 117**,** 275-300.

JIAN, P., NIESEL, J., LOEW, A., SHIQIANG, Z. and JIE, W. 2015. Evaluation of Satellite and Reanalysis Soil Moisture Products over Southwest China Using Ground-Based Measurements. *Remote Sensing,* 7**,** 15729-15747.

JORDAN, P., SEED, A. and AUSTIN, G. 2000. Sampling errors in radar estimates of rainfall. *Journal of Geophysical Research: Atmospheres,* 105**,** 2247-2257.

JORDAN, P. W., SEED, A. W. and WEINMANN, P. E. 2003. A Stochastic Model of Radar Measurement Errors in Rainfall Accumulations at Catchment Scale. *Journal of Hydrometeorology,* 4**,** 841-855.

JOSS, J. and LEE, R. 1995. The Application of Radar-Gauge Comparisons to Operational Precipitation Profile Corrections. *Journal of Applied Meteorology,* 34**,** 2612-2630.

JUN, W., JACKSON, T. J., BINDLISH, R., HSU, A. Y. and SU, Z. B. 2005. Retrieval of Soil Moisture and Vegetation Water Content Using SSM/I Data over a Corn and Soybean Region. *Journal of Hydrometeorology,* 6**,** 854-863.

JUNG, H. C., JASINSKI, M., KIM, J.-W., SHUM, C. K., BATES, P., NEAL, J., LEE, H. and ALSDORF, D. 2012. Calibration of two-dimensional floodplain modeling in the central Atchafalaya Basin Floodway System using SAR interferometry. *Water Resources Research,* 48**,** n/a-n/a.

KALMAN, R. E. 1960. A new approach to linear filtering and prediction problems. Transactions of the ASME. *Journal of Basic Engineering,* . 82**,** 35-45.

KAY, A. L., JONES, D. A., CROOKS, S. M., CALVER, A. and REYNARD, N. S. 2006. A comparison of three approaches to spatial generalization of rainfall-runoff models. *Hydrological Processes,* 20**,** 3953-3973.

KERR, Y. H., WALDTEUFEL, P., WIGNERON, J. P., MARTINUZZI, J., FONT, J. and BERGER, M. 2001. Soil moisture retrieval from space: the Soil Moisture and Ocean Salinity (SMOS) mission. *Geoscience and Remote Sensing, IEEE Transactions on,* 39**,** 1729-1735.

KERR, Y. H., WALDTEUFEL, P., WIGNERON, J. P., DELWART, S., CABOT, F., BOUTIN, J., ESCORIHUELA, M. J., FONT, J., REUL, N., GRUHIER, C., JUGLEA, S. E., DRINKWATER, M. R., HAHNE, A., MARTI, X, N-NEIRA, M. and MECKLENBURG, S. 2010. The SMOS Mission: New Tool for Monitoring Key Elements ofthe Global Water Cycle. *Proceedings of the IEEE,* 98**,** 666-687.

KERR, Y. H., WALDTEUFEL, P., RICHAUME, P., WIGNERON, J. P., FERRAZZOLI, P., MAHMOODI, A., BITAR, A. A., CABOT, F., GRUHIER, C., JUGLEA, S. E., LEROUX, D., MIALON, A. and DELWART, S. 2012. The SMOS Soil Moisture Retrieval Algorithm. *IEEE Transactions on Geoscience and Remote Sensing,* 50**,** 1384-1403.

KIDD, C. and LEVIZZANI, V. 2011. Status of satellite precipitation retrievals. *Hydrology and Earth System Sciences,* 15**,** 1109-1116.

KIM, B. S., KIM, B. K. and KIM, H. S. 2008. Flood simulation using the gauge-adjusted radar rainfall and physics-based distributed hydrologic model. *Hydrological Processes,* 22**,** 4400-4414.

KIM, G. and BARROS, A. P. 2002. Downscaling of remotely sensed soil moisture with a modified fractal interpolation method using contraction mapping and ancillary data. *Remote Sensing of Environment,* 83**,** 400-413.

KIM, S., LIU, Y. Y., JOHNSON, F. M., PARINUSSA, R. M. and SHARMA, A. 2015. A global comparison of alternate AMSR2 soil moisture products: Why do they differ? *Remote Sensing of Environment,* 161**,** 43-62.

KOBOLD, M. and SUŠELJ, K. 2005. Precipitation forecasts and their uncertainty as input into hydrological models. *Hydrol. Earth Syst. Sci.,* 9**,** 322-332.

KOKKONEN, T., KOIVUSALO, H. and KARVONEN, T. 2001. A semi-distributed approach to rainfall-runoff modelling—a case study in a snow affected catchment. *Environmental Modelling & Software,* 16**,** 481-493.

KOMMA, J., BLÖSCHL, G. and RESZLER, C. 2008. Soil moisture updating by Ensemble Kalman Filtering in real-time flood forecasting. *Journal of Hydrology,* 357**,** 228-242.

KRAJEWSKI, W. F., VILLARINI, G. and SMITH, J. A. 2010. RADAR-Rainfall Uncertainties. *Bulletin of the American Meteorological Society,* 91**,** 87-94.

KRZYSZTOFOWICZ, R. 1999. Bayesian theory of probabilistic forecasting via deterministic hydrologic model. *Water Resources Research,* 35**,** 2739-2750.

KUMAR, S., SEKHAR, M. and BANDYOPADHYAY, S. 2009. Assimilation of remote sensing and hydrological data using adaptive filtering techniques for watershed modelling. *Current Science,* 97**,** 1196-202.

KUNDZEWICZ, Z. W. 2012. *Changes in Flood Risk in Europe*, Taylor & Francis.

LACAVA, T., BROCCA, L., CALICE, G., MELONE, F., MORAMARCO, T., PERGOLA, N. and TRAMUTOLI, V. 2010. Soil moisture variations monitoring by AMSU-based soil wetness indices: A long-term inter-comparison with ground measurements. *Remote Sensing of Environment,* 114**,** 2317-2325.

LACAVA, T., MATGEN, P., BROCCA, L., BITTELLI, M., PERGOLA, N., MORAMARCO, T. and TRAMUTOLI, V. 2012. A first assessment of the SMOS soil moisture product with in situ and modeled data in Italy and Luxembourg. *IEEE Transactions on Geoscience and Remote Sensing***,** 1612.

LAI, X., LIANG, Q., YESOU, H. and DAILLET, S. 2014. Variational assimilation of remotely sensed flood extents using a 2-D flood model. *Hydrology & Earth System Sciences,* 18**,** 4325-4339.

LARSON, L. W. and PECK, E. L. 1974. Accuracy of precipitation measurements for hydrologic modeling. *Water Resources Research,* 10**,** 857-863.

LEAHY, C., BADDILEY, P. and SOORIYAKUMARAN, S. 2008. Comparison of Two Continuous Soil Moisture Accounting Models for Flood Forecasting. *International Conference on Water Resources and Environment Research,* Engineers Australia, Causal Productions, Modbury, Adelaide, Australia**,** 341-352.

LEE, C. K., LEE, G. W., ZAWADZKI, I. and KIM, K.-E. 2009. A preliminary analysis of spatial variability of raindrop size distributions during stratiform rain events. *Journal of Applied Meteorology and Climatology,* 48**,** 270-283.

LEROUX, D. J., PELLARIN, T., VISCHEL, T., COHARD, J. M., GASCON, T., GIBON, F., MIALON, A., GALLE, S. and PEUGEOT, C. 2016. Assimilation of SMOS soil moisture into a distributed hydrological model and impacts on the water cycle variables over the Ouémé catchment in Benin. *Hydrol. Earth Syst. Sci. Discuss.,* 2016**,** 1-26.

LI, H., ZHANG, S., QIU, C. and ZHANG, W. 2010. A Study of Retrieving the Soil Moisture Profile by Combining the Four-Dimensional Variational Data Assimilation with the Ensemble Square Root Filter. *Journal of Tsinghua University (Science and Technology),* 34**,** 193-201.

LI, L. and GAISER, P. WindSat soil moisture algorithm and validation. Geoscience and Remote Sensing Symposium, 2007. IGARSS 2007. IEEE International, 23-28 July 2007 2007. 1188-1191.

LI, Y., RYU, D., WANG, Q. J., THOMAS, P., WESTERN, W. A., HAPUARACHCHI, P. and TOSCAS, P. 2011. Assimilation of streamflow discharge into a continuous flood forecasting model. *Proceedings of Symposium H03 held during IUGG GA 2011, Melbourne, Australia, IAHS Publ***,** 107-113.

LI, Y., RYU, D., WESTERN, A. W. and WANG, Q. J. 2013. Assimilation of stream discharge for flood forecasting: The benefits of accounting for routing time lags. *Water Resources Research,* 49**,** 1887-1900.

LI, Y., RYU, D., WESTERN, A. W., WANG, Q. J., ROBERTSON, D. E. and CROW, W. T. 2014. An integrated error parameter estimation and lag-aware data assimilation scheme for real time flood forecasting. *Journal of Hydrology,* 519**,** 2722-2736.

LIANG, X., ZHENG, X., ZHANG, S., WU, G., DAI, Y. and LI, Y. 2012. Maximum likelihood estimation of inflation factors on error covariance matrices for ensemble Kalman filter assimilation. *Quarterly Journal of the Royal Meteorological Society,* 138**,** 263-273.

LIEVENS, H., TOMER, S. K., AL BITAR, A., DE LANNOY, G. J. M., DRUSCH, M., DUMEDAH, G., HENDRICKS FRANSSEN, H. J., KERR, Y. H., MARTENS, B., PAN, M., ROUNDY, J. K., VEREECKEN, H., WALKER, J. P., WOOD, E. F., VERHOEST, N. E. C. and PAUWELS, V. R. N. 2015. SMOS soil moisture assimilation for improved hydrologic simulation in the Murray Darling Basin, Australia. *Remote Sensing of Environment,* 168**,** 146-162.

LINDSTRÖM, G. 1997. A Simple Automatic Calibration Routine for the HBV Model. *Hydrology Research,* 28**,** 153-168.

LINSLEY, R. K. RAINFALL-RUNOFF MODELS - AN OVERVIEW. Rainfall-Runoff Relationship (Proceedings of the International Symposium on Rainfall-Runoff Modeling). 1982 Mississippi State, MS, Can. Water Resources Publ, 3-22.

LIU, Y. and GUPTA, H. V. 2007. Uncertainty in hydrologic modeling: Toward an integrated data assimilation framework. *Water Resources Research,* 43**,** W07401.

LIU, Y. Y., PARINUSSA, R. M., DORIGO, W. A., DE JEU, R. A. M., WAGNER, W., VAN DIJK, A. I. J. M., MCCABE, M. F. and EVANS, J. P. 2011. Developing an improved soil moisture dataset by blending passive and active microwave satellite-based retrievals. *Hydrology & Earth System Sciences,* 15**,** 425-436.

LIVINGSTONE, C. E., SIKANETA, I., GIERULL, C., CHIU, S. and BEAULNE, P. RADARSAT-2 System and Mode Description. 2006. NATO, 13.

LOUMAGNE, C., CHKIR, N., NORMAND, M., OTTLÉ, C. and VIDAL-MADJAR, D. 1996. Introduction of the soil/vegetation/atmosphere continuum in a conceptual rainfall/runoff model. *Hydrological Sciences Journal,* 41**,** 889-902.

LOUVET, S., PELLARIN, T., AL BITAR, A., CAPPELAERE, B., GALLE, S., GRIPPA, M., GRUHIER, C., KERR, Y., LEBEL, T., MIALON, A., MOUGIN, E., QUANTIN, G., RICHAUME, P. and DE ROSNAY, P. 2015. SMOS soil moisture product evaluation over West-Africa from local to regional scale. *Remote Sensing of Environment,* 156**,** 383-394.

MAPIAM, P. P. and SRIWONGSITANON, N. 2008. Climatological Z-R relationship for radar rainfall estimation in the upper Ping river basin. *Science Asia,* 34**,** 215-22.

MAPIAM, P. P., SRIWONGSITANON, N., CHUMCHEAN, S. and SHARMA, A. 2009. Effects of rain gauge temporal resolution on the specification of a Z-R relationship. *Journal of Atmospheric and Oceanic Technology,* 26**,** 1302-14.

MARZBAN, C. and SANDGATHE, S. 2006. Cluster Analysis for Verification of Precipitation Fields. *Weather and Forecasting,* 21**,** 824-838.

MASSARI, C., BROCCA, L., BARBETTA, S., PAPATHANASIOU, C., MIMIKOU, M. and MORAMARCO, T. 2014. Using globally available soil moisture indicators for flood modelling in Mediterranean catchments. *Hydrol. Earth Syst. Sci.,* 18**,** 839-853.

MATGEN, P., HENRY, J.-B., HOFFMANN, L. and PFISTER, L. Assimilation of remotely sensed soil saturation levels in conceptual rainfall-runoff models. 2006. IAHS Press, 226-234.

MATHEVET, T. 2005. *Which rainfall–runoff model at the hourly time-step? Empirical development and intercomparison of rainfall–runoff models on a large sample of watersheds, PhD Thesis, ENGREF, Paris, France (in French).*

MERLIN, O., CHEHBOUNI, A., BOULET, G. and KERR, Y. 2006. Assimilation of Disaggregated Microwave Soil Moisture into a Hydrologic Model Using Coarse-Scale Meteorological Data. *Journal of Hydrometeorology,* 7**,** 1308-1322.

MERLIN, O., CHEHBOUNI, A., WALKER, J. P., PANCIERA, R. and KERR, Y. H. 2008. A simple method to disaggregate passive microwave-based soil moisture. *IEEE Transactions on Geoscience and Remote Sensing***,** 786.

MERLIN, O., RUDIGER, C., BITAR, A. A., RICHAUME, P., WALKER, J. P. and KERR, Y. H. 2012. Disaggregation of SMOS Soil Moisture in Southeastern Australia. *IEEE Transactions on Geoscience and Remote Sensing,* 50**,** 1556-1571.

MLADENOVA, I., LAKSHMI, V., WALKER, J. P., PANCIERA, R., WAGNER, W. and DOUBKOVA, M. 2010. Validation of the ASAR global monitoring mode soil moisture product using the NAFE'05 data set. *IEEE Transactions on Geoscience and Remote Sensing***,** 2498.

MOHAMED ABOU, N., MICHEL, N., MONIQUE, B. and ISABELLE, P. 2012. Digital Mapping of Soil Drainage Classes Using Multitemporal RADARSAT-1 and ASTER Images and Soil Survey Data. *Applied and Environmental Soil Science*.

MOORE, R. J. 1999. Real-Time Flood Forecasting Systems: Perspectives and Prospects. *In:* CASALE, R. & MARGOTTINI, C. (eds.) *Floods and Landslides: Integrated Risk Assessment.* Springer Berlin Heidelberg.

MOORE, R. J. 2007. The PDM rainfall-runoff model. *Hydrology and Earth System Sciences,* 11**,** 483-499.

MORADKHANI, H., SOROOSHIAN, S., GUPTA, H. V. and HOUSER, P. R. 2005. Dual state-parameter estimation of hydrological models using ensemble Kalman filter. *Advances in Water Resources*, 28**,** 135-147.

MULUYE, G. Y. 2011. Deriving meteorological variables from numerical weather prediction model output: A nearest neighbor approach. *Water Resources Research,* 47**,** W07509-W07509.

NASCIMENTO, N. O. 1995. Appréciation à l'aide d'un modèles empirique des effects d'action anthropiques sur la relation pluie-débit à l' échelle du basin versant. *Ph.D. Thesis***,** CERGRENE/ENPC, Paris, France 550 p.

NASH, J. E. and SUTCLIFFE, J. V. 1970. River flow forecasting through conceptual models part I — A discussion of principles. *Journal of Hydrology,* 10**,** 282-290.

NICHOLS, N. K. Data assimilation: aims and basic concepts. *In:* SWINBANK, R., SHUT˜NISAEV, V. P. & LAHOZ, W. A., eds., 2003. Boston, Kluwer Academic Publishers, 9-20.

NJOKU, E. G. and ENTEKHABI, D. 1996. Passive microwave remote sensing of soil moisture. *Journal of Hydrology,* 184**,** 101-129.

NJOKU, E. G., JACKSON, T. J., LAKSHMI, V., CHAN, T. K. and NGHIEM, S. V. 2003. Soil moisture retrieval from AMSR-E. *IEEE Transactions on Geoscience and Remote Sensing,* 41**,** 215-29.

O'CONNELL, P. E., NASH, J. E. and FARRELL, J. P. 1970. River flow forecasting through conceptual models; Part II, The Brosna catchment at Ferbane. *Journal of Hydrology,* 10**,** 317-329.

OWE, M., DE JEU, R. and WALKER, J. 2001. A methodology for surface soil moisture and vegetation optical depth retrieval using the microwave polarization difference index. *IEEE Transactions on Geoscience and Remote Sensing,* 39**,** 1643-54.

OWE, M. and DE JEU, R. A. M. Retrieving surface soil moisture and vegetation optical depth from satellite microwave observations. IGARSS 2001. Scanning the Present and Resolving the Future. Proceedings. IEEE 2001

International Geoscience and Remote Sensing Symposium, 9-13 July 2001, 2001 Piscataway, NJ, USA. IEEE, 15-18.

OWE, M., DE JEU, R. and HOLMES, T. 2008. Multisensor historical climatology of satellite-derived global land surface moisture. *JOURNAL OF GEOPHYSICAL RESEARCH-EARTH SURFACE,* 113**,** F01002.

PAGANO, T. C., WANG, Q. J., HAPUARACHCHI, P. and ROBERTSON, D. 2010. Continuous rainfall-runoff model comparison and short-term daily streamflow forecast skill evaluation. *CSIRO: Water for a Healthy Country National Research Flagship Technical Report*.

PAGANO, T. C., WANG, Q. J., HAPUARACHCHI, P. and ROBERTSON, D. 2011. A dual-pass error-correction technique for forecasting streamflow. *Journal of Hydrology,* 405**,** 367-381.

PANCIERA, R., WALKER, J. P., KALMA, J. D., KIM, E. J., SALEH, K. and WIGNERON, J.-P. 2009. Evaluation of the SMOS L-MEB passive microwave soil moisture retrieval algorithm. *Remote Sensing of Environment,* 113**,** 435-444.

PARAJKA, J., NAEIMI, V., BLOSCHL, G., WAGNER, W., MERZ, R. and SCIPAL, K. 2006. Assimilating scatterometer soil moisture data into conceptual hydrologic models at the regional scale. *Hydrology and Earth System Sciences,* 10**,** 353-368.

PARAJKA, J. and BLOSCHL, G. 2008. Spatio-temporal combination of MODIS images - Potential for snow cover mapping. *Water Resources Research,* 44.

PARAJKA, J., NAEIMI, V., BLOSCHL, G. and KOMMA, J. 2009. Matching ERS scatterometer based soil moisture patterns with simulations of a conceptual dual layer hydrologic model over Austria. *Hydrology and Earth System Sciences,* 13**,** 259-271.

PARKER, D. and FORDHAM, M. 1996. An evaluation of flood forecasting, warning and response systems in the European Union. *Water Resources Management,* 10**,** 279-302.

PATHE, C., WAGNER, W., SABEL, D., DOUBKOVA, M. and BASARA, J. B. 2009. Using ENVISAT ASAR Global Mode Data for Surface Soil Moisture Retrieval Over Oklahoma, USA. *Geoscience and Remote Sensing, IEEE Transactions on,* 47**,** 468-480.

PAUWELS, V. R. N., HOEBEN, R., VERHOEST, N. E. C., DE TROCH, F. P. and TROCH, P. A. 2002. Improvement of TOPLATS-based discharge predictions through assimilation of ERS-based remotely sensed soil moisture values. *Hydrological Processes,* 16**,** 995-1013.

PAUWELS, V. R. N. and DE LANNOY, G. J. M. 2006. Improvement of modeled soil wetness conditions and turbulent fluxes through the assimilation of observed discharge. *Journal of Hydrometeorology,* 7**,** 458-477.

PAUWELS, V. R. N. and DE LANNOY, G. J. M. 2009. Ensemble-based assimilation of discharge into rainfall-runoff models: A comparison of approaches to mapping observational information to state space. *Water Resources Research,* 45.

PAUWELS, V. R. N. and DE LANNOY, G. J. M. 2015. Error covariance calculation for forecast bias estimation in hydrologic data assimilation. *Advances in Water Resources,* 86**,** 284-296.

PECHLIVANIDIS, I. G., MCINTYRE, N. R. and WHEATER, H. S. 2010. Calibration of the semi-distributed PDM rainfall–runoff model in the Upper Lee catchment, UK. *Journal of Hydrology,* 386**,** 198-209.

PELEG, N., BEN-ASHER, M. and MORIN, E. 2013. Radar subpixel-scale rainfall variability and uncertainty: Lessons learned from observations of a dense rain-gauge network. *Hydrology and Earth System Sciences,* 17**,** 2195-2208.

PELLENQ, J., KALMA, J., BOULET, G., SAULNIER, G. M., WOOLDRIDGE, S., KERR, Y. and CHEHBOUNI, A. 2003. A disaggregation scheme for soil moisture based on topography and soil depth. *Journal of Hydrology,* 276**,** 112-127.

PERRIN, C., MICHEL, C. and ANDREASSIAN, V. 2003. Improvement of a parsimonious model for streamflow simulation. *Journal of Hydrology,* 279**,** 275-289.

PICCOLO, F. and CHIRICO, G. B. 2005. Sampling errors in rainfall measurements by weather radar. *Advances in Geosciences,* 2**,** 151-155.

PILES, M., CAMPS, A., VALL-LLOSSERA, M., CORBELLA, I., PANCIERA, R., RUDIGER, C., KERR, Y. H. and WALKER, J. 2011. Downscaling SMOS-Derived Soil Moisture Using MODIS Visible/Infrared Data. *IEEE Transactions on Geoscience and Remote Sensing,* 49**,** 3156-3166.

PILES, M., SANCHEZ, N., VALL-LLOSSERA, M., CAMPS, A., MARTINEZ-FERNANDEZ, J., MARTINEZ, J. and GONZALEZ-GAMBAU, V. 2014. A Downscaling Approach for SMOS Land Observations: Evaluation of High-Resolution Soil Moisture Maps Over the Iberian Peninsula. *IEEE Journal of Selected Topics In Applied Earth Observations And Remote Sensing,* 7**,** 3845-3857.

PLAZA, D. A., DE KEYSER, R., DE LANNOY, G. J. M., GIUSTARINI, L., MATGEN, P. and PAUWELS, V. R. N. 2012. The importance of parameter resampling for soil moisture data assimilation into hydrologic models using the particle filter. *Hydrology & Earth System Sciences,* 16**,** 375-390.

PRATOLA, C., BARRETT, B., GRUBER, A. and DWYER, E. 2015. Quality Assessment of the CCI ECV Soil Moisture Product Using ENVISAT ASAR Wide Swath Data over Spain, Ireland and Finland. *Remote Sensing,* 7**,** 15388-15423.

PURI, K., DIETACHMAYER, G., STEINLE, P., DIX, M., RIKUS, L., LOGAN, L., NAUGHTON, M., TINGWELL, C., XIAO, Y., BARRAS, V., BERMOUS, I., BOWEN, R., DESCHAMPS, L., FRANKLIN, C., FRASER, J., GLOWACKI, T., HARRIS, B., LEE, J., LE, T., ROFF, G., SULAIMAN, A., SIMS, H., SUN, X., SUN, Z., ZHU, H., CHATTOPADHYAY, M. and ENGEL, C. 2013. Implementation of the initial ACCESS numerical weather prediction system. *Australian Meteorological and Oceanographic Journal,* 63**,** 265-284.

RAUPACH, M. R., BRIGGS, P. R., HAVERD, V., KING, E. A., PAGET, M. and TRUDINGER, C. M. 2009a. Australian Water Availability Project (AWAP), CSIRO Marine and Atmospheric Research Component: Final Report for Phase 3. *CAWCR Technical Report No. 013, Centre for Australian Weather and Climate Research (Bureau of Meteorology and CSIRO), Melbourne, Australia***,** 67 pp.

RAUPACH, M. R., BRIGGS, P. R., HAVERD, V., KING, E. A., PAGET, M. and TRUDINGER, C. M. 2009b. Australian Water Availability Project (AWAP), CSIRO Marine and Atmospheric Research Component: Final Report for Phase 3. CAWCR Technical Report No. 013, Centre for Australian Weather and Climate Research (Bureau of Meteorology and CSIRO), Melbourne, Australia, 67 pp. .

REICHLE, R. H., MCLAUGHLIN, D. and ENTEKHABI, D. Variational data assimilation of soil moisture and temperature from remote sensing observations. ModelCARE'99 Conference, September 20, 1999 - September 23, 1999, 2000 Zurich, Switz. IAHS Press, 353-359.

REICHLE, R. H., ENTEKHABI, D. and MCLAUGHLIN, D. B. 2001. Downscaling of radio brightness measurements for soil moisture estimation: A four-dimensional variational data assimilation approach. *Water Resources Research,* 37**,** 2353-2364.

REICHLE, R. H. and KOSTER, R. D. 2004. Bias reduction in short records of satellite soil moisture. *Geophysical Research Letters,* 31**,** 4 pp.

REICHLE, R. H., DE LANNOY, G. J. M., FORMAN, B. A., DRAPER, C. S. and LIU, Q. 2014. Connecting Satellite Observations with Water Cycle Variables Through Land Data Assimilation: Examples Using the NASA GEOS-5 LDAS. *Surveys in Geophysics,* 35**,** 577-606.

RENNIE, S. J. 2012. Doppler weather radar in Australia. *CAWCR Technical Report* 55**,** 1-42.

REZACOVA, D., SOKOL, Z. and PESICE, P. 2007. A radar-based verification of precipitation forecast for local convective storms. *Atmospheric Research,* 83**,** 211-224.

RICHARD, E., COSMA, S., BENOIT, R., BINDER, R., BUZZI, A. and KAUFMANN, P. 2003. Intercomparison of mesoscale meteorological models for precipitation forecasting. *Hydrology and Earth System Sciences,* 7**,** 799-811.

RIDLER, M.-E., MADSEN, H., STISEN, S., BIRCHER, S. and FENSHOLT, R. 2014. Assimilation of SMOS-derived soil moisture in a fully integrated hydrological and soil-vegetation-atmosphere transfer model in Western Denmark. *Water Resources Research,* 50**,** 8962-8981.

RINEHART, R. E. 1991. *Radar for meteorologists, or, You too can be a radar meteorologist,* Grand Forks, N.D., R.E. Rinehart.

ROBERTS, N. 2008. Assessing the spatial and temporal variation in the skill of precipitation forecasts from an NWP model. *Meteorological Applications,* 15**,** 163-9.

ROBERTS, N. M. and LEAN, H. W. 2008. Scale-selective verification of rainfall accumulations from high-resolution forecasts of convective events. *Monthly Weather Review,* 136**,** 78-97.

ROBERTS, N. M., COLE, S. J., FORBES, R. M., MOORE, R. J. and BOSWELL, D. 2009. Use of high-resolution NWP rainfall and river flow forecasts for advance warning of the Carlisle flood, north-west England. *Meteorological Applications,* 16**,** 23-34.

ROBERTSON, D. E., SHRESTHA, D. L. and WANG, Q. J. 2013. Post-processing rainfall forecasts from numerical weather prediction models for short-term streamflow forecasting. *Hydrol. Earth Syst. Sci.,* 17**,** 3587-3603.

ROBINSON, W. D., KUMMEROW, C. and OLSON, W. S. 1992. A technique for enhancing and matching the resolution of microwave measurements from the SSM/I instrument. *IEEE Transactions on Geoscience and Remote Sensing***,** 419.

RODELL, M. and HOUSER, P. R. 2004. Updating a land surface model with MODIS-derived snow cover. *Journal of Hydrometeorology,* 5**,** 1064-1075.

ROY, A., ROYER, A. and TURCOTTE, R. 2010. Improvement of springtime streamflow simulations in a boreal environment by incorporating snow-covered area derived from remote sensing data. *Journal of Hydrology,* 390**,** 35-44.

RÜDIGER, C. 2006. Streamflow Data Assimilation for Soil Moisture Prediction. PhD thesis, Dep. of Civ. and Environ. Eng., Univ. of Melbourne, Melbourne, Victoria, Australia**,** 407 pp.

RÜDIGER, C., WALKER, J. P., KERR, Y. H., MIALON, A., MERLIN, O. and KIM, E. J. 2011. Validation of the Level 1c and Level 2 SMOS products with airborne and ground-based observations. *19th International Congress on Modelling and Simulation, Perth, Australia.*

SCHREIDER, S. Y., WHETTON, P. H., JAKEMAN, A. J. and PITTOCK, A. B. 1997. Runoff modelling for snow-affected catchments in the Australian alpine region, eastern Victoria. *Journal of Hydrology,* 200**,** 1-23.

SCIPAL, K., DRUSCH, M. and WAGNER, W. 2008. Assimilation of a ERS scatterometer derived soil moisture index in the ECMWF numerical weather prediction system. *Advances in Water Resources,* 31**,** 1101-1112.

SEBASTIANELLI, S., RUSSO, F., NAPOLITANO, F. and BALDINI, L. 2010. Comparison between radar and rain gauges data at different distances from radar and correlation existing between the rainfall values in the adjacent pixels. *Hydrol. Earth Syst. Sci. Discuss.,* 7**,** 5171-5212.

SENARATH, S. U. S., OGDEN, F. L., DOWNER, C. W. and SHARIF, H. O. 2000. On the calibration and verification of two-dimensional, distributed, Hortonian, continuous watershed models. *Water Resources Research,* 36**,** 1495-1510.

SÉNÉGAS, J., WACKERNAGEL, H., ROSENTHAL, W. and WOLF, T. 2001. Error covariance modeling in sequential data assimilation. *Stochastic Environmental Research and Risk Assessment,* 15**,** 65-86.

SEO, D.-J., KOREN, V. and CAJINA, N. 2003. Real-time variational assimilation of hydrologic and hydrometeorological data into operational hydrologic forecasting. *Journal of Hydrometeorology,* 4**,** 627-641.

SEO, D.-J., CAJINA, L., CORBY, R. and HOWIESON, T. 2009. Automatic state updating for operational streamflow forecasting via variational data assimilation. *Journal of Hydrology,* 367**,** 255-275.

SHAHRBAN, M., WALKER, J. P., WANG, Q. J. and ROBERTSON, D. E. On the importance of soil moisture in calibration of rainfall-runoff modelling: Two case studies. *Hydrological Processes*, In Review.

SHAHRBAN, M., WALKER, J. P., WANG, Q. J., SEED, A. and STEINLE, P. 2011. Comparison of weather radar, numerical weather radar, numerical weather prediction and gauge-based rainfall estimates. *MODSIM, 19th International Congress on Modelling and Simulation,*, Modelling and Simulation Society of Australia and New Zealand, Perth, Australia, 3384-3390.

SHAHRBAN, M., WALKER, J. P., WANG, Q. J., SEED, A. and STEINLE, P. 2016. An evaluation of numerical weather prediction based rainfall forecasts. *Hydrological Sciences Journal,* 61**,** 2704-2717.

SHAMSELDIN, A. Y. and O CONNOR, K. M. 2001. A non-linear neural network technique for updating of river flow forecasts. *Hydrology and Earth System Sciences,* 5**,** 577-598.

SHIMADA, M., ISOGUCHI, O., TADONO, T. and ISONO, K. 2009. PALSAR radiometric and geometric calibration. *IEEE Transactions on Geoscience and Remote Sensing***,** 3915.

SHRESTHA, D. L., ROBERTSON, D. E., WANG, Q. J., PAGANO, T. C. and HAPUARACHCHI, H. A. P. 2013. Evaluation of numerical weather prediction model precipitation forecasts for short-term streamflow forecasting purpose. *Hydrology and Earth System Sciences,* 17**,** 1913-1931.

SILVESTRO, F. and REBORA, N. 2014. Impact of precipitation forecast uncertainties and initial soil moisture conditions on a probabilistic flood forecasting chain. *Journal of Hydrology,* 519, Part A**,** 1052-1067.

SILVESTRO, F., GABELLANI, S., RUDARI, R., DELOGU, F., LAIOLO, P. and BONI, G. 2015. Uncertainty reduction and parameter estimation of a distributed hydrological model with ground and remote-sensing data. *Hydrol. Earth Syst. Sci.,* 19**,** 1727-1751.

SLATER, A. G. and CLARK, M. P. 2006. Snow data assimilation via an ensemble Kalman filter. *Journal of Hydrometeorology,* 7**,** 478-493.

SMITH, A. B., WALKER, J. P., WESTERN, A. W., YOUNG, R. I., ELLETT, K. M., PIPUNIC, R. C., GRAYSON, R. B., SIRIWARDENA, L., CHIEW, F. H. S. and RICHTER, H. 2012. The Murrumbidgee Soil Moisture Monitoring Network data set. *Water Resources Research,* 48.

SMITH, J. A., SEO, D. J., BAECK, M. L. and HUDLOW, M. D. 1996. An Intercomparison Study of NEXRAD Precipitation Estimates. *Water Resources Research,* 32**,** 2035.

SMITH, J. M. 1977. *Mathematical modeling and digital simulation for engineers and scientists / Jon M. Smith,* New York, Wiley.

STEINER, M. and SMITH, J. A. 2000. Reflectivity, Rain Rate, and Kinetic Energy Flux Relationships Based on Raindrop Spectra. *Journal of Applied Meteorology,* 39**,** 1923-1940.

SU, C.-H., RYU, D., YOUNG, R. I., WESTERN, A. W. and WAGNER, W. 2013. Inter-comparison of microwave satellite soil moisture retrievals over the Murrumbidgee Basin, southeast Australia. *Remote Sensing of Environment,* 134**,** 1-11.

SUTANUDJAJA, E. H., VAN BEEK, L. P. H., DE JONG, S. M., VAN GEER, F. C. and BIERKENS, M. F. P. 2014. Calibrating a large-extent high-resolution coupled groundwater-land surface model using soil moisture and discharge data. *Water Resources Research,* 50**,** 687-705.

TALAGRAND, O. 1987. *Variational Assimilation of Meteorological Observations With the Adjoint Vorticity Equation. I: Theory*

Quarterly Journal of the Royal Meteorological Society.

TANG, Q. and LETTENMAIER, D. P. 2010. Use of satellite snow-cover data for streamflow prediction in the Feather River Basin, California. *International Journal of Remote Sensing,* 31**,** 3745-3762.

THIELEN, J., BARTHOLMES, J., RAMOS, M. H. and DE ROO, A. 2008. The European Flood Alert System - Part 1: Concept and development. *Hydrology and Earth System Sciences Discussions,* 5**,** 257-287.

THIREL, G., MARTIN, E., MAHFOUF, J. F., MASSART, S., RICCI, S. and HABETS, F. 2010a. A past discharges assimilation system for ensemble streamflow forecasts over France - Part 1: Description and validation of the assimilation system. *Hydrology and Earth System Sciences,* 14**,** 1623-1637.

THIREL, G., SALAMON, P., BUREK, P. and KALAS, M. 2011. Assimilation of MODIS snow cover area data in a distributed hydrological model. *Hydrol. Earth Syst. Sci. Discuss.,* 8**,** 1329-1364.

THIREL, G., SALAMON, P., BUREK, P. and KALAS, M. 2013. Assimilation of MODIS Snow Cover Area Data in a Distributed Hydrological Model Using the Particle Filter. *Remote Sensing,* 5**,** 5825-50.

TRAMBLAY, Y., BOUVIER, C., MARTIN, C., DIDON-LESCOT, J.-F., TODOROVIK, D. and DOMERGUE, J.-M. 2010. Assessment of initial soil moisture conditions for event-based rainfall-runoff modelling. *Journal of Hydrology,* 387**,** 176-187.

TRAMBLAY, Y., BOUVIER, C., AYRAL, P. A. and MARCHANDISE, A. 2011. Impact of rainfall spatial distribution on rainfall-runoff modelling efficiency and initial soil moisture conditions estimation. *Nat. Hazards Earth Syst. Sci.,* 11**,** 157-170.

TSUTSUI, H., KOIKE, T. and GRAF, T. Snow satellite algorithm development and verification based on the ground snow observation using a ground microwave radiometer. 2006 IEEE International Geoscience and Remote Sensing Symposium, IGARSS, July 31, 2006 - August 4, 2006, 2006 Denver, CO, United states. Institute of Electrical and Electronics Engineers Inc., 751-754.

TUSTISON, B., HARRIS, D. and FOUFOULA-GEORGIOU, E. 2001. Scale issues in verification of precipitation forecasts. *Journal of Geophysical Research,* 106**,** 11775-84.

VAZE, J., CHIEW, F. H. S., PERRAUD, J. M., VINEY, N., POST, D., TENG, J., WANG, B., LERAT, J. and GOSWAMI, M. 2010. Rainfall-runoff modelling across southeast Australia: Datasets, models and results. *Australian Journal of Water Resources,* 14**,** 101-116.

VAZE, J., POST, D. A., CHIEW, F. H. S., PERRAUD, J. M., TENG, J. and VINEY, N. R. 2011. Conceptual rainfall-runoff model performance with different spatial rainfall inputs. *Journal of Hydrometeorology*, 12**,** 1100-1112.

VELASCO-FORERO, C. A., SEMPERE-TORRES, D., CASSIRAGA, E. F. and JAIME GOMEZ-HERNANDEZ, J. 2009. A non-parametric automatic blending methodology to estimate rainfall fields from rain gauge and radar data. *Advances in Water Resources,* 32**,** 986-1002.

VRUGT, J. A., DIKS, C. G. H., GUPTA, H. V., BOUTEN, W. and VERSTRATEN, J. M. 2005. Improved treatment of uncertainty in hydrologic modeling: Combining the strengths of global optimization and data assimilation. *Water Resources Research,* 41**,** 1-17.

WAGNER, W., LEMOINE, G. and ROTT, H. 1999. A method for estimating soil moisture from ERS Scatterometer and soil data. 70**,** 191-207.

WAGNER, W., BLOESCHL, G., PAMPALONI, P., CALVET, J.-C., BIZZARRI, B., WIGNERON, J.-P. and KERR, Y. 2007. Operational readiness of microwave remote sensing of soil moisture for hydrologic applications. *Nordic Hydrology,* 38**,** 1-20.

WAGNER, W., DORIGO, W., DE JEU, R., FERNANDEZ, D., BENVENISTE, J., HAAS, E. and ERTL, M. 2012. FUSION OF ACTIVE AND PASSIVE MICROWAVE OBSERVATIONS TO CREATE AN ESSENTIAL CLIMATE VARIABLE DATA RECORD ON SOIL MOISTURE. *ISPRS Ann. Photogramm. Remote Sens. Spatial Inf. Sci.,* I-7**,** 315-321.

WAGNER, W., DRUSCH, M., LEROUX, D. J., KERR, Y. H., CALVET, J. C., JACKSON, T. J., WESTERN, A., CHUN-HSU, S., DE JEU, R., RYU, D., HAHN, S., DRAPER, C., REICHLE, R., NAEIMI, V. and PAULIK, C. 2014. Clarifications on the 'comparison between SMOS, VUA, ASCAT, and ECMWF soil moisture products over four Watersheds in U.S.'. *IEEE Transactions on Geoscience and Remote Sensing***,** 1901.

WALKER, J. P., WILLGOOSE, G. R. and KALMA, J. D. 2001. One-dimensional soil moisture profile retrieval by assimilation of near-surface observations: A comparison of retrieval algorithms. *Advances in Water Resources,* 24**,** 631-650.

WALKER, J. P., HOUSER, P. R. and WILLGOOSE, G. R. 2004. Active microwave remote sensing for soil moisture measurement: a field evaluation using ERS-2. *Hydrological Processes,* 18**,** 1975-1997.

WALKER, J. P. and HOUSER, P. R. 2005. Hydrologic Data Assimilation. *In:* ASWATHANARAYANA, A. (ed.) *Advances in Water Science Methodologies.* A.A. Balkema, The Netherlands.

WANDERS, N., BIERKENS, M. F. P., DE JONG, S. M., DE ROO, A. and KARSSENBERG, D. 2014a. The benefits of using remotely sensed soil moisture in parameter identification of large-scale hydrological models. *Water Resources Research,* 50**,** 6874-6891.

WANDERS, N., KARSSENBERG, D., DE ROO, A., DE JONG, S. M. and BIERKENS, M. F. P. 2014b. The suitability of remotely sensed soil moisture for improving operational flood forecasting. *Hydrol. Earth Syst. Sci.,* 18**,** 2343-2357.

WEERTS, A. H. and EL SERAFY, G. Y. H. 2006. Particle filtering and ensemble Kalman filtering for state updating with hydrological conceptual rainfall-runoff models. *Water Resources Research,* 42**,** W09403.

WERNINGHAUS and R. BUCKREUSS, S. 2010. The TerraSAR-X mission and system design. *IEEE Transactions on Geoscience and Remote Sensing***,** 606.

WEYGANDT, S. S., LOUGHE, A. F., BENJAMIN, S. G. and MAHONEY, J. L. 2004. Scale sensitivities in model precipitation skill scores during IHOP. *22 nd Conference Severe Local Storms, American Meteorological Society, Hyannis, MA, 4–8 October*.

WHEATER, H., SOROOSHIAN, S. and SHARMA, K. D. 2007. *Hydrological modelling in arid and semi-arid areas, ISBN9780521869188*, Cambridge University Press, Cambridge.

WHITAKER, J. S. and HAMILL, T. M. 2002. Ensemble Data Assimilation without Perturbed Observations. *Monthly Weather Review*, 130**,** 1913.

WILKS, D. S. 1995. Statistical Methods in the Atmospheric Sciences. An Introduction. Academic Press, San Diego**,** 467pp.

WOOD, S. J., JONES, D. A. and MOORE, R. J. 2000. Accuracy of rainfall measurement for scales or hydrological interest. *Hydrology and Earth System Sciences,* 4**,** 531-543.

WOODHOUSE, I. H. 2005. *Introduction to microwave remote sensing*, Boca Raton, FL : Taylor&Francis, 2005.

WU, Q., LIU, H., WANG, L. and DENG, C. 2016. Evaluation of AMSR2 soil moisture products over the contiguous United States using in situ data from the International Soil Moisture Network. *International Journal of Applied Earth Observation and Geoinformation,* 45, Part B**,** 187-199.

WU, X., WALKER, J. P., C, R., X00FC, DIGER and PANCIERA, R. 2015. Effect of Land-Cover Type on the SMAP Active/Passive Soil Moisture Downscaling Algorithm Performance. *IEEE Geoscience and Remote Sensing Letters,* 12**,** 846-850.

XIANGJUN, T., ZHENGHUI, X., AIGUO, D., CHUNXIANG, S., BINGHAO, J., FENG, C. and KUN, Y. 2009. A dual-pass variational data assimilation framework for estimating soil moisture profiles from AMSR-E microwave brightness temperature. *Journal of Geophysical Research - Part D - Atmospheres,* 114**,** D16102 (12 pp.).

YANG, X. and MICHEL, C. 2000. Flood forecasting with a watershed model: a new method of parameter updating. *Hydrological Sciences Journal*, 45**,** 537-546.

YATES, E., ANQUETIN, S., DUCROCQ, V., CREUTIN, J.-D., RICARD, D. and CHANCIBAULT, K. 2006. Point and areal validation of forecast precipitation fields. *Meteorological Applications,* 13**,** 1-20.

YEE, M. S. 2016. Remote sensing error assessment for subsequent use in model confrontation. Submitted PhD thesis, Dep. of Civ. Eng., Monash Univ., Melbourne, Victoria, Australia**,** 270 pp.

YILMAZ, M. T. and CROW, W. T. 2013. The Optimality of Potential Rescaling Approaches in Land Data Assimilation. *Journal of Hydrometeorology,* 14**,** 650-660.

YIN, J., ZHAN, X., ZHENG, Y., LIU, J., HAIN, C. R. and FANG, L. 2014. Impact of quality control of satellite soil moisture data on their assimilation into land surface model. *Geophysical Research Letters,* 41**,** 7159-7166.

YU, W., LIN, C. A., BENOIT, R. and ZAWADZKI, I. High resolution model simulation of precipitation and evaluation with Doppler radar observation. Proceedings of the 1997 3rd International Workshop on Rainfall in Urban Areas, December 4, 1997 - December 7, 1997, 1998 Pontresina, Switz. Elsevier Ltd, 179-186.

ZAKERMOSHFEGH, M., NEYSHABOURI, S. A. A. S. and LUCAS, C. 2008. Automatic calibration of lumped conceptual rainfall-runoff model using particle swarm optimization. *Journal of Applied Sciences,* 8**,** 3703-8.

ZHAN, X., HOUSER, P. R., WALKER, J. P. and CROW, W. T. 2006. A method for retrieving high-resolution surface soil moisture from hydros L-band radiometer and Radar observations. *Geoscience and Remote Sensing, IEEE Transactions on,* 44**,** 1534-1544.

ZHANG, Y., CHIEW, F. H. S., ZHANG, L. and LI, H. 2009. Use of remotely sensed actual evapotranspiration to improve rainfall-runoff modeling in Southeast Australia. *Journal of Hydrometeorology,* 10**,** 969-980.

ZHANG, Y. Q., VAZE, J., CHIEW, F. H. S. and LIU, Y. Incorporating vegetation time series to improve rainfall-runoff model predictions in gauged and ungauged catchments. 19th International Congress on Modelling and Simulation - Sustaining Our Future: Understanding and Living with Uncertainty, MODSIM2011, December 12, 2011 - December 16, 2011, 2011 Perth, WA, Australia. Modelling and Simulation Society of, 3455-3461.

ZHENG, X. 2009. An adaptive estimation of forecast error covariance parameters for Kalman filtering data assimilation. *Advances in Atmospheric Sciences,* 26**,** 154-160.

Appendix A1

Evaluation of Joint-calibration to Streamflow and CDF-matched OzNet Observations

This Appendix contains evaluation results from joint-calibration to OzNet soil moisture observations when the in-situ data were CDF-matched to model predictions as compared to the results from calibration to streamflow observations alone and joint-calibration to streamflow and normalized OzNet soil moisture observations (joint-cali). Table A1.1 compares the NSE scores and RMSE for calibration period in 2007 to 2010 (Cal.) and validation period using operational rainfall data in 2011 to 2012 (Val.), and the optimized values for soil storage capacity parameter in the models for SF-calibration, joint-calibration with normalized/CDF-matched soil moisture observations. In Figures A1.1 to A1.4, the modelled soil moisture from calibration to streamflow alone (Sim SF-cali) and joint-calibration to streamflow and soil wetness observations (Sim Joint-cali) (%), which were shown in the original thesis, are compared to the results from the joint-calibration to streamflow and soil moisture observations (mm) when the soil moisture observations (% m^3/m^3) are CDF-matched to the modelled soil moisture (mm) (Sim Joint-cali-cdf). Note that for the first and third panels, the blue line is the original average of volumetric soil moisture (Obs) before the CDF-matching which is shown on the secondary vertical axis while the grey line is the CDF-matched observation and the other lines are modelled soil water after either SF-calibration or joint-calibration. The blue line in the second and fourth panels is the soil wetness obtained by normalisation alone and the other lines are the soil wetness obtained by normalising CDF-matched soil water values. OzNet rainfall data are used for the calibration. The error statistics in the figures are shown for three calibrations which are between the normalised observation and model prediction for SF-cali and Joint-cali and between the CDF-matched observation and the model prediction for Joint-cali-cdf.

Table A1.1: NSE scores of streamflow modelling, RMSE (%) of soil wetness simulations and observations, and soil moisture storage capacity C_{max} (mm) from calibration to streamflow alone (SF-cali), calibration to both streamflow and normalised soil moisture (Joint-cali) and calibration to streamflow and CDF-matched soil moisture (Joint-cali-CDF)in the Kyeamba (K) and Adelong (A) subcatchments for the GR4H and PDM models. The NSE scores are shown for Calibration with OzNet rainfall (2007-2010, Cal.) and validation with operational rainfall (2011-2012, Val.) in the left hand column; the RMSE results are shown for Cal. and Val. in the right hand column.

Sub. Catch	Model	SF-cali					Joint-cali					Joint-cali-CDF				
		Cal.		Val.		C_{max}	Cal.		Val.		C_{max}	Cal.		Val.		C_{max}
K	GR4H	0.71	9.7	0.63	10.6	286	0.68	9.6	0.58	11.4	194	0.71	10.8	0.63	13.5	246
	PDM	0.75	10	0.59	11.4	245	0.75	9.4	0.61	10.3	247	0.73	11.2	0.57	15.2	232
A	GR4H	0.80	20.7	0.80	18.4	108	0.79	17.9	0.83	15.3	167	0.80	14.6	0.80	15.5	110
	PDM	0.83	26.6	0.20	22.4	358	0.81	11.4	0.35	17.3	309	0.82	12.6	0.32	31.8	345

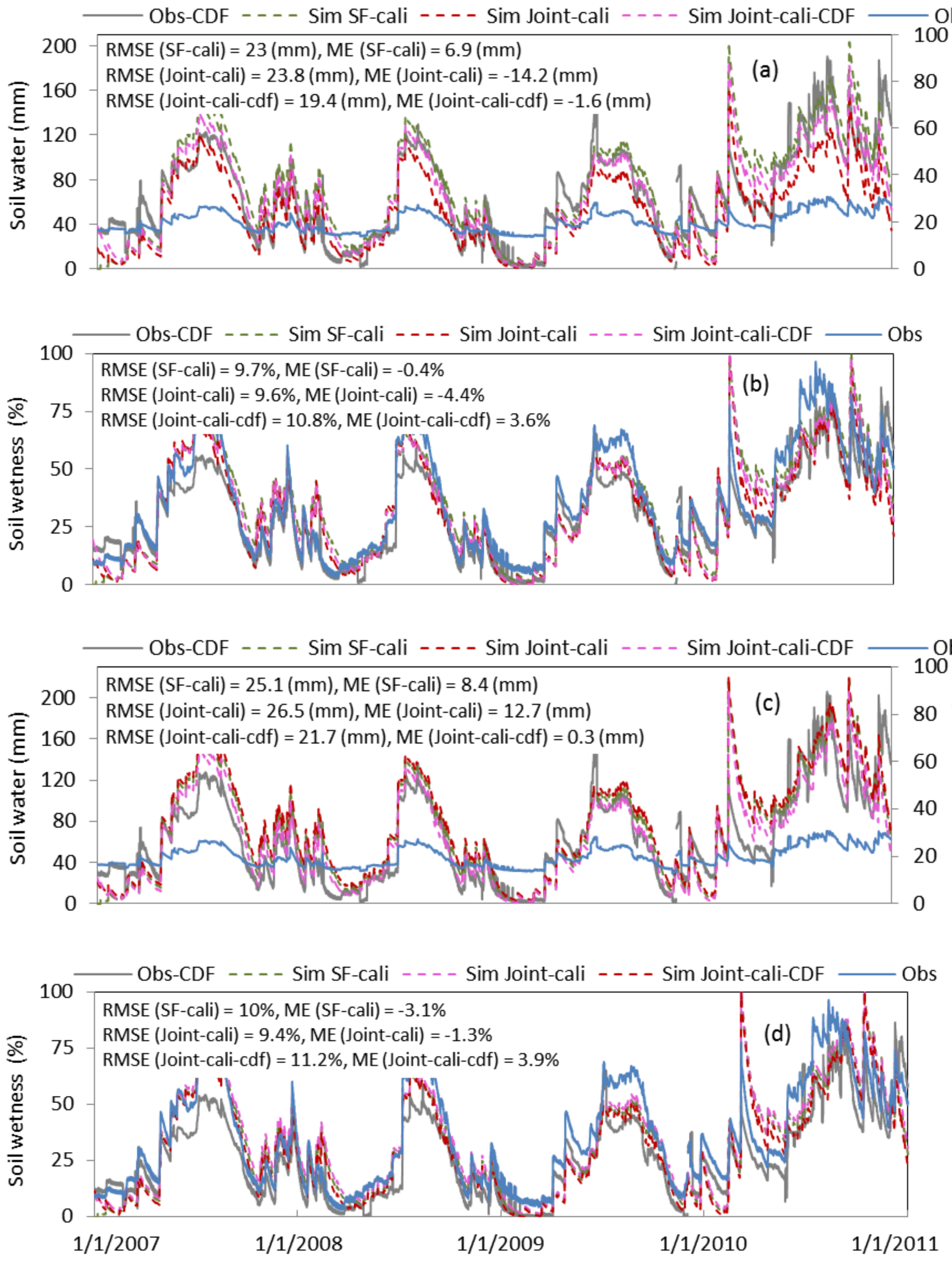

Figure A1.1: Comparison between OzNet soil moisture (Obs) or rescaled OzNet soil water/wetness observation (Obs-CDF) and modelled soil water/wetness from GR4H (a and b) and PDM (c and d) models for calibration to streamflow alone (SF-cali), calibration jointly to streamflow and normalised soil moisture observations (Joint-cali), and calibration jointly to streamflow and CDF-matched soil moisture observations (Joint-cali-CDF) for the calibration period in the upper Kyeamba catchment.

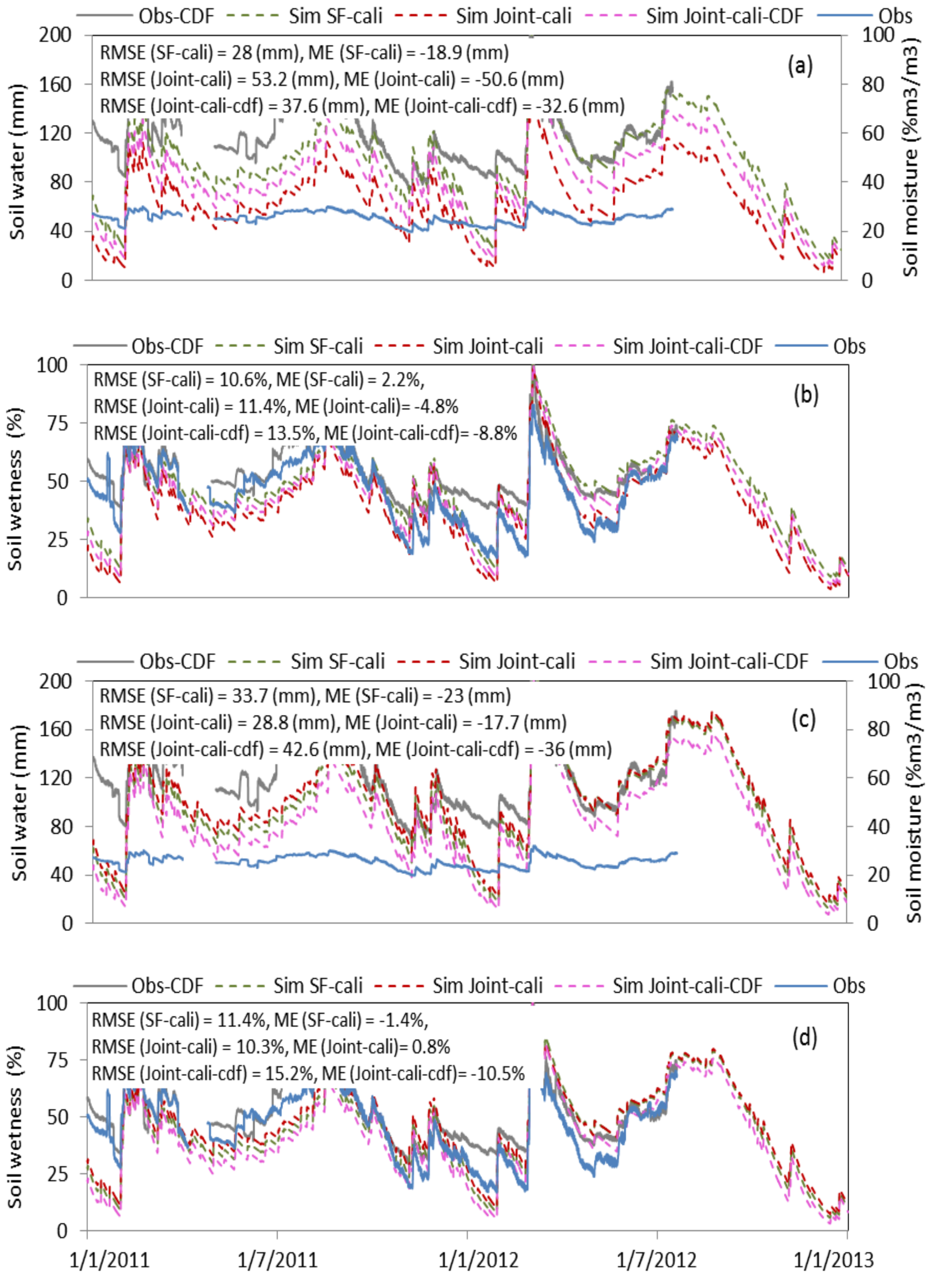

Figure A1.2: Same as Figure A1.1, but shown for the validation period. Note that the operational rainfall data are used for the validation.

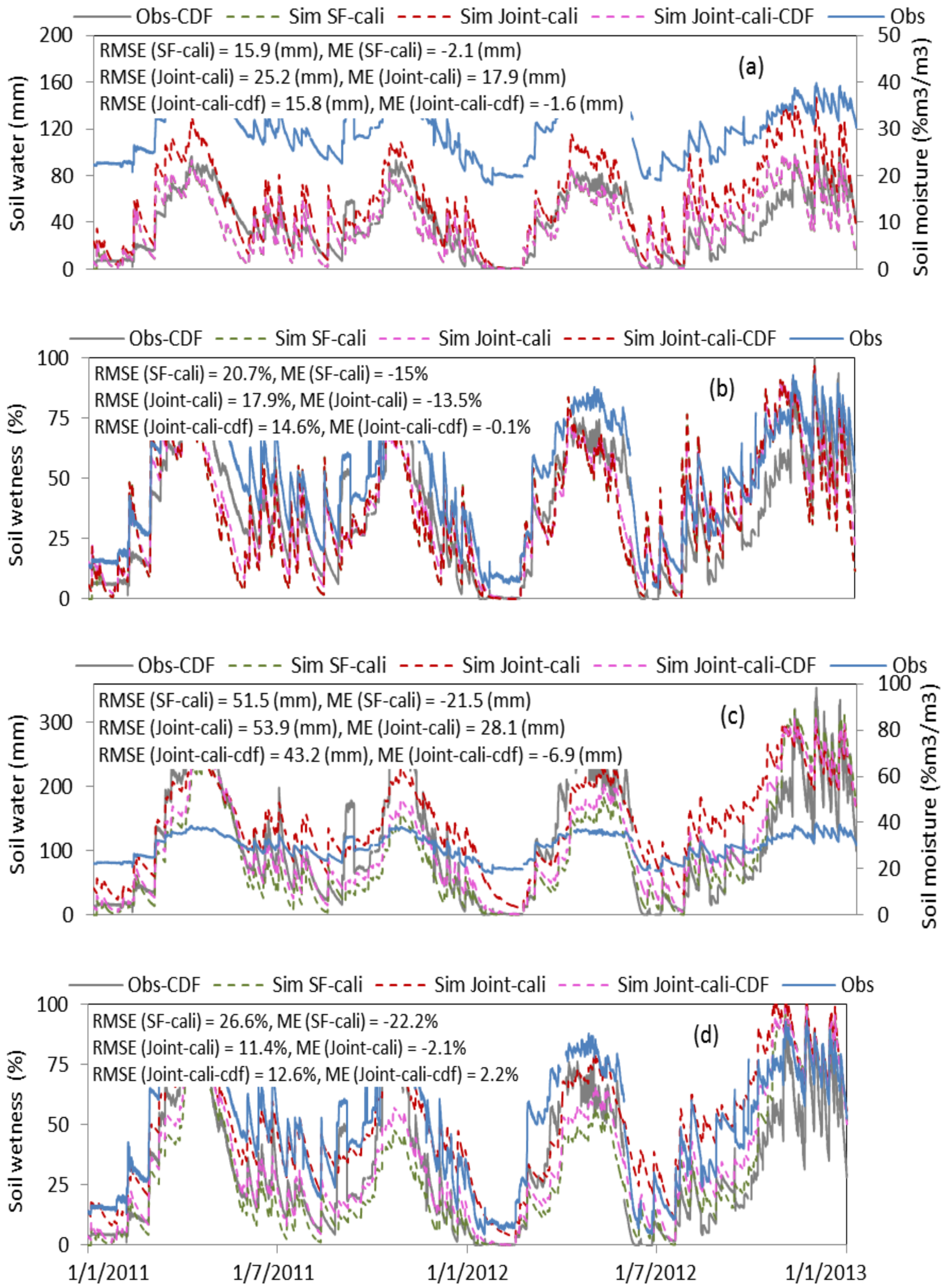

Figure A1.3: Same as Figure A1.1, but for the Adelong Creek catchment.

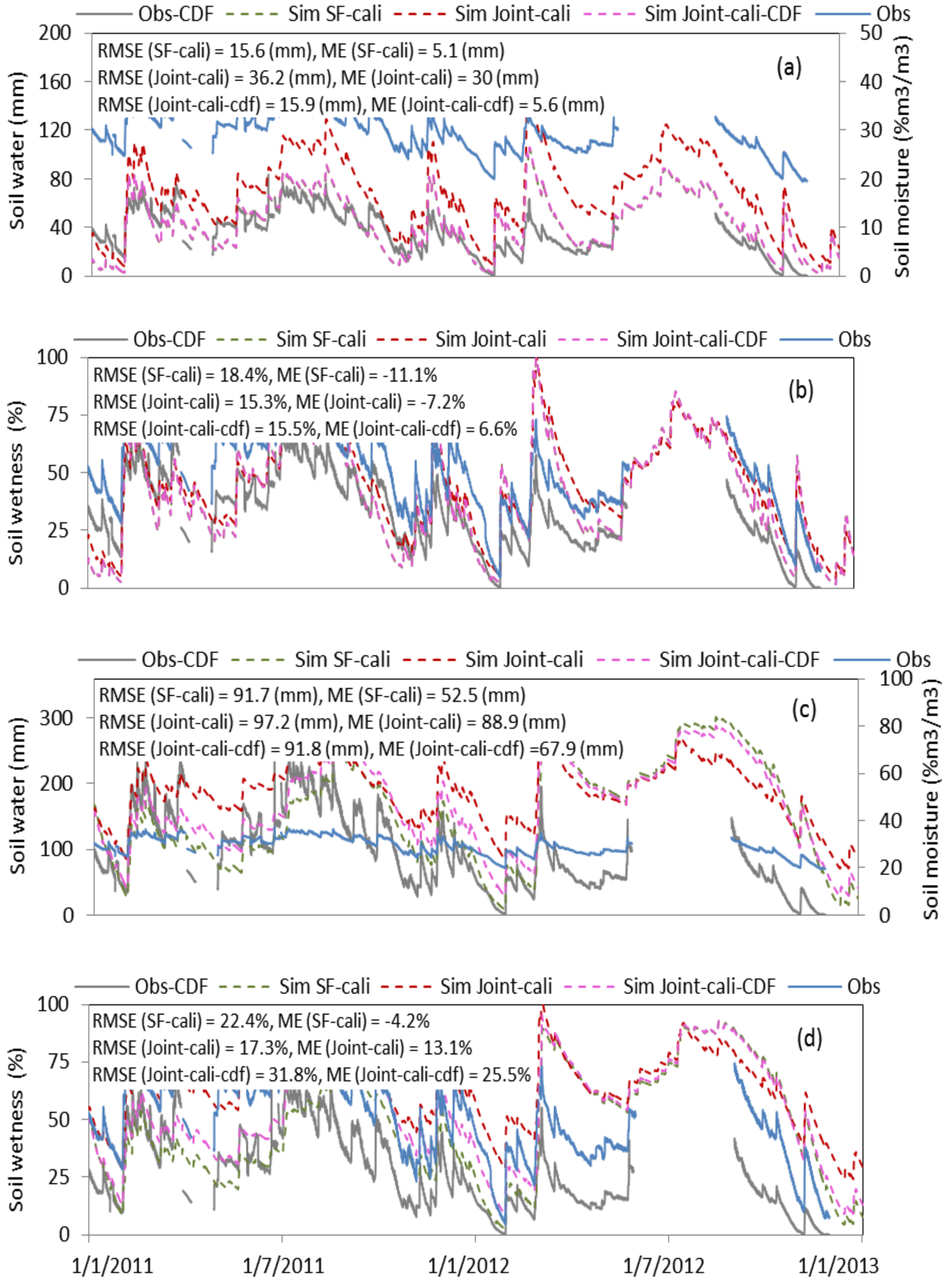

Figure A1.4: Same as Figure A1.3, but for the validation period.

Appendix A2

Evaluation of CDF-matching Rescaling Approach for SMOS Estimation

The exponential filtered/moving averaged satellite-based estimations have been rescaled to either OzNet root-zone volumetric soil moisture data or root-zone modelled soil moisture predictions using CDF-matching approach. The new SMOS soil moisture data estimated from CDF-matching to OzNet root-zone volumetric soil moisture (m^3/m^3) data (SMOS-exp-filt-cdf1, SMOS-move-ave-cdf1) or model soil moisture predictions (mm) (SMOS-exp-filt-cdf2, SMOS-move-ave-cdf2) are compared to the OzNet and model data in Figures A2.1 to A2.6. The skill scores between all SMOS estimations and OzNet data or model predictions are presented in Table A2.1 and A2.2. For further evaluation, the different SMOS estimations have been assimilated into the GR4H model using the nudging approach with a weighting factor (G) of 0.8 and direct insertion (ie. G=1.0) as illustrated in Figures A2.7 to A2.10. Table A2.3 summarizes NSE and Vol E at 10 stream gauges located at 10 subcatchments outlets within the entire study area down to Wagga Wagga station (see Figure 5.1 in the thesis) before (Sim) and after nudging or direct insertion of SMOS estimations obtained by exponential filtering alone (Nudge, DI), CDF-matching to OzNet data after exponential filtering (Nudge-cdf1, DI-cdf1), and CDF-matching to model predictions after exponential filtering (Nudge-cdf2, DI-cdf2).

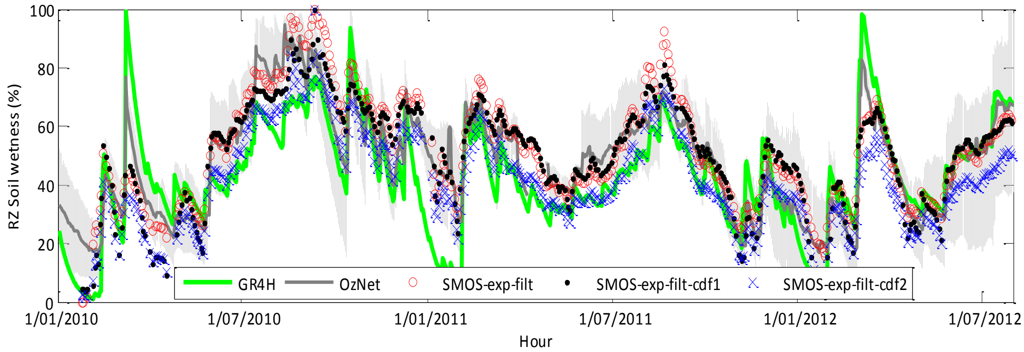

Figure A2.1: Comparison between normalised OzNet and SMOS-based root-zone data and modelled soil wetness from GR4H for exponential filtering approach after normalisation alone (exp-filt), after CDF-matching to the OzNet data (exp-filt-cdf1), and after CDF-matching to model estimations (exp-filt-cdf2) in the Kyeamba catchment; data are from January 2010 to July 2012 and OzNet observation range has been shown in light grey colour.

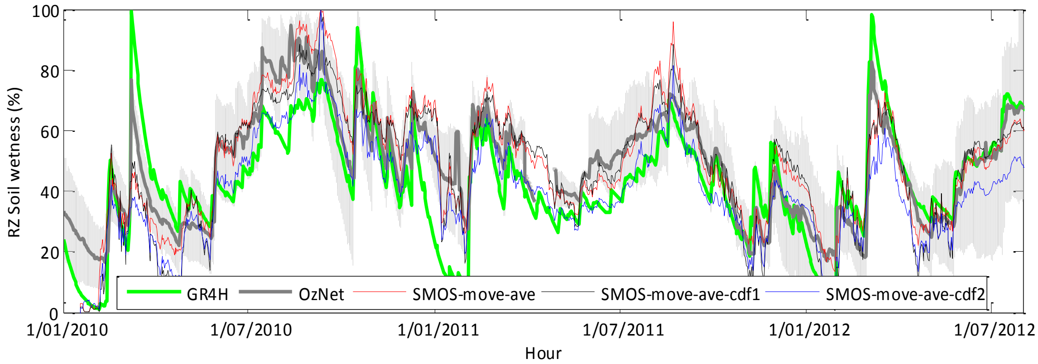

Figure A2.2: Same as Figure A2.1, but for moving average approach.

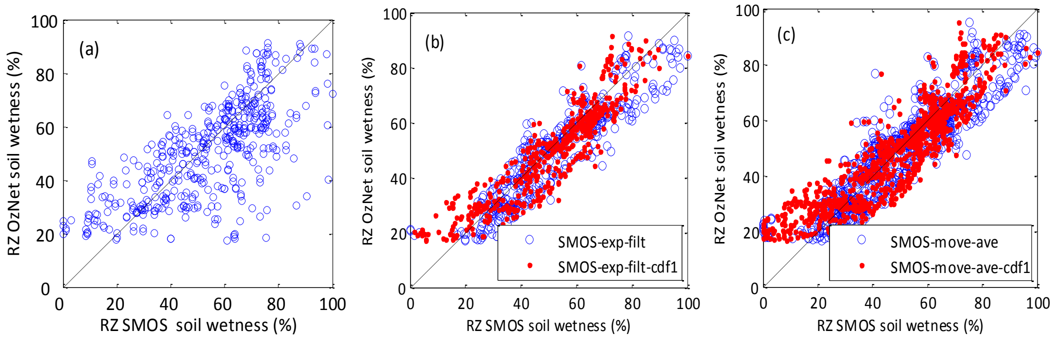

Figure A2.3: Scatter plots of mean OzNet soil wetness over depth 0-90 cm and normalised SMOS-based root-zone estimations after CDF-matching to the OzNet root-zone data alone (a), after exponential filtering (exp-filt)/moving average (move-ave) alone (blue circles in (b) and (c)), and after exponential filtering/moving average and CDF-matching to OzNet root-zone data (red dots in (b) and (c)) in the Kyeamba catchment; data are from January 2010 to July 2012.

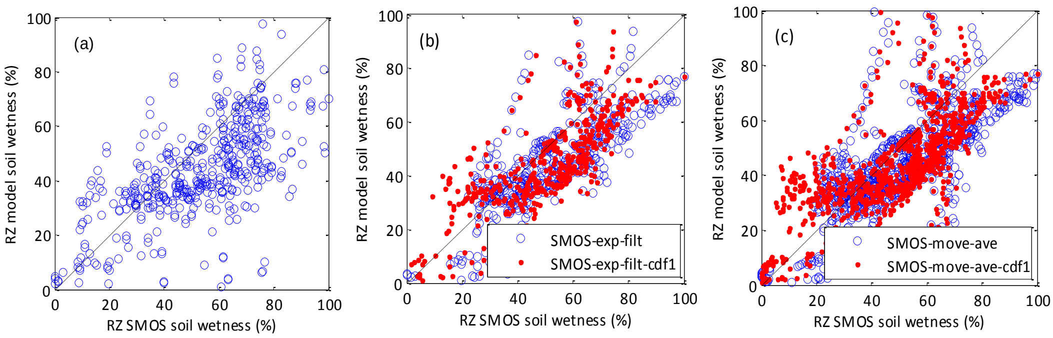

Figure A2.4: Scatter plots of GR4H model soil wetness and normalised SMOS-based root-zone estimations after CDF-matching to the OzNet root-zone data alone (a), after exponential filtering (exp-filt)/moving average (move-ave) alone (blue circles in (b) and (c)), and after exponential filtering/moving average and CDF-matching to OzNet root-zone data (red dots in (b) and (c)) in the Kyeamba catchment; data are from January 2010 to July 2012.

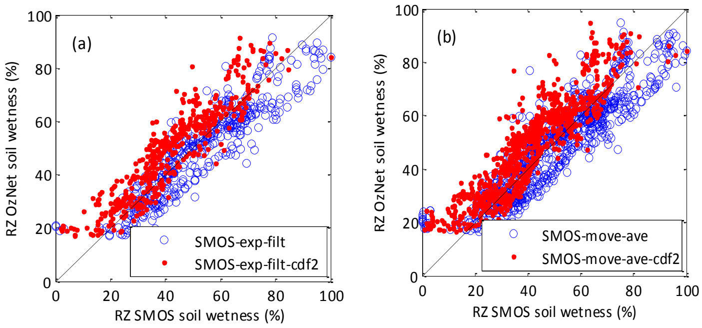

Figure A2.5: Scatter plots of mean OzNet soil wetness over depth 0-90 cm and normalised SMOS-based root-zone estimations after exponential filtering (exp-filt)/moving average (move-ave) alone (blue circles in a and b), and after exponential filtering/moving average and CDF-matching to GR4H model soil moisture estimations (red dots in (a) and (b)) in the Kyeamba catchment; data are from January 2010 to July 2012.

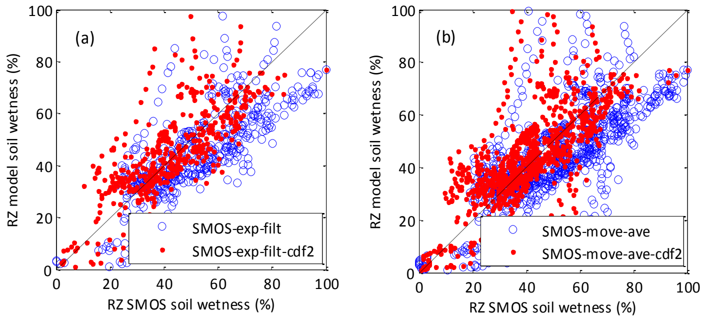

Figure A2.6: Scatter plots of GR4H model soil wteness and normalised SMOS-based root-zone estimations after exponential filtering (exp-filt)/moving average (move-ave) alone (blue circles in a and b), and after exponential filtering/moving average and CDF-matching to GR4H model soil moisture estimations (red dots in (a) and (b)) in the Kyeamba catchment; data are from January 2010 to July 2012.

Table A2.1: RMSD (%), bias (%) and correlation coefficient (R) between OzNet root-zone soil wetness and normalised SMOS-based root-zone estimations for CDF-matching to the OzNet data alone (cdf), exponential filtering/moving average (Exp-filt, Mov-ave), exponential filtering/moving average and CDF-matching to the OzNet data (Exp-filt-cdf1, Move-ave-cdf1), and exponential filtering/moving average and CDF-matching to GR4H model predictions (Exp-filt-cdf2, Move-ave-cdf2) in the Kyeamba subcatchment; data are from January 2010 to July 2012.

cdf			Exp-filt			Exp-filt-cdf1			Exp-filt-cdf2			Move-ave			Move-ave-cdf1			Move-ave-cdf2		
RMSD	Bias	R	RMSD	Bias	R	RMSD	Bias	R	RMSD	Bias	R	RMSD	Bias	R	RMSD	Bias	R	RMSD	Bias	R
15.6	3.1	0.7	7.2	1.4	0.93	7.9	-0.6	0.91	9.8	-6.8	0.93	7.9	1.5	0.92	9.2	-0.7	0.9	10.8	-7.6	0.9

Table A2.2: RMSD (%), bias (%) and correlation coefficient (R) between modelled soil wetness from GR4H and normalised SMOS-based root-zone estimations for CDF-matching to OzNet data alone (cdf), exponential filtering/moving average (Exp-filt, Mov-ave), exponential filtering/moving average and CDF-matching to the OzNet data (Exp-filt-cdf1, Move-ave-cdf1), and exponential filtering/moving average and CDF-matching to GR4H model predictions (Exp-filt-cdf2, Move-ave-cdf2) in the Kyeamba subcatchment; data are from January 2010 to July 2012.

cdf			Exp-filt			Exp-filt-cdf1			Exp-filt-cdf2			Move-ave			Move-ave-cdf1			Move-ave-cdf2		
RMSD	Bias	R	RMSD	Bias	R	RMSD	Bias	R	RMSD	Bias	R	RMSD	Bias	R	RMSD	Bias	R	RMSD	Bias	R
19.5	9.7	0.63	15	8	0.76	14.4	6.1	0.74	12.2	-1.9	0.75	15	8	0.74	14.9	4.6	0.73	13	-2.8	0.74

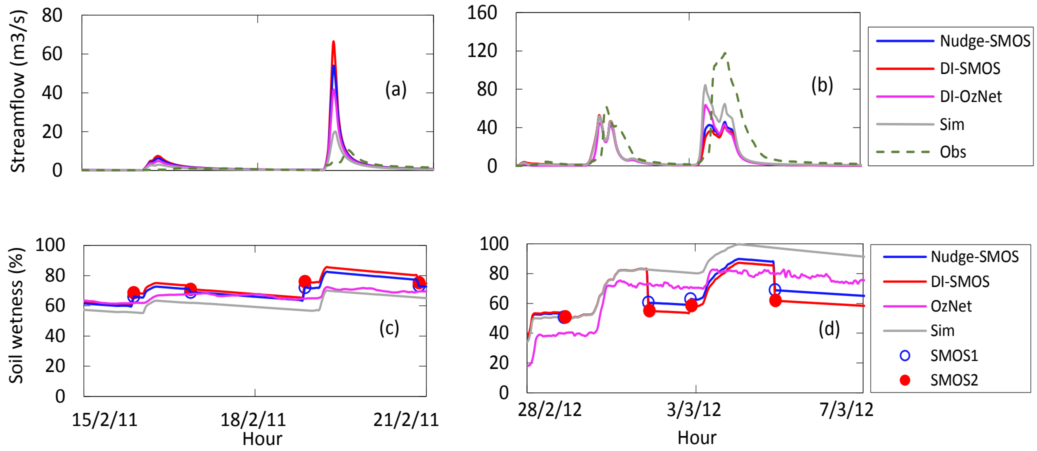

Figures A2.7: Comparison of observed (Obs) and modelled streamflow and root-zone soil wetness for open simulation (sim) and after direct insertion of OzNet data (DI-OzNet), or after assimilation with G equal to 0.8 (Nudge-SMOS) or 1.0 (DI-SMOS) using estimated SMOS root-zone soil wetness obtained from exponential filter alone for the GR4J model in the Kyeamba subcatchment for a small event in 2011 (a and c) and a major event in 2012 (b and d). SMOS1 and SMOS2 in the second panel are estimated SMOS soil wetness for G equal to 0.8 and 1.0 respectively.

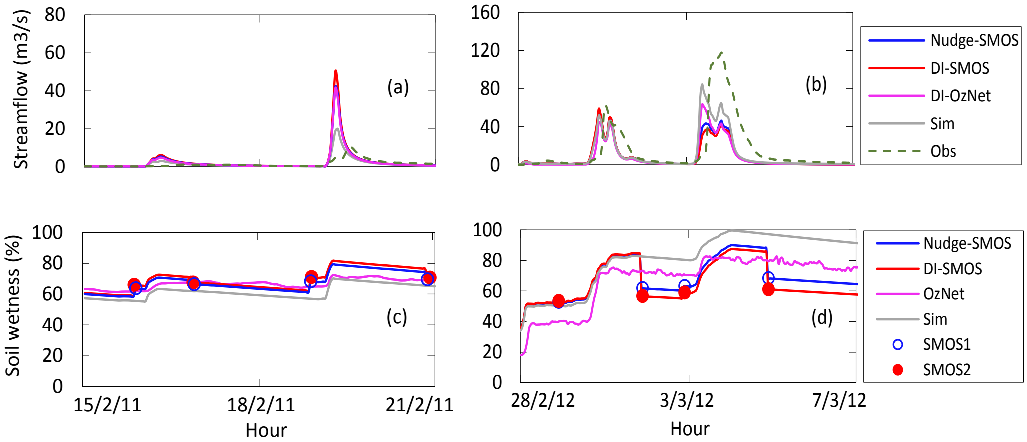

Figures A2.8: Same as Figures A2.7, but for SMOS root-zone soil wetness obtained from exponential filtering and CDF-matching to OzNet data.

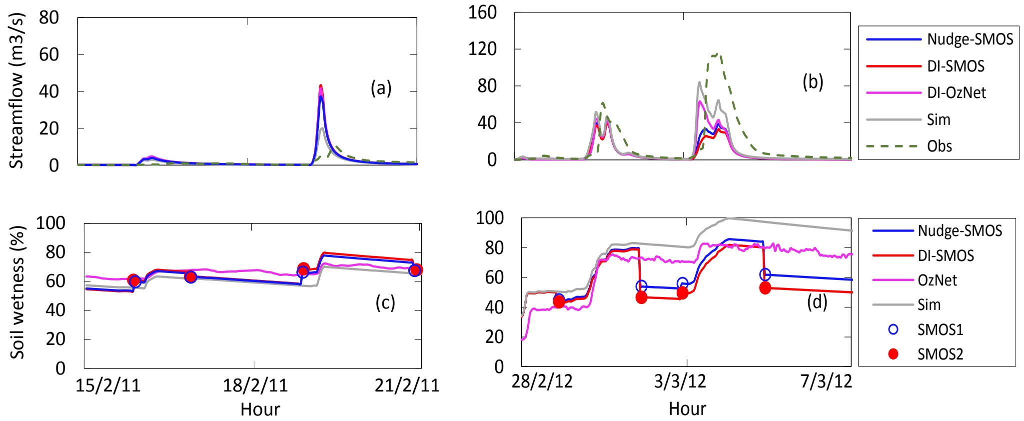

Figures A2.9: Same as Figure A2.7, but for SMOS root-zone soil wetness obtained from exponential filtering and CDF-matching to model predictions.

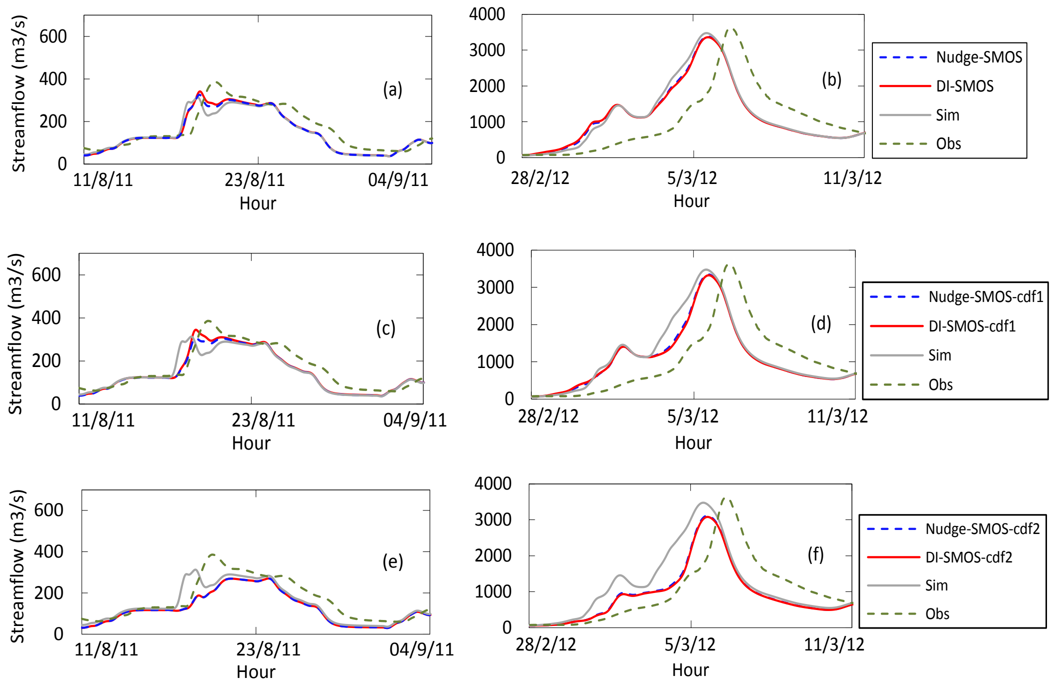

Figure A2.10: Comparison of observed (Obs) and modelled streamflow before (sim) and after assimilation of estimated SMOS root-zone soil wetness obtained from exponential filtering alone (a, b), from exponential filtering with CDF-matching to OzNet data (c, d), and from exponential filtering with CDF-matching to model predictions (e,f) with G equal to 0.8 (Nudge-SMOS, Nudge-SMOS-cdf1, Nudge-SMOS-cdf2) or 1.0 (DI-SMOS, DI-SMOS-cdf1, DI-SMOS-cdf2) at Wagga Wagga station for a moderate event in 2011 and a major event in 2012.

Table A2.3: Comparison of Nash-Sutcliffe Efficiency (NSE) and Vol E (%) for streamflow modelling at 10 stream gauges within the study area down to Wagga Wagga station for open simulation (Sim), and after nudging with G equals to 0.8 and direct insertion using SMOS estimations from exponential filtering alone (Nudge, DI), exponential filtering with CDF-matching to OzNet data (Nudge-cdf1, DI-cdf1), and exponential filtering with CDF-matching to model prediction (Nudge-cdf2, DI-cdf2).

Stream gauge	Sim		Nudge		DI		Nudge-cdf1		DI-cdf1		Nudge-cdf2		DI-cdf2	
	NSE	Vol E	NSE	Vol E	NSE	Vol E	NSE	Vol E	NSE	Vol E	NSE	Vol E	NSE	Vol E
171	0.26	71.2	0.20	83.1	0.20	83.1	0.10	88.5	0.10	88.5	0.15	74.1	0.15	75.1
206	0.90	1.9	0.90	1.7	0.90	1.8	0.90	1.3	0.90	1.2	0.89	-2.7	0.89	-2.8
214	0.79	67.5	0.63	43.0	0.56	40.8	0.62	34.1	0.55	31.4	0.15	-63.1	0.12	-66.5
245	0.73	-54.4	0.69	-51.7	0.66	-49.8	0.67	-39.3	0.63	-33.1	0.24	-87.0	0.19	-88.1
216	0.96	-1.2	0.95	0.1	0.95	0.8	0.95	0.5	0.94	1.6	0.93	-6.8	0.93	-7.0
218	0.83	-37.2	0.84	-28.8	0.82	-24.3	0.63	-67.7	0.51	-71.9	0.41	-83.8	0.35	-85.8
229	0.73	-14.8	0.74	-25.7	0.73	-26.2	0.25	-81.8	0.26	-86.4	0.28	-93.8	0.12	-94.5
241	0.60	-42.7	0.50	-33.3	0.45	-28.6	0.51	-35.8	0.46	-32.0	0.49	-49.2	0.43	-49.2
242	0.64	-23.8	0.39	-66.5	0.33	-72.2	0.36	-94.3	0.11	-97.7	0.10	-91.5	0.08	-92.5
Wagga Wagga	0.61	-4.1	0.64	-3.9	0.64	-3.2	0.69	-6.5	0.67	-5.8	0.72	-14.3	0.72	-14.6